Mechanisms of central nervous system damage and recovery in demyelinating and other neurological disorders: structural and functional MRI studies

David John Werring

A thesis submitted to the University of London for the degree of

Doctor of Philosophy

September 2000

NMR Research Unit

Department of Clinical Neurology

Institute of Neurology, University College London

Queen Square

London WC1N 3BG

United Kingdom

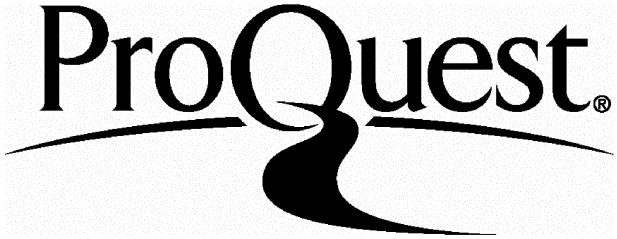

Abstract

This thesis is concerned with multiple sclerosis (MS), a chronic, multifocal demyelinating disease of the central nervous system (CNS). In its early stages MS is characterised by reversible deficits, but with time recovery usually becomes incomplete, causing progressive disability. To understand this transition requires knowledge of mechanisms of recovery and fixed neurological deficit.

Functional recovery from demyelination can occur despite irreversible conduction abnormalities and axon loss in affected pathways, suggesting that cortical adaptive mechanisms may contribute. To investigate this hypothesis, patients who had recovered from a single episode of optic neuritis were studied using functional magnetic resonance imaging (fMRI). Monocular visual stimulation to the recovered eye induced an anatomically and temporally abnormal response in areas outside the visual cortex, to which activation in control subjects was confined. The extra-occipital activation was most marked in those with delayed optic nerve conduction, suggesting a role in adaptation to persistently abnormal visual input.

Mechanisms of tissue damage in MS were investigated using MR diffusion imaging, which quantifies water molecule mobility non-invasively and is sensitive to tissue structural integrity. Heterogeneous diffusion properties were demonstrated in MS lesions, and subtle abnormalities in the magnitude and directional restriction (anisotropy) of diffusion were found in widespread areas of normal-appearing white matter (NAWM). Diffusion in lesions correlated with that in NAWM, suggesting that the underlying pathogenic mechanisms are closely linked. In patients with ischaemic stroke, anisotropy changes were demonstrated in tracts distant to the lesion, indicating an ability to detect fibre degeneration.

Finally, fMRI and diffusion imaging were combined to obtain complementary functional and structural information. In a traumatic CNS injury causing hemiplegia, excellent motor recovery was associated with a preservation of corticospinal tract structural integrity and motor cortex activation. In the human visual system, fibre tract structure and orientation, and cortical activation were demonstrated in single maps.

Acknowledgements

All of the work described herein was performed in the NMR Research Unit at the Institute of Neurology, which is funded by a generous grant from the MS Society of Great Britain and Northern Ireland. My research post was funded by the Brain Research Trust and funds available to Professor Alan Thompson. I thank all of the patients who kindly gave their time to participate in the studies.

Many thanks are due to my principle supervisor, Professor Alan Thompson, who provided enthusiastic support and encouragement throughout, enabling me to see the work in a wider context, yet at the same time showing meticulous attention to detail. I am grateful to Professor David Miller for supervising many aspects of the projects, but particularly for guidance in the interpretation of diffusion MRI data. Dr Gareth Barker provided expert supervision, patient explanations of physics principles, and solved many analysis and computer problems. It has been a privilege to work with Professor Ian McDonald, who gave invaluable encouragement and guidance, especially on the optic neuritis project.

I warmly thank Dr Christopher Clark for help with understanding and applying diffusion imaging, and Dr Martin King for statistical advice. Thanks to Dr Geoff Parker for useful discussions and help in displaying diffusion tensor imaging data. Dr Aidan Droogan collected some of the EPI diffusion data, and gave guidance on storing and manipulating it. Dr Peter Brex helped to recruit the patients for the optic neuritis study. Dr Ahmed Toosy contributed to analysing the optic neuritis and stroke studies. I am grateful to Drs Ed Bullmore, Mick Brammer and Vincent Giampietro for expert assistance with implementing fMRI analysis.

I wish to thank David MacManus, who provided radiographic assistance, particularly in the early days of applying the new techniques. I thank the many other members of the NMR Reasearch Unit with whom I worked during the project. In particular, Dr Siobhan Leary and Andrew Lowe helped me to remain (reasonably) sane throughout by providing support and reassurance, often over a drink or two. Drs Jeremy Hobart and Alex Leff could always be relied upon for words of humour and encouragement. Finally, I thank Lucy Wood for continuing moral support and proof reading the manuscript.

Publications associated with this thesis

Werring DJ, Clark CA, Barker GJ, Miller DH, Parker GJM, Brammer MJ, Bullmore ET, Giampietro VP, Thompson AJ. The structural and functional mechanisms of motor recovery: complementary use of diffusion tensor and functional magnetic resonance imaging in a traumatic injury of the internal capsule. J Neurol Neurosurg Psychiatry 1998; 65: 863-869.

Werring DJ, Clark CA, Miller DH, Thompson AJ, Barker GJ. A direct demonstration of both structure and function in the visual system: combining diffusion tensor imaging with functional magnetic resonance imaging. Neuroimage 1999; 9: 352-361.

Werring DJ, Clark CA, Barker GJ, Thompson AJ, Miller DH. Diffusion tensor imaging of lesions and normal appearing white matter in multiple sclerosis. Neurology 1999; 52: 1626-1632.

Werring DJ, Bullmore ET, Toosy AT, Miller DH, Barker GJ, MacManus DG, Brammer MJ, Giampietro VP, Brusa A, Brex PA, Moseley IF, Plant GT, McDonald WI, Thompson AJ. Recovery from optic neuritis is associated with a reorganisation of the cerebral response to visual stimulation. J Neurol Neurosurg Psychiatry 2000; 68: 441-9. (*see also*: "Brain may reorganise to compensate for damage caused by multiple sclerosis." Lancet 1999; 354: 1361; "Flexible thinking." Daily Telegraph Oct 28, 1999,p24.)

Werring DJ, Toosy AT, Clark CA, Parker GJM, Barker GJ, Miller DH, Thompson AJ. Diffusion tensor imaging can detect and quantify corticospinal tract degeneration after stroke J Neurol Neurosurg Psychiatry 2000; 69: 269-72.

Droogan AG, Clark CA, **Werring DJ**, Barker GJ, McDonald WI, Miller DH. Comparison of multiple sclerosis clinical subgroups using navigated spin-echo diffusion-weighted imaging. Magnetic Resonance Imaging 1999; 17: 653-661.

Werring DJ, Brassat D, Droogan AG, Clark CA, Symms MR, Barker GJ, MacManus DG, Thompson AJ, Miller DH. The pathogenesis of lesions and normal-appearing white matter changes in multiple sclerosis: a serial diffusion MRI study. Brain 2000; 123: 1667-76.

Clark CA, **Werring DJ**, Miller DH. Diffusion imaging of the spinal cord in vivo: estimation of the principle diffusivities and application to multiple sclerosis. Magn Reson Med 2000; 43: 133-8.

Parker GJM, Schnabel JA, Symms MR, **Werring DJ**, Barker GJ. Nonlinear smoothing for reduction of systematic and random errors in diffusion tensor imaging. J Magn Reson Imaging 2000; 11: 702-10.

Table of Contents

Page

Chapter 3. Mechanisms of recovery in demyelinating disease: fMRI studies in optic neuritis.

Page

Chapter 4. Mechanisms of central nervous system damage in multiple sclerosis and stroke: studies using MR diffusion imaging.

Page

Chapter 6. Conclusions

List of Figures

Chapter 3

Chapter 5

List of Tables

Chapter 1

Introduction to demyelinating diseases and the principles of magnetic resonance imaging

Introduction

In the last two decades, magnetic resonance imaging (MRI) has revolutionized clinical practice and research in neurology by its ability to probe, non-invasively, the physical and chemical properties of the central nervous system (CNS). MRI methods can visualize, quantify and monitor pathological changes *in vivo*, characterizing their effects on nervous tissue in detail. In multiple sclerosis (MS), a common and disabling condition defined by plaques of inflammatory demyelination in CNS white matter, the impact of MRI has been dramatic in understanding disease mechanisms and monitoring the effects of new treatments. This thesis is concerned with investigating the mechanisms of CNS damage and recovery in neurological diseases, particularly demyelinating conditions including MS. The methods used – namely, magnetic resonance (MR) diffusion imaging, and functional magnetic resonance imaging (fMRI) – offer new opportunities to study the mechanisms of pathological damage and its functional effects on surviving systems, respectively. In this chapter, introductory accounts of MS (the most prevalent demyelinating disease), and the basic principles of MRI, are presented. This information provides a foundation for subsequent descriptions of diffusion and functional MRI, and a brief overview of their clinical applications.

1.1 Multiple Sclerosis

Background

MS is a chronic, multifocal disease of the CNS in which demyelinating lesions are disseminated in space and time. It commonly presents in young adults, and has a profound impact upon individuals and society. The course of the disease is unpredictable, but progressive disability often occurs; community studies indicate that half of those affected will require help with walking after 15 years (Weinshenker et al., 1989). MS is the commonest cause of neurological disability in young adults in the Western world and has stimulated research for well over a hundred years.

The early stages of MS are characterized by reversible neurological deficits, but ultimately most patients enter a phase of progressive disability. A key challenge is to understand why this transition occurs, which in turn requires an understanding of the mechanisms of symptom remission and of fixed or progressive neurological deficit. These mechanisms underpin the work contained in this thesis. Although repair processes, including remyelination and remodeling of sodium channels along affected fibres contribute, clinical recovery can occur despite persistently abnormal conduction in affected pathways. Furthermore, there is increasing evidence that axons are damaged even at the earliest stages of the disease, when remissions are usual. Recovery despite persistent conduction block or axonal loss suggests that compensatory mechanisms must play a role. Continued structural damage, including irreversible demyelination and axonal loss, is likely to be an important factor in the irrecoverable deficit typical of the

later disease stages.

Charcot, who first recognized MS as a distinct clinico-pathological entity in the last three decades of the 19th century, was not hopeful of any possibility of treatment, stating: "...the time has not yet come when such a subject can seriously be considered." However, following recent clinical trials with immunomodulatory treatments including the interferons, the modification of the natural history of the disease (albeit to a limited degree) is now a real possibility. Ultimately, a fuller understanding of the mechanisms of deficit and recovery will provide opportunities to develop and monitor novel treatment strategies. The relatively new MRI techniques used in this thesis provide an invaluable opportunity to study the functional response of the brain to demyelinating lesions, and to investigate the structural substrates of progressive disability.

Aetiology

MS is thought to result from a complex interplay between genetic and environmental factors, which results in an immune-mediated inflammatory response that targets one or more structural components of white matter.

Genetic susceptibility

MS is a common disorder in Northern Europe, North America and Australasia, but much less common in the Orient, Africa and the Arabian peninsula; there are also gradients of prevalence within areas of high frequency. In Northern Europe, for example, the United Kingdom has a higher prevalence (in excess of 100 per

100,000) than France or Spain (approximately 20 per 100,000). Furthermore, the frequency of MS may differ considerably between areas that are geographically close but genetically diverse; these patterns are interpreted to indicate that racial susceptibility influences the geographical distribution of the disease.

Other lines of evidence suggesting a genetic influence include family studies showing higher risk in first or second degree relatives of probands (e.g. Sadovnick and Baird, 1988) and twin studies, indicating stronger concordance in monozygotic than in dizygotic twins (e.g. Mumford et al., 1994). However, the limited concordance in monozygotic twins and the unpredictable pattern of inheritance from pedigree studies argue against a purely genetic aetiology, whilst the rarity of conjugal pairs and low concordance in dizygotic twins do not favour the hypothesis of a transmissible environmental agent. Recent complete genome screens indicate that susceptibility to MS depends on the independent effects of several genes with small individual effects (Chataway et al., 1998). The biological relevance of the loci identified awaits further study, but may help to elucidate different pathogenetic mechanisms, resulting in indistinguishable phenotypes of clinically definite MS.

Environmental influences

The geographical distribution of MS cannot be explained by genetic susceptibility alone. The relatively low prevalence of MS in Australians of Northern European origin suggests that the environment of the Southern hemisphere is relatively protective (Hammond et al., 1988). Further evidence of an altered risk comes from first-generation descendents of black immigrants to the United Kingdom, who are

reported to have a prevalence approaching that of the white population (Elian and Dean, 1987). Studies of migration from regions of high to low risk have been influential. Dean (1967) showed that those migrating to South Africa from Northern Europe as adults retain the high risk of their country of origin, whereas those migrating in childhood acquire the low risk characteristic of native-born inhabitants. These data suggest that susceptibility to MS is conferred at some point during childhood.

The geographical clustering of cases of MS has naturally led to the speculation that an infective agent is important. Clusters have been described in the Faroe Islands, Iceland, Shetland Isles and the Orkneys, but the interpretation of these data remains controversial. The risk of MS appears to be increased in individuals who develop certain viral illnesses in late childhood, including measles, mumps, rubella and Epstein-Barr Virus (Compston et al., 1986); the importance of timing of exposure appears to indicate a narrow age range of susceptibility.

The available evidence suggests that environmental factors including a variety of viral pathogens interact upon a background of genetic susceptibility during late childhood, causing a change in immune system function that results in inflammatory damage to the CNS.

Clinical course, symptoms and diagnosis

Clinical course

The course of MS is unpredictable and variable, but some characteristic patterns of disease can be usefully identified. Most patients (approximately 85%) present with episodes that recover fully (Runmarker and Andersen, 1993), commonly with isolated, or mixed, sensory or motor symptoms. Further episodes then typically occur at unpredictable intervals for a variable period but with an average frequency of approximately 1.5 per year (*relapsing-remitting MS*). It is usual for these episodes to become less frequent with less complete remission. The disease becomes slowly progressive (*secondary progressive MS*) in approximately 50% of relapsing-remitting patients after 10 years (Runmarker and Andersen, 1993). Relapses may continue or cease during this progressive phase. A minority (10-15%) of patients has a progressive illness from onset without relapses (*primary progressive MS*); these patients tend to present in later life with a progressive paraparesis or, less commonly, a progressive hemiparesis or ataxia (Thompson et al., 1997). Another group has been defined as having minimal disability after 10 or more years of disease (*benign MS*), but this is a somewhat artificial distinction. Rarely, patients present with fulminant demyelination that can be rapidly fatal. The typical duration of disease from presentation has been estimated at over 25 years, with the majority of deaths not directly attributable to MS.

Clinical symptoms

The symptoms and signs of MS are as variable as its clinical course, but are generally consistent with the pattern of CNS demyelination; the most frequently and severely affected structures at post mortem are the optic nerves, cervical spinal cord, brainstem and cerebellum (Matthews, 1998). These sites are affected in most patients at some point during their illness. The common symptoms found in one community study of MS are listed in Table 1. It should be noted that whilst some symptoms have a clear anatomical substrate (for example, motor disability may reasonably be attributed to the involvement of cortico-spinal pathways), others, such as the common complaint of fatigue, do not have an obvious structural explanation. A variety of paroxysmal symptoms also occurs; these are typically short-lived and stereotyped in an individual patient. Paroxysmal symptoms include trigeminal neuralgia, dysarthria, ataxia and tonic spasms, and typically begin suddenly, followed usually by full remission over days to months.

Interestingly, the symptomatology of MS varies with geographical location; the most striking observation is the very high incidence of optic neuritis in oriental countries. In a comparison between British and Japanese patients, the onset of MS with monocular visual loss in the former group was 21%, compared to 48% in the Japanese patients (Shibasaki et al., 1981). Paroxysmal symptoms also seem to be more prevalent in Oriental patients.

Table 1.1. *Frequency of symptoms in MS (%). Adapted from Swingler and Compston, 1992.*

Symptom	At onset	Ever
Weakness	22	89
Sensory symptoms	34	87
Ataxia	11	82
Bladder symptoms	1	71
Fatigue	2	57
Diplopia	8	51
Visual symptoms	13	49

Diagnosis

The diagnosis of MS rests firmly upon the history and clinical examination findings, which often allow a diagnosis to be made with considerable confidence. However, confirmatory evidence from investigations (for example, visual evoked potentials or MRI) may be sought, particularly if disease-modifying treatments are to be considered. In conducting research, it is also important to define precisely the population of patients studied. A number of diagnostic classifications have been proposed, but there is wide acceptance of the criteria proposed by the Poser committee (Poser et al., 1983). The essential criteria are the demonstration of lesions disseminated in time and space, age 10-59 years at onset, with no better explanation of symptoms assessed by a competent neurologist. Data from evoked potentials, neuroimaging and laboratory analysis of CSF are also included.

Application of the Poser criteria allows a patient to be classified as either definite or probable MS, with each group further subdivided into clinical and laboratory supported categories (Table 2). More recently, criteria for the diagnosis of primary progressive MS have been presented (Thompson et al., 1999). The power of magnetic resonance imaging (MRI) to detect disease activity in MS may lead to its increasing incorporation into future diagnostic criteria.

Table 1.2. *Poser committee criteria (Poser et al., 1983)*

Category	Relapses	Sites of CNS clinically involved		Paraclinical evidence of CNS abnormality	CSF oligoclonal bands
Clinically definite	2	2			
	2	1	*and*	1	
Clinically probable	2	1			
	1	2			
	1	1	*and*	1	
Laboratory supported definite	2	1	*or*	1	+
	1	2			+
Laboratory supported probable	1	1	*and*	1	+
	2				+

Pathology

The most characteristic pathological feature of MS is the demyelinated plaque: a focal area of inflammation associated with the destruction of myelin sheaths. The first macroscopic depictions of these lesions as discoloured, indurated areas of white matter were by Carswell (1838). Plaques vary in size from millimetres to centimetres and show a predilection for the optic nerves, cervical spinal cord and periventricular regions. Cortical plaques are also well recognized (Brownell and Hughes, 1962; Kidd et al., 1998). The histopathological characteristics of MS lesions - demyelination, relative preservation of axon cylinders, gliosis and inflammation – were well described in the last century (Charcot, 1868); it was also appreciated early on that plaques were invariably centred around a blood vessel. The pathological features in MS lesions have been reviewed by Lassman (1998).

A number of histopathological features suggest disease activity within a lesion. Some plaques display features of inflammation, with perivascular monocyte cuffing and lymphocytic infiltration of the demyelinated area. Larger lesions may have a peripheral zone of inflammatory cells and myelin breakdown products (Lumsden, 1970). Inflammatory activity in lesions may be associated with oedema (McDonald et al., 1992). Recent myelin breakdown is indicated by the presence of neutral fat particles and numerous lipid-laden macrophages.

Chronic lesions that do not exhibit inflammatory activity or evidence of myelin degradation have been classified as two distinct types (Barnes et al., 1991): these are the "closed" lesions containing intact axons and extensive glial proliferation; and the "open" lesions in which axonal loss is extensive and gliosis sparser, causing an expanded extracellular space. Transitional forms showing

intermediate characteristics are also commonly seen.

The heterogeneity of pathological findings in MS lesions may reflect different pathogenetic mechanisms in different patients. A study of a large number of post-mortem cases (Luchinetti et al., 1999) has emphasized the variation of the topology and extent of oligodendrocyte damage in active lesions, with differential patterns of loss of myelin, mature or progenitor oligodendrocytes observed in different clinical subsets of MS patients. These observations could reflect genetic heterogeneity, and may have important implications for the targeting of therapeutic strategies.

Although classical studies established destruction of myelin with *relative preservation* of axons as the pathological signature of MS, loss of axons occurs in practically all lesions and may be extensive (Charcot 1868, Adams and Kubik 1952, Lassmann et al., 1994). Recent work has refocused interest upon axonal damage (Ferguson et al., 1997; Trapp et al., 1998), which has been observed in lesions at the earliest disease stages (Trapp et al., 1998). These findings are relevant in understanding recovery mechanisms (see section on Pathophysiology, below).

Remyelination is often observed, but its extent varies with the stage of disease. In early MS (for example during the first or second clinical episode), many oligodendrocytes are often present within demyelinated lesions, which may facilitate the extensive remyelination observed (Lassman et al., 1983, Bruck et al., 1994). However, in plaques studied later in the disease, remyelination is usually limited to the periphery of the lesions and the resulting myelin is abnormally thin and incomplete (Prineas and Connell, 1979). Gliosis is seen in all MS plaques, but may be particularly dense in chronic lesions.

The macroscopically normal white matter (or normal-appearing white matter, NAWM) has attracted less attention than the plaques of MS. However, histopathological and quantitative MRI studies indicate that pathological damage occurs to the NAWM. Diffuse astrocytic gliosis, lyphocytic infiltration and biochemical abnormalities in lysosomal enzymes have been reported (Allen et al., 1979; Newcombe et al., 1980); and NAWM contains a higher proportion of water than healthy tissue (Tourtellotte et al., 1968). A recent study has demonstrated extensive axonal loss in the NAWM of the corpus callosum in MS (Evangelou et al., 2000).

Pathophysiology

A complete account of the pathophysiology of MS (i.e. the mechanisms underlying the clinical expression of the disease) should explain the following features: firstly, the variety of symptoms, including both negative phenomena (e.g. paresis and sensory loss) and positive phenomena (e.g. paroxysmal symptoms); secondly, the initial recovery from relapses and progressive deficit in the later stages; and thirdly, the poor correlation between plaque size and location and the severity of clinical impairment. In the following brief account these aspects will be discussed

Conduction disturbances

Intact myelinated fibres are capable of saltatory conduction, allowing the faithful transmission of rapid trains of impulses in individual axons. Damage to myelin

may have several effects including complete conduction block or slowing, fibre hyperexcitability, and cross-talk between neighbouring axons.

Conduction block. Direct experimental evidence for abrupt conduction failure (conduction block) due to demyelination was first obtained by recording from the dorsal root ganglia of cats demyelinated by the systemic administration of diphtheria toxin (McDonald, 1963). The same phenomenon was later shown in a CNS (spinal cord) model (McDonald and Sears, 1970). In man, evidence for conduction block can be obtained noninvasively by recording visual evoked potentials (VEPs) (Halliday et al., 1972). VEPs are recorded during monocular visual stimulation (often a reversing black-and-white checker-board pattern), providing an estimate of the timing and magnitude of the afferent volley reaching the cortex.

The role of conduction block in symptom production is clearly demonstrated by the correlation between conduction block and clinical deficits (Youl et al., 1991). In acute optic neuritis, complete conduction block in all fibres in the optic nerve results in an absent or reduced amplitude cortical potential, and coincides with near complete visual loss. As vision recovers, a well-formed but delayed evoked potential reappears. Reduced visual evoked potential amplitude without delay suggests conduction block in a proportion of fibres, though dispersal of response due to asynchronous delays in different fibres may also contribute.

Demyelination is not the only mechanism invoked to explain conduction block. A role for inflammation has been suggested by a strong relationship between contrast enhancement on optic nerve MRI following the administration of gadolinium-diethylenetriamine pentaacetic acid (Gd-DTPA) (indicating

inflammatory leakage of the blood-brain barrier; see later in this chapter), and reduced evoked potential amplitude (implying conduction block) (Youl et al., 1991). The mechanisms by which inflammation may influence conduction are not known. A heat-labile serum "synaptic blocking factor" has been identified in animals with experimental allergic encephalomyelitis (EAE), an experimental model of inflammatory demyelination, as well as in patients with MS (Seil, 1977), but its structure and role remain undefined. More recently a number of inflammatory mediators (cytokines), including interleukin 2 (Gallo et al., 1988), interleukin 6 (Weller et al., 1991), interleukin 1β and tumour necrosis factor (TNF) (Tsukada et al., 1991) have been found in the CSF of patients with acute MS, whilst interleukin 1 and tumour necrosis factor have been demonstrated in plaques (Cannella and Raine, 1995). Immunologically active molecules can alter the conduction properties of neurons (Koller et al., 1996): indeed, a clinical deterioration has been observed in patients treated with campath-1H, which is associated with an increase in circulating TNFα (Moreau et al., 1996). Nitric oxide has recently been shown to induce a reversible conduction block (with demyelinated fibres being particularly susceptible) at physiological concentrations (Redford et al., 1997), and is found at increased concentrations in the CSF of MS patients (Giovannoni, 1998). The role of oedema in the origin of conduction block is not known, but could conceivably play a role, particularly in the optic nerve which is tightly encased in a narrow bony canal and may be subject to compressive injury.

Intermittent conduction block may also result from demyelination, causing an inability of affected fibres to conduct trains of impulses faithfully at physiological frequencies (McDonald and Sears, 1970). This is due to an increased

refractory period in fibres traversing the lesion. Failure of transmission thus occurs at lower impulse frequencies than in intact fibres, and has been shown to correlate with peripheral sensory disturbance in MS (Sclabassi et al., 1974). Sustained trains of impulses are necessary for effective muscle contraction; intermittent conduction block may therefore contribute to paresis in MS.

The refractory period is known to increase with temperature, and when a certain point is reached complete block occurs even in intact fibres. In demyelinated fibres, the temperature at which conduction block occurs is reduced (Davis and Jacobson, 1971). This provides a rational explanation for the exacerbation of symptoms in MS by a hot bath or exercise (Uhtoff's phenomenon), and correlates with neurological impairment. Impaired vision following exercise is associated with reduced visual evoked potential amplitude, indicating conduction block (Persson and Sachs, 1981).

Conduction Slowing. Demyelination is associated with a reduction in the maximum velocity of conduction (McDonald, 1961); the degree of slowing is related to the degree of demyelination (McDonald, 1963). Evidence for conduction slowing was first obtained in man using VEPs in acute optic neuritis (Halliday et al., 1972); the delay in the cortical potential may be considerable (on average about 30 milliseconds). Although the cortical potential depends on conduction in central visual pathways in addition to the optic nerve, the consistent association of demyelinating optic neuritis with a delayed but preserved waveform suggests that optic nerve demyelination is the most important mechanism of slowing.

Increased excitability of demyelinated axons. Damage to myelin makes fibres more excitable. This has been demonstrated in a study of experimental demyelination of the posterior columns (Smith and McDonald, 1982). Prolonged continuous regular discharges were often observed either spontaneously or due to very slight mechanical deformations. These phenomena in sensory pathways may account for some characteristic symptoms often reported in MS; for example the paraesthesiae induced by neck flexion (Lhermitte's symptom); the phosphenes induced by eye movement following optic neuritis; and facial myokymia. Recent work suggests that internodal potassium currents can become hyperexcitable in regions of demyelination; this may be one mechanism of hyperexcitability and ectopic discharge (Chiu et al., 1981). Electrical cross-talk between fibres has long been known to be associated with demyelination (Katz and Schmitt, 1940), and has been suggested to be responsible for some paroxysmal symptoms in MS, including tonic spasms and paroxysmal dysarthria.

Mechanisms of Recovery

A striking feature of MS in the early disease stages is the complete recovery from individual relapses. At least three mechanisms may contribute. Firstly, function may be restored in the damaged fibres; secondly, surviving pathways may adapt to compensate for the damage; and thirdly, intact fibres may suffer a transient, reversible functional disturbance due to humoral or inflammatory factors.

We have seen that abnormal conduction in demyelinated fibres may explain many of the symptoms commonly seen in MS. It is therefore reasonable to suppose that restoration of conduction contributes to recovery from symptoms.

There are two possible mechanisms: either persistently demyelinated axons may recover the ability to conduct electrical impulses, or damaged fibres may be remyelinated.

Restoration of conduction in demyelinated fibres. There is evidence that conduction can be restored in demyelinated nerve fibres in the peripheral nervous system (PNS) (Rasminsky et al., 1978), but there is less evidence that it occurs in the CNS. Felts et al. (1997) have, however shown that a labelled demyelinated fibre (in an experimental mammalian spinal preparation) can conduct impulses. Evidence is also provided from a patient with bilateral optic neuritis who had documented visual function four days prior to death from a massive pulmonary embolus (McDonald et al., 1976). At post-mortem both optic nerves were found to be completely demyelinated over several centimetres; in the absence of alternative pathways, conduction along the optic nerves must therefore have been occurring. One important contributory mechanism is likely to be the insertion of sodium channels into demyelinated segments (Moll et al., 1991). Increased numbers of sodium channels along demyelinated fibres have been shown in the PNS (England et al., 1990) and CNS (Black et al., 1991). In mice, little functional deficit is observed when increased numbers of sodium channels are present along the demyelinated axons (Rivera-Quinones et al., 1998). Interestingly, in the PNS at least, small diameter demyelinated fibres can more readily recover the ability to conduct than larger fibres. This may explain the frequent remission observed following optic nerve or corticospinal tract demyelination in MS, since in both of these pathways most fibres are smaller than four microns in diameter.

Remyelination. Experimental studies have confirmed that remyelination in the CNS restores conduction (Smith et al., 1981). The time course of conduction recovery closely parallels that of remyelination, suggesting that remyelination may be a contributory factor. Indirect evidence for remyelination in man is provided by the return to normal of the VEP latency following optic neuritis in some adults and, more commonly, in children (Kriss et al., 1988). However, the contribution made by remyelination to functional recovery in this setting is unclear since rapid recovery often occurs from optic neuritis despite persistent evoked potential delay.

Recovery following axonal degeneration. Some axons are lost in lesions at the earliest stages of MS, when complete remissions are usual (Trapp et al., 1998). This suggests that functional recovery can occur despite irreversible axonal loss in affected pathways. More direct evidence is provided by the excellent visual recovery following optic neuritis, even with considerable retinal fibre layer loss (a measure of axonal density in the optic nerve) and marked optic atrophy (MacFayden, 1988; Steel and Waldeck, 1998). This observation suggests that compensatory processes in the cerebral cortex may contribute to the recovery of vision when the pattern of sensory input to the brain is irreversibly disrupted.

Experimental studies also suggest that adaptive mechanisms contribute to the recovery from demyelinating lesions in eloquent pathways. McDonald (1963) studied animals recovering from sensory ataxia due to experimental demyelination in the sacral afferent nerve roots. In those with only minimal residual functional impairment there was persistent histological evidence of demyelination, and electrophysiological evidence of reduced compound action potential amplitude and delay. The return of normal proprioceptive input cannot therefore have been

the explanation for clinical recovery. These data indicate that recovery depended on adaptive changes in surviving CNS networks that allowed the persistently abnormal input to be interpreted effectively.

In the visual system, Jacobson et al. (1979) studied the recovery of visual function in cats with experimentally induced degenerative lesions in the intracranial optic nerve. Visual function was quantified by the ability to recognize stripes of different degrees of contrast (contrast sensitivity) and spatial frequencies. Following training, the lesion was made and the recovery of function was monitored. An initial rapid recovery was seen in parallel with a considerable resolution of optic nerve oedema. A less rapid recovery of the ability to recognize the thinner stripes was demonstrated over several months. Histological analysis showed that this recovery could occur even when up to 77% of optic nerve fibres were destroyed. In the absence of any known alternative anterior visual pathways these results suggest that adaptive changes in the brain must contribute to visual recovery after optic nerve damage. The possible role of cortical adaptation in recovery from demyelination in humans has not been widely studied, in part due to a lack of available techniques to investigate brain function, but also because of the considerable methodological difficulties in applying them to a multifocal, variable and often progressive disease like MS.

Mechanisms of persistent deficit

In the later stages of MS, irrecoverable deficit is usual. At least two types of mechanism can be suggested: firstly, repair and compensatory processes may begin to fail as the disease progresses; and secondly, continued axon loss may

occur. The first suggestion remains largely speculative and has not been widely investigated. However, there is now good evidence that axonal loss plays an important role in the development of persistent disability.

The measurement of the volume of a structure in the CNS provides evidence for a loss of tissue that is likely to, at least in part, result from axonal loss. Loss of volume (atrophy) of the cervical spinal cord correlates strongly with clinical disability measured by the expanded disability status scale (EDSS) described by Kurtzke (Kurtzke 1983) (Kidd et al., 1996, Losseff et al., 1996a). Furthermore, an increase in atrophy has been demonstrated over a one year period in progressive patients (Stevenson et al., 1998). Similarly, cerebral atrophy is correlated with functional deficit and progresses over time (Losseff et al., 1996b). Interestingly, atrophy appears to be seen even in the early stages of MS (Rudick et al., 1999).

Atrophy may result from the destruction of myelin or glial cells in addition to axonal loss. A putative, more specific, marker for neuronal integrity and function is N-acetyl aspartate (NAA), an amino acid that is found only in neurons in the adult brain and which can be detected non-invasively by magnetic resonance spectroscopy. In dominant cerebellar atrophy, a condition known to result from loss of axons, the concentration of NAA in the cerebellum is reduced (Davie et al., 1995). In MS patients with prominent ataxia, there are similar reductions in cerebellar NAA and cerebellar volume (Davie et al., 1995), which are not seen in MS patients without ataxia. A widespread reduction of NAA has also been shown in the macroscopically normal or normal-appearing white matter in MS patients (Davie et al., 1994, Husted et al., 1994). Changes in NAWM NAA concentration have been reported to correlate with accumulated disability, lending further weight

to the hypothesis that axonal loss contributes to this outcome (Fu et al., 1998).

Although there is strong evidence for axonal loss at all stages of MS, the pathogenetic mechanisms are not fully understood. Axons are certainly damaged in focal lesions, and this appears to be closely related to inflammatory activity; demyelinated axons seem to be particularly vulnerable to attack by a variety of inflammatory molecules present in plaques (Trapp et al., 1999). There is also evidence that chronic demyelination in lesions, in the absence of active inflammation, can cause axonal loss (Trapp et al., 1998). The latter process could account for a progressive, irreversible loss of axons in the later stages of MS. An important outstanding question is whether axonal loss can occur independently of focal inflammatory demyelination. That this may occur is suggested by the progressive disability – presumably due to axonal loss – that is seen in primary progressive MS, in which there are relatively few episodes of focal lesion activity compared to other subgroups. One proposed mechanism is of a primary immune attack on axons, which has been demonstrated in acute motor axonal neuropathy (McKhann et al., 1993); whether this or similar mechanisms play a role in the progression of MS is not known.

Clinical expression and silence

Since the studies of Charcot (1868), it has been shown that there is a broad correspondence between the presence of lesions and symptoms and signs consistent with their anatomical location. We have seen that the locations that are most severely demyelinated (the optic nerves, cerebellum and cervical spinal cord) are generally consistent with the common clinical symptoms seen in MS.

However, post mortem and more recently MRI studies (see later in this chapter) emphasize that the relationship between detectable nervous tissue damage and symptoms may be complex. Ghatak et al. (1974) reported the presence at post mortem of a large demyelinating spinal cord lesion in a patient with no symptoms in life. Namerow and Thompson (1969) described a patient who died of an overdose five years after developing MS, who had a number of lesions at post mortem which had been asymptomatic. Although the posterior columns of the spinal cord were extensively demyelinated, examination shortly before death had revealed only minimal impairment of the sensory modalities subserved by these tracts (joint position and vibration sense). Similarly, corticospinal fibres were demyelinated across several cervical segments, but no abnormal clinical signs were elicited in the upper limbs. There are also reports of normal visual function despite extensive optic nerve demyelination (Ulrich and Groebke-Lorenz, 1976; McDonald, 1976). It is well known that patients in the very earliest disease stages (or who have had a single episode suggestive of demyelination) often have evidence of extensive periventricular lesions on MRI, but with little recognisable clinical deficit.

How can the lesions of MS be clinically silent? Plaques in the periventricular regions may not cause symptoms because they are located in clinically "non eloquent" areas and do not interrupt important white matter fibre tracts unless they are very large. [It should be noted, however, that periventricular lesion volume on MRI has been shown to correlate with cognitive impairment (Ron et al., 1991)]. This cannot be the explanation for lesions in eloquent pathways such as the spinal cord or optic nerve. One possibility is that only a proportion of the fibres are damaged by the demyelinating lesion, allowing

compensatory reorganization in surviving pathways. There is evidence from a PET study of patient who sustained a traumatic spinal cord transection sparing only a part of one anterolateral quadrant and yet retained good posterior column sensory function (Danziger et al., 1996), that cortical adaptation may occur even when a high proportion of eloquent fibres are damaged. Cortical reorganization has also been demonstrated following recovery from damage to subcortical motor tracts due to stroke (Weiller et al., 1992). The potential role of adaptive (or "plastic") cortical changes in neurological recovery is discussed in further detail in chapters 3 and 4. Another possibility is that there is a discrepancy between the apparent structural damage and the functional disturbance upon conduction; some of the mechanisms of restoration of conduction in demyelinated fibres (including remodelling of sodium channels) may have no histological or MRI counterparts.

1.2 Magnetic Resonance Imaging

Physical description of nuclear magnetic resonance

MRI is a non-invasive technique that can be used to create pictures of the soft tissues of the human body. It involves no ionizing radiation (unlike x-rays and other radiological methods) making it safe for repeated investigations. The spatial resolution of MRI is potentially very high, and it may be made sensitive to a number of tissue properties including some that vary with the haemodynamic consequences of neural activity (see later section on functional MRI). These characteristics make MRI an important technique in clinical neurology and neuroscience.

MRI is based on the phenomenon of nuclear magnetic resonance (NMR). The NMR phenomenon can be summarized as the application of a pulse of radiofrequency energy to a sample, in the presence of a magnetic field, followed by the collection of radiofrequency signal emitted by the sample. NMR depends on the interactions that occur when certain atomic nuclei are placed in an external magnetic field. Specifically, nuclei with an odd number of nucleons (i.e. protons + neutrons = odd integer) have the special property of "spin". Since they are also charged, these spinning nuclei will create a magnetic field; each nucleus behaves like a magnetic dipole with a magnetic moment. For the purposes of this thesis we are concerned solely with the particular case of the hydrogen nucleus (proton) which is abundant in biological tissues, usually in the form of water. Each spinning proton may be visually represented as a vector showing the direction of its magnetic moment (Fig. 1.1).

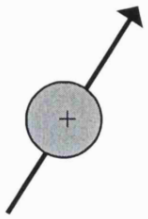

Fig. 1.1. Magnetic moment. Protons are charged particles, which have the property of spin and possess their own magnetic moment, which may be represented by a vector.

Consider what happens when an object is placed in an MRI scanner, essentially a powerful (usually superconducting) magnet; in clinical scanners the magnetic field is commonly of 1.5 Tesla strength and oriented horizontally. (For comparison the earth's magnetic field is approximately 5×10^{-5} Tesla). Protons in a sample, when placed in this strong external magnetic field (conventionally designated B_0), will align themselves in one of two ways (parallel or anti-parallel). Since these two states have different energy levels, a majority of the protons will adopt the lower energy (parallel) state. This excess of parallel oriented protons means that the subject in the scanner is magnetized with a small net magnetic moment, M_0 (Fig. 1.2). This magnetic moment is also termed longitudinal magnetization, and is directly proportional to B_0.

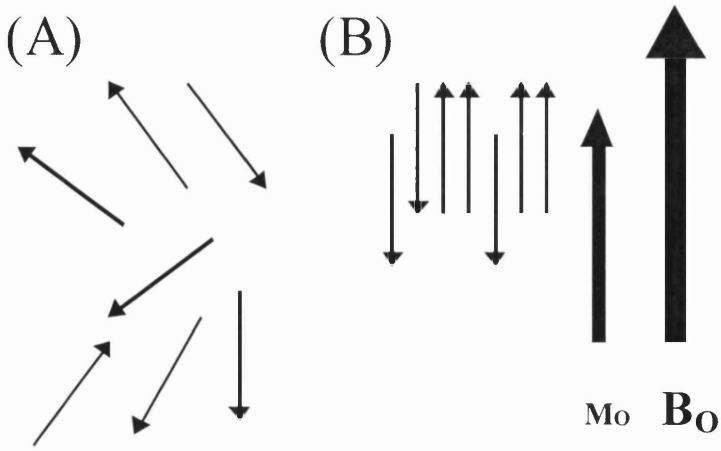

Fig. 1.2. Alignment of protons in an external magnetic field. (A) Proton magnetic moments ("spins") are normally oriented randomly. (B) When placed in an external field (B_0) they become aligned in parallel or anti-parallel states, causing them to acquire a net magnetic moment, M_0.

When protons are placed in a magnetic field they exhibit a type of motion called *precession*. This motion can be conceptualized as the vector representing the magnetic dipole describing the shape of a cone (Fig. 1.3).

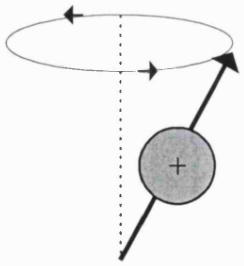

Fig. 1.3. Precession of a proton in an external magnetic field.

The precession frequency depends on the strength of the applied magnetic field and the molecular species under consideration, and is given by the Larmor equation:

$$\omega = \gamma B_0$$

where ω is the angular precession frequency (radians s^{-1}), γ is the gyromagnetic ratio (which is different for different materials), and B_0 is the strength of the applied field (T).

If a short duration oscillating magnetic field of the correct frequency is applied perpendicular to B_0, energy is exchanged with the protons and they are induced to resonate. The frequency required is directly related to the precession (Larmor) frequency which for protons in a 1.5T magnetic field is approximately 64 MHz; this falls in the radiofrequency band of the electromagnetic spectrum, so that the applied field is generally referred to as a radiofrequency (RF) pulse. The application of a RF pulse has two effects on precessing protons: firstly, some will gain energy and become realigned in the higher energy antiparallel state; and secondly the protons will begin to precess in a more coherent way (i.e. they precess in phase) (Fig. 1.4). The former effect causes a reduction in the longitudinal magnetization of the sample (because the excess of parallel oriented protons has reduced). The latter effect causes the sample to acquire a transverse oriented magnetic moment (which is rotatory due to the in-phase precession of the protons).

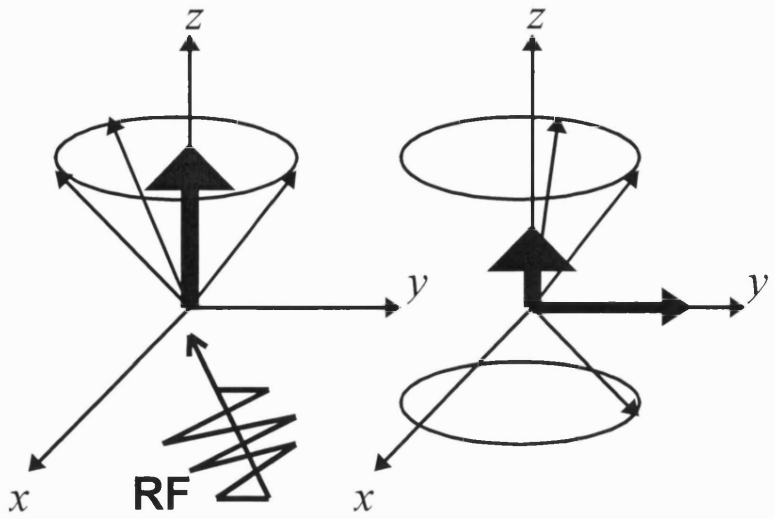

Fig. 1.4. Effect of a radiofrequency pulse. When an RF pulse is applied at the appropriate frequency (*left)* protons lose longitudinal magnetization and gain transverse magnetization (*right).*

In this process, known as *nutation* the protons are effectively 'tipped' from their previously longitudinal alignment by an angle, α. If this angle is 90° then the RF pulse is commonly termed a "90 degree pulse." The greater the amplitude and duration of the RF pulse, the larger the nutation angle. The transverse magnetization induced following the RF pulse forms the signal from which all NMR measurements are made. Because transverse magnetization is effectively an oscillating magnetic field (Fig. 1.5), it can induce an electrical current in an appropriately placed receiver coil; the way in which this detected signal changes when the RF pulse is switched off is the starting point for creating an MR image.

When the RF pulse stops, the protons will return to their equilibrium position, in alignment with the external magnetic field. This process is called *relaxation.* The longitudinal magnetization will increase back to its original size, M_0, and the newly acquired transverse magnetization will dephase due to slight

differences in the precession rates of individual protons (Fig. 1.5).

The former process is termed longitudinal relaxation and is described by a time constant, T1; the latter is termed transverse relaxation and is described by a second time constant, T2. Longitudinal relaxation takes much longer than transverse relaxation (dephasing is a very rapid process). T1 in brain tissues is usually of the order of hundreds of milliseconds, T2 of the order of tens to hundreds of milliseconds.

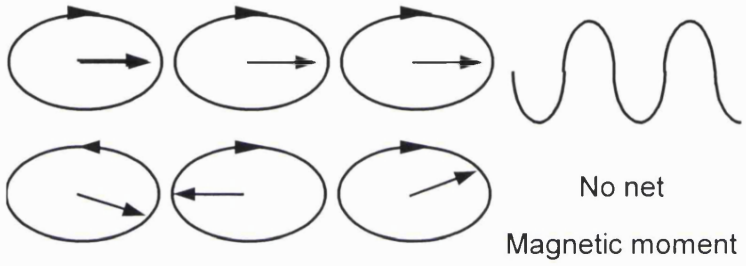

Fig. 1.5. Only when protons precess in phase *(top row)* do they create a net oscillating magnetic field that can induce a signal in a receiver coil.

Longitudinal relaxation occurs because, in the absence of the RF pulse, the protons will naturally return to the state of lowest energy, in alignment with B_0 with an excess of parallel oriented protons. The extra energy that the protons possessed in the excited state is dissipated to their surroundings (the *lattice*) so this relaxation is also referred to as *spin-lattice relaxation.* Transverse relaxation occurs because each proton experiences a slightly different magnetic field (due to inhomogeneities in the B_0 field and to interactions with surrounding protons), causing each one to naturally precess at a different frequency. The net result is that when the RF pulse is switched off, protons lose their phase coherence and the

transverse magnetization decays. Because this process depends on interactions between spinning protons it is also known as *spin-spin relaxation.* If efforts are made to minimize the external field inhomogeneities (see below) then transverse relaxation is described by the constant T2; if inhomogeneities are present then the dephasing will be more rapid, and the process is described by a shorter constant termed T2* ("T2 star").

Classical MRI depends on the fact that the relaxation properties of protons depend on the physico-chemical environment, which is different in different tissue types, and is affected by pathological changes. Some protons are tightly bound within large molecules such as lipids, proteins or carbohydrates and thus lose their magnetization very quickly to surrounding molecules (i.e. they have very short relaxation constants). This means that they are not "seen" on conventional scans. It is the unbound or "free" water protons (with a relatively long T2), both intracellular and extracellular, that make the most important contribution to MRI.

Simple spin echo experiment

The most common pulse sequence is the spin echo sequence, which can be used to image tissues with different T1 and T2 relaxation properties. This results in *T1-weighted* or *T2-weighted* images, that is images in which the contrast depends mainly on the T1 or T2 of tissues respectively. It is important to understand the principles of this type of NMR experiment before considering other methods of generating image contrast.

Firstly, a 90° RF pulse is applied to tip the protons in the sample into the xy plane. This generates an oscillating transverse magnetization component which

is able to induce a signal in a receiver coil, but this is rapidly lost due to dephasing as a result of T2* decay. A second radiofrequency pulse is then applied that allows the lost phase coherence to be retrieved. This pulse tips the protons by 180° in the transverse plane. This has the effect of speeding up the protons that are precessing more slowly, allowing them to "catch up" with the faster precessing ones (Fig. 1.6). This makes the protons once more (briefly) precess coherently so that they generate an oscillating magnetic field, detectable by a receiver. The 180° pulse is also known as a *refocusing* pulse. This rephasing of protons and detection of the signal is often termed the *echo* or *echo collection.*

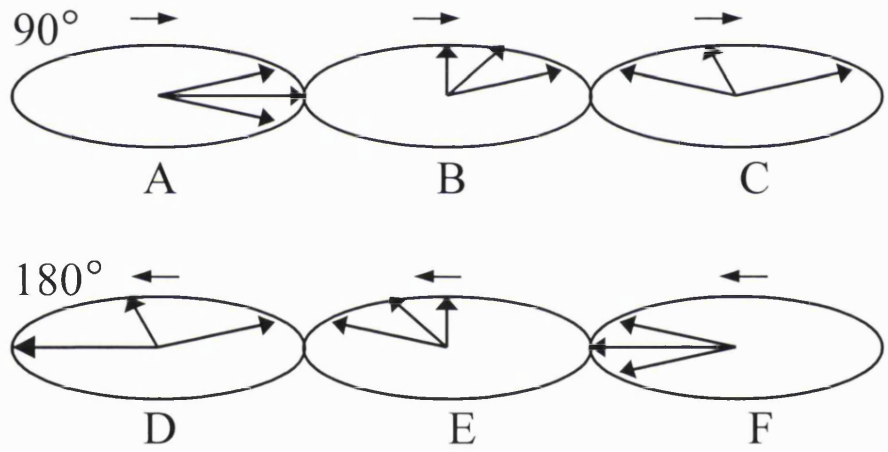

Fig. 1.6. Effect of 180°pulse. After the RF pulse is switched off the protons dephase (A, B, C; *top*). The 180° pulse reverses their precession directions, restoring phase coherence (D, E, F; *bottom*).

The time between the 90° pulse and the collection of the spin echo is termed TE (time to echo). The experiment must be repeated many times to create an image; the time between successive 90° pulses is the TR (time to repeat). The spin echo sequence may be depicted by a pulse sequence diagram:

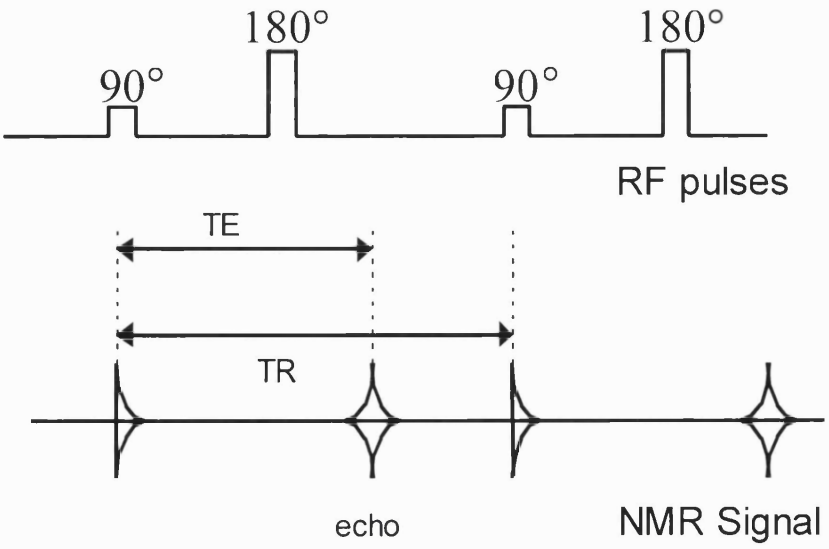

Fig. 1.7. Pulse sequence diagram for a simple spin echo NMR experiment.

By varying the TE and TR of a spin echo experiment, the type of contrast in the resulting image can be manipulated. If a long TE is used, at the time of echo collection protons with a short T_2 will have dephased, whereas those with a longer T_2 (relative to the TE) will not. This results in a strongly T_2-weighted image in which tissues with a short T_2 return little NMR signal (and appear dark) whilst those with a longer T_2 return a high signal and appear bright. If a T1-weighted image is required, a short TR is chosen. This means that tissues with long T_1 will not have had time to regain their equilibrium longitudinal magnetization following a particular echo, and will give a smaller NMR signal following their next excitation. This allows tissues of short T_1 to be distinguished from those of long T_1; if the T_1 is short, the signal will be high (bright on the image); if T_1 is long, the signal will be low (dark on the image). A long TR with a short TE results in an image that has neither strong T_1 nor T_2 weighting, but depends largely on the concentration (density) of free protons. This results in a *proton density weighted* image.

The T_1 and T_2 properties of protons tend to vary together. In biological tissues, T_1 is usually of the order 300 to 2000ms, T_2 of the order 30 to 150ms. Where protons are very mobile in tissue they take longer to relax, so that cerebrospinal fluid (CSF) has a long T_1 and a long T_2. More structured tissues contain protons that are less mobile and readily exchange energy with their surroundings, so that protein, lipid and other macromolecules have a short T_1 and a short T_2. Pathology generally (but not exclusively) increases the mobility of protons in tissue, in association with increased water content, so lengthens the T_1 and T_2 of healthy tissues.

Making an image

Although the principles of NMR were first described in the 1940s by Bloch and Purcell, culminating in their being awarded the Nobel Prize for physics in 1952, the use of this phenomenon to create images was first suggested only relatively recently, by Paul Lauterbur in 1973. In order to create a meaningful image, the different NMR signals from different parts of the sample being studied must be distinguished, and ultimately displayed. This is accomplished using magnetic field gradients that are applied briefly during the imaging sequence along the three orthogonal axes of the scanner magnet coordinate system. These gradients are designated the slice selection (z axis), frequency encoding (x axis) and phase encoding (y axis) gradients, for reasons that will become clear. These magnetic gradients can induce protons in different positions along them to have different precession frequencies.

The slice-select gradient, as its name suggests, allows a slice of tissue to be

selectively excited, depending on the range of frequencies (or band width) of the RF pulse applied. This is because the Larmor frequency of protons at different positions along the gradient will be different (Fig. 1.8), and only some of them will match that of the RF pulse.

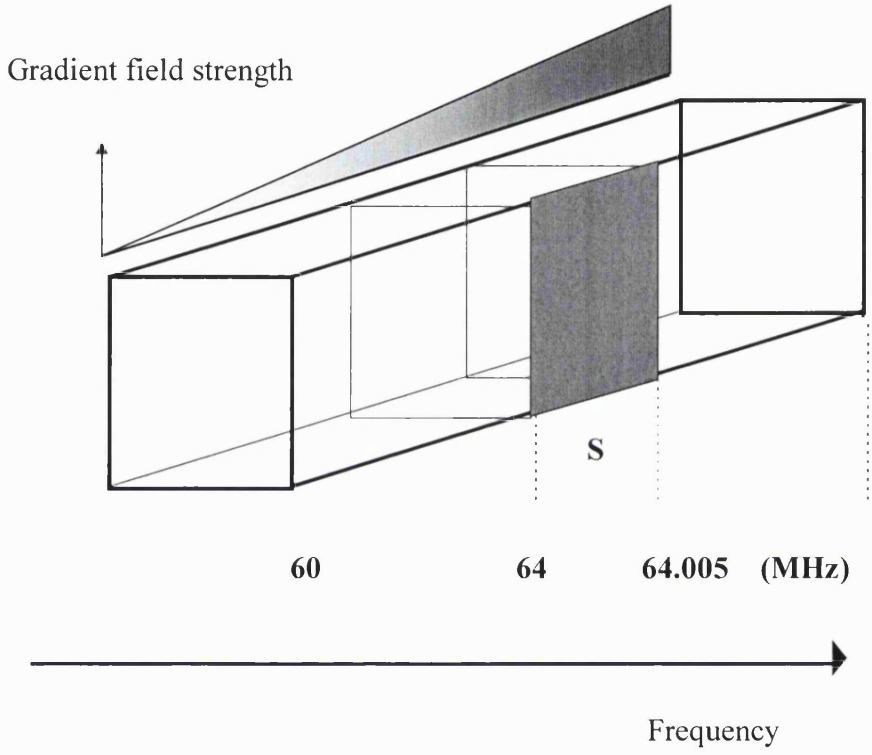

Fig. 1.8. Slice selection. A slice-select gradient is superimposed upon the main B_0 field in the z direction so that protons at different positions along the sample have different resonant frequencies. A 'slice' of the sample can then be excited by applying an RF pulse of a specific frequency range (or bandwidth); in the example a pulse of 64 to 64.005 MHz excites a slice of thickness S.

After the slice-select gradient has been switched off, the protons in the slice will all be precessing in phase at the same frequency, forming an echo that can induce a signal in a receiver coil. To determine the point on the slice from which a given signal arises, the two other gradients (frequency- and phase-encoding gradients) are used to alter the signal so that it contains the information needed to localize protons within different voxels in the slice.

The frequency-encoding gradient is applied after the slice-selecting gradient in the x axis direction, resulting in different precession frequencies along this axis (Fig. 1.9).

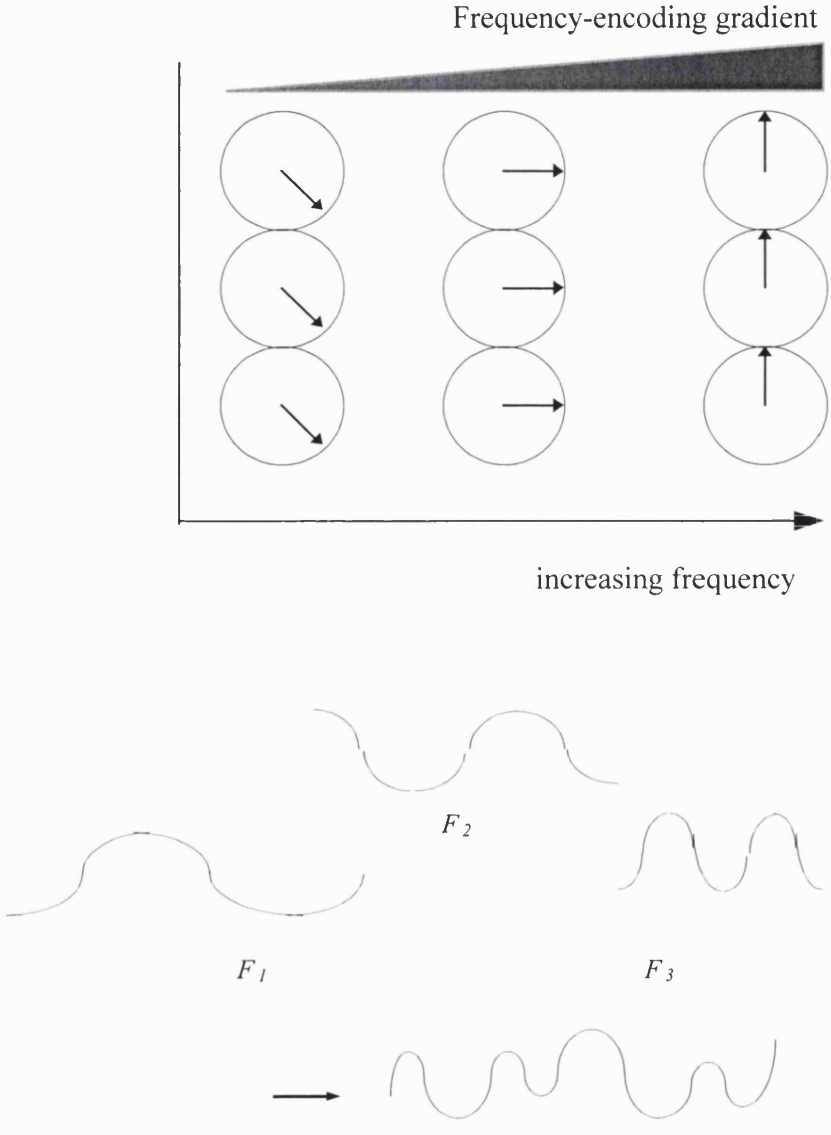

Fig. 1.9. Frequency encoding. A gradient is applied in the x direction (left to right) causing protons at different locations along the x axis to precess at different frequencies. The emitted NMR signal is made up of these frequency components (F_1, F_2 and F_3 in this illustration).

Each of the resulting signals of different frequencies will contribute to the net NMR signal emitted by the slice. The different frequency signals from protons at different positions along the x coordinate are calculated by a *Fourier transformation.* Stated briefly, Fourier transform theory shows that any complex signal can be modelled by combining a (possibly infinite) series of sine waves at different frequencies (Fig. 1.10).

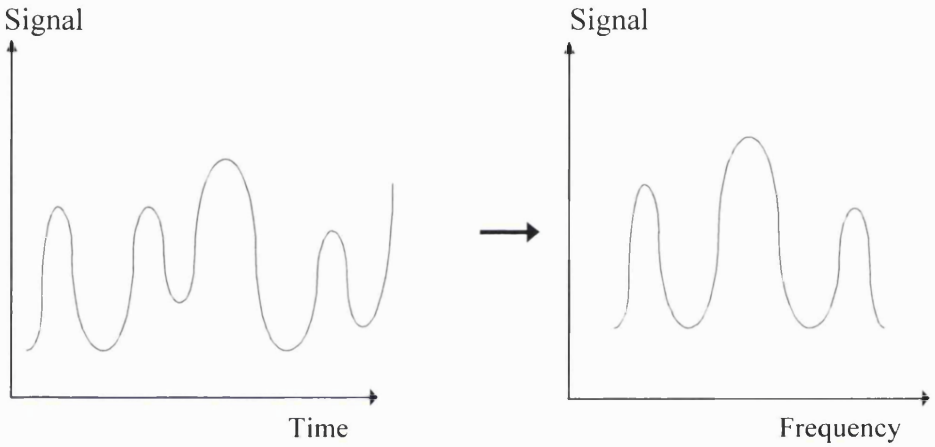

Fig. 1.10. Fourier transformation of the complex NMR signal results in a frequency spectrum (i.e. converts signal/time data to signal/frequency data).

To finally localize a given tissue volume element or voxel a third, y axis, gradient is applied very briefly before the frequency-encoding gradient. This results in a different precession frequency along the y axis. When this gradient is switched off the protons revert back to their previous uniform precession frequency, but have now dephased slightly, allowing their y axis positions to be differentiated (those protons that experienced the highest magnetic field will have precessed through a larger phase angle). In conventional imaging the frequency-encoding (or "readout") gradient is applied during signal acquisition, whilst the

phase encoding gradient is applied briefly immediately prior to signal readout; a number of phase encoding gradients are applied, one per excitation. This is repeated until the required spatial information in the x and y axes of the image slice is collected. It should be noted that the frequency- and phase-encoding gradients may each be applied to either the x or y axis.

The concept of k-space

In MRI, the frequency- and phase-encoding gradients are used to localize the NMR signal from each voxel. In other words these encoding gradients convert information about physical position into frequency data. The achievable spatial resolution of the image is determined by the gradient-time product of the spatial encoding gradient. This is because larger field gradients enable spins that are closer together to be differentiated. For example, a field gradient of 10^{-3} T/m will cause protons 1cm apart to differ in precession frequency by approximately 4258 Hz (from the Larmor equation). If the gradient is applied for 1/4258 s, spins 1 cm apart differ in phase by 360° and can be differentiated in position by Fourier transformation. To increase the resolution to 1mm the gradient must either be applied for 10 times as long or have 10 times the amplitude. The gradient-time product is known as *k:*

$$k = Gt$$

where G represents the gradient amplitude, and t the time for which it is applied. NMR signals are collected in the presence of encoding gradients. Because the

spatial resolution is directly determined by the maximum value of *k*, as the MR signal is collected, information about smaller and smaller image features is received.[1]

The NMR signal is in fact sampled digitally at different time points (2^n depending on the desired image resolution, i.e. 64, 128, 256 or 512 points) during spatial encoding. The complex data from each successive phase-encoding step are stored in a two-dimensional matrix, representing the signal at each point in *k*-space. In order to form an image, Fourier transformation of *k-space* is performed, which requires that complete data is available from all four quadrants of *k-space*, symmetrically about the origin (although the data have intrinsic symmetry so that sometimes only half of the matrix has actually to be acquired). In conventional spin echo imaging each line of data is collected following a separate excitation, so that the time between collecting each line is equal to the TR of the pulse sequence (Fig. 11).

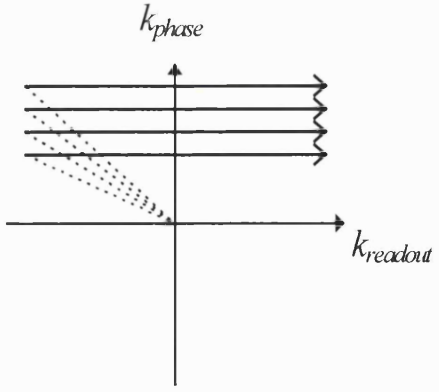

Fig. 1.11. Conventional *k-space* encoding. Each readout line is collected in the presence of a frequency encoding (x) gradient. A y gradient (phase-encoding) is pulsed immediately prior to collecting each line, resulting in a line by line filling of *k-space*.

[1] This is not strictly true for a spin echo experiment, where k-space is scanned from $-k_{max}$, through k=0 to $+k_{max}$ (i.e. small details are received at both ends of the echo, with contrast information being obtained in the middle of the echo.)

It will be clear from the above that the larger the *k-space* matrix being acquired, the longer the acquisition time required. As a simple example, let us assume that an image resolution of 256 x 256 is required (which would be typical of a clinical MRI scan of the brain). The time between each excitation must be greater than the time taken for recovery of longitudinal magnetization, described by the T_1 constant. T_1 in biological tissues is on the order of 500 ms so that the TR will be at least approximately this long. This gives an image acquisition time of 256 x 500ms, or about 2 minutes.

Echoplanar Imaging

In the conventional spin echo experiment described above, many excitations and echo collections are performed in order to generate an MR image. Echoplanar imaging (EPI), first proposed by Mansfield in 1977, is a technique that allows image data to be collected from a single excitation pulse, in a single *shot* (i.e. the TR is effectively infinite). This makes EPI the fastest clinically useful MRI technique. It will be seen that EPI makes a number of special applications feasible for the first time, including functional MRI and diffusion tensor imaging; these techniques form a substantial part of this thesis.

EPI collects the whole of the *k-space* matrix following a single excitation, by traversing the matrix in a single pass. To allow this to be done, all data must be collected in the time taken for the NMR signal to decay (i.e. at an echo time < T_2, and a total acquisition time ~T2*, or about 30-100 ms). There are a number of ways to traverse *k-space* rapidly, but all require rapid switching of large magnetic

field gradients, which necessitates the use of special MR hardware. Large gradients are necessary to provide an adequate gradient-time product (which determines spatial resolution) in each spatial dimension. Two commonly used methods of acquiring EPI data are illustrated in Fig. 1.12. There are many other approaches available that are beyond the scope of this brief discussion.

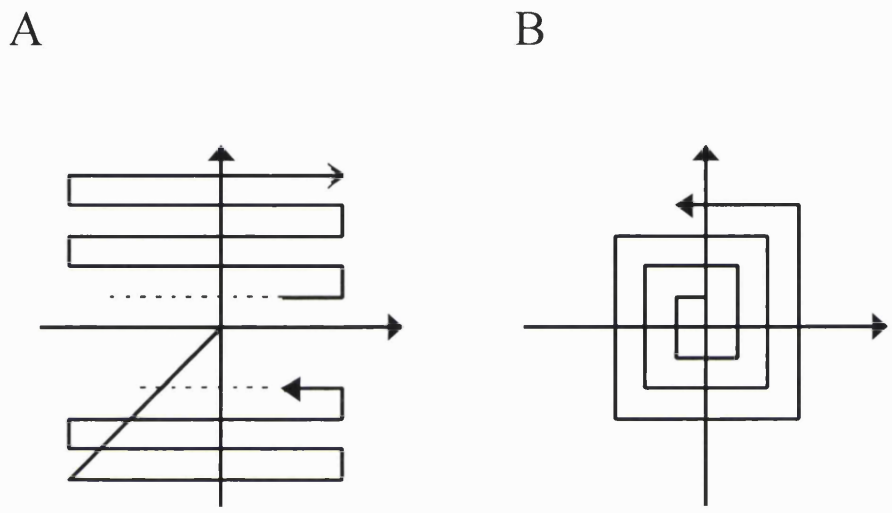

Fig. 1.12. Two different possible k-space traversals. (A) Raster-like acquisition; (B) Spiral acquisition.

All EPI methods share certain disadvantages, including significant time-varying magnetic fields within biological tissue that may induce currents in neural tissue and cause stimulation. This is one of the ultimate limiting factors in EPI, along with the availablility of large and rapidly-switching gradients. EPI is also inherently more vulnerable to certain types of image artefact and distortion. These include distortion at interfaces between tissue types, especially air and bone, known as magnetic susceptibility artifact. This is manifest as areas of signal

dropout and geometric distortion in the MR image. EPI with specific reference to functional and diffusion MRI will be considered in detail in later chapters.

The role of magnetic resonance imaging in multiple sclerosis

In the last 10-15 years, MRI has revolutionized the diagnosis and understanding of neurological illnesses, with arguably its greatest impact in MS. The contributions from MRI in MS may be considered under the following broad categories: diagnosis; prognosis; disease mechanisms (pathogenesis and pathophysiology); newer MRI techniques; and therapeutic monitoring. These will be discussed in turn.

Diagnosis

The first MRI images of lesions in the brain of patients with MS were obtained by Young et al. (1981). These images demonstrated the exquisite sensitivity of MRI in detecting the plaques of MS, which were hitherto often inconspicuous or undetected on CT scans. Subsequently, the abnormal areas on MRI scans were shown to correspond to histopathologically defined abnormalities (Ormerod et al., 1987). Brain MRI is abnormal in over 95% of patients with clinically definite MS (Ormerod et al., 1987). The appearances seen in MS on MRI scans, although not specific, may be quite characteristic. Typical features include ovoid or irregular, laterally oriented periventricular lesions, corpus callosum involvement, and lesions at the cortico-medullary junction. Nevertheless, a number of neurological conditions cause white matter abnormalities that are similar to those of MS. These

include acute disseminated encephalomyelitis (ADEM), sarcoidosis, systemic lupus erythematosus, Behçet's disease, phenylketonuria and leucodystrophies (Fieschi et al., 1997). Criteria that exploit the features most typical of MS have been developed by Fazekas et al. (1988) in order to increase the specificity of diagnosing MS. The use of these criteria in 1500 consecutive patients has shown a specificity of 89% for the diagnosis of MS (Offenbacher et al., 1993). More recently, the characteristics typical of MS lesions have been defined in an effort to predict the likelihood of conversion to clinically definite MS after a first symptom (Barkhof et al., 1997). Spinal cord imaging may also play a role in diagnosing MS, particularly in older subjects who may have non-specific brain MRI white matter abnormalities of vascular origin (Thorpe et al., 1996).

The limited pathological specificity of MRI is easily appreciated if the mechanisms of MR contrast - namely, the density and physico-chemical environment of water protons - are remembered, since such changes will not be specific for any single pathological process. Thus, MRI alone is not sufficient to establish a diagnosis of MS and must always be considered together with the clinical context.

Prognosis

It is now well established that the MRI abnormalities present at the time of a first clinically isolated syndrome suggestive of demyelination (including optic neuritis, partial myelitis, and brainstem disturbance) are helpful in predicting outcome. The presence and number of lesions on T2-weighted imaging strongly predict the development of clinically definite MS at 1, 5 and 10 years after the presenting

event. The longest published period of follow-up to date has been 10 years (O'Riordan et al., 1998). This study showed that of patients with a normal scan at presentation 11% had progressed to clinically definite MS, whereas 83% of those with an abnormal scan had done so. A further refinement of the risk prediction may be obtained by measuring the number of lesions or lesion volume at presentation (Sailer et al., 1999). The presence of new enhancing lesions at three months after first presentation has also recently been reported to be a strong predictor of the future development of MS Brex et al., 1999).

Disease mechanisms

The acute lesion and its evolution. MRI provides for the first time an opportunity to visualize safely and non-invasively the evolution of MS lesions *in vivo* in serial studies. Gadolinium-diethylenetriamine pentaacetic acid (Gd-DTPA) is a paramagnetic contrast agent that normally is unable to penetrate the blood-brain barrier to enter the brain parenchyma. However, when there is an increase in the permeability of the blood-brain barrier in association with inflammation, Gd-DTPA is able to leak into brain tissue and can be seen as bright or "enhancing" areas on appropriately T_1-weighted scans. This has been shown in the model of experimental allergic encephalomyelitis (Hawkins et al., 1990) as well as in a patient with MS who died of unrelated causes 10 days after a contrast-enhanced MR examination (Katz et al., 1993). In the latter study, enhancing areas on MRI revealed intense perivascular inflammation, a feature not seen in non-enhancing lesions.

The earliest detectable change in the majority of lesions studied is a focal

increase in blood-brain barrier permeability demonstrated with Gd-DTPA (Miller et al., 1988; Kermode et al., 1990). An area of abnormality then appears (visible on unenhanced scans) within about one week (Kermode et al., 1990), which enlarges to its maximum size at approximately four to six weeks (Isaac et al., 1988, Willoughby et al., 1989, Kermode et al., 1990). This region frequently exceeds the area of blood-brain barrier damage as indicated by enhancement. Enhancement ceases around this time, to leave a smaller lesion; 98% of lesions no longer enhance at 8 weeks (Thompson et al., 1991, Harris et al., 1991). There is strong evidence that the "disappearing element" corresponding to enhancement is oedema (Larsson et al., 1988; McDonald et al., 1992) since the patterns of T_1 and T_2 relaxation in areas of enhancement are identical with those of experimental vasogenic oedema. The area of lesion visible on unenhanced scans subsequently diminishes further, although most leave some residual area of abnormality.

The chronic lesion. It seems intuitive that persistent damage in chronic lesions might contribute to the irreversible deficit seen in the later stages of MS. One study performed quantitative and contrast-enhanced MRI together with both light and electron microscopy of longstanding lesions (Barnes et al., 1991). In all, the authors examined 53 lesions that shared certain properties. All had prolonged T_1 and T_2 relaxation times and the T_2 relaxation decay process showed two components in the majority of lesions. The first finding suggests an increase in tissue water content in these chronic lesions, whilst the latter suggests a shift of water into the extracellular space. A wide range of relaxation times was found both within and between patients, indicating a degree of heterogeneity in the lesions. This was confirmed on the histological and electron microscopy material,

which revealed a great variety in the extent of axonal loss and extracellular space expansion. Two broad classes of lesions could be defined: firstly, "open" lesions with a highly expanded extracellular space (up to 87% of their total area) and severe axonal loss; and secondly, "closed" lesions with less expansion of the extracellular space and dense glial infiltration. Only 17% of lesions examined enhanced with Gd-DTPA, and in all cases to a lesser extent than acute lesions.

Relationships between MRI and clinical activity

MRI has provided a unique opportunity to observe dynamic changes in disease activity (as indicated by changes in the properties, number or extent of lesions on MRI scans) in parallel with changes in clinical expression of the disease. A fundamental contribution has been to convincingly demonstrate that there is considerably more disease activity than is expressed as clinical symptoms and signs. Early studies showed that changes in the number or size of MRI lesions occur much more frequently than changes in clinical state (Isaac et al., 1988; Willoughby et al., 1989). Subsequent work using the contrast agent Gd-DTPA showed that the number of focal areas of enhancement may exceed the number of clinical relapses by a factor of up to 10-fold (Thompson et al., 1991).

Serial studies of patients with differing clinical courses have been instructive. Patients with early relapsing-remitting disease (within 5 years of onset) showed approximately 20 new enhancing lesions per patient per year of which 87% enhanced, in contrast to patients with primary progressive MS (approximately 3 lesions per patient per year of which only 5% enhanced) (Thompson et al., 1991). This suggests that inflammatory activity is greater in

relapsing than primary progressive patients and that progression in the latter group may be due to a non-inflammatory process culminating in irreversible structural damage. Within the phenotype of secondary progressive MS, some patients continue to have superimposed relapses, and evidence suggests that these patients show more frequent enhancement than those with steady progression (Kidd et al., 1996). This again suggests that inflammation (as judged by Gd-DTPA enhancement) is not a necessary prerequisite for disease progression, but plays an important role in acute exacerbations.

Limitations of conventional MRI

Conventional MRI detects the white matter lesions of MS with excellent sensitivity and has an established role in diagnosis. However, both cross sectional and longitudinal studies show only a modest relationship between T2-weighted cranial MRI abnormalities and the severity and progression of disability. An important contributory factor is the lack of pathological specificity of T2-weighted signal change: all of the pathological hallmarks of MS (inflammation, oedema, demyelination, gliosis, axonal loss) are likely to alter tissue water content and thus T2-weighted signal, but may have very different effects on neuronal function and clinical deficit. Furthermore, axonal loss, which may be a major determinant of functional deficit, may be difficult to detect on conventional MRI or at post mortem, as the nervous tissue may contract in response to the lost tissue, thus not causing obvious disruption of tissue architecture.

Newer MRI techniques

A number of newer MRI techniques have been developed with the aim of increasing pathological specificity and the ability to detect the structural changes that underpin clinical disability. These include magnetization transfer imaging (a putative marker for demyelination and/or axonal loss); spectroscopy of N-acetyl aspartate (a measure of axonal loss or dysfunction); T1-weighted imaging (in which the hypointensity of lesions may relate to the degree of axonal loss); and quantification of brain or cord atrophy. These newer techniques will be discussed briefly in turn.

Magnetization transfer imaging. Protons associated with macromolecules (e.g. protein, lipids) in the brain have very short transverse relaxation times as they readily give up their energy to the lattice. This makes them effectively "invisible" to conventional MRI. Magnetization transfer imaging may best be understood by modeling the biological system as two compartments, one containing water protons (free spins) and one containing macromolecular protons (bound spins). The spins in these two compartments have different resonant properties, so that an RF pulse may be applied to saturate the "bound" pool selectively. This energy is subsequently transferred to the "free" pool by cross-relaxation, chemical exchange and other processes, resulting in a decrease in the "free" proton NMR signal and a consequent reduction in tissue signal intensity. The greater the magnetization transfer from macromolecular protons, the greater is the signal attenuation. A magnetization transfer ratio (MTR) may be calculated, which should reflect the presence and integrity of macromolecules. MTR values have been shown to be

reduced in MS lesions compared to normal tissue, with a range of abnormality indicating a heterogeneity in lesion structure (Dousset et al., 1992). Reduced MTR has also been demonstrated in NAWM, implying that MTR imaging may be able to detect subtle pathological changes in tissue (Filippi et al., 1995a). MTR abnormalities have been reported in NAWM *before* a lesion is detectable on Gd-DTPA enhanced or T2-weighted scans (Filippi et al., 1998; Goodkin et al., 1998), challenging the notion that all lesions evolve in a stereotyped pattern in which focal leakage of the blood-brain barrier is the initiating event.

That the changes detected by MTR might contribute to clinical deficit is supported by a correlation of mean lesion MTR and disability (Gass et al., 1994). One promising recent technique for assessing the total "burden" of tissue abnormalities throughout the brain is the generation of histograms based on calculated MTR (van Buchem et al., 1997; van Buchem et al., 1998). In normal brain these histograms are characterized by a single sharp peak due to intact white matter pixels; in MS the peak height is reduced and the area under the peak is shifted toward lower MTR values.

T_1 Hypointense lesions. The first description of T1 hypointense lesions in MS was by Uhlenbrock and Sehlen (1989) who noted that such lesions were more common in MS than in subcortical arteriosclerosis. There is evidence that such lesions might represent those in which tissue destruction is most severe; several factors may contribute. One histopathological and MRI study suggested that the degree of T1 hypointensity in lesions is influenced by the extent of axonal loss, extracellular oedema, and the degree of demyelination and/or remyelination (Bruck et al., 1997). Another direct comparison of histopathological abnormalities with

corresponding T1-weighted images (van Walderveen et al., 1998) found that axonal loss was the main feature associated with T1 hypointensity and that demyelination and gliosis were less important, although this study did not examine acute enhancing lesions. T1 hypointense lesions have low magnetization transfer ratios, indicating severe structural loss (Hiehle et al., 1995); moreover, T1 relaxation time shows an inverse correlation with MTR (van Waesberghe et al., 1997).

Change in T1 hypointense "lesion load" has been shown to correlate with the progression of clinical disability in follow up studies, suggesting that these lesions correspond to irreversible loss of functionally important tissue (van Walderveen et al., 1995, Truyen et al., 1996). In summary, T1 hypointense lesions appear to have greater pathological specificity than conventional T2-weighted images. Further clinical and histopathological studies are needed to establish the role of T1 hypointensities as a marker of clinical progression or fixed structural damage.

Proton NMR Spectroscopy. Proton NMR spectroscopy has the potential to detect chemical changes corresponding to specific pathological changes *in vivo*. Water suppressed, localized proton NMR spectra of the normal human brain are characterized by three major resonances: these are due to phospholipids containing choline; creatine or phosphocreatine; N-acetyl aspartate (NAA); and lactate. NAA is of particular interest since it is found only in neurons in the mature brain and is therefore considered a marker for neuronal loss or dysfunction. Reduced NAA/creatine ratios have been demonstrated both in acute (Miller et al., 1991) and chronic (Matthews et al., 1991) MS lesions. Dynamic changes in choline

(found in membrane phospholipids) have been found in evolving acute lesions, which may reflect the release of lipid membrane components in association with myelin breakdown (Davie et al., 1994). Reduced NAA is not confined to lesions visible on MRI, but is also found in the NAWM (Husted et al., 1994; Davie et al., 1997), supporting the idea that subtle diffuse axonal damage (or dysfunction) occurs outside focal lesions in MS.

Functional relevance of changes in NAA concentration is suggested by a study demonstrating a reduced NAA concentration in the cerebellum of ataxic MS patients compared to MS patients who are not ataxic, or normal controls. Furthermore, a similar reduction in NAA was found in patients with a hereditary form of ataxia known to be associated with axonal loss (Davie et al., 1995). This result supports the hypothesis that axonal loss is important in the development of clinical disability in MS. Further support is provided by longitudinal studies, which showed that progression in disability correlated with reduction in NAA (Fu et al., 1998). NAA may be transiently reduced, emphasizing that neuronal dysfunction or altered relative volume, rather than destruction, may also contribute to NAA changes. A temporary reduction in NAA has recently been reported in anatomically homologous regions contralateral to an acute demyelinating lesion of the type seen in MS (De Stefano et al., 1999), which may represent axonal damage or dysfunction secondary to fibre transection within the acute lesion. These changes appear to be transmitted selectively to brain regions directly connected to the acute lesion, implicating projection fibres in their pathogenesis.

Atrophy measurement. Atrophy (a reduction in tissue volume) has recently attracted considerable interest in MS since it seems to be closely linked to clinical

disability. Initial studies concentrated on quantifying atrophy in the spinal cord, a site where pathological damage is likely to contribute significantly to motor disability. Kidd et al. (1996) examined 80 patients with MS and found that those patients with marked atrophy had higher disability on the EDSS than those without atrophy, although there was no significant difference in cord area between the relatively disabled progressive patients and the less disabled benign and relapsing groups. It was subsequently demonstrated that the techniques used in this study lacked scan-re-scan reproducibility and the technique was refined to improve this component. Losseff et al. (1996a) using a new, highly reproducible method of measuring spinal cord atrophy, showed a strong correlation of cord area with disability. Another study examined periventricular atrophy over time (Losseff et al., 1996b) and demonstrated a reduction in tissue volume, beyond the measurement error of the technique, over 18 months. Furthermore, atrophy was greater in those with sustained progression in disability. The pathological mechanisms underlying atrophy are not known, but axonal loss is likely to be a major factor. As discussed above, evidence from other MRI techniques in progressive patients indicates that axonal loss occurs in association with disability, and it has been suggested that the CNS responds to this destruction by reorganization and shrinkage manifest as atrophy (Losseff et al., 1998).

Therapeutic Monitoring

Preliminary trials. The unpredictability of MS, in particular the natural tendency for some patients to remit, makes the assessment of the effects of therapeutic interventions challenging. The ability of MRI to detect more disease activity than

is clinically apparent has led to the widespread use of serial scanning as a primary outcome measure in pilot studies to evaluate new therapeutic agents in relapsing-remitting or secondary progressive disease (Miller et al., 1996). A positive effect of treatment on the number of new enhancing lesions can be demonstrated in a smaller number of patients, studied for a shorter time than that required to show a change in clinical relapse rate. The size of the sample required to show an effect has been calculated for different anticipated effect sizes (McFarland et al., 1992). A number of treatments have shown a convincing reduction in enhancing lesions including beta interferon 1b (Stone et al., 1995), campath-1H (Moreau et al., 1994) and mitoxantrone (Edan et al., 1997). Typical protocols typically used currently in pilot treatment trials involve monthly T2-weighted and Gd-DTPA-enhanced scans, but other strategies including more frequent scanning, contrast manipulation to increase the number of detectable lesions, and different contrast agent doses are also being investigated.

Definitive trials. Until relatively recently no treatment had been shown to have a definitively favourable, long term influence on the course of MS. The first study to demonstrate such an effect was the North American interferon beta 1b study (IFNB MS Study group, 1993). A highly significant effect on the rate of accumulation of MRI lesions was demonstrated (Paty et al., 1993) whilst the relapse rate was also significantly reduced. The powerful MR effect was not, however associated with a significant effect on progression of disability. This may have been due to a number of factors including the limited responsiveness of the EDSS, the relatively low level of disability of the patient group, the relatively short duration of the trial, and the limited pathological specificity of MRI that has

already been discussed (McDonald et al., 1994). Furthermore, the relationship between MRI findings and subsequent progression of disability is not clearly understood. At present, MRI is considered to have an important role in screening new therapies, but is an adjunct rather than a primary outcome measure in definitive trials. The role of newer MRI techniques that may have greater power to detect the pathological changes that underlie disability (e.g. Magnetization transfer, atrophy) in clinical trials has yet to be defined.

Chapter 2

Introduction to the principles and clinical applications of functional MRI and magnetic resonance diffusion imaging

2.1 Functional Magnetic Resonance Imaging

Basic principles of brain functional organization

Although the concept that different functions or behaviours are broadly localized to particular areas of the brain has gained wide acceptance (Phillips et al., 1984), its origin was surrounded by controversy. Early evidence for cerebral localization arose from phrenology, based upon the work of Gall, which described correlations between personality traits and the configuration of skull prominences. Phrenology was increasingly popular until about 1820, when Flourens proposed in contrast that the brain acted as a whole, citing in support the similar and diffuse effects caused by damage to different brain regions. Subsequently, powerful evidence emerged for cerebral localization of function. In 1861, Broca demonstrated that disordered language function followed damage to the left inferior frontal gyrus; in the latter part of the nineteenth century, Fritsch and Hitzig published the effects of localized motor cortex stimulation in soldiers with head injuries and in animals. Ferrier (1889) demonstrated that lesions in particular cortical areas could induce specific functional deficits in primates. These experiments were refined and

expanded in the 20th century by detailed cortical stimulation experiments performed in awake patients prior to neurosurgery (Penfield and Boldrey, 1937).

It has become increasingly apparent that functional localization in itself does not provide a satisfactory description of cerebral organization. As early as 1881, Goltz emphasized the extent of functional recovery that followed irreversible injury to parts of the cerebral cortex, and the non-specific, general functional deficits caused by focal experimental lesions (Phillips et al., 1984). These observations were difficult to reconcile with a strict localization of cortical function. An important, more recent contribution was the pioneering work on disconnection syndromes described by Geschwind (1965). Distinct clinical patterns of deficit (due to single brain lesions) were elegantly explained by a disruption of (interhemispheric) connecting pathways, rather than dysfunction of a specific area. A comprehensive explanation of at least some cerebral functions thus requires an interaction (or *functional integration)* between anatomically distinct, functionally specialized (*functionally segregated*) areas of the brain. For example, in the visual system, distinct cortical regions are specialized for processing different aspects of the visual scene (Zeki et al., 1998). Current models of brain function propose that many cognitive or sensorimotor processes depend upon activity in parallel, distributed neural systems. This account, in retrospect, encompasses both sides of the controversy between localizationism and disconnectionism. In modern functional imaging experiments, a subject is asked to perform a task, during which the response of different brain regions is measured in some way (see below). The principles of functional segregation and integration are central to the interpretation of the regions "activated" during such experiments. Note that in the above account functional segregation differs subtly from

localization, which holds that *entire* behavioural functions, rather than component processes, can be ascribed to single brain areas.

Functional imaging: historical overview

The idea that neural activity is associated with haemodynamic changes was first clearly put forward over a hundred years ago by Roy and Sherrington (1890), They suggested that there may be "an automatic mechanism by which the blood supply of any part of the cerebral tissue is varied in accordance with the activity of the chemical changes which underlie the functional action of that part". It was not until nearly 40 years later that direct evidence supporting this hypothesis was obtained in man. Fulton (1928) studied a patient with an occipital arterio-venous malformation that was found to be inoperable. After surgery the patient had a small skull defect through which a bruit could be detected and recorded. It was demonstrated that this bruit intensified during visual stimulation (for example reading a newspaper), but not during other types of activity. This may be considered to be one of the earliest "functional imaging" experiments.

In the last 20 years, methods of imaging the brain have developed rapidly. Computerized axial tomography (CAT) provided the first opportunity to image the brain non-invasively in the 1970s and quickly replaced previous techniques of pneumoencephalography and angiography. It subsequently became possible to label molecules of biological interest with radionuclides and map their distribution in the brain, using positron emission tomography (PET) and single photon emission computed tomography (SPECT). These methods can be used to monitor regional cerebral blood flow and metabolism. Alongside these developments,

increasingly sophisticated methods of detecting electrical and magnetic field changes accompanying neural activity (e.g. using electroencephalography and magnetoencephalography) have emerged to provide excellent temporal resolution, albeit with limited localizing power.

The advent of MRI in the 1980s has revolutionized neurological clinical practice and provided a non-invasive research tool whose versatility in probing the structure and physico-chemical properties of brain tissue is unprecedented. The idea that MRI could be used to map brain activity was developed relatively recently, in the early 1990s.

Principles of functional imaging using magnetic resonance

When a population of neurons is functionally "activated", there are changes in membrane polarization that cause measurable local electrical and magnetic potential fluctuations, together with synaptic activity requiring neurotransmitter synthesis and release. These processes require energy, which is provided by an increase in local neuronal metabolism; through incompletely understood mechanisms, this causes local haemodynamic fluctuations (in blood *flow*, blood *volume* and blood *oxygenation*). All modern functional imaging techniques are based on detecting the electromagnetic, metabolic or haemodynamic consequences of neural activity. The following discussion will include only methods of detecting haemodynamic changes using MRI, with an emphasis on blood oxygenation changes. Methods of investigating blood volume and flow will be briefly considered first, however.

Blood volume

The first experiments using MRI to detect blood volume changes relied upon the susceptibility contrast caused by a paramagnetic contrast agent (Gd-DTPA) (see Chapter 1), which can be detected using EPI to generate maps of cerebral blood volume. In brief, a bolus of contrast agent is injected intravenously, after which T2*-weighted images are rapidly acquired (approximately one per second). The contrast agent enters the cerebral vasculature, creating susceptibility gradients that dephase proton spins and result in a local attenuation of the NMR signal. The signal attenuation is a linear function of the concentration of contrast agent which is in turn related to blood volume. This technique was first successfully used in a human subject by Belliveau and colleagues (1991), who tracked the passage of gadolinium through the occipital cortex whilst the subject viewed a flashing visual stimulus. Average increases in cerebral blood volume in the visual cortex of approximately 30% were demonstrated in this study.

Blood flow

Although imaging of blood flow in large cerebral vessels has been used clinically since the early 1980s, the microvascular flow associated with neural activity has proven more difficult to detect. Several approaches have been proposed. LeBihan et al. (1988) developed the intravoxel incoherent motion model of blood flow, in which flow within a voxel can be measured by virtue of a diffusion-like attenuation of the MR signal (a discussion of how molecular diffusion influences the MR signal is provided in the second part of this chapter). This technique

suffers a number of practical limitations, including difficulty obtaining an adequate signal to noise ratio and artefact due to cerebrospinal fluid and other tissue motion.

Another approach has been to 'label' arterial spins flowing into the brain by saturating them with a radiofrequency pulse applied outside the imaging plane (usually in the neck). Because the T1 of protons in blood is rather long, these labelled spins retain this longitudinal magnetization as they enter the part of the brain of interest. Following exchange of magnetization with bulk brain water at a capillary level, the regional concentration of labelled spins is related to regional cerebral tissue blood flow. Other methods of imaging flow with MRI using inversion pulses have also been developed but are beyond the scope of this brief overview.

Blood Oxygenation

It has long been known that the magnetic susceptibility of haemoglobin varies with its oxygen saturation (Pauling and Coryell, 1936). This is because oxyhaemoglobin contains diamagnetic oxygen-bound iron, whilst deoxyhaemoglobin contains paramagnetic iron. This phenomenon means that the transverse relaxation properties of tissues differ depending on the presence of oxyhaemoglobin and deoxyhaemoglobin; specifically, deoxyhaemoglobin causes more rapid spin-spin dephasing and so shortens the T2* relaxation time. This was predicted and demonstrated by Thulborn et al. (1982). Thus, changes in blood oxygenation (and thus oxy- and deoxyhaemoglobin concentrations) should alter the NMR signal detected by an appropriate susceptibility-sensitized pulse

sequence. In 1990, Ogawa et al. confirmed that the MR signal in perfused brain tissue of experimental animals studied at high field strength decreased as the blood oxygenation was lowered using various anaesthetic agents (Ogawa et al., 1990). A similar effect was subsequently demonstrated in animals breathing an oxygen-deprived atmosphere (Turner et al., 1991). This mechanism of image contrast was named blood oxygenation level dependent (BOLD) contrast.

The first demonstration that BOLD contrast could be used to image human brain activation was in 1991 at the meeting of the Society for Magnetic Resonance in Medicine (Brady, 1991). Subsequent papers reported an increase in local MR signal in the visual cortex during visual stimulation using susceptibility-weighted, gradient-echo pulse sequences (Kwong, et al., 1992, Ogawa et al., 1992). In these experiments periods of photic stimulation, presented using lightproof goggles, alternated with darkness. Simple subtraction of "off" from "on" images demonstrated highly significant signal increases in visual cortex grey matter.

The mechanism underlying BOLD contrast is not yet fully understood, but a widely accepted model of the sequence of events is the following: increased neuronal activity causes a local dilation of the cerebral vasculature, causing an increase in local blood flow. This delivers oxygenated haemoglobin into the area that exceeds the needs of the tissue. There is therefore a decrease in the local concentration of deoxyhaemoglobin, causing reduced susceptibility differences in the vascular structures, increased spin coherence and increased signal on T2*-weighted images (Fig. 2.1). For a 1.5T scanner, this signal increase is of the order of 2-5% in visual cortex during photic stimulation.

Important outstanding questions include whether excitatory and inhibitory synaptic events affect the BOLD signal in a similar way, and how they interact.

The effect of prolonged neuronal activity on the BOLD response also remains controversial. The complex relationship between neural activity and the BOLD signals is considered further in chapter 3.

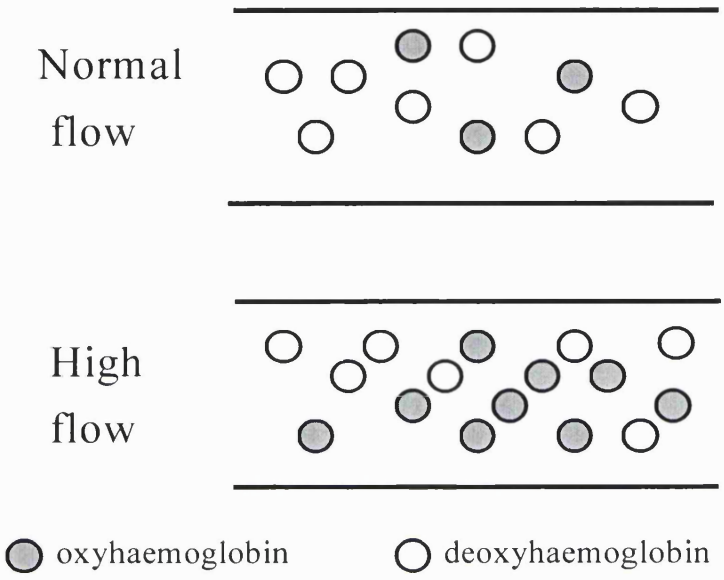

Fig. 2.1. The BOLD effect. When neurons are activated there is an increase in blood flow relative to the resting state. This delivers an excess of oxygenated haemoglobin molecules to the brain region causing a relative decrease in deoxyhaemoglobin concentration. This in turn causes increased MR signal on T2*-weighted images (see text).

Functional MRI using BOLD contrast

The BOLD contrast method of fMRI has been used very widely and successfully since the pioneering experiments described above and is arguably now the technology of choice for human brain mapping studies. The remainder of this section will be concerned solely with this technique, which was used for all of the functional imaging studies described in this thesis. Despite its brief history, it has become clear that BOLD fMRI offers a unique combination of non-invasiveness

and resolution in time and space with which to study brain function. Some practical and theoretical aspects of BOLD fMRI will now be considered.

fMRI data acquisition and hardware

The essential requirement for data acquisition is a scanner that can rapidly acquire a series of images with appropriate T2*-weighted contrast. Rapid imaging is desirable for the following reasons. Firstly, it is important to minimize the effects of head motion by keeping scan times as short as possible, ensuring optimum subject compliance; secondly, repeated sampling during neural activity increases the probability that detected signal changes are due to the task or stimulus under investigation, rather than system noise or signal drift. EPI, as we have seen, allows the acquisition of MR images in a fraction of a second, and has been crucial to the practical implementation of BOLD fMRI. (Although fMRI activation has been observed using conventional hardware, acquisition of multislice data is difficult due to the relatively long imaging times). EPI is therefore the acquisition method of choice for fMRI. Gradient-echo sequences are generally used, as they are inherently sensitive to T2* contrast and provide larger signal changes than other techniques.

EPI is not without drawbacks, however. The spatial resolution is generally less than that of slower MRI techniques, although the amount of image information acquired per unit time is highest for EPI (and variants thereof). EPI images suffer from signal loss due to bulk susceptibility differences across the image; gradient echo EPI is particularly affected by this problem. This is because by making the sequence deliberately sensitive to T2* contrast (i.e. to spin-spin

dephasing due to susceptibility differences) *macroscopic* susceptibility differences also have a significant effect on the image. The problem is particularly marked at interfaces between air and bone, for example in the region of the petrous temporal bone or the frontal air sinuses, and causes local signal loss. Furthermore, geometric distortions are prominent in EPI. One suggested approach has been to correct for these distortions in post-processing (Jezzard and Balaban, 1995). Clearly, it would be advantageous to minimize the distortions present in the acquired images, but there is a trade-off between minimizing inhomogeneity across the image and maintaining adequate BOLD contrast sensitivity.

In a typical fMRI experiment, the subject lies horizontally in the bore of the magnet and attends to a stimulus, often visual or auditory. Visual stimuli may be simple or complex; lightproof goggles have been widely used to present simple visual stimuli. More complex patterns can be presented on a projector screen viewed via a mirror above the subject, or by a liquid crystal display (LCD) video projector. Auditory input may be provided via headphones, and a number of strategies to reduce the acoustic noise inherent to EPI acquisition (due to large and rapid gradient switches) have been developed. The subject may be instructed to attend to a particular aspect of the stimulus and/or to make a specific response (e.g. pressing a button).

Using EPI, typically three to ten images are acquired per second for an experimental period of about five to ten minutes. Multiple slices are ideally acquired, usually 10 or more of thickness approximately five mm to provide reasonable brain coverage. The in-plane resolution will generally be between two and four mm (field of view 16-24cm^2, matrix size 64 to 128^2). The TE is chosen to be close to the T2* of brain tissue, about 40-50ms to optimise the ability to detect

BOLD contrast. The TR is typically 3000 to 5000 ms to allow the acquisition of multiple data slices, and to minimize the effects of flow on the image. With these parameters, the effects of cardiorespiratory pulsations on areas of activation are minimized and are confined mainly to large vessels and CSF (Le and Hu, 1996).

Most fMRI studies to date have used a 1.5T imaging system, giving a BOLD signal increase during primary sensory stimulation of approximately 2-5%. The signal to noise ratio (SNR) scales with the field strength to the power of 7/4. Using a 4T magnet therefore gives a considerable improvement in the signal to noise ratio. 3T systems have been approved in the USA by the food and drug administration (FDA) so may be clinically useful in the foreseeable future. However, increasing field strength may exacerbate other problems, including neural stimulation in the subject and image susceptibility distortions. Few high field systems are available worldwide, in contrast to 1.5T systems, which are in widespread diagnostic and research use.

Experimental design

There are three fundamental experimental designs for fMRI studies: these are categorical, parametric and factorial. A categorical design (Fig. 2.2) is conceptually straightforward, being based upon contrasting periods (epochs) of two different experimental conditions, often task performance (or sensory stimulation) and rest. The resulting regions of differences in brain activity between the two conditions should represent areas involved in a particular brain function. Categorical designs have the advantages of simplicity, and the availability of a number of statistical tools with which to investigate differences in BOLD signal

between rest and active epochs. Disadvantages include the limited temporal resolution (epochs are usually between 20 and 40s in duration) and the inability to examine unpredictable or aperiodic types of brain activity. An assumption implicit in a categorical design is that the difference between the two experimental conditions represents a separable cognitive or sensorimotor process, and that the resultant activation maps depict the brain areas involved in this process. Whether this assumption is justified in all cases is difficult to validate and remains controversial.

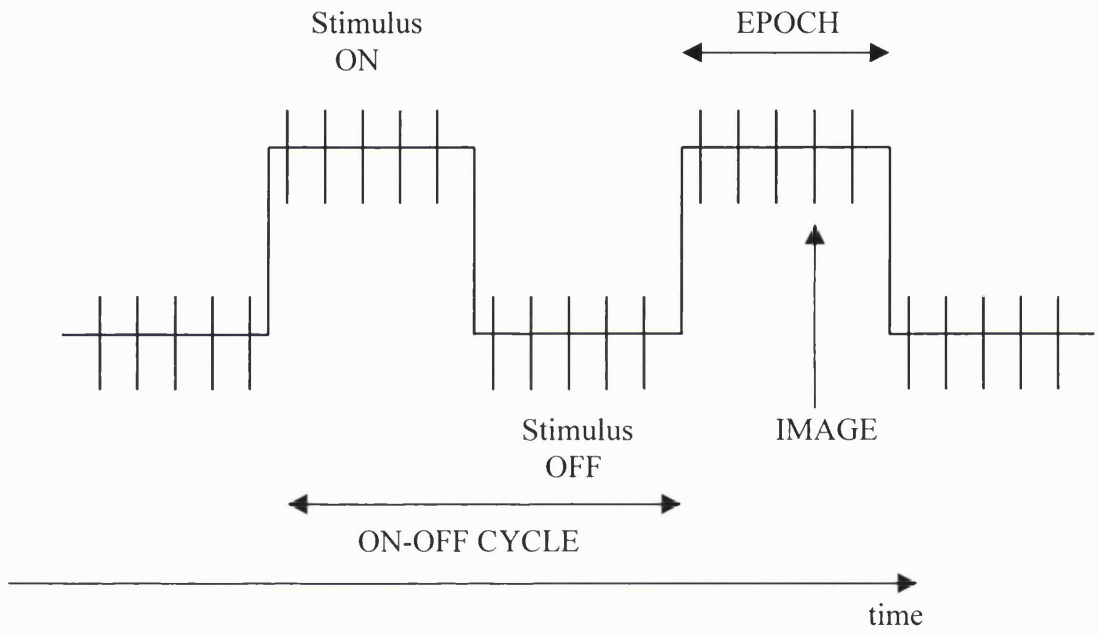

Fig. 2.2. Simple block design categorical fMRI experiment.

A second experimental design is a *parametric* study in which the properties of a stimulus or task are systematically varied (e.g. increasing frequency of word presentation) and the areas of the brain whose behaviour correlates with the changing stimulus are detected statistically. The underlying assumption in a

parametric design is that regional brain activity will vary systematically with the amount of cognitive or sensorimotor processing.

Thirdly, the interactions of two or more different conditions may be investigated using a *factorial* study design. Two factors are combined in a single experiment. Each factor may be varied to investigate how this affects the response to the other factors, described statistically by an *interaction* term. For example, one of the factors may be time, in which case the interaction between regional activity and time implies an adaptive cerebral response which could be related to habituation or learning. Because the signal changes due to brain activation are of small magnitude compared to the baseline signal and may be contaminated by the noise inherent in the MRI signal, the activity or stimulus being investigated must usually be repeated a number of times. Therefore, in all types of study discussed, a 'blocked' trial design is usual, i.e. multiple performances of a task are combined in a block during the experiment. A fuller discussion of experimental design may be found in Friston et al. (1998a).

Responses to *single* tasks or stimuli may be averaged over a number of trials in a way analogous to evoked potential recordings; this technique (*event-related* fMRI) is attracting increasing interest for exploring the timings of neural changes with respect to the onset of a stimulus or task. Single-trial responses have been detected using a cognitive task (Buckner et al., 1996). Memory tasks have also been investigated successfully with event-related studies (Brewer et al., 1998, Wagner et al., 1998). The optimization of experimental design and method of response characterization remain active areas of research (e.g. Friston et al., 1998b, Friston et al., 1998c). Event-related fMRI designs are likely to become the approach of choice for investigating the temporal patterns of neural activity.

Other factors to be considered in fMRI experiments include the scanner environment, which is noisy and may cause claustrophobia. Subjects should be familiar with the magnet and relaxed prior to any study. Task monitoring or feedback is desirable, so that the subject confirms performance of the required task. Habituation or fatigue effects may result from prolonged task performance or stimulation and there may be learning effects from experiment to experiment. Head motion is a major source of artifact in fMRI studies. Many strategies have been used to attempt to minimize head motion including inflatable inserts, cranial moulds and bite bars. Instrument manufacturers provide simple foam inserts which may be placed around the subjects head, and are comfortable and effective.

Spatial and temporal resolution

The ultimate spatial resolution of fMRI will be limited by how tightly cortical vascular responses are spatially linked to neuronal activation. Direct mapping with optical imaging methods (Frostig et al., 1990) indicates that vascular responses may be localized to the level of cortical columns. For fMRI to localize activation to this spatial resolution requires voxel sizes in the order of 100 microns. An unfortunate consequence of reducing voxel size is a reduction in the signal measured from the voxel, whilst the noise level remains constant. This reduces the signal to noise ratio (SNR), which scales with the cube of the linear voxel dimensions.

Another limiting factor in fMRI is the ability to detect signal change arising from the cortical microvasculature, rather than from larger blood vessels. Indeed, it has been suggested that fMRI detects signal changes in large draining

veins (Lai et al., 1993) that are spatially distinct from activated neurons. The contribution of vessels of different calibre (capillaries, venules, veins) to the BOLD signal remains controversial; the sensitivity of fMRI to vessels of different sizes may depend on the type of sequence used (e.g. gradient echo versus spin echo EPI) and sequence parameters (e.g. TE). Notwithstanding the above potential limiting factors, fMRI, using a 1.5T magnet, has been shown to reliably distinguish between activations separated by ~1mm in the visual cortex (Engel et al., 1997).

The theoretical limit in temporal resolution of fMRI depends upon the temporal characteristics of the BOLD response. The BOLD effect lags neuronal activity, which occurs within 50ms of stimulus onset. The latency of the BOLD response in primary visual or motor cortex is about five to eight seconds from stimulus onset to 90% of the maximum signal. However, there is evidence that this latency varies with anatomical region (Bandettini and Wong, 1998). Anatomical variation may reflect different haemodynamic coupling or other physiological or anatomical differences between regions. Studies of the temporal properties of neuronal responses have generally used event-related designs. The upper limit of temporal resolution has been estimated at approximately 1 second, although this remains an area of active research. A diagram depicting the relative spatial and temporal resolving power of different investigative methods is shown in Fig. 2.3.

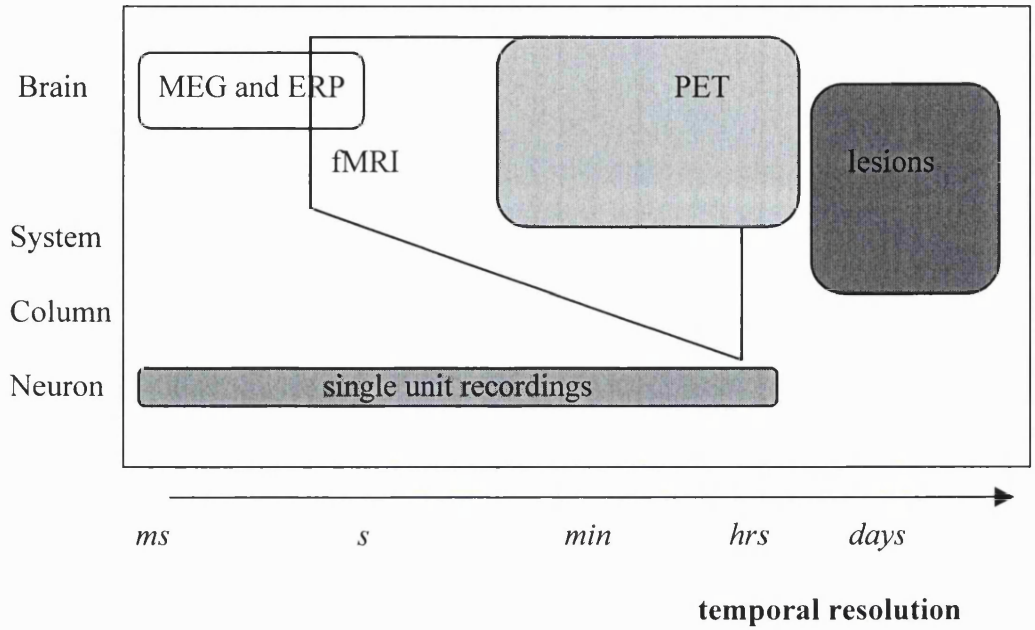

Fig. 2.3. Approximate spatial and temporal resolution of different brain imaging methods. The darker the shading the more invasive the method. fMRI offers a unique combination of spatial and temporal resolution and non-invasiveness.

Data analysis

The aim of fMRI data analysis is to detect areas of significant brain activation associated with a particular experimental manipulation, for example presentation of a sensory stimulus alternating with a rest condition. There are numerous statistical tools with which to detect activations; the following discussion will briefly describe the basic principles, and will be limited to block design trial analyses. The format of data from such a study will be of a series of images (usually from multiple brain slices) taken at sequential time points

(corresponding to the repetition time) from the beginning of the experiment (Fig. 2.4).

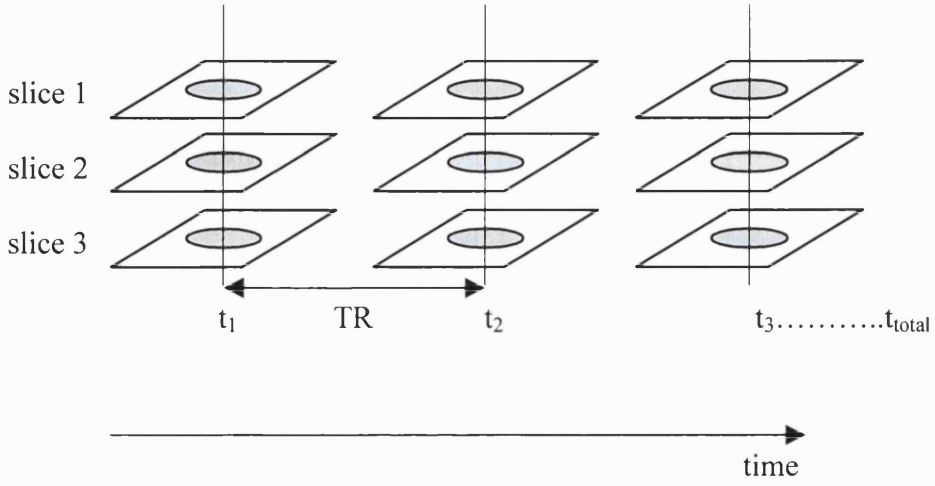

Fig. 2.4. Illustration of the form of a typical fMRI dataset which consists of a time series of images (t_1.....t_{total}) at each of a number of different brain slices.

Subject head motion is a major concern in the analysis of fMRI data since it may cause artifactual changes in voxel signal intensity that may or may not correlate with the experimental design. This may have the effect of obscuring true activation or generating spurious areas of activation. Motion correction is therefore generally considered a vital step, prior to statistical tests for activation. There are many methods of varying complexity used to correct for head motion, which even in a cooperative subject will at best be of the order of 1mm. The Woods algorithm (Woods et al., 1992), originally developed for PET images, is widely used. In this method, images are realigned by translation and rotating each image in the time series to make their voxel-by-voxel features and position most nearly uniform. There are other methods based on similar principles of minimizing differences between the images in the time series. Even after optimal image

alignment, however, some movement related (artifactual) signal changes may remain. This is because the MR signal in a given voxel depends not only upon its current position, but also upon its *previous* position (or *spin history*). This is because the T1 saturation experienced by spins will alter if out of plane motion occurs, since the TR in multislice data depends on slice position. A method of correcting for this phenomenon has been proposed by Friston et al. (1996).

After motion correction, statistical methods are used in order to distinguish areas of activation in the image. Many methods are available, but all aim to perform the same task - namely, to determine how likely it is that an observed result occurred due to the experimental design rather than by chance. In other words, the aim is to reject the *null hypothesis* (i.e. that the result is due to chance), in order to establish that the result was very *unlikely* to be due to chance. How unlikely this must be is given by the significance level, α. Conventionally this will be set at $\alpha<0.05$ or lower to minimize the false positive rate or Type I error. The second important property in a statistical approach is not to miss areas of significant response, so minimizing the number of false-negative declarations (Type II error, given by significance level β). To perform these statistical tests, the distribution of the data under the null hypothesis must be modeled and then compared with the observed data. Ascertainment of the test statistic under the null distribution can be done in three ways: first, theoretically (requiring certain assumptions to be made about the null distribution, for example that it is normally distributed); second, experimentally (by collecting data when the null hypothesis is known to be true, for example with the subject at rest in the magnet); or third, by randomization or permutation of experimental data. Having ascertained the null distribution, the observed experimental data must then be statistically compared

with this. This is normally done on a voxel-by-voxel basis in order to give a statistical map that must then be evaluated to minimize the number of type I and type II errors. This involves many separate statistical comparisons (for a 128x128 image over 10,000), which must be corrected for in some way; for example the voxel-wise false positive probability can be made more stringent.

An "activation map" of significantly activated voxels is usually superimposed upon an anatomical template, typically a structural MRI image of the patient's own brain. The ability of fMRI to generate single subject, single study maps is in fact one of its potential strengths. However, the geometry of the template may not closely match the geometry of the images used to create the functional map (the latter generally derived from EPI such that they are subject to the distortions and susceptibility signal loss previously described). The activation map must therefore be transformed to fit the anatomical template, a process that may involve image manipulation including linear and non-linear transformations. This may affect anatomical localization, a point that will later be considered in the experimental chapters on fMRI.

Although an important advantage of fMRI is its ability to localize brain regions activated by an experimental task in a single individual, often it is desirable that fMRI data from groups of individuals be combined in some way in order to allow the generalization of individual subject results to populations. For example, in clinical research the common effect that a particular disease has on the activation pattern in a group of patients may be of more interest than the variability of responses between each patient. This requires the combination of the individual activation maps into "group maps" presented in some common anatomical reference space. The most widely adopted co-ordinate system currently

is the atlas of Talairaich and Tournoux (1988), originally developed to assist stereotactic surgery to the deep grey matter nuclei, and based upon the brain of a 65-year-old French female. The process of transforming individual activation maps into a common space - to map the group response at each voxel - is complex. Important steps include image registration, spatial transformation and smoothing; details of the methods used for the group analysis in this thesis are provided in detail in chapter 3.

The techniques for analyzing fMRI data continue to develop rapidly, but there is currently no consensus regarding the optimum method. It will be apparent that the method of choice must be able to specify the properties of data under the null hypothesis. It must also be able to take into account the complex delay and morphology of the BOLD response, its variation across brain regions, and deal with physiological, instrumental and experimental sources of noise or artifact. Further work is required in many of these areas, and it is likely that different analyses will be appropriate for different types of experimental questions.

A large number of different software packages have been used for the analysis of fMRI data; three used in the NMR Research Unit will be outlined briefly. STIMULATE (Strupp et al., 1996) is easy to use and offers correlation analyses with options to choose a number of reference waveforms as models of the periodic haemodynamic response in block design experiments. However, image realignment must be performed on data prior to using this software. Statistical parametric mapping (SPM) (Friston et al., 1995), originally developed for PET image analysis, utilizes a sophisticated statistical approach based on the general

linear model.[1] The software package includes image realignment and the ability to coregister images from different modalities. Generic brain activation mapping (GBAM) is a nonparametric approach (Brammer et al., 1997) based upon permutation testing and sinusoidal modeling of data that accounts for variations in haemodynamic delay and dispersion across the brain, and includes image realignment and the image processing steps necessary for combining groups of subjects. GBAM will be discussed in detail in chapter 3.

Overview of some applications

Since the early fMRI experiments described, the range of applications has expanded at a rapid rate. Studies were initially performed using simple sensory or motor paradigms designed to activate areas of primary cortex in attempts to validate the technique, but these have been followed by an increasing number of studies involving more subtle cognitive paradigms and innovative experimental designs. It is clear that fMRI data from primary cortex activation studies are in good agreement with other functional imaging modalities, including PET and electrophysiological studies. The results in more complex studies involving cognitive processes present greater challenges for interpretation, but emphasize the enormous potential of fMRI to contribute to our understanding of higher cerebral functions. Selected fMRI studies will be considered in the following brief and selective overview.

[1] In a PET experiment sequential scans are treated as independent observations; because of the delay in the BOLD haeodynamic response, the images in fMRI time series show *autocorrelation*, violating this assumption and reducing the true degrees of freedom. SPM methodology has since been developed to extend the application of the general linear model to accommodate autocorrelation.

Visual system

The important early papers describing BOLD fMRI in humans used simple photic stimulation (Kwong et al. 1992, Ogawa et al., 1992). Stimuli were presented using lightproof goggles containing a matrix of red light-emitting diodes (LEDs) in each eyepiece that may be flickered at different frequencies. The flicker frequency for maximum cerebral blood flow changes was previously shown to be 8Hz, using PET (Fox and Raichle, 1985); fMRI studies confirmed that peak BOLD signal change also occurs at this frequency (Kwong et al., 1992). Subsequent work has exploited the high spatial resolution of fMRI to map the retinotopic organization of visual cortical areas (Schneider et al., 1993). Elegant experiments using stimuli in which the stimulus presentation is manipulated in a periodic fashion have allowed functionally specialized areas in the human visual system to be precisely located (e.g. Sereno et al., 1995; Engel et al., 1997). An example of an experiment of this type is the use of a repeatedly contracting ring shape in the visual field of the subject. If the stimulus moves at constant velocity, each point in the visual field experiences the same frequency of stimulus, giving neurons receiving input from each point the same frequency of periodic stimulus, inducing a periodic BOLD signal. Neurons responding to the periphery of the field will respond earlier than those responding to the fovea, so that the phase of the response defines the receptive field position. This type of retinotopic mapping method is termed a *phase-encoded* experimental design.

Ocular dominance columns are thin sheets of visually responsive neurons with common functional properties, which represent fundamental units of functional organization in the visual cortex. Alternating columns preferentially

respond to input from either the right or left eye. The demonstration of ocular dominance columns using fMRI at high field strength has been reported (Menon et al., 1997), which probably approaches the ultimate limit of spatial resolution of fMRI.

To date, relatively few studies have been performed in the visual system with patients. One early study demonstrated abnormal lateralization of the cortical response to a monocular stimulus in albino patients, in which an abnormally high proportion of temporal retinal fibres cross in the optic chiasm (Hedera et al., 1994), indicating the potential of fMRI to detect activation changes related to abnormal fibre projections. A significant increase in the magnitude of BOLD response to photic stimulation has been reported in schizophrenic patients compared with control subjects (Renshaw et al., 1994). Another study found that patients with schizophrenia showed a reduced visual cortex response to photic stimulation during visual hallucinations (Howard et al., 1995). Visual processing has been studied using fMRI in dyslexic patients, with an abnormal lack of response to moving stimuli in area MT (V5) demonstrated in comparison to matched healthy control subjects (Eden et al., 1996). The effect of unilateral occipital cortex damage in a patient exhibiting "blindsight"- the phenomenon of being able to perform a visual discrimination task without conscious visual perception - has been investigated (Sahraie et al., 1997). In this study, during "unaware" discriminatory tasks a shift in activation from neocortex to subcortical structures was reported in comparison to the "aware" mode.

Motor system

The first motor experiments with fMRI involved simple finger to thumb opposition or hand squeezing (Kwong et al., 1992) and subsequently, more complex movements (Rao et al., 1993). Somatotopic mapping of the hand and foot primary motor areas was reported by Rao et al. (1995); a somatotopic organization has also been reported in the cerebellum (Nitschke et al., 1996). More recently, activation of basal ganglia structures during motor tasks has been described (Lehericy et al., 1998). In patients, studies have successfully correlated the areas activated by fMRI with areas eliciting limb movement by direct cortical stimulation during surgery for tumours (Jack et al., 1994; Atlas et al., 1996). Motor fMRI has also been performed in patients with partial epilepsy (Morris et al., 1994).

fMRI studies may illuminate the effects of brain pathology upon the motor system. For example, a study has reported abnormal motor organization in patients with schizophrenia (Schroder et al., 1995). Patients recovered from hemiplegic stroke have been reported to activate areas of motor cortex ipsilateral to the stroke, suggesting a functional reorganization of the motor system associated with recovery (Cramer et al. 1998); a variability in the pattern of plastic changes was also found in this study. Work using functional neuroimaging to investigate mechanisms of recovery will be discussed further in chapter 3.

Language.

A large study of 100 subjects has confirmed that language processing is strongly lateralized, to a similar degree, in both men and women (Frost et al., 1999). A potential clinical application of fMRI is in the identification of the language-dominant hemisphere in patients undergoing evaluation for epilepsy surgery (Prichard and Cummings, 1997). Preliminary data indicate that fMRI allows identification of language-mediating areas during word generation tasks that correlate with more invasive electrocorticography studies (Hertz-Pannier et al, 1997). Pre-surgical mapping with fMRI may also be of value in patients with brain tumours or vascular malformations.

2.2 Magnetic resonance diffusion imaging

Background

Diffusion is the random translational motion of molecules in a fluid system and may be illustrated by a simple two-compartment diagram containing two molecular species. When the barrier between the two compartments is removed, the diffusive motion of the two species causes the molecules to mix together (Fig. 2.5). A similar mixing occurs with a single molecular species, more accurately termed *self-diffusion.*

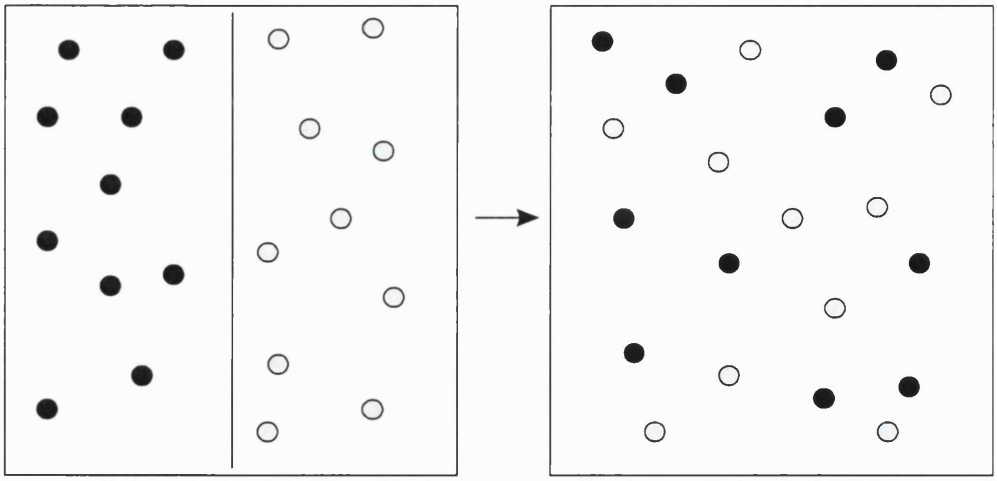

Fig. 2.5. Classical model of diffusion of two molecular species (see text).

A large proportion of the living brain is in a fluid state due to its high water content, and diffusion plays a vital role in the transport of metabolites and regulation of the tissue environment. The diffusion of water molecules in the brain is influenced by the microstructural components of tissue including cell membranes and organelles; the measurement of water diffusion thus gives unique information about tissue structure. Measuring the self-diffusion of water diffusion in biological tissues *in vivo* has considerable potential as a research and clinical tool. MRI is the only method currently available with which to measure molecular displacements non-invasively.

Diffusion may be understood by conceptually following a water molecule in a glass vessel, whose direction is altered each time it interacts with another water molecule. The longer the molecule is observed, on average, the further it has travelled from its original position when the observation began. The *diffusion coefficient* relates the observation time to the average distance travelled, and is a characteristic of the particular fluid under consideration. Diffusion is, of course, a three-dimensional process and when, as in a glass of water, it is the same in any

direction in space, it is termed *isotropic* diffusion. Because the diffusion coefficient is related to the kinetic or motional energy of molecules its value is approximately proportional to temperature.

Diffusion-weighted imaging

MRI is unique in its ability to measure diffusion coefficients non-invasively. The technique is based on the application of large pulsed field gradients, which sensitize the NMR signal to diffusive motion (Stesjkal and Tanner, 1965). This sensitization results in an irreversible dephasing of the transverse magnetization, which causes attenuation of the NMR signal. In a diffusion-weighted image (DWI), regions of high diffusion such as the cerebrospinal fluid show marked signal attenuation, whilst areas with lower diffusion such as the brain parenchyma (where there are more restricting boundaries; see below) have relatively less signal attenuation. This approach can yield useful information, for example by revealing reduced water diffusion in acute cerebral infarction (Warach et al., 1992), a phenomenon which may reflect a shift of water into cells from the extracellular space ("cytotoxic oedema"). Interpreting DWIs is qualitative, however, and may be complicated by T2 relaxation in addition to the effects of diffusion. It is therefore desirable to quantify water diffusion in the brain.

Quantification of water diffusion

The degree of signal attenuation is related to the diffusion coefficient of the sample and the properties (including the magnitude, separation and duration) of

the diffusion sensitizing gradients, described by the *gradient b factor*. There is a linear relationship between the logarithm of the NMR signal and the b factor used. Therefore, by experimentally collecting a series of signals at different b factor values it is possible to calculate the diffusion coefficient of a sample. In biological tissues the value of the diffusion coefficient is less than it would be in free water at the same temperature. This is because the structural components of tissue, including cell membranes and organelles, present obstacles to water diffusion. If a water molecule is observed for a sufficiently long time it will eventually reach an element of the cellular structure. If a cell membrane is impermeable to water molecules the molecule will be reflected back so that their progress across the membrane is impeded; this is termed *restricted* diffusion. If the membrane is semi-permeable then only a proportion of the water molecules proceed across the membrane, causing a more modest reduction in the apparent diffusion coefficient, termed *hindered* diffusion. Measuring diffusion in the brain therefore results in an *apparent* diffusion coefficient (ADC), so named to distinguish it from true free diffusion (LeBihan et al., 1986). The ADC can be calculated by collecting images with different degrees of diffusion sensitization (b factors) and fitting the data to the following exponential function:

$$\frac{S}{S_0} = \exp(-bADC)$$

where S is the attenuated NMR signal in the presence of diffusion gradients, S_0 is the signal in their absence, and b is the gradient b factor. Diffusion sensitized MRI can thus provide a novel type of tissue contrast based upon water molecule displacements, and facilitates the computation of maps of diffusion coefficients

throughout the brain on a pixel-by-pixel basis (LeBihan and Breton, 1985, Taylor and Bushell, 1985, Merboldt et al., 1985).

Anisotropy

In some biological tissues the degree of restriction or hindrance of diffusion may change with direction due to oriented structural barriers to diffusion such as axonal membranes, myelin and the neurofilamentary cytoskeleton. In this situation, where the diffusion coefficient is directionally dependent, diffusion is said to be *anisotropic*. Anisotropy has been observed in the white matter tracts of the brain by applying the diffusion sensitizing gradients in two or more directions (Chien et al., 1990; Chevenert et al., 1990). A higher ADC is seen parallel to the fibre direction than is the case perpendicular to the fibres. Anisotropy in the brain depends on the structural coherence of fibre tracts, and is therefore of potential interest in assessing the impact of pathology on tract integrity, but accurate quantification requires a more sophisticated approach than that described thus far.

The diffusion tensor

Full quantitative assessment of diffusion in anisotropic tissues requires the acquisition of data relating to the diffusion of water molecules in all directions. An ADC map produced by one diffusion gradient direction will only give information about water diffusion in that direction. Attempts to estimate anisotropy by using two diffusion gradient directions assume that the largest ADC is measured along the longitudinal axis of the anisotropic structure, whereas the

smallest ADC is perpendicular to it. It is clearly impossible to arrange the required measurement directions in tissues where the orientation of structure is not uniform, as in brain white matter. In practice, this means that tissue anisotropy cannot be accurately measured using two or three diffusion gradient axes; one study has shown that three axis measurements underestimate white matter anisotropy (Pierpaoli and Basser, 1996). At its most extreme the error may be so severe as to cause obliquely oriented fibres to appear to be isotropic.

Diffusion imaging has been revolutionized by the recognition that the diffusion tensor, D (a matrix that includes six independent scalar elements, each representing a different diffusion direction; Fig. 2.6) is required to fully characterize diffusion in anisotropic, heterogeneously oriented tissues, and that it may be estimated using MRI (Basser et al., 1994; Basser et al.,1996).

The magnitude of diffusion as measured by the diffusion tensor (known as the mean diffusivity) has the special property of rotational invariance. This means that, unlike the ADC calculated with only one axis of sensitization, mean diffusivity has the same value regardless of the orientation of the brain, relative to the magnet. This property is particularly desirable for longitudinal patient studies, or studies involving different laboratories. Furthermore it has been shown that true quantification of diffusion anisotropy is possible using indices derived from the diffusion tensor (Basser and Pierpaoli, 1996; Pierpaoli and Basser, 1996); proposed anisotropy indices include fractional anisotropy and the volume ratio.

$$\begin{matrix} D_{xx} & D_{xy} & D_{xz} \\ D_{xy} & D_{yy} & D_{yz} \\ D_{xz} & D_{yz} & D_{zz} \end{matrix}$$

Fig. 2.6. The diffusion tensor matrix. D_{xx}, D_{yy}, and D_{zz} are the diagonal elements, corresponding to the ADCs in the x, y and z directions, respectively. It should be noted that the off-diagonal elements (D_{xy}, D_{xz}, and D_{yz}) do not represent ADCs along the oblique directions; they indicate how strongly ADCs are correlated in the x, y, and z directions. If the off diagonal elements are zero, then the tissue is either isotropic or the fibres lie parallel to the x, y or z axes. Note that the matrix is symmetrical about the diagonal, meaning that only six elements must be measured to estimate the full diffusion tensor.

The diffusion within a given voxel may be most fully and naturally described by the three principle diffusivities (eigenvalues λ_1, λ_2, and λ_3) derived from the diffusion tensor. The process by which the eigenvalues and eigenvectors are obtained from the diffusion tensor is known as *diagonalization.*

These eigenvalues represent the principle diffusion coeffecients measured along the three intrinsic coordinate directions within the voxel. This intrinsic or local "fibre" frame of reference is independent of the magnet coordinate orientation or the subject orientation. Each eigenvalue is associated with an eigenvector (or principle diffusion direction) that is also intrinsic to the tissue. In the analysis of diffusion tensor data the three eigenvalues are sorted by order of decreasing magnitude (λ_1, λ_2, and λ_3). In a sample of parallel white matter fibre bundles, λ_1 represents the diffusion coefficient along the fibre direction, whilst λ_2 and λ_3 represent the mutually perpendicular transverse diffusion coefficients (ie $\lambda_1 >> \lambda_2 \approx \lambda_3$; Fig. 2.7). There are two other basic possible eigenvalue combinations; the 'planar' case, where the diffusion may be thought of as a 'pancake' shape, and

$\lambda_1 \approx \lambda_2 >> \lambda_3$ (less likely to be found frequently *in vivo*); and finally, the 'spherical' case, where $\lambda_1 \approx \lambda_2 \approx \lambda_3$ and diffusion is isotropic.

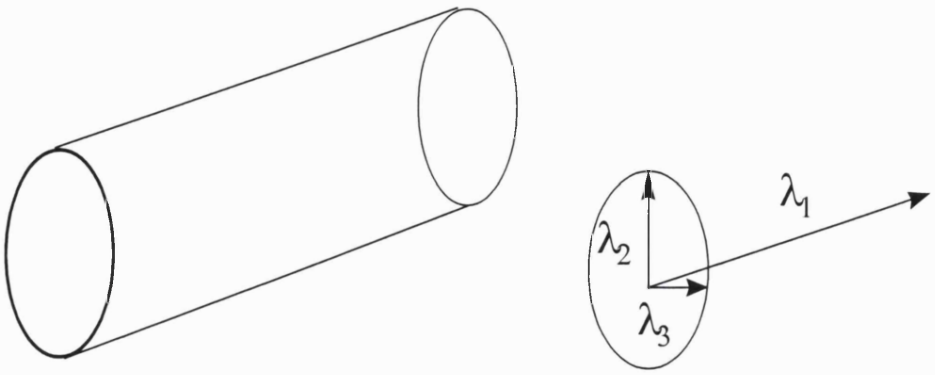

Fig. 2.7. Diagram showing the eigenvectors for an anisotropic, cylindrical structure in which $\lambda_1 >> \lambda_2 \approx \lambda_3$.

Motion artifacts in diffusion imaging

Unfortunately, sensitization of the imaging sequence to diffusion also results in greatly increased sensitivity to patient motion. Early diffusion imaging studies were limited by severe motion artefacts, resulting in an inaccurate assessment of the ADC. A number of strategies have been employed to circumvent this problem including the use of cardiac gating and navigator echoes which correct for the effects of bulk subject motion (Ordidge et al., 1994). Perhaps the most notable development, however, has been the use of EPI (Turner et al., 1990). This method (see Chapter 1) effectively avoids the motion problem and is sufficiently rapid to enable the collection of DWIs with the multiple b factors and axes of sensitization required for imaging the diffusion tensor. EPI is now becoming more widely used on many commercial MRI systems for diffusion imaging. Thus, diffusion imaging

has benefited from a number of methodological improvements, which today make DWI and DTI realistic tools for clinical investigation. Although the optimum strategy for DTI is an area of active development and there have been few clinical studies so far, the application of DTI in clinical research is attracting considerable interest and it is likely that the number of studies will increase rapidly in the coming years.

Clinical applications of diffusion MRI

Acute stroke

Diffusion-weighted imaging has detected changes in animal models of acute stroke within an hour of vascular occlusion (Moseley et al., 1990). In humans it is also clear that diffusion changes precede those seen on conventional T2-weighted images. Acute infarction is visualized as an area of hyperintensity on DWIs, which represents a reduction in water diffusion. The ADC decreases in the first four days after ischaemia and subsequently normalizes at about five to 10 days; after this time the ADC is elevated (Lutsep et al., 1997). The most widely accepted mechanism for the early diffusion decrease is that of cytotoxic oedema, in which a massive influx of water and ions from the freely-diffusing extracellular compartment into the more restricted intracellular compartment occurs. This process may in part be dependent upon continued calcium ion influx and a failure of active membrane pumps as their capacity becomes saturated. The diffusion coefficient then rises with the presence of vasogenic oedema, and ultimately remains increased in comparison to normal tissue, due to cell lysis with

consequent expansion of the extracellular space. Diffusion imaging in stroke has potentially important clinical implications. In addition to aiding early diagnosis, diffusion imaging may also help to identify the area of potentially salvageable tissue within an infarct (the 'penumbra') that may help to rationalize the use of neuroprotective or reperfusion therapies. Although at present, the clinical impact of diffusion imaging in stroke remains limited, there has recently been a resurgence in its use to evaluate acute stroke syndromes (Prichard and Grossman, 1999).

Neoplasia

Diffusion MRI has shown some promise in elucidating the physical properties of intracranial mass lesions, which potentially could have an important influence upon clinical management. In a preliminary study, (Tsuruda et al., 1990) the ADC of arachnoid cysts was shown to be higher than that of epidermoid tumours, confirming the more solid nature of the latter. The result was confirmed in a subsequent study (Maeda et al., 1992). A more recent study (Krabbe et al., 1997) compared the ADC values in cerebral metastases with high-grade gliomas, and found that metastases had higher ADC values, particularly within cystic or necrotic areas. A role in distinguishing between brain abscess and tumour has also been suggested recently (Noguchi et al., 1999).

Multiple sclerosis

Diffusion MRI has not yet been widely applied to the study of MS, despite the well recognized limited pathological specificity of conventional T2-weighted MRI (discussed in chapter 1). MR diffusion imaging is sensitive to the orientation, shape and geometry of water spaces in tissue, and should detect subtle abnormalities in tissue microstructure due to the pathological changes in MS. It may also have the potential to quantify the severity of structural damage, and to distinguish between different aspects of the pathological process, particularly if both the magnitude and anisotropy of diffusion are examined. The first report of water diffusion in MS was published in 1992 (Larsson et al., 1992). Although limited by motion artefact, this work demonstrated higher diffusion in MS plaques than in normal appearing white matter (NAWM). Plaques judged to be less than three months old showed the highest diffusion values, perhaps due to greater inflammatory oedema in comparison to chronic lesions. A subsequent paper (Christiansen et al., 1993) used bipolar gradients and cardiac gating to reduce (but not eliminate) motion artefact, which resulted in more stable measurements and confirmed the previous observations. In this study it was also noted that patient NAWM showed higher diffusion than NAWM in healthy control subjects, consistent with a subtle, diffuse abnormality of structure in tissue appearing normal on conventional MRI. These early studies suffered from technical limitations, particularly of motion artefact, limited brain coverage and an ability to examine only large lesions with diffusion gradients applied in a single direction. A study by Horsfield et al. (1996) used a volume selective technique, which permitted three axis diffusion measurements in a reasonable time frame without

major motion artefact, although only large lesions could be studied. No significant differences in ADC were detected between benign and secondary progressive phenotypes of MS. The finding of increased ADC in lesions was again confirmed, and a single acute lesion had the highest value with subsequent normalization almost to the NAWM value. Patient NAWM was found to exhibit higher water diffusion than in normal controls, in keeping with earlier work. The method used in this study did not allow lesion morphology and the surrounding structure to be visualized on ADC maps. These diffusion studies demonstrate the promise of diffusion MRI to study tissue structure changes in the brains of patients with MS. In chapter 4, work that has further developed the application of diffusion MRI (including DTI) in MS will be described.

Chapter 3

Mechanisms of recovery in demyelinating disease: fMRI studies in optic neuritis

3.1 Introduction

Mechanisms of neurological recovery: the concept of cerebral plasticity

Recovery is common following many types of neurological injury but, until recently, the mechanisms have been difficult to study in humans *in vivo*. With non-invasive functional neuroimaging, it is now possible to investigate how the human brain responds following damage. In contrast to longstanding concepts of "hardwired" functional pathways, evidence has emerged for functional reorganization (or "plasticity") in the adult CNS following injury (see, for example, Benecke et al., 1991; Chollet et al., 1991; Frackowiak, 1998). The basic underlying mechanisms underlying CNS plasticity and its role in recovery remain speculative. In animal studies, changes in the expression of presynaptic protein markers of axonal sprouting have been described local to a focal ischaemic lesion (Li et al., 1998); similar synaptic remodelling may also contribute to neurological recovery in humans.

In its most general sense, plasticity in the nervous system means a change in structure or function due to development, experience or injury; to be relevant to recovery, reorganization should occur in a pattern that may plausibly help to

compensate for the deficit induced by injury. A working definition of the concept of plasticity has been proposed by Frackowiak as a "long-term alteration in patterns of behaviour-related activity in distributed brain systems." (Frackowiak, 1998). This defines a phenomenon that can be investigated with functional imaging methods, which are able to map the distribution of cerebral activity during performance of a task involving appropriate brain systems after injury.

There are likely to be a number of general mechanisms involved in neurological recovery. Changes at the site of tissue injury may contribute, particularly in the very early stages, and include the resolution of inflammation and oedema, and the re-absorption of necrotic tissue. However, considerable recovery is often observed for months or years after CNS injury, a phenomenon not explicable by these acute local changes. Other processes occurring over a longer period must therefore contribute: in MS, for example, remyelination of damaged fibres may occur over weeks to months. However, restitution of function in MS and other neurological conditions may occur despite the destruction or degeneration of some of the axons in affected pathways. Recovery must therefore depend, at least in part, on adaptive changes in surviving components of either the damaged pathway, or other intact systems. Plasticity in this context implies that undamaged brain regions can somehow compensate by "taking over" the function of the damaged tissue. Proposed mechanisms include the strengthening or unmasking of existing functional connections (perhaps linked with bilateral cerebral representation of function); the formation of new connections; or the release of inhibition from cerebral areas local to, or remote from, the injury. For example, lost brain function due to a cortical injury might be engaged by tissue adjacent to the lesion, by areas in the unaffected hemisphere, or by connected

subcortical structures. To illustrate the concept of plasticity, and the way in which functional imaging may be used to investigate it, some of the evidence obtained following two types of CNS injury - motor stroke and spinal cord injury - will be discussed.

Motor stroke

Motor stroke is a common cause of neurological disability, often followed by a variable functional recovery, which has been widely studied with functional neuroimaging. A series of studies used PET to measure regional cerebral blood flow (rCBF) changes in patients who had recovered from a first hemiplegic stroke. On moving the recovered hand, a bilateral activation of motor cortices occurred, in contrast to the unilateral pattern observed for the unaffected hand (Chollet et al., 1991); this observation suggests that pathways between the affected limb and the ipsilateral motor cortex contribute to the recovery process. A number of possible confounding explanations of the observed result have been put forward, including the presence of involuntary 'mirror movements' of the unaffected hand when moving the recovered hand. Neurophysiological work has also cast doubt on the role of fast ipsilateral descending pathways in recovery (Palmer et al., 1992), although this does not exclude a contribution from slower, polysynaptic pathways. In a second paper, Weiller et al. (1992) compared recovered motor stroke patients with normal subjects, and reported a widespread increase in activation in areas including motor cortex ipsilateral to the hand performing the task, contralateral cerebellum, bilateral lower parietal cortex and insula in patients compared to controls. A third paper examined the individual patterns of activation in patients

compared to a group of 10 normal controls (Weiller et al., 1993) and found a large variability in the areas of significant activation differences between individuals and the control group. Bilateral motor cortex activation was observed in four patients (though these all exhibited involuntary synkinetic "mirror movements" of the unaffected arm). Another observation in this study was that of an expansion of the hand field of the normal contralateral motor cortex representation ventrally (i.e. toward the face area) in four patients with posterior capsular limb damage.

fMRI is a relatively recent technology, and at the time of writing there have been few published data on neurological recovery. One study (Cramer et al., 1997) demonstrated patterns of reorganization after hemiparetic stroke that were largely consistent with those seen with earlier PET studies, including activation contralateral to the deficit in unaffected hemisphere motor cortex, and in the ipsilateral cerebellum. This study noted that in general recovered finger tapping by patients activated similar motor regions to controls, but to a larger extent.

The role of changes in cerebral activation patterns in recovery is difficult to investigate. There is some experimental evidence that motor recovery from a small cortical infarct is associated with an expansion of representation of the affected hand into adjacent cortical areas, but only in the context of rehabilitative training (Nudo et al., 1996). An exciting direction for future functional imaging research will be to investigate the effect of rehabilitation on patterns of functional reorganization, and clinical recovery, following stroke in humans.

Spinal cord injury

Spinal cord injury may damage pathways ascending to or descending from the cerebrum, and the degree of functional recovery is variable. Alteration in input or output pathways might be expected to cause a functional reorganization of brain sensorimotor areas. A study using ^{18}F fluorodeoxyglucose PET (Roelcke et al., 1997) examined 11 patients with complete paraplegia or tetraplegia following spinal cord injury (between six months and 16 years prior to the study) and compared them to healthy controls. Reduced global cerebral metabolism was found in patients at rest, as expected from a loss of afferent and efferent cortical projections. However areas of increased glucose metabolism in brain regions involved in movement preparation or execution, including supplementary motor cortex, putamen and anterior cingulate cortex were seen, which were thought to reflect a release of inhibition to these areas. Another study investigated a single patient following a near-complete spinal cord transection sparing only a part of one anterolateral quadrant (Danziger et al., 1996), 18 years following the injury. The patient had retained some sensory functions classically believed to depend upon intact dorsal spinal cord pathways, including light touch and joint position sense. Furthermore, PET activation studies of vibration of the hand or foot showed a very abnormal pattern, with activation of cerebral areas beyond the usual somatotopic representations. The data from these studies suggest that injury to the spinal cord may cause a reorganization of the cortical areas connected with ascending or descending pathways, although the functional significance of these changes remains unclear.

These studies illustrate the following general points: firstly, functional imaging techniques are powerful tools with which to investigate plasticity or "functional reorganization" associated with recovery from CNS injury; secondly, the interpretation of the data may be complex due to factors including artefactual causes of altered activation patterns and the heterogeneity of response between individuals; and thirdly, the contribution of altered activation patterns to neurological recovery may be difficult to establish.

Recovery in demyelinating disease

The remarkable capacity for full recovery is a hallmark of relapses in the early stages of MS. The mechanisms have been discussed in detail in chapter 1, but will briefly be reiterated here. In the acute phase, contributory factors include the resolution of oedema and inflammation and the release of conduction block (Youl et al., 1991). However, a slower process of recovery continues in spite of persistent structural damage to myelinated axons in affected pathways. Part of the explanation may be that functional conduction can be restored in persistently demyelinated axons (McDonald et al., 1976; Smith et al., 1994), probably due to changes in the distribution and concentration of ionic sodium channels.

Nevertheless, recovery of function after demyelination may occur despite persistent significant axonal degeneration or conduction disturbance in the affected pathway. In patients following an excellent recovery from optic neuritis, atrophy of the retinal nerve fibre layer (MacFayden et al., 1988; Steel and Waldock, 1998), and persistent VEP delay (Halliday et al., 1972) are frequent. In certain peripheral demyelinating neuropathies, clinical recovery may also occur

despite enduring neurophysiological evidence of conduction block (McLeod, 1981; Lewis et al., 1982).

Experimental studies provide further evidence for functional recovery despite axonal loss in eloquent pathways (see chapter 1). Jacobson et al. (1979) describe a delayed phase of visual recovery following experimental optic neuropathy, despite extensive destruction of fibres in the affected nerves. In the absence of regeneration or remyelination of fibres traversing the experimental lesion (Eames et al., 1977) these data raise the possibility that adaptive synaptic changes in the brain (or retina) may contribute to the slow phase of visual recovery after optic neuritis. Since axonal loss probably occurs to some extent in the majority of MS lesions, regardless of their location (Adams and Kublik, 1952) or the stage of disease (Trapp et al., 1998), compensatory plastic changes may also contribute to the recovery from lesions in other systems, for example in corticospinal pathways.

Hypothesis

The data discussed in the previous section suggest that local changes in a demyelinated pathway cannot fully account for the temporal pattern and extent of functional recovery commonly observed. In the absence of significant functionally effective regeneration, recovery, despite persistent conduction block or axonal loss, may depend on adaptive changes in the cerebral cortex or surviving pathways. With functional neuroimaging, it is now possible to begin to investigate this possibility. As a first step, we have generated a hypothesis that is testable using functional magnetic resonance imaging:

Following an episode of demyelination in an eloquent CNS pathway, the pattern of activation of the brain induced by a task involving that pathway is different from that induced by a task involving a comparable, unaffected pathway.

3.2 Methodological considerations

Study design: problems

Patient selection

Testing the formulated hypothesis presents considerable difficulties in MS, in which lesions are disseminated throughout the cerebral white matter. Lesions may have functional effects upon the pathways in which they are located, but more often are clinically silent. Furthermore, lesions may influence remote cerebral areas if they disrupt connecting fibre pathways (the phenomenon of *diaschisis*). Remote dysfunction may occur if lesions interrupt connections, between cortical and subcortical structures or between the cerebral hemispheres. There is evidence from PET that MS patients have a general disturbance of cerebral neuronal metabolism, and that lesions can indeed cause diaschisis (Brooks et al., 1984; Pozzilli et al., 1992; Blinkenberg et al., 1996; Bakshi et al., 1998). Thus, in a patient with disseminated disease it will be difficult (if not impossible) firstly, to state with certainty, which lesion is responsible for a given clinical deficit; and secondly, to anticipate what effects multiple lesions will have upon the fMRI activation pattern. Furthermore, widespread disturbances of blood flow and volume, which may affect the BOLD response, have been reported in patients with inflammatory CNS disease associated with HIV infection (Tracey et al., 1998) and

may also be relevant in MS. These considerations have implications for designing a functional imaging experiment with which to investigate mechanisms of recovery following demyelination.

The hypothesis put forward requires the demonstration of a different brain activation pattern in response to a task involving an affected, in comparison to an unaffected, eloquent pathway. To test this, patients following or during recovery from demyelination in the pathway under consideration may be studied. The activation pattern induced by repeated trials of a stimulus or task involving the affected pathway can then be compared to the pattern obtained from an unaffected contralateral pathway (if available), and to an equivalent pathway in control subjects. However, the presence of multiple lesions is likely to make the detection of differences due to a specific pathway lesion between patients and controls more difficult due to complex effects on both local and remote cerebral function.

Technical considerations

The use of fMRI as a clinical research tool, although developing at a rapid rate, remains limited compared with its use in studying brain function in healthy individuals. For this preliminary study, the specific problems to address were: firstly, the development of a simple experimental paradigm allowing selective testing of affected and unaffected pathways in patients and controls; secondly, the acquisition of data allowing the reliable detection of BOLD contrast; and thirdly, the analysis of data with the objective of constructing activation maps for each experiment (i.e. affected or unaffected pathways) in standard anatomical space.

Study design: solutions

Patient selection

In the earliest disease stages of MS, patients often present with clinically isolated syndromes suggestive of demyelination (Miller et al., 1989). In these cases, the likelihood of identifying which lesion is responsible for a particular symptom is much higher than for patients with established disease. Such isolated syndromes include spinal cord or brainstem disturbances, and optic neuritis. Brain MRI may or may not show evidence of disease outside the clinically affected pathway in these patients (Miller et al., 1989b), a finding which indicates an increased likelihood of developing MS (chapter 1).

Optic neuritis is of particular value in the investigation of adaptive responses to focal demyelination for the following reasons. Firstly, optic neuritis has a characteristic pattern of clinical evolution: typically, unilateral visual loss (often accompanied by pain on eye movement) progresses over hours to several days, reaching its nadir within a week with subsequent recovery to normal or near normal visual acuity by about two months. Secondly, visual function is readily evaluated using simple bedside clinical tests (e.g. visual fields, acuity and colour appreciation). Thirdly, it is possible to assess conduction through the lesion using electrophysiological measures derived from the VEP (Halliday et al., 1972). Finally, the clinically unaffected nerve may also be investigated for comparison, with the proviso that clinically silent demyelination as indicated by a delayed VEP (Halliday et al., 1972) is well documented.

For this initial study patients were selected from a cohort originally recruited as part of a study of patients presenting with clinically isolated syndromes suggestive of demyelination (O'Riordan et al., 1998). Essential criteria for inclusion were a full recovery from a single episode of clinically unilateral optic neuritis, and the absence of clinical or MRI evidence of disease elsewhere in the CNS. Thus, the confounding effects of multiple disseminated lesions in the brain were avoided, allowing the fMRI results to be more easily interpreted. By studying a group of such patients it should be possible to investigate the effects of a single demyelinating lesion located in the optic nerve upon the cerebral activation pattern induced by a visual stimulus, by comparing it to that induced by stimulating the contralateral optic nerve, and to control subjects.

Technical considerations

Development of a simple visual stimulation paradigm. Choice of experimental design is particularly important in a clinical setting since patients may have neurological impairment that makes complex designs more difficult to implement. Although the patient group included in this study (following a single episode of demyelinating optic neuritis) do *not* have marked visual impairment, a simple apparatus was nevertheless used, consisting of a pair of goggles in which each eyepiece contains a matrix of nine red light-emitting diodes (LEDs) (Grass Instruments Model S10VSB, Quincy, MA). The LEDs can be flashed at different rates to provide a powerful, homogeneous visual stimulus to the whole visual field of one or both eyes. Many studies employing this apparatus have reported robust activation of visual cortical areas in healthy subjects (see, for example, Belliveau

et al., 1991; Kwong et al., 1992; Ogawa et al., 1992) and in a range of clinical settings including albinism (Hedera et al., 1993), schizophrenia (Renshaw et al., 1994; Howard et al., 1995) and MS (Rombouts et al., 1998). A flash frequency of 8Hz was used; the peak BOLD signal has been shown to occur at this frequency (Thomas and Menon, 1998), in agreement with PET studies of regional blood flow (Fox and Raichle, 1995).

Most previous studies using flash stimulation have used a binocular stimulus. For the present study a monocular visual stimulus was chosen in order to allow selective stimulation of the clinically affected optic nerve, thus allowing a comparison of activation patterns between the affected and unaffected eyes in patients, and between patient affected eyes and unaffected control eyes. A block design was used, in which epochs of monocular stimulus alternated with no stimulus. Since the goggles are lightproof (or nearly so), the baseline condition is binocular darkness. This was further ensured by dimming all non-essential lights within the scanner room during the experiments.

An epoch length of 20 seconds was used to allow the fMRI signal to peak and stabilize following the haemodynamic lag of 5-8 seconds (see chapter 2). The epoch length must be sufficiently long to allow the BOLD response to return to its baseline level after cessation of the stimulus, otherwise no modulation of the BOLD response by the stimulus can be detected (Thomas and Menon, 1998). Using a similar photic stimulus, Thomas and Menon showed that the shortest epoch length at which modulation of the haemodynamic response could still be detected was approximately seven seconds. Before the patient study was commenced, a pilot study (in 15 healthy volunteers) was performed to ensure that the stimulus apparatus and the BOLD fMRI sequence were functioning

appropriately, and that reliable activation was detectable in the visual cortex. Acquisition parameters were chosen in order to provide consistent activation in striate visual cortex using a monocular stimulus, with a minimum of noise.

Image acquisition. A standard gradient-echo EPI sequence similar to that previously used in other laboratories was used. An echo time close to the expected T2* of brain tissue (TE=40ms) was chosen to maximize the BOLD response in capillaries compared to larger vessels, with a relatively long repetition time to minimize flow effects (TR=4000ms). The matrix size was 96x96 (reconstructed as 128x128), with a field of view of 240x240mm, giving an in-plane resolution of 2.5mm x 2.5mm (1.9x1.9mm after reconstruction). This sequence gave adequate signal-to-noise ratio (SNR) to provide reliable activation in pilot studies in normal subjects. Ten 5mm axial slices (interslice gap 0.5mm) through visual cortical areas were acquired, providing approximately 60% brain coverage. Whole brain fMRI coverage was not possible at the time of scanning due to limited data storage availability. In order to map the partial brain fMRI data into a standard space to allow group activation maps to be constructed, a high resolution, whole brain, anatomical dataset was also acquired. An EPI sequence was used with similar geometric distortions to the fMRI data. The advantages of matching the geometric distortions of functional and anatomical images are discussed in detail in chapter 5. Further details of the mapping procedure are given in the following methods section.

3.3 Recovery from optic neuritis is associated with a change in the distribution of cerebral response to visual stimulation: a functional MRI study

Introduction

A group of patients who had made an excellent recovery from a single episode of unilateral optic neuritis, without evidence of disease elsewhere in the CNS, were studied using functional MRI. The objective was to investigate the pattern of cerebral response to a simple visual stimulus in this group of patients in comparison to normal individuals.

Patients and Methods

Subjects

Seven patients (mean age 37.8 years; 3 male, 4 female) were studied who had attended The National Hospital for Neurology and Neurosurgery or The Moorfields Eye Hospital with a single episode of typical, strictly unilateral, acute optic neuritis diagnosed according to standard criteria (Compston et al., 1978), and who had made a good recovery. Patients with any abnormalities on brain MRI were excluded (see previous section). Seven normal volunteers (mean age 31.0 years; 3 male, 4 female) were also studied. All subjects gave informed written consent. The study was approved by the National Hospital and Institute of Neurology ethics committee.

Clinical evaluation

All patients had been evaluated by a consultant neurophthalmologist at their original presentation; four of seven had undergone whole field VEP recordings. On the day of the fMRI study, visual acuity was measured using the Snellen chart and colour vision was assessed using Ishihara colour plates. Whole field VEP recordings were performed using pattern-reversal as described elsewhere (Brusa et al., 1995).

Imaging

Structural MRI. Gradient echo EPI MR images were acquired using a 1.5 Tesla GE Signa Horizon Echospeed system (General Electric, Milwaukee, Wisconsin, United States) using a standard quadrature head coil. This system was used for all subsequent studies described in this thesis. Multishot, high resolution mildly T2-weighted EPI near-axial images of the whole brain were obtained (TR=6000ms, TE=40ms, matrix 256x256, FOV 24cm), together with high resolution fat-suppressed spin echo images of the optic nerves (FSE 3250/68, matrix 512x512, FOV 20cm) (Gass et al., 1995). The structural MRI brain and optic nerve scans were evaluated for any abnormalities by a neuroradiologist (with blinding to clinical details).

Functional MRI. 120 T2*-weighted single-shot EPI images depicting blood oxygenation level dependent (BOLD) contrast were acquired in each 8 minute experiment at each of 10 near-axial non-contiguous 5mm thick slices through visual cortex approximately parallel to the AC-PC line: sequence parameters as

determined during the pilot study (see above).

Experimental Design

Subjects passively viewed visual stimuli which alternated periodically between 20 second epochs of two contrasting conditions: (ON) red 8Hz photic stimulation to the whole visual field was presented to one eye using the lightproof goggles whilst the other eye received no visual stimulation; (OFF) no visual stimulation (darkness) was presented to both eyes. In total, 12 cycles of alternation between the ON and OFF conditions were presented over the course of each experiment; condition OFF (no stimulation) was always presented first. Each subject was studied once for each side of monocular stimulation; the order of experiments was randomly decided.

Analysis

Detailed descriptions of the analysis methods used in this study are provided elsewhere (Bullmore et al., 1996a; Bullmore et al., 1996b; Brammer et al., 1997), but the essential steps are now summarized as follows.

Motion correction and realignment. Images were corrected for head motion prior to time series analysis. This procedure consists of generating a "base" image volume of mean signal intensity, by averaging the 120 images acquired in each plane. The sum of differences in grey-scale values between each "match" image volume and the base image volume was computed, and the translations and

rotations in three dimensions that minimized these differences estimated. The match volumes were then realigned to the base volume by tricubic spline interpolation. A spin history correction (see chapter 2) was applied at each voxel (Friston et al., 1996).

Detecting activation. The next stage of analysis determined the power of experimentally determined signal change at the frequency of alternation between ON and OFF conditions. In order to do this, a model of expected data behaviour is compared with a model under the null hypothesis that there is no experimentally determined effect. The motion-corrected time-series $\{Y_t\}$, t = 1,2,3..., 120 images, observed at each image voxel, was modelled by:

$$Y_t = \gamma \sin(\omega t) + \delta \cos(\omega t) + \gamma' \sin(2\omega t) + \delta' \cos(2\omega t) + \gamma'' \sin(3\omega t) + \delta'' \cos(3\omega t) + \alpha + \beta t + \varepsilon_t$$

This model includes a combination of sine and cosine waves (i.e. phase-shifted sine waves) at the fundamental frequency of ON-OFF alternation and at its first and second harmonic frequencies (Bullmore et al., 1996b), parameterized by coefficients γ and δ respectively. Here Y_t is the T2*-weighted signal intensity value for each time point; ω is the (fundamental) frequency of alternation between ON and OFF conditions; $\alpha + \beta t$ is a (nuisance) linear trend and ε_t is the residual error at time point t. The phase of periodic response was estimated from the sinusoidal regression coefficients used in the model (phase, $\phi = \delta/\gamma$).

This sinusoidal regression model was fitted to the observed data at each voxel by the method of pseudogeneralized least squares.[1] The power of experimentally determined response was computed as the fundamental power quotient (FPQ) - a measure of the power of periodic response at each voxel, divided by its standard error (see Bullmore et al., 1996b) - allowing a map of the FPQ at each intracerebral voxel of the observed data to be constructed. To determine the FPQ distribution under the null hypothesis (i.e. that the observed data are not determined by experimental design) the time series images were randomly permuted 10 times. The FPQ was then calculated at each intracerebral voxel exactly as before, and its distribution determined from all voxels and all permutations. (The FPQ distributions obtained in this way have been shown to be indistinguishable from data collected when the null hypothesis is known to be true, e.g. when no periodic task or stimulus was undertaken [Bullmore et al., 1996b]). If the observed FPQ at a voxel exceeded the $(100-\alpha)^{th}$ percentile of the randomized distribution of FPQ values then the null hypothesis was refuted by a one-tailed test at that voxel with probability of Type I error = α. Voxel locations at which the null hypothesis was refuted were coloured and overlaid upon the individual subject's high resolution image to form an individual brain activation map, or IBAM.

Measuring activated volumes. The area of activation in the occipital visual cortex was determined by outlining all activated clusters on the IBAM using a semi-automated contouring technique. Clusters of a single voxel were not included to improve the presumed biological significance of activations (Forman et al., 1995).

[1] Pseudogeneralized least squares is a model fitting technique used in preference to ordinary least squares (which may be spuriously influenced by autocorrelation in the fMRI time series.)

The borders of V1 were not formally defined, but the region selected included only occipital cortex up to the anterior border of the temporo-occipital junction (approximate Brodmann areas 17, 18, 19). The activated areas for each slice were then summed and multiplied by the slice thickness to give a total activated volume (referred to for the remainder of this chapter as occipital activation) in response to stimulation of each eye. The area of activation outside this region (referred to in the remainder of this chapter as extra-occipital activation) was also calculated in a similar way. To make comparison of data between patients and controls easier the relative activated volume (V_{REL}) in each experiment was expressed as a fraction of the average activation observed in the control group for the appropriate eye (i.e. left or right) (Rombouts et al., 1998). This gives a simple quantitative estimate of the extent to which each experimental activated volume differs from the average result in our control population.

Mapping data into stereotactic space. To allow the combination of data from individuals and to perform between-group comparisons, the observed and permuted FPQ maps were relocated into standard space (Talairach and Tournoux, 1988). The structural EPI dataset (covering the whole brain) was rescaled by linear interpolation to the same voxel dimensions as the functional BOLD volume acquired at each time point. The intensity of the rescaled structural image was then histogram matched to the "base" functional image volume. The rotations, translations and linear rescaling factors required to minimize the grey scale differences between the structural and functional datasets were then derived. The same processing steps were used to minimize the grey-scale differences between the structural dataset and a template in standard space created by transforming the

high resolution structural datasets from a group of healthy subjects into this space using AFNI software (Cox, 1995) and then averaging all of the images. The transformations defining the previous two steps (i.e. structural to functional, and structural to standard space) were then sequentially applied to the observed and randomized FPQ maps, and the FPQ values written to new locations in standard space by nearest-neighbour interpolation. All maps were smoothed by a two dimensional Gaussian filter with full width at half maximum (FWHM) = 5mm, to accommodate error in estimation of transformation parameters and individual variability in sulco-gyral anatomy.

At every voxel where the FPQ maps overlapped sufficiently well, the median observed and randomized FPQs were computed. The median statistic was chosen in preference to the mean in order to minimize the effect of outlier observations (a potential problem when using a small number of subjects). If the observed median at a voxel exceeded the $(100-\alpha)^{th}$ percentile of the randomized distribution of median FPQ then the null hypothesis was refuted by a one-tailed test at that voxel with probability of Type I error = α. Voxel locations at which the null hypothesis was refuted were coloured and overlaid upon the Talairach template derived from the subjects individual high resolution images to form a generic brain activation map, or GBAM.

The power of periodic response was compared between groups and between eyes within group by analysis of variance (ANOVA). The following one-way ANOVA model was fitted at each intracerebral voxel in standard space:

$$FPQ = \mu + \beta \cdot F + \varepsilon$$

where FPQ is the fundamental power quotient, μ is the overall mean power at the i^{th} voxel, F is a factor coding group membership (patient or control) or stimulated eye (right or left), and ε is an error. The coefficient β was tested by permutation at those voxels that were generically activated in one or both of the groups of data being compared. For these analyses, we set the two-tailed probability of false positive error $p=0.05$. This relatively lenient threshold is justified by the restricted search volume for between-group comparisons.

The relationship between extent of abnormal (extra-occipital) activation and VEP evidence for persistently delayed optic nerve conduction was also investigated in the patients. The correlation between the volume of extraoccipital brain activation and VEP latency was assessed by a scatter plot and significance test of Spearman's correlation coefficient.

Results

The patient characteristics are shown in Table 3.1. All patients had a typical clinical history of strictly unilateral acute optic neuritis with documented loss of visual acuity at presentation (between 0.5 and 14 years [mean 8 years] previously), and by the time of our study had recovered normal visual acuity and colour vision. All had normal eye movements, and were able to fixate normally during formal visual field perimetry. Four patients had VEP recordings at presentation; three were abnormal (two were delayed and one absent). All patients had VEP recordings at the time of our study. The three previously abnormal VEPs now had normal latencies; two of the remaining three cases (with shorter clinical histories) had delayed responses. MRI of the affected optic nerve was abnormal in five of

the seven cases (e.g. Fig. 3.1).

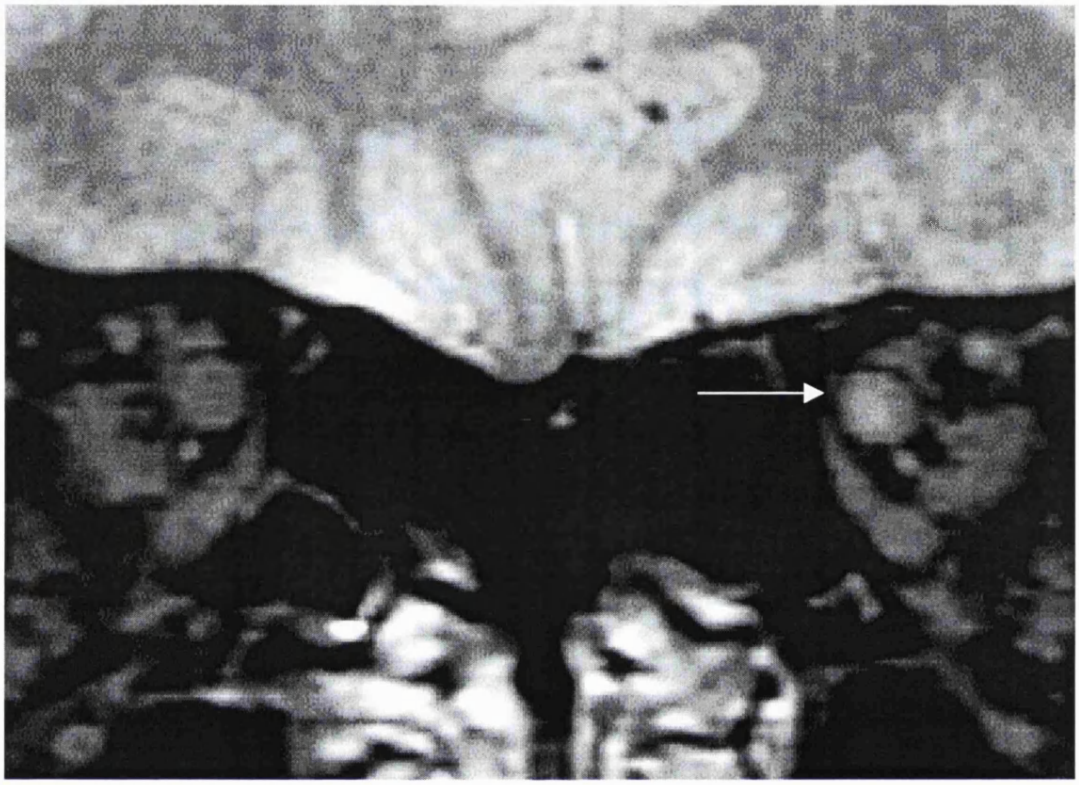

Fig. 3.1. Coronal MRI scan through the optic nerves in a patient following a single episode of left unilateral optic neuritis 14 years previously. Note the abnormal high signal in the affected nerve (*right of panel, arrowed*), indicating persisting structural abnormality despite the excellent clinical recovery observed.

Table 3.1: Characteristics of patients

Age	Sex	Years from diagnosis	Side of affected eye	Worst Documented visual acuity	MRI brain	Acuity on day of study R	Acuity on day of study L	Colour vision on day of study R	Colour vision on day of study L	MRI optic nerves	VEP latency at presentation (ms) Affected	VEP latency at presentation (ms) Unaffected	VEP latency at follow up (ms) Affected	VEP latency at follow up (ms) Unaffected
38	F	14	R	6/9	Normal	6/5	6/5	17/17	17/17	Abnormal (R)	119.0	108.0	101.1	97.1
49	M	13	L	6/36	Normal	6/5	6/5	17/17	16/17	Normal	114.0	112.5	103.1	101.6
31	M	0.5	L	6/18	Normal	6/5-2	6/5-2	17/17	15/17	Abnormal (L)	ND	ND	121.5	102.6
33	F	12	L	6/60	Normal	6/4	6/4	16/17	15/17	Abnormal(L)	147.0	106.0	99.6	98.6
35	M	3	L	6/24	Normal	6/5-2	6/6	16/17	15/17	Abnormal (L)	ND	ND	118.6	103.3
34	M	1	L	NPL	Normal	6/4	6/5	17/17	16/17	Normal	ND	ND	97.2	96.2
45	F	12	L	CF	Normal	6/5	6/5	17/17	15/17	Abnormal (L)	No pattern	107.0	98.1	96.6

NPL = no perception of light; CF = counting fingers; ND = not done

Acuity = smallest type seen on the Snellen chart, Colour vision = number of Ishihara plates correctly identified

Individual subject activation map analysis

The activated volumes in occipital and extra-occipital areas for patients and controls are shown in Tables 3.2 and 3.3, respectively.

Occipital visual cortex. All subjects studied activated the visual cortex in response to monocular stimulation of either eye. Six of seven controls showed greater activation on stimulation of the right compared to the left eye. Four of seven patients (all with left optic neuritis) showed greater activation on stimulating the unaffected (right) eye than the affected (left) eye. Patients tended to have smaller volumes of occipital activation than controls for both affected and unaffected eyes. The volume of occipital cortex activated in patients was lower than the control mean (i.e. $V_{REL} < 1.0$) for both eyes (affected and unaffected) in four of seven subjects, for the affected eye only in two subjects, and for neither eye in one subject. The affected eye on average showed a greater reduction in occipital activated volume (average $V_{REL} = 0.78$) than the unaffected eye (average $V_{REL} = 0.90$).

Extra-occipital areas. All patients showed extra-occipital activation on stimulation of the affected and unaffected eyes; in five, this extra-occipital activation was greater than the control mean volume for both affected and unaffected eyes. The extent of extra-occipital activation was much greater for the affected eye (mean $V_{REL}=7.1$) than the unaffected eye (mean $V_{REL}=1.53$).

Table 3.2. *Occipital activation volumes from individual activation maps in patients and controls*

	PATIENTS				CONTROLS			
	Affected eye volume (side) /cm^3	V_{REL}	*Unaffected eye volume /cm^3*	V_{REL}	*Right eye volume /cm^3*	V_{REL}	*Left eye volume /cm^3*	V_{REL}
	23.1 (R)	0.91	19.8	1.13	12.8	0.50	9.2	0.53
	3.1 (L)	0.22	6.1	0.23	34.2	1.34	17.8	1.02
	14.1 (L)	0.81	8.8	0.34	40.8	1.60	24.6	1.41
	11.8 (L)	0.68	3.6	0.14	36.4	1.43	31.2	1.79
	30.1 (L)	1.73	68.8	2.70	0.5	0.02	15.7	0.90
	14.1 (L)	0.81	18.4	0.72	30.9	1.21	15.9	0.91
	17.1 (L)	0.98	32.4	1.27	23.2	0.91	7.4	0.43
Mean	**14.3**	**0.78**	**25.1**	**0.90**	**25.5**	**1.00**	**17.4**	**1.00**

$$V_{REL} = \frac{\text{Volume of activation}}{\text{Volume of activation (matched control eye mean)}}$$

Table 3.3. *Extra-occipital activation volumes from individual maps in patients and controls*

	PATIENTS				CONTROLS			
	Affected eye volume (side) /cm^3	V_{REL}	*Unaffected eye volume /cm^3*	V_{REL}	*Right eye volume /cm^3*	V_{REL}	*Left eye volume/cm^3*	V_{REL}
	0.2 (R)	0.06	0.2	0.19	0	0	0	0
	5.3 (L)	5.14	13.6	4.25	0.50	0.16	0.64	0.62
	22.8 (L)	22.1	8.2	2.56	8.5	2.66	4.94	4.80
	15.6 (L)	15.1	3.5	1.09	0.62	0.19	0.71	0.69
	10.1 (L)	9.81	6.0	1.88	0	0	0	0
	4.8 (L)	4.66	4.0	1.25	7.8	2.43	0.9	0.87
	0.2 (L)	0.19	0	0	4.9	1.53	0	0
Mean	**7.4**	**7.1**	**5.1**	**1.53**	**3.2**	**1.00**	**1.03**	**1.00**

$$V_{REL} = \frac{\text{Volume of activation}}{\text{Volume of activation (matched control eye mean)}}$$

Four of seven controls showed extra-occipital activation in response to both right and left eye stimulation, one to right eye stimulation only, but this activation was much less extensive than in the patients.

Two general observations can be made from this analysis: firstly, patients showed less occipital activation than controls, particularly during stimulation of their affected eyes; and secondly, patients showed more extra-occipital activation than controls, again to a greater extent during stimulation of the affected eye. The individual map analyses presented in Tables 3.2 and 3.3 emphasize the variability in individual responses in patients and control subjects.

Generic Brain Activation maps

There were no significant differences between the control and patient groups in stimulus correlated motion during the fMRI studies, which was estimated by the power of a periodic trend at the frequency of AB alternation in the time series of rotations and translations of the head in three dimensions (Bullmore et al., 1999). Selected slices from generic brain activation maps (Brammer et al., 1997) for patients and control subjects are shown in Fig. 3.2. Coordinates of the main foci of activation in standard space (Talairach and Tournoux, 1988), cluster sizes and FPQ values are given in Table 3.4.

In controls (Fig. 3.2A and 3.2B), stimulation of either eye induced activation almost exclusively in visual cortex (approximate Brodmann areas (BA) 17,18 and 19). A visual impression of asymmetry in response between left and right eyes was investigated using a repeated measures one-way ANOVA thresholded at $p<0.05$ (Fig. 3.3).

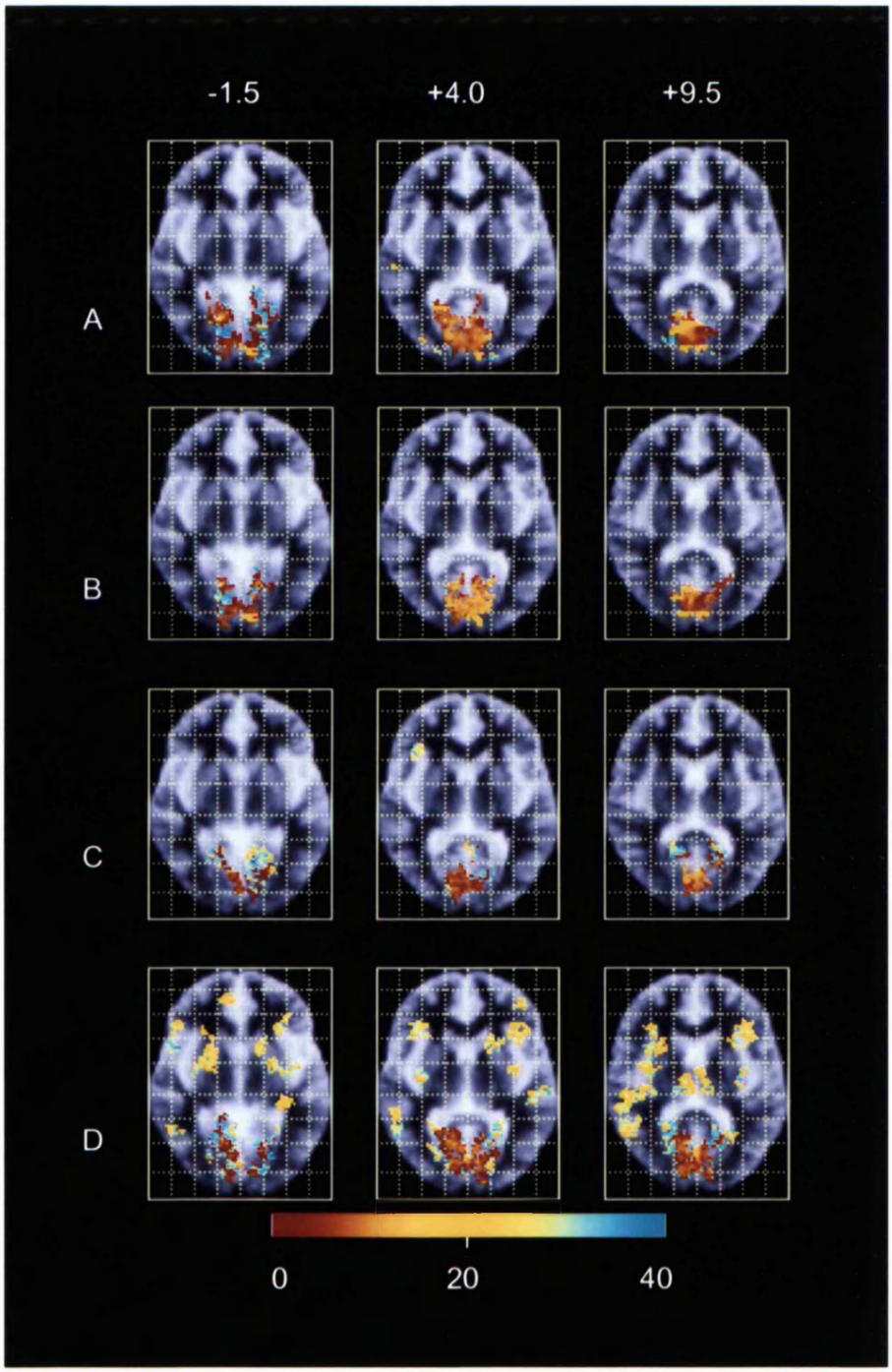

Fig. 3.2 Generic brain activation maps from seven control subjects and seven patients following optic neuritis, showing areas of significant response to monocular photic stimulation compared with binocular darkness. The one-tailed probability of false positive activation $p < 0.0001$ for each voxel; activated voxels are colour coded according to the delay (in seconds) of periodic response relative to the onset of photic stimulation. The left side of each map represents the right side of the brain; z coordinates in standard space are given for each slice in mm (top of figure). **(A)** Controls (left eye); **(B)** Controls (right eye); **(C)** Patients (unaffected eye); **(D)** Patients (affected eye).

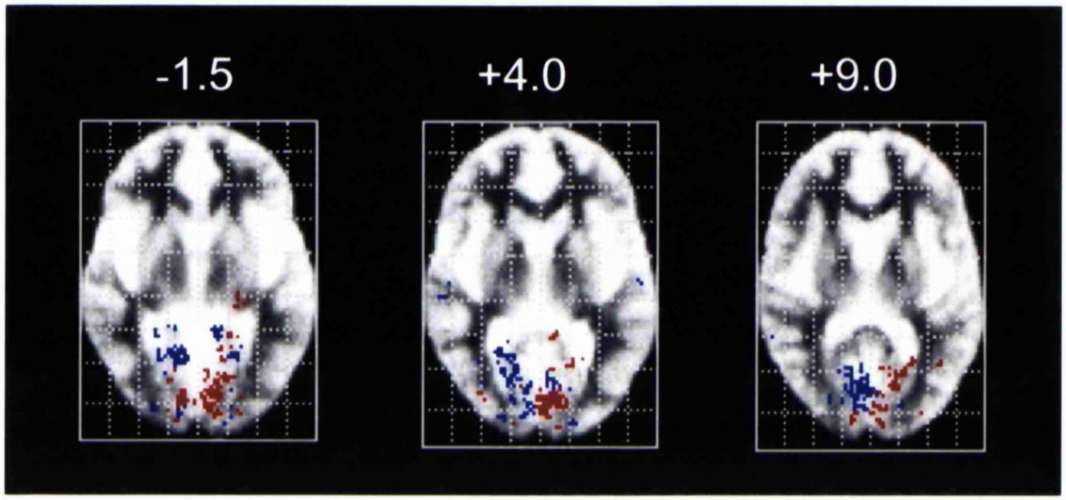

Fig. 3.3. Repeated measures one-way ANOVA comparing periodic right eye monocular stimulation in controls (n=7) with periodic left eye monocular stimulation in controls (n=7). Coloured voxels indicate regions in which the power of response differs between the two experiments. Left eye > right eye (blue) = 293 voxels; right eye > left eye (red) = 245 voxels. Search volume = 1197 voxels, $p>0.05$. Talairaich *z* co-ordinates are shown (mm) at the top of the figure. The right side of the brain is on the left side of each panel.

Table 3.4. *Main areas of activation in generic brain activation maps for patients and controls.*

(a) Control subjects - left eye stmulation Talairach coordinates (mm)

Area of activation	Brodmann area (BA)	x	y	z	FPQ[2]	Cluster size (voxels)
Visual cortex	17,18,19	+11	-65	+4	10.4	253
Visual cortex	17	+9	-63	+9	13.8	177
Visual cortex	18,19	-13	-56	-2	6.2	99
Visual cortex	17,18	+11	-82	-2	8.1	143
Visual cortex	17,18	+6	-68	+15	7.6	104
Visual cortex	19	-9	-70	-2	5.7	67

(b) Control subjects - right eye stimulation Talairach coordinates (mm)

Area of activation	Brodmann area (BA)	x	y	z	FPQ	Cluster size (voxels)
Visual cortex	17,18,19	-11	-72	-2	10.6	257
Visual cortex	17,18	-9	-72	+4	13.9	230
Visual cortex	18,19	-2	-74	+9	7.8	175
Visual cortex	17,18	0	-75	+15	6.7	53
Visual cortex	17,18	-17	-65	-7	5.8	49
Visual cortex	19	+17	-58	-7	7.2	33

[2] FPQ is the fundamental power quotient, a measure of the power of periodic response to the stimulus for each cluster.

Table 3.4 */continued*

(c) Optic neuritis - unaffected eye stimulation Talairach coordinates (mm)

Area of activation	Brodmann area (BA)	x	y	z	FPQ	Cluster size (voxels)
Visual cortex	17,18	0	-74	+4	10.5	195
Visual cortex	17,18	-17	-67	-2	5.6	160
Visual cortex	17,18	-11	-60	+15	7.0	121
Visual cortex	18,19	-15	-58	-7	5.6	94
Visual cortex	17	0	-74	+9	6.4	92
Visual cortex	17,18	0	-75	-2	8.6	91
Visual cortex	18	-15	-60	+9	5.8	56
Visual cortex	19	-19	-51	-13	4.5	37
Visual cortex	19	+17	-53	-13	4.1	25
Visual cortex	18	-2	-74	+20	5.0	23
Insula	14-16	+36	+28	+4	3.5	21

Table 3.4 */continued*

(d) Optic neuritis - affected eye stimulation Talairach coordinates (mm)

Area of activation	Brodmann area (BA)	x	y	z	FPQ	Cluster size (voxels)
Visual cortex	17,18	+8	-58	+4	7.0	371
Visual cortex	17,18	+13	-56	+9	7.8	329
Visual cortex	18	0	-72	+15	5.6	219
Visual cortex	18	+4	-77	-2	5.3	193
Visual cortex	18	+11	-61	-7	4.0	129
Visual cortex	18,19	-13	-60	-7	4.3	106
Visual cortex	18	+6	-74	+9	5.5	95
Insula-claustrum	14-16	+32	+2	+15	3.5	78
Insula-claustrum	14-16	+26	+11	+9	3.8	75
Insula-claustrum	14-16	-36	+28	+9	3.8	71
Insula-claustrum	14-16	-42	+23	+4	3.6	47
Insula-claustrum	14-16	-38	-4	-2	3.2	46
Insula / corpus striatum	14-16	+23	+12	-2	4.2	79
Corpus striatum	-	+11	+18	+15	4.2	123
Corpus striatum	-	-32	+21	+15	4.3	80
Lateral temporal cortex	21,22	+49	-23	+9	3.7	81
Lateral temporal cortex	21,22	55	-47	+9	3.7	50
Lateral temporal cortex	21,22	53	-35	+4	3.7	44
Posterior parietal cortex	40	45	-19	+20	3.5	66
Posterior parietal cortex	40	-47	-23	+20	4.1	63
Orbitofrontal cortex	11	55	+11	+15	3.6	63
Thalamus	-	+8	-11	+9	4.5	43

Stimulating the clinically unaffected eye in patients induced additional activation in the right insula-claustrum (BA 14) (Figure 3.2C). To confirm that this apparent visual difference between the group activation maps was of statistical significance, a one-way ANOVA comparing the generic map for the patient unaffected eyes with the generic map for the control right eye studies was performed (Figure 3.4; Table 3.5). (Only the six patients with a left optic neuritis were included, to remove possible confounding effects of fMRI activation asymmetry during monocular stimulation). This comparison confirmed increased activation in the right insula-claustrum region in patients compared to controls, but also showed a significantly larger response in visual cortex (approximate BA 17,18,19) in controls.

In response to stimulating the recovered eye, additional extensive activations were observed bilaterally in the insula-claustrum (BA14, 15, 16), lateral temporal cortex (BA 21,22), posterior parietal cortex (BA 39,40), orbitofrontal cortex (BA 11), corpus striatum and thalamus (Figure 3.2D). A one-way ANOVA comparison between the affected eye generic activation maps (again including only the six individuals with a left optic neuritis) and the left eye maps from controls, confirmed greater activation in patients in the orbitofrontal cortex, anterior insula bilaterally, and the corpus striatum (Figure 3.4; Table 3.6). Significantly greater power of response was observed in visual cortical areas (approximate BA 17, 18, 19) in controls.

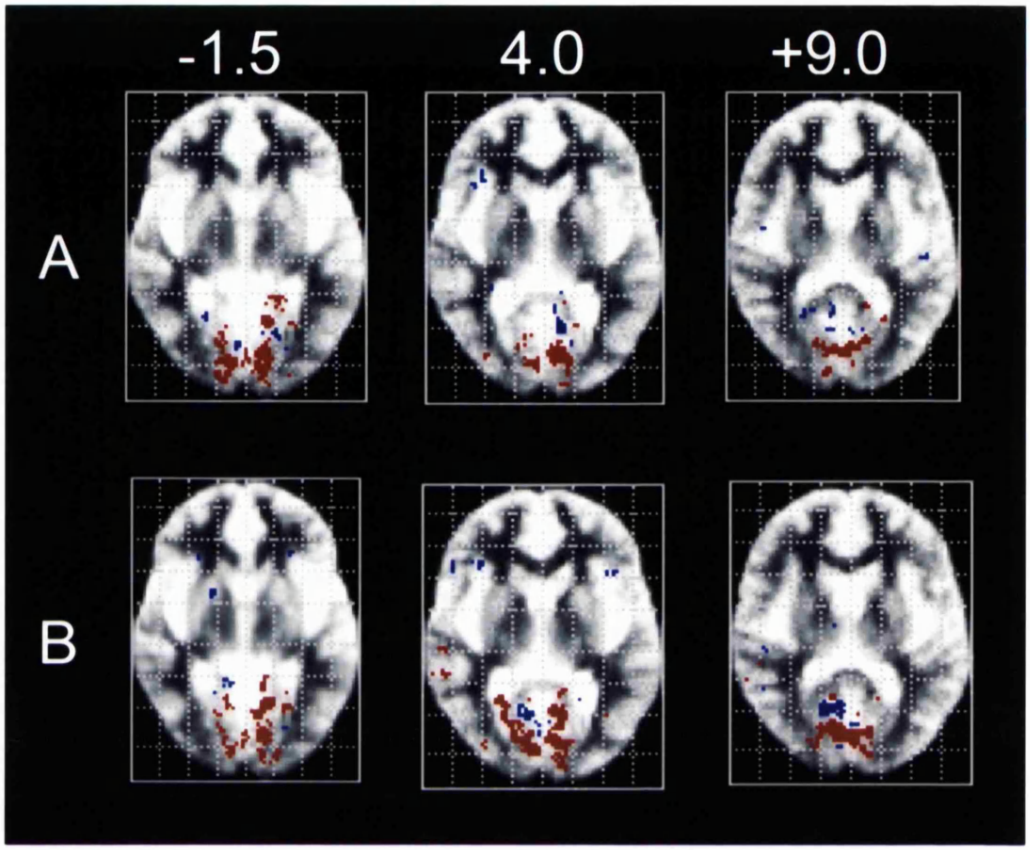

Fig. 3.4. (A) One-way ANOVA comparing the generic activation map for patient unaffected right eye stimulation (n=6) with control right eye stimulation (n=7). Coloured voxels show a different power of response between the two experiments. Patients > controls (blue) =125 voxels; controls > patients (red) = 305 voxels. Search volume = 1476 voxels, $p<0.05$.**(B)** One-way ANOVA comparing the generic activation map for patient affected left eye stimulation (n=6) with control left eye stimulation (n=7). Patients > controls (blue) = 125 voxels; controls > patients (red) = 424 voxels. Search volume = 2471 voxels, $p<0.05$.

Table 3.5. *One-way ANOVA comparison between generic brain activation maps for stimulation of the unaffected eye in patients following left optic neuritis, and the right eye in controls.*

Areas of significantly greater response in patients	Talairach co-ordinates		
	Approx. BA	x (mm)	y (mm)	z (mm)
Right anterior insula	14-16	-35	+28	+4
Right visual cortex	19	-27	-54	-1
Right visual cortex	18	-5	-72	-1
Left visual cortex	18	+20	-63	-1
Left visual cortex	19	+15	-62	-8
Left visual cortex	18	+10	-62	+4
Left visual cortex	18	+6	-46	+4
Left visual cortex	18	+16	-70	+4
Left visual cortex	17	+5	-75	+12
Left visual cortex	18	+5	-81	+12
Right lateral temporal cortex	22	-48	-5	+8
Left lateral temporal cortex	22	+49	-22	+8
Right cingulate gyrus	31	-7	-52	+8
Right cingulate gyrus	31	-8	-63	+8
Left cingulate gyrus	31	+7	-65	+12
Right cingulate gyrus	23	-25	-53	+8
Right inferior frontal gyrus	45	-38	+24	+4
Right visual cortex	19	-18	-62	-8
Right visual cortex	19	-32	-61	-8

Table 3.5 */continued*

Areas of significantly greater response in controls		Talairach co-ordinates		
	Approx. BA	x (mm)	y (mm)	z (mm)
Right visual cortex	18	-10	-82	-1
Right visual cortex	18	-16	-70	-1
Left visual cortex	17	+5	-94	-1
Left visual cortex	18	+7	-80	-1
Left visual cortex	19	+12	-60	-1
Left visual cortex	19	+18	-42	-1
Right visual cortex	18	-34	-78	+4
Right visual cortex	18	-9	-82	+4
Left visual cortex	17	+12	-95	+4
Left visual cortex	18	+7	-75	+4
Right visual cortex	17	-10	-82	+8
Right visual cortex	17	-10	-75	+8
Left visual cortex	17	+10	-75	+8
Right visual cortex	18	-10	-82	+12

Search volume 1476 voxels, $p < 0.05$. Patients > controls = 125 voxels, controls > patients = 305 voxels

Table 3.6. *One-way ANOVA comparison between generic brain activation maps for stimulation of the affected eye in patients following left optic neuritis, and the left eye in controls.*

Areas of significantly greater response in patients	Talairach co-ordinates		
	Approx. BA	x (mm)	y (mm)	z (mm)
Right orbitofrontal cortex	11	-22	+40	-12
Right insula-claustrum	14-16	-28	+28	-1
Left insula-claustrum	14-16	+27	+29	-1
Right insula-claustrum	14-16	-31	+25	+4
Left insula-claustrum	14-16	+35	+20	+4
Right corpus striatum	-	-20	+3	-1
Right inferior frontal cortex	45	-52	+26	+4
Right visual cortex	19	-12	-45	-1
Right visual cortex	18	-14	-55	+4
Right visual cortex	17	-13	-70	+12
Right cingulate gyrus	23	-14	-60	+8
Right lateral temporal cortex	22	-49	-25	+8
Right cingulate gyrus	23	-13	-61	+12
Left cingulate gyrus	23	+8	-61	+12

Table 3.6 */continued*

Areas of significantly greater response in controls		Talairach co-ordinates		
	Approx. BA	x (mm)	y (mm)	z (mm)
Left visual cortex	18	+21	-64	-8
Right visual cortex	18	-8	-80	-1
Right visual cortex	19	-12	-55	-1
Left visual cortex	18	+5	-85	-1
Left visual cortex	18	+11	-77	-1
Left visual cortex	18	+12	-61	-1
Left visual cortex	19	+25	-61	-1
Left visual cortex	19	+12	-44	-1
Right superior temporal gyrus	22	-53	-20	+4
Right middle temporal gyrus	22	-55	-37	+4
Right visual cortex	18	-32	-78	+4
Right visual cortex	18	-25	-75	+4
Left visual cortex	17	+5	-85	+4
Left visual cortex	18	+7	-75	+4
Left visual cortex	18	+10	-61	+4
Right visual cortex	17	-10	-72	+8
Left visual cortex	17	+6	-75	+8
Right visual cortex	17	-10	-75	+12
Left visual cortex	18	+20	-80	+16

Search volume 2471 voxels, $P < 0.05$. Patients > controls =125 voxels, controls > patients = 424 voxels

The finding of extra-occipital activation during stimulation of the affected eye in patients was seen (to varying degrees) in all seven individual activation maps, indicating that the group result was not due to a small number of outlier observations.

A generic brain activation map for stimulation of the affected eye in the two patients with definite VEP delay at the time of fMRI scanning showed a greater extent of extra-occipital activation than that for the five patients without VEP delay (Fig. 3.5). Furthermore, whole field VEP latency showed a strong positive correlation with the volume of extra-occipital activation (Spearman's rho=0.71, p=0.005) (Fig. 3.6). No correlation was found between VEP amplitude and extra-occipital activated volume, nor was there significant correlation between occipital activated volume and either VEP latency or amplitude.

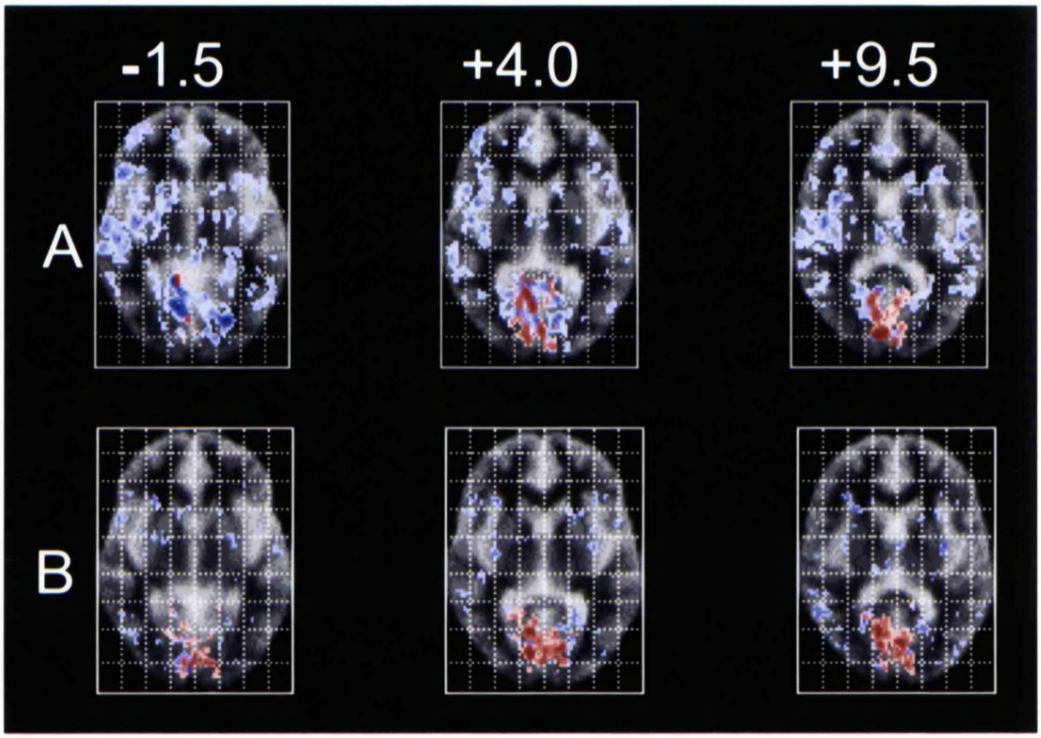

Fig. 3.5. Generic brain activation maps obtained during periodic stimulation of the affected eye in patients following recovery from optic neuritis. **(A)** With VEP delay (defined as a latency prolongation of >109 ms for those under 40 years old, and >122 ms for those over 40 years old); and **(B)** without VEP delay. Talairach z co-ordinates are shown in mm (top of figure). The phase of response is coded as red (maximum fMRI signal during the stimulus condition) or blue (maximum fMRI signal during the baseline condition). The deepness of hue represents the magnitude of the fundamental power quotient (FPQ) at each voxel (see text).

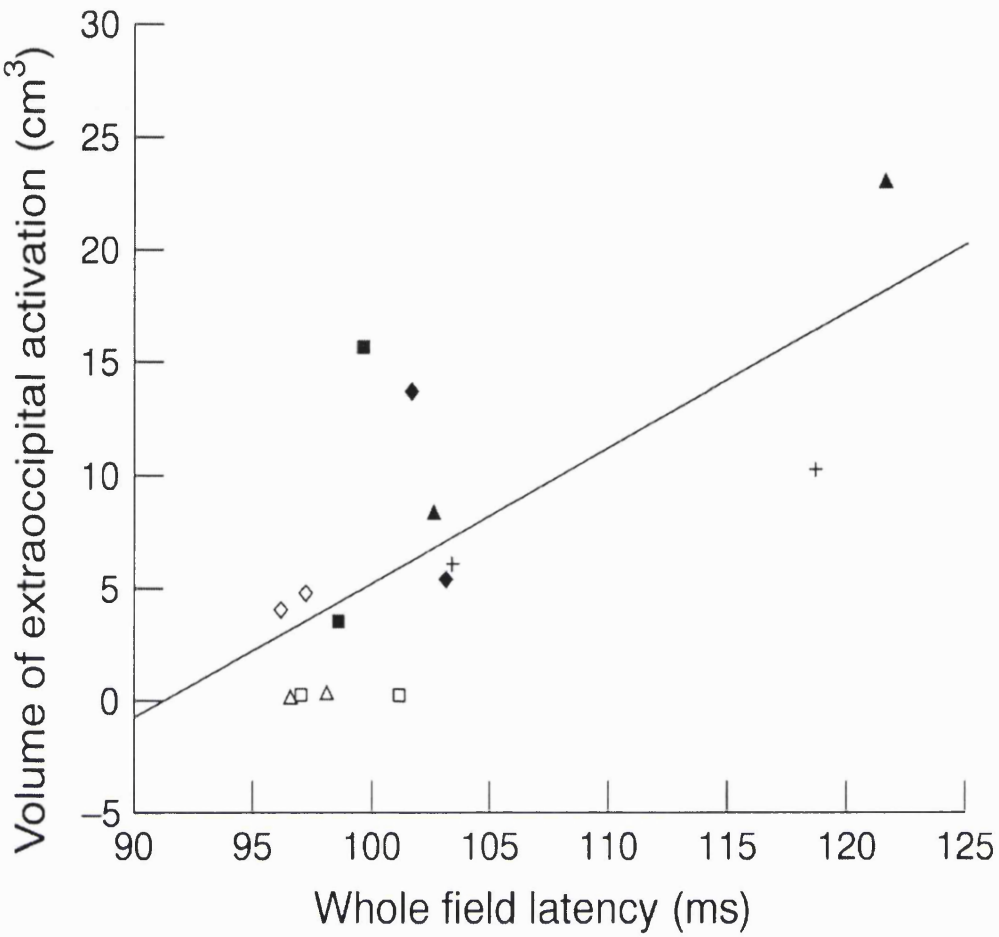

Fig. 3.6. Correlation between the volume of extra-occipital activation and whole field VEP latency (including both affected and unaffected optic nerves) for seven patients following unilateral optic neuritis. Each patient is coded by a different symbol to show the paired nature of the data.

Whilst occipital regions were activated in the patient group with MR signal maximum during the photic stimulation condition, as in the control group, areas of extra-occipital activation showed a different pattern of response, with signal maximum during the early part of the dark condition; Figures 3.2 and 3.7.

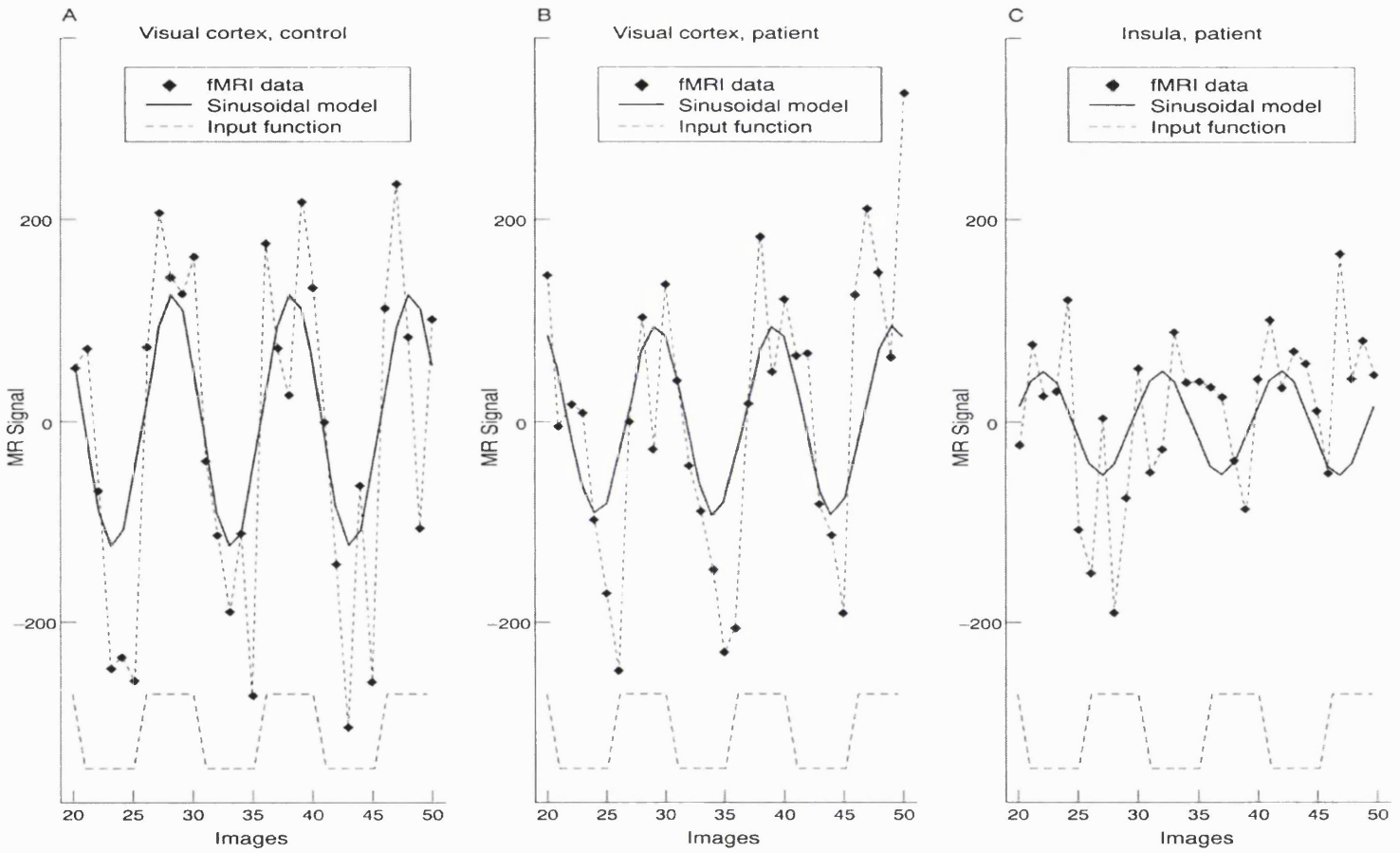

Fig. 3.7. fMRI data acquired during periodic monocular photic stimulation, alternating with binocular darkness. The diamonds and dotted lines represent the raw data; the solid line is the best fit sinusoidal model (see text); the dotted square wave (bottom of figure) shows the experimental input function. (A) Control, visual cortex; (B) patient, visual cortex; (C) patient, insula. Note the delayed timing of the peak BOLD response in the patient insula (C).

Discussion

Comparison with previous work

There have, to date, been few studies of demyelinating optic neuritis using fMRI, and none have investigated a directly comparable group of patients following isolated unilateral optic neuritis. However, several groups have investigated optic neuritis in the context of MS. Rombouts et al. (1998) studied nine patients with variable recovery from optic neuritis, eight of whom had clinically definite MS. In common with the present study, a reduced volume of visual cortex activation was observed in patients on stimulating either the affected or the unaffected eye in comparison to control subjects (Table 3.2). The present study has additionally shown a reduced *power* of fMRI response in regions of the visual cortex in patients compared to controls for both affected and unaffected eyes (Tables 3.5 and 3.6).

However, in contrast to the present data, Rombouts et al. (1998) reported no extra-occipital activation. This could reflect several methodological differences. Firstly, the patients in the present study were more homogeneous in their clinical and MRI characteristics. It is possible that this highly selected group show different visual activation patterns compared with a heterogeneous group of patients with variable recovery and disseminated disease. Secondly, the stimulus used in the present study was of 20-second duration compared to 40 seconds; it is known that epoch length affects the modulation of the fMRI signal (Thomas and Menon, 1998), and this could conceivably have different effects in different parts of the brain. The response in patients with optic neuritis to a 40 second stimulus

will be addressed in the next section. Thirdly, the analysis method used in the present study takes account of locally variable haemodynamic delay and response shape and allows an accurate estimation of the phase of periodic response in different brain regions; the time-shifted boxcar approach used by Rombouts et al. (1998) may not be sensitive to extra-occipital activation if it is phase-shifted with respect to the visual stimulus.

Two other fMRI studies of patients with optic neuritis in the context of MS (Gareau et al., 1999; Langkilde et al., 1999) included clinically heterogeneous populations of patients using data acquisition and analysis methods that were not designed to detect extra-occipital activation. Gareau et al. (1999) studied four patients with MS, three of whom had experienced an episode of unilateral optic neuritis using a surface MR receiver coil, which cannot detect activation in anterior brain regions. Langkilde et al. (1999) investigated eight patients (five with definite or probable MS) with varying degrees of clinical recovery after optic neuritis, acquiring images in the coronal plane with limited antero-posterior coverage; these data do not include anterior brain regions in which extra-occipital activation was observed in recovered patients.

Gareau et al. (1999) report time series data from one patient that suggests a smaller BOLD signal change than that seen in a dataset from a normal subject; this is in contrast to Rombouts et al. (1998) who reported no abnormality in the BOLD signal response in nine patients after optic neuritis. This difference between studies may reflect differences in data acquisition or patient selection. Further studies in larger cohorts of patients may help to clarify the effect of demyelinating lesions on the morphology of the BOLD response arising from stimulation of the affected pathway. It is possible that different types of pathological damage (e.g.

demyelination, axonal degeneration) cause different disturbances of the form of the BOLD signal.

Individual Brain Activation Maps

The stimulus used reliably activates visual cortical areas in both patient and control groups (Table 3.2).

Controls. Right eye stimulation activated a larger area than left eye stimulation in six of seven healthy individuals studied. Few previous studies have investigated monocular stimulation in normal subjects. One study has reported that subjects generally activated a larger area of occipital cortex upon stimulating the dominant eye (Rombouts et al., 1996). The determination of ocular dominance relies on a test in which a near object (e.g. a pencil) is aligned with a distant point on a wall that is being focused upon with both eyes open (Porac and Coren, 1976). Each eye is closed in turn; only when the dominant eye is open will the pencil remain in good alignment with the wall. The concept of ocular dominance has been suggested to reflect one eye input being favoured over the other (Rombouts et al., 1996). The present findings in control subjects could therefore perhaps be explained by right eye dominance, although not all subjects were assessed; two of three subjects who were assessed had right eye dominance (the other being unclear), but all three had larger activation from right eye stimulation.

The value of the concept of ocular dominance has been challenged by reports of the variability of dominance depending upon the method used for its determination. Its value in the interpretation of visual fMRI studies has not been

investigated, nor can dominance always be reliably assessed clinically (Porac and Cohen, 1976). Ocular dominance may be of limited use in interpreting studies of optic neuritis, which may change the pattern of dominance (Rombouts et al., 1998).

Patients. In seven of eight patients, stimulation of the affected eye induced a smaller activated area than the unaffected eye in the occipital cortex. The volume activated in patients was less than the mean area activated in an appropriate control eye (i.e. V_{REL} <1.0) for six of seven affected eyes and for four of seven unaffected eyes. The reduced activation was seen regardless of the degree of clinical recovery, the presence of VEP abnormality or of optic nerve MRI abnormality. These data suggest that reduced fMRI activation could potentially be a marker for persistently abnormal visual input, and that abnormalities may remain for longer than VEP abnormalities, consistent with the notion of a persistently abnormal pattern of input to the visual cortex following optic neuritis. However, the data also show the great variability of the activated volume in both controls and patients, which may limit its specificity and clinical usefulness. Although further studies with larger numbers of controls may help to establish the mean activated volume induced by a monocular stimulus, allowing individual patients to be compared against the mean, a method of ensuring comparability of data across different subjects is also needed due to the considerable individual anatomical variation in the visual cortex. One way of addressing this is to map each study into standard space (as in the next section) with image smoothing to minimize inter-individual anatomical differences.

Individual patient activation maps showed extra-occipital activation for all seven affected eyes, and for six of seven unaffected eyes (Table 3.3). There was considerable inter-individual variation (affected eye range 0.2 to 22.8 cm^3, unaffected eye range 0.2 to 13.6 cm^3). In five of seven patients, the volumes for both affected and unaffected eyes were larger than the mean for the appropriate eye in the control group (i.e. V_{REL} >1.0). Individual control activation maps revealed small volumes of extra-occipital activation in five of seven subjects (Table 3.4) for both left and right eye stimulation, but to a lesser extent than for stimulation of either affected or unaffected eyes in patients. These observations are in keeping with the generic activation map results (see below), but demonstrate the variability of the extent of extra-occipital activation, particularly in patients.

Generic Brain Activation Maps

Control subjects. The generic brain activation maps in controls, as expected, revealed activation in visual cortex. An asymmetry was noted, with a larger area activated in the hemisphere contralateral to the side of monocular stimulation. Moreover, the ANOVA comparisons between left and right monocular stimulation in controls indicate the presence of regions in visual cortex that respond with greater *power* to stimulation of one eye compared to the other. The lateralization of response to monocular photic stimulation has not been widely studied. Although Rombouts et al. report in detail on the size of area activated by monocular stimulation of either eye, with assessment of the effect of ocular dominance (Rombouts et al., 1997), the lateralization of response was not investigated. Hedera et al. (1994) used fMRI with an 8Hz simple visual stimulus

to study visual cortical responses in six patients with oculocutaneous albinism and six normal subjects. In this study, no asymmetry was found in normal subjects, in contrast to the predominant contralateral visual cortex activation seen in albino subjects, though no formal statistical comparisons of activation maps were made, and group activation maps were not computed. The present findings indicate that monocular stimulation induces asymmetric patterns in both the spatial extent and power of activation in the visual cortex; this should be taken into account in the analysis and interpretation of fMRI data from patients with visual deficits.

The asymmetry in response demonstrated during monocular stimulation is consistent with anatomical studies of the visual system in animals and humans. In many mammalian species the retina of each eye projects to both hemispheres (see for example Stone et al., 1966). Fibres from the temporal part of the retina are largely uncrossed at the optic chiasm and project (via the lateral geniculate nucleus and optic tract) to the anterior visual cortex in the ipsilateral hemisphere, whilst nasal fibres cross at the optic chiasm and project mostly to the posterior visual cortex in the contralateral hemisphere. The data presented here indicate that each eye has a greater functional representation in the contralateral compared to the ipsilateral visual cortex. Several lines of anatomical evidence may contribute to this observation: firstly, in the cat there is evidence that some fibres arising from the temporal retina project contralaterally in addition to the normal temporal crossed projection (Stone et al., 1966); secondly, the density of ganglion cells is up to two to three times greater in the nasal retina compared to the temporal retina in monkeys (Perry and Cowey, 1985); and thirdly, there is a modest bias toward crossing fibres in the optic chiasm (Kupfer et al. 1967), which is greater at the level of the lateral geniculate nucleus, achieving a crossed:uncrossed ratio of

approximately 60:40 (Le Gros Clark 1941; Chacko 1948; Connolly and Van Essen, 1984).

Ocular dominance columns are thin strips of cortex containing cells that receive a greater input from one or other eye. The columns responding to each eye alternate with one another in the striate cortex. LeVay et al. (1985) examined the ocular dominance columns in the macaque monkey by autoradiography. The stripes for the contralateral eye were significantly wider than the ipsilateral eye, which may contribute to the present findings. A possible explanation for the enlargement of contralaterally responding dominance columns could be a naturally occurring form of visual deprivation due to the partial obstruction of the nasal field of view (which is received by the ipsilaterally-projecting temporal retina) by the nose. In support of this, the ocular dominance stripe patterns seen in this study closely matched those seen after experimentally produced monocular deprivation (LeVay 1980). Several other studies have documented nasotemporal asymmetries in ocular dominance column width or area in primates, with a consistent bias favouring inputs from the nasal retina (Rosa et al. 1988, Tychsen and Burkhalter, 1997).

Patients. The generic maps in patients show that there is indeed a change in the distribution of cortical activation by a simple visual stimulus in patients who have recovered from acute optic neuritis compared with normal individuals. Activation in response to stimulating the recovered eye occurs not only in the occipital visual cortex, but also in the insula-claustrum, lateral temporal, posterior parietal and orbito-frontal cortices, corpus striatum and thalamus. Although these sites are not normally activated by a simple visual stimulus, they are known to have extensive

connections with visual processing areas, and some of them have been proposed as areas of multimodal sensory integration (Mesulam, 1998). The claustrum is a small nucleus whose function remains uncertain. It is well developed in primates, and its size increases approximately in proportion to the volume of cerebral cortex (Sherk, 1986). It has complex projections to many cortical regions, in particular with BA 17, 18 and 19 and the visual thalamus (Sherk, 1986), and receives input from both visual fields (Olsen and Graybiel, 1980); furthermore, the claustrum can functionally modulate the response properties of neurons in primary visual cortex (BA 17) (Tsumoto and Suda, 1982). The claustrum receives input from, and projects to, multimodal visual and auditory areas; it has recently been proposed as a site of transfer of information between tactile and visual modalities (Hadjikhani and Roland, 1998). These extensive visual connections provide a plausible physiological substrate for activation of the claustrum during simple visual stimulation.

The insula has also been proposed as a multimodal convergence area (Mesulam and Mufson, 1986), and damage to the insula in humans causes a syndrome of multimodal neglect (Berthier et al., 1987). The anterior insula has substantial connections with orbitofrontal cortex and the thalamus as well as limbic areas (Mesulam and Mufson, 1986). The posterior insula has connections with frontal, temporal and parietal cortices and the thalamus (Mesulam and Mufson, 1986). The medial pulvinar thalamic nucleus in turn projects to higher order multimodal association cortex (Mufson and Mesulam, 1984). The lateral temporal cortex (BA 21 and 22) and posterior parietal cortex (BA 39 and 40) were activated in patients in response to simple visual stimulation of the affected eye, but not in normal controls. These areas have been suggested to be sites of

multimodal sensory processing based on homologies with primate multimodal areas (Mesulam, 1988). Finally, there is experimental evidence that the corpus striatum, although classically thought to have mainly a motor role, receives functional input from the visual cortex (Nieuollon et al., 1978).

Thus, the areas that are activated during stimulation of the affected eye in patients constitute a cortical and subcortical network of areas known to be involved in visual or multimodal sensory processing. The activation map for the unaffected eye showed a limited activation of this network, confined to the right insula-claustrum region at the statistical threshold used in this study. One possible mechanism is that the change in activation pattern is a response to abnormal input due to clinically silent abnormality of conduction in the unaffected optic nerve (a well recognized phenomenon) (Halliday et al., 1972). Another possibility, suggested by the fact that visual input to the claustrum is binocular (Olsen and Graybiel, 1980), is that a change in functional organization in the claustrum due to disease in one eye could result in altered activation additionally upon stimulating the other, clinically unaffected, eye. Why this activation is lateralized to the right side is uncertain, though it is noteworthy that six of seven unaffected eyes were on the right.

Although the significance of these areas of extra-occpital activation in the recovery process in optic neuritis remains to be determined, the reported here indicate that they may, at least in part, be influenced by the degree of recovery of the VEP latency. Firstly, the greater extent of extra-occipital activation from stimulating the affected eye in patients with VEP delay compared to those without VEP delay suggests that slowed conduction in the optic nerve is a contributory factor in producing, and sustaining, an abnormal distribution of cerebral response

to visual stimulation. Secondly, there is a strong correlation between the volume of extra-occipital activation and the VEP latency. The origin of a prolonged VEP latency is complex, but is likely to be in part due to slowed conduction in completely or partially demyelinated axons; a reduction and dispersion of the normal input due to unequal slowing in different fibres may also contribute (Youl et al., 1991). In the acute phase of optic neuritis, there is a decrease in amplitude and an increase in the latency of the VEP. As recovery of vision occurs the amplitude recovers to a variable extent, but the prolonged latency persists for much longer, even when full visual recovery has occurred (Youl et al., 1991; Jones et al., 1993). The present findings suggest that the extra-occipital network activated in patients after optic neuritis may represent an adaptive cerebral response to VEP delay, which could contribute to the recovery process.

The phase of periodic fMRI signal change in the extra-occipital areas activated only by patients was delayed relative to the phase of response to photic stimulation in visual cortex; Figures 3.2C and 3.2D, Figure 3.8. On the assumption that locally increased BOLD magnetic resonance signal reflects increased synaptic activity, whether excitatory or inhibitory (Bullmore et al., 1996a), there are several possible explanations for this observation. Firstly, extra-occipital multimodal areas could be excited by delayed propagation of neural activity from primary visual areas. The delay that observed between occipital visual cortex and these areas (of approximately 10 seconds) is, however, considerably longer than delayed hierarchical excitation of visual cortical processing areas [shown by electrophysiological studies to be of the order of milliseconds (Zeki et al., 1998)], making this unlikely. A second possibility is that multimodal regions are actively inhibited in patients during the dark condition (causing locally increased fMRI

signal), from which they are released (disinhibited) at the onset of photic stimulation. Disinhibition (by experimental reduction of inhibitory input to the superior colliculus, a putative subcortical multimodal region) has been suggested as a contributory mechanism in recovery from experimental injury to mammalian visual cortical areas (the Sprague effect) (Ciaramitaro et al., 1997), but the role of such a process in recovery from anterior visual pathway lesions has not been investigated. A third possibility is that extra-occipital areas show a relative increase in activity during the baseline condition that may be suspended during visual stimulation. Finally, the peak fMRI signal could occur later in multimodal areas due to a different, delayed haemodynamic response. There is evidence that the response to a semantic decision task in multimodal lateral frontal areas in normal subjects is delayed by approximately 10 seconds compared to the response to pure tone discrimination in primary auditory cortex (Bandettini et al., 1995a; Bandettini et al., 1998). Further experiments, described in section 3.4, have been performed to help to clarify the phase and time course of activations and their relationship to the stimulus.

One potential artefactual source of increased fMRI signal during the resting phase is from involuntary eye movements, which could not be monitored with the apparatus used in this study, and could potentially induce activation in areas including frontal eye fields. This is unlikely to have contributed to the different activation patterns we have observed between patients and normal subjects for the following reasons: first, patients were able to fixate normally during visual field perimetry and had no clinical evidence of any eye movement disorder; second, classical areas in which activation would be expected during eye movements (frontal eye fields, intraparietal sulcus) were not imaged in this study

so could not have contributed to the observed differences; and third, the extra-occipital responses demonstrated in patients would not be anticipated to be activated by eye movements.

In summary, the present study has revealed a previously unsuspected degree of functional reorganization of the brain after acute unilateral optic neuritis implicating a distributed cortical and subcortical network of cerebral areas that are not normally involved in a simple visual stimulation experiment. These areas have extensive visual connections. Whether and how these changes might contribute to the recovery process and its maintenance remains to be determined. Components of this network have been identified in other functional imaging studies as potential areas of cross-modal integration between different sensory inputs, for example when "seen" speech influences the perception of "heard" speech (Calvert and Brammer, 1998). Our results may thus reflect a greater than normal contribution of such higher processing areas (so-called 'top-down' processing) in patients compared to controls. One possibility is that multimodal regions contribute to suppression of the abnormal input from the affected eye; there is experimental evidence that when the two eyes receive dissimilar visual inputs there is a long latency suppression of response from one eye that may be mediated by cortico-thalamic pathways (Varela and Singer, 1987). Alternatively, a recent study has reported activation in a network including posterior parietal, occipito-temporal cortex and anterior insula during a spatial attention task (Gitelman et al., 1999), and it is possible that activation of these areas in our data reflects increased attention and thus perhaps perceptual enhancement of a pathologically degraded stimulus. However, the data presented cannot rule out a possible contribution from increasing fatigue (or reduced arousal) in patients at the end of the baseline period

to the extra-occipital activation. At this stage it is clear that temporary visual loss in optic neuritis has previously unexpected long-term consequences for the pattern of activation of the brain by simple visual stimuli.

3.4 A functional MRI investigation of the mechanism of abnormal cerebral response to visual stimulation following recovery from optic neuritis

Introduction

The results presented in the previous section indicate that recovery from optic neuritis is associated with a change in the distribution of the cerebral response to a simple visual stimulus in patients compared to control subjects. The timing of the fMRI response in these extra-occcipital regions was demonstrated to be different to the response in occipital visual cortex; the peak fMRI signal change occurred during the baseline condition of binocular darkness, in contrast to the peak during monocular visual stimulation observed in occipital visual cortical areas. As discussed above, there are several possible explanations for this observation. The aim of the present study was to attempt to determine which of the proposed mechanisms are most likely to contribute to the timing of extra-occipital response.

Further data were collected, in a group of eight patients (the original seven, and an additional one who also fulfilled identical clinical criteria to the previous study) and eight controls (different from those in the previous study), using a visual stimulus with an epoch duration of 40 seconds (compared to 20 seconds in the previous study). If the extra-occipital response is due to increased BOLD signal due to excitatory or inhibitory neural activity in the baseline period, rather

than a delayed response to the stimulus, then the phase of the activated extra-occipital areas should remain the same as in the previous study. If, however, these areas show a constant delay from stimulus onset (which judging from the previous study would be approximately 10 seconds), then with the longer epoch length their phase should change; i.e. they should show maximum fMRI signal during the stimulus phase.

Patients and methods

Subjects. Eight patients (mean age 37.1 years; 4 male, 4 female) following a single episode of typical unilateral acute optic neuritis and eight normal controls (mean age 34.0 years; 4 male, 4 female), were studied. As before, on the day of study visual acuity was measured using the Snellen chart and colour vision was assessed using Ishihara colour plates. Visual evoked potentials were recorded as previously. A repeat brain MRI was performed to confirm the absence of new disseminated lesions.

Imaging, experimental design and analysis. Structural and functional brain imaging were performed as described in the previous study, with the exception of optic nerve MRI, which was not repeated. Subjects passively viewed a visual display which alternated periodically between 40 second epochs of two contrasting conditions: (ON) red 8Hz photic stimulation to the whole visual field was presented to one eye using lightproof goggles whilst the other eye received no visual stimulation; (OFF) no visual stimulation (darkness) was presented to both eyes. In total, six cycles of alternation between the ON and OFF conditions were

presented over the course of each experiment; condition OFF (no stimulation) was always presented first. Analysis involved the generation of individual brain activation maps with subsequent computation of generic brain activation maps in standard space for patients and controls. Activated volumes in occipital and extra-occipital areas were measured as before.

Results

All subjects had normal visual acuity and colour vision. The volumes of occipital and extra-occipital activation in each individual are shown in Tables 3.6 and 3.7. Selected slices from the generic brain activation maps in controls and patients are shown in figure 3.8. In the control subject group, generic brain activation maps for monocular stimulation to either eye revealed activation almost exclusively in occipital visual cortex. As in the previous study, monocular stimulation resulted in an asymmetric visual cortex activation pattern, with a larger activated area in contralateral compared to ipsilateral cortex (Figure 3.8A and 3.8B). This visual impression was investigated by performing a formal one-way ANOVA comparing the response to right and left eye stimulation in controls (Fig 3.9).

In patients, stimulation of the clinically unaffected eye (six right and two left eyes) induced a pattern of visual cortex response similar to that seen during monocular stimulation in controls, but with additional extra-occipital activation in the insula-claustrum. Unlike the previous study, stimulation of the affected eye induced a smaller spatial extent of visual cortex activation, but with similar additional activation in extra-occipital areas including anterior insula-claustrum

and the orbitofrontal, posterior parietal and lateral temporal cortices (Figure 3.8D), which was not as extensive as that observed with the 20 second epoch length.

Table 3.7. *Occipital activation volumes from individual activation maps in patients and controls (40s epoch length)*

	PATIENTS				CONTROLS			
	Affected eye volume (side) /cm³	V_{REL}	*Unaffected eye volume /cm³*	V_{REL}	*Right eye volume /cm³*	V_{REL}	*Left eye volume /cm³*	V_{REL}
	6.11 (R)	0.54	0.62	0.04	0.40	0.04	16.16	1.00
	0.15 (L)	0.01	0.15	0.01	21.16	1.86	9.73	0.60
	0.84 (L)	0.05	4.50	0.40	3.23	0.28	35.98	2.23
	2.99 (L)	0.19	8.16	0.72	16.77	1.48	17.09	1.06
	4.36 (L)	0.27	16.05	1.41	7.64	0.67	5.82	0.36
	0.35 (L)	0.02	1.40	0.09	19.23	1.69	27.18	1.69
	13.50 (L)	0.84	27.95	2.46	16.00	1.41	13.42	0.83
	5.53 (R)	0.34	16.40	1.02	6.42	0.57	3.47	0.22
Mean	**4.23**	**0.28**	**9.40**	**0.77**	**11.36**	**1.00**	**16.11**	**1.00**

$$V_{REL} = \frac{\text{Volume of activation}}{\text{Volume of activation (matched control eye mean)}}$$

Table 3.8. *Extra-occipital activated volumes from individual activation maps in patients and controls (40s epoch length)*

	PATIENTS				CONTROLS			
	Affected eye volume (side) /cm³	V_{REL}	*Unaffected eye volume /cm³*	V_{REL}	*Right eye volume /cm³*	V_{REL}	*Left eye volume/cm³*	V_{REL}
	10.17 (R)	37.7	0.70	0.39	0.00	0.00	1.36	0.76
	0.63 (L)	0.35	1.67	6.19	0.30	1.11	5.70	3.20
	0.00 (L)	0.00	0.00	0.00	0.00	0.00	0.97	0.54
	0.50 (L)	0.28	0.61	2.26	0.80	2.96	2.21	1.24
	0.17 (L)	0.10	1.55	5.74	0.00	0.00	1.23	0.69
	0.49 (L)	0.28	2.22	8.22	1.04	3.85	0.64	0.36
	0.00 (L)	0.00	0.52	1.93	0.00	0.00	2.11	1.19
	9.88 (R)	36.6	20.36	11.44	0.00	0.00	0.00	0.00
Mean	**2.73**	**9.41**	**3.45**	**4.52**	**0.27**	**1.00**	**1.78**	**1.00**

$$V_{REL} \quad \frac{\text{Volume of activation}}{\text{Volume of activation (matched control eye mean)}}$$

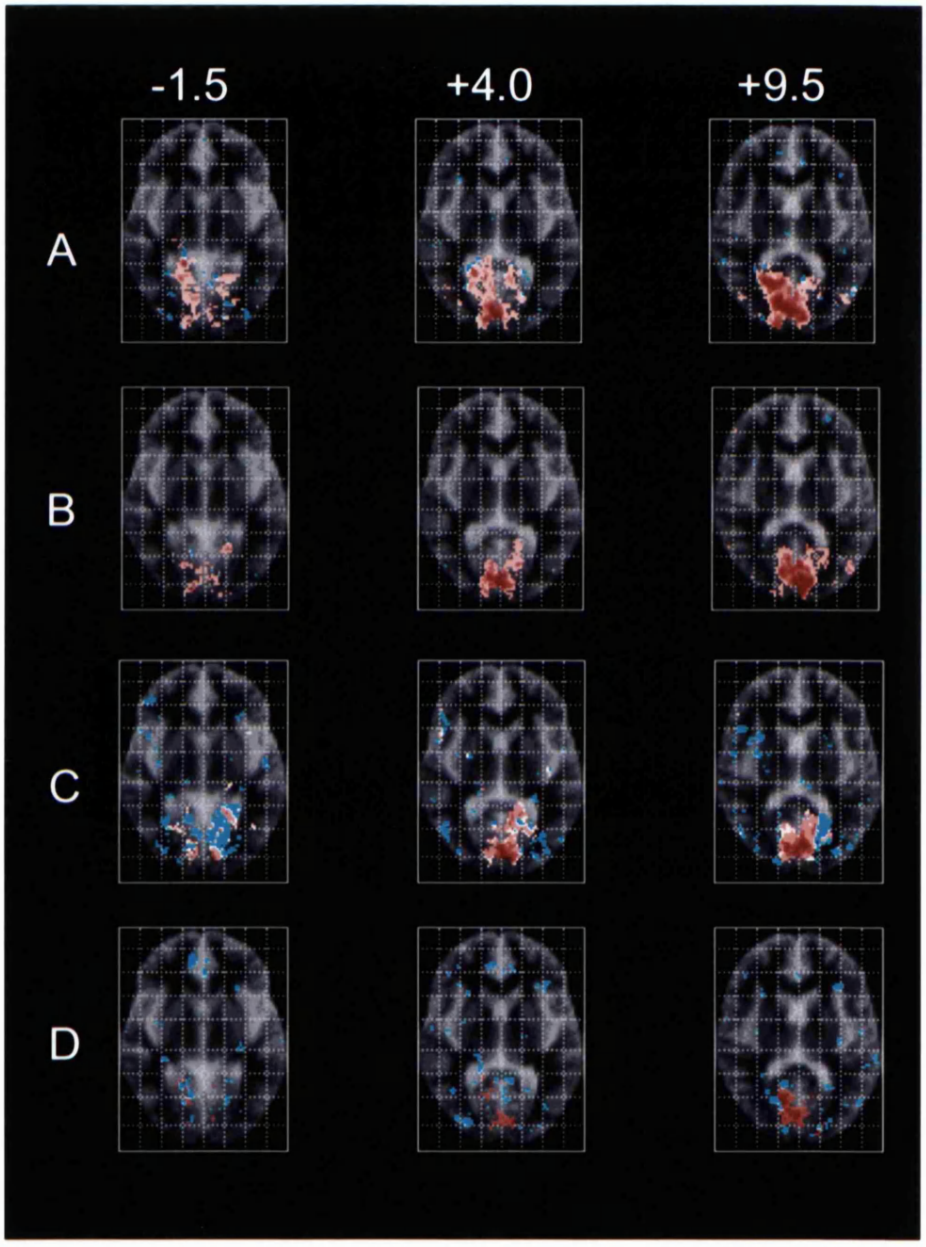

Fig. 3.8. Generic brain activation maps from eight control subjects and eight patients following optic neuritis, showing areas of significant response to monocular photic stimulation compared with binocular darkness (epoch length = 40 seconds). The one-tailed probability of false positive activation $p < 0.0001$ for each voxel. Voxels showing maximum fMRI signal during the stimulus condition are coloured red; those showing maximum response during the baseline condition are coloured blue. The deepness of hue represents the magnitude of the fundamental power quotient (FPQ) at each voxel (see text). **(A)** Controls (left eye); **(B)** Controls (right eye); **(C)** Patients (unaffected eye); **(D)** Patients (affected eye).

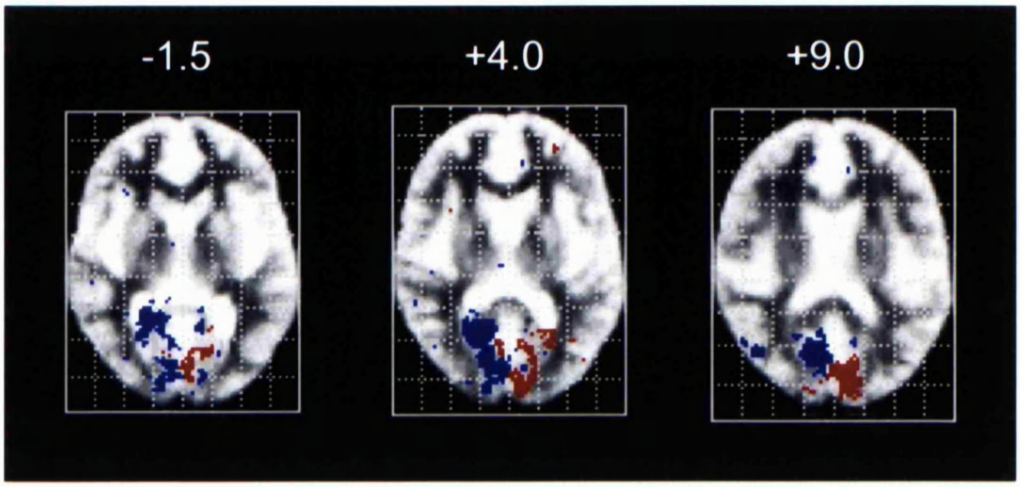

Fig. 3.9. One-way ANOVA comparison between left and right eye periodic photic stimulation (epoch length = 40 seconds) in control subjects (n=8). Voxels at which left eye stimulation induces a greater power of response than right eye stimulation are coloured blue (562 voxels); those with greater power of response during right eye stimulation are coloured red (268 voxels). Search volume = 1591 voxels, $p < 0.05$. Talairach z co-ordinates are shown in mm (top of figure); the left of the brain is on the right side of the figure.

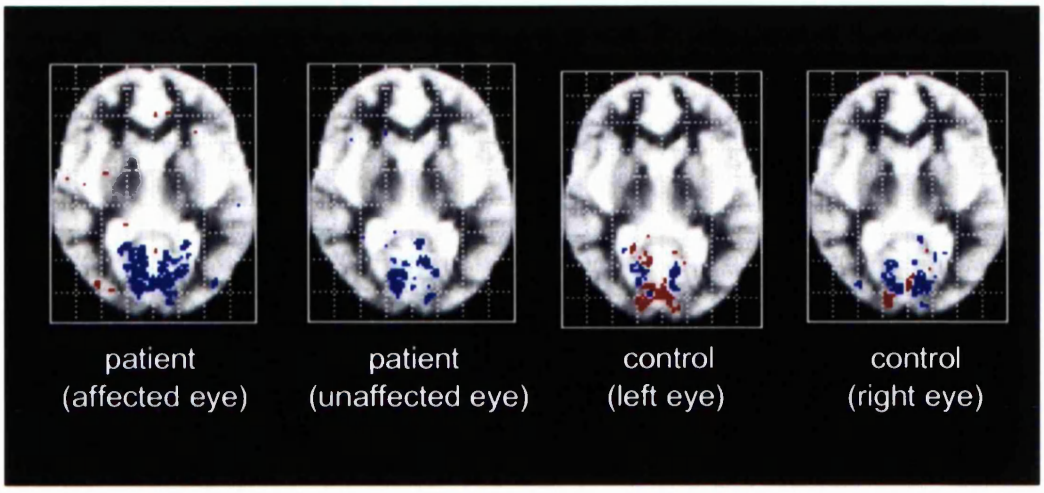

Fig. 3.10. One-way ANOVA comparing the activation induced by long epoch (40 seconds) compared to short epoch (20 second) periodic photic stimulation, for patients (affected eyes and unaffected eyes) and controls (left and right eyes). Voxels showing a greater power of response during the short epoch study than during the long epoch study are coloured blue; those showing a greater power of response during the long epoch study are coloured red. For all slices the Talairach z co-ordinate is 1.5mm; the left side of the brain is on the right side of the figure.

The phase of response in occipital visual cortex showed most voxels with peak signal during the stimulus, as expected, in controls (Red voxels, Figs 3.8A and 3.8B). The visual cortex activation in patients showed a more heterogeneous phase pattern, with some voxels having peak BOLD signal during the baseline condition (mixture of red and blue voxels, 3.8C and 3.8D), whilst the extra-occipital activation in patients almost exclusively showed peak signal change during the baseline condition.

For each experimental group (control left, control right; patient affected, patient unaffected), a one-way ANOVA model, thresholded at $P<0.05$ was fitted at each intracerebral activated voxel in standard space to assess the difference in activation between the generic maps for the 40s epoch and 20s epoch experiments (Fig. 3.10). In all groups, areas of reduced power of response for the 40s study compared to the 20s study were demonstrated in occipital cortex (blue voxels); these areas were more extensive for the affected eye than for the unaffected eye (or either eye in control subjects). These results indicate a generally reduced extent of response across groups to the longer stimulus duration, but with the largest effect in the affected eye.

Discussion

This study aimed to determine the mechanism of extra-occipital activation in patients after optic neuritis, by performing experiments using a 40 second epoch length and comparing the findings to those obtained using a shorter (20 second) epoch length (section 3.3) in similar patient and control groups. The results were similar in both studies, with a greater extent of extra-occipital activation in patients compared to control subjects consistently observed. Furthermore, the maximum BOLD response in extra-occipital regions occurs consistently during the baseline condition of binocular darkness. This qualitative similarity in data from both sets of experiments suggests that the findings are robust, although caution in generalizing the findings is necessary with the relatively small sample size studied, since outliers may still exert considerable influence on the group data. Nonetheless, in conjunction with the previous data, the present observations allow some of the proposed mechanisms for the extra-occipital activation to be discounted. The constancy of phase of the extra-occipital activation in both studies indicates that a fixed delay in the timing of peak BOLD response to the stimulus (either due to delayed neuronal propagation, or a long haemodynamic response rise time) cannot explain the observations. If such mechanisms were responsible then the peak fMRI signal in extra-occipital areas in the present study would occur in phase with the stimulus (providing the lag is less than the epoch length of 40 seconds).

The present results therefore indicate that there is a consistent increase in BOLD signal in extra-occipital areas during the baseline condition relative to the stimulus condition during simple monocular stimulation in patients following

optic neuritis. This pattern, of a relative decrease in fMRI signal (often termed "deactivation") associated with task performance has been observed in numerous previous fMRI studies of visual or cognitive tasks (LeBihan et al., 1995; Bullmore et al., 1996; Clark et al., 1996), but the mechanisms and physiological significance are not well understood. Measurements of neurotransmitter cycling rates using NMR measurements of labelled molecules suggest that neurotransmitter activity during resting states is not negligible and may only show a 10% increase during task activity (Shulman et al., 1998). These data support the idea that brain areas may show significant neural activity during an experimental baseline or reference phase.

There are several possible explanations for an increased BOLD response during the baseline condition. It is generally agreed that the BOLD signal is a measure of neural activity that may be either excitatory or inhibitory (Bullmore et al., 1996a). This suggests at least two broad explanations for a baseline phase response in a simple alternating stimulation-rest experimental design of the type we have performed. Firstly, the increased BOLD response may reflect excitatory synaptic activity due to ongoing processes in extra-occipital areas, in keeping with psychological data suggesting that conscious humans are perpetually engaged in cognitive adaptation to their continuously changing environment. Interruption of these processes by a task (i.e. suppression of the BOLD signal at task onset; task-induced deactivation) would thus reduce neural activity, and the BOLD signal during the stimulus phase, accounting for the apparent signal peak in the baseline condition (Binder et al., 1999). PET evidence suggests, however, that a similar "resting" state provides a consistent, reliable control in functional imaging studies across a variety of different experiments involving visual attention in normal

subjects (Shulman et al., 1997). Unconstrained eye movements could contribute to the observed results, but are unlikely to be a major confounding factor as previously discussed in section 3.3.

Secondly, the peak fMRI response during the resting phase could be due to ongoing *inhibitory* synaptic activity in extra-occipital areas, which are released from inhibition (disinhibited) during visual stimulation. Classically, all fibres projecting from cortical regions are excitatory to their target subcortical or cortical structures (Okazi et al., 1990). However, in the areas to which they project, inhibitory interneurones - which constitute some 20% of the number of excitatory neurones - may be located and have significant functional effects (Buchkremer-Ratzmann and Witte, 1996); experimental studies have demonstrated inhibitory (GABA-ergic) synapses within the striate visual cortex and between striate and extrastriate visual areas (McDonald and Burkhalter, 1993). It is therefore likely that some signals detected by BOLD fMRI during visual stimulation experiments are due to inhibitory neuronal activity. There are many reports of long-range inhibitory interactions in cerebral cortex, particularly those mediated across the corpus callosum (Swadlow, 1974, Diao et al., 1983). A striking example of reduction of tonic inhibition (i.e. disinhibition) in the visual cortex has been described by Sandell and Schiller (1982), who found that some striate neurons become more responsive to visual stimulation after cooling the region. The possible role of disinhibition in recovery from experimental visual system injury has been mentioned (the Sprague effect) (Ciarametro et al., 1997), but the model investigated in that study was of cortical damage rather than optic neuritis. Nevertheless, it is possible that distortion of the normal visual input via one or both optic nerves, as occurs in optic neuritis, causes an adaptive recruitment of

higher-order multimodal processing regions during visual stimulation that is mediated by releasing them from inhibitory control. Experimental studies indicate that widespread remote disinhibition is a common consequence of focal ischaemic cortical injuries in the motor and somatosensory systems (Buchkremer-Ratzmann and Witte, 1996), and that this process may facilitate plastic changes in neurological recovery. Whether a similar process can occur in response to impaired sensory input to the brain is not known.

A third, less likely explanation is that areas with increased resting BOLD signal are activated in response to darkness, and are unrelated to the stimulus. This seems unlikely in that there is no obvious reason to explain a response to darkness by brain regions known to have connections with visual processing areas, some of which have been proposed as sites of multimodal integration.

Finally, it is possible that the fMRI signals we have observed in patients are not related to neural activity differences between the active and resting states, but have a more prosaic explanation relating to a redistribution of the cerebral blood supply. In the PET literature, during activation there is an increased regional cerebral blood flow (rCBF) in cortex activated by the task, but this area is surrounded by regions of reduced flow which may extend for considerable distances (Ingvar, 1975). The type of sequence used for most fMRI studies (usually a gradient echo variant with T2* weighting) involves a compromise between sensitization to the BOLD effect and the effect of flow (due simply to an influx of blood with a different degree of nuclear magnetization into the imaged volume) (Frahm et al., 1994). It is commonly assumed that, using a repetition time of approximately 4000ms (as used here), flow makes a very small contribution to fMRI images, but a recent study has suggested that a redistribution of cerebral

blood flow during visual stimulation could explain BOLD responses with peak signal during the baseline condition (Guy et al., 1999). The hypothesis put forward was that blood flow is diverted towards the visual cortex during stimulation, causing a reduced BOLD signal in the areas from which blood is "stolen" due to reduced flow. It was also suggested that the "load" of the stimulus (determined by the complexity of the visual task) might affect the form and delay of the haemodynamic response, an observation that may be relevant in patients with a distorted pattern of visual input through an affected optic nerve. It is possible that in optic neuritis patients there is an exaggeration of this physiological phenomenon due to increased metabolic demands placed upon the visual cortex.

A noteworthy finding in the group activation maps for the 40-second epoch experiments is that stimulation of the affected eye activates a much smaller area (both within and outside the occipital visual cortex) than the clinically unaffected eye. This was not observed in the group maps from the previous study, and suggests that lengthening the duration of the visual stimulus has a selective effect in diminishing the extent of activation induced by stimulation of the eyes previously affected by optic neuritis. This suggestion is supported by the results of fitting a one-way ANOVA model, which demonstrates a more extensive reduction in power of response for the affected eye in the longer epoch experiment compared to the 20s epoch study (Figure 3.10). It should be noted, however, that the 40s epoch length also resulted in areas of less powerful response across the other groups (control left, control right and patient unaffected eyes), albeit to a lesser extent than for the affected eyes. Inspection of individual activated volumes also shows that the longer epoch length induces smaller volumes of activation across groups, but the effect is most marked for the affected eye.

There are several possible explanations for a reduced BOLD response in visual cortex for a long compared to a short simple visual stimulus. One possibility is that attending to a 40s stimulus is more fatiguing than to a 20s stimulus, so that the degree of vigilance decreases during stimulus epochs, thus reducing the power of periodic response. This could explain the general reduction in response observed across groups, and may contribute to the greater reduction in power and extent of activation from stimulation of the affected eye, which may receive a degraded input pattern.

The phenomenon of reduced visual function after viewing a prolonged bright light (termed "photostress") may be relevant to our findings. Following such a stimulus, a central scotoma is induced, with recovery of normal vision over about 10-15 seconds in healthy subjects. Photostress causes a transient increase in latency and decrease in amplitude of the VEP that recovers in normal subjects over about 70 seconds. In patients following optic neuritis (with good recovery) an impaired recovery of the VEP after photostress induced by 30 second exposure to a 200W bulb at 20 cm has recently been demonstrated (Parisi et al., 1998). The VEP latency and amplitude were seen to return towards normal at 40 and 60s after the photostress in patients and controls, but this was significantly slower in the affected compared to the unaffected eyes. Pattern electro-retinograms (PERGs) indicated that the delayed recovery may in part be due to an impairment of proximal retinal layer function. Photostress and recovery may involve the bleaching of retinal pigments and their resynthesis, but the precise mechnanisms are not well understood. There have been no investigations of photostress using fMRI in either controls or patients after optic neuritis, but it is possible that this phenomenon contributes to our finding of impaired fMRI activation in affected

eyes with a prolonged visual stimulus. The duration of stimulus used in our experiment, at 40 seconds, is comparable to that shown to induce photostress, and the luminance of our apparatus should be similar, based upon information provided by the manufacturer and standard luminance calculations (GJ Barker, personal communication). This possibility could be investigated further in optic neuritis patients by using an event-related experimental design to examine the haemodynamic response during individual stimulus epochs of differing lengths.

The photostress phenomenon is not confined to patients with optic nerve damage, and has been widely documented in normal controls, albeit to a lesser extent. Photostress could contribute to the present finding of areas in normal visual cortex with reduced power of response to the longer stimulus duration. The effect of photostress on fMRI activation may be relevant to the controversy regarding changes in the BOLD response during prolonged neural activity induced by visual stimulation. Some studies have demonstrated decay in BOLD signal during prolonged visual stimulation (Hathout et al., 1994; Frahm et al., 1996), whilst others did not (Bandettini et al., 1995b; Howseman et al., 1998). Explanations put forward for a diminishing BOLD response include a recoupling of blood flow with metabolism (the basis of the BOLD effect is generally agreed to reflect a transient excess of flow over neuronal metabolism at the onset of neural activity, causing a decrease in deoxyyhaemoglobin concentration - see Chapter 2) or an habituation of cortical neurons (Hathout et al., 1994). The present data suggest that factors in the *anterior* visual pathway may contribute to the BOLD response pattern in the visual cortex induced by a sustained bright stimulus, and that the epoch length has an important experimental influence upon the BOLD response.

In summary, this study has confirmed an abnormality of cerebral reponse to visual stimulation in patients who have recovered from optic neuritis, and has helped to clarify the mechanism of the neural response in extra-occipital areas. These putative multimodal regions show an increased neural response with a consistent signal peak during the baseline or resting phase of a simple visual stimulation experiment. It should be emphasized that at this stage the interpretation of the mechanisms of resting phase responses remains speculative, and that more work is required. The data we have presented suggests that they may have physiological significance in the recovery of function after CNS injury and deserve further study.

Chapter 4

Mechanisms of central nervous system damage in multiple sclerosis and stroke: studies using MR diffusion imaging

4.1 Introduction

Background

The excellent clinical recovery experienced by patients following an isolated optic neuritis (studied in Chapter 3) is similar to that commonly seen in relapses early in the course of MS. However, this selected group are not representative of the general MS patient population. Most patients ultimately enter a phase characterized by a progressive accrual of neurological deficit, probably related to continued, irreversible structural damage including axonal loss (see chapter 1). Abnormalities visualized by conventional MRI do not clearly correlate with clinical disability, at least in part due to its limited pathological specificity. The following chapter describes work performed with the aim of investigating the structural abnormalities in the brain in patients with clinically definite MS (and in a smaller number of patients with stroke) using MR diffusion imaging.

When MRI was first applied to MS in the early 1980s, it provided a striking visualization of signal abnormalities that corresponded to the location of demyelinating plaques (Young et al., 1981; Stewart et al., 1984; Ormerod et al.,

1987). However, the extent of focal disease (i.e. lesions) visible on conventional MRI (by which is generally meant images with varying degrees of T2-weighting) has shown at best only a modest correlation with disability (e.g. Thompson et al., 1990; Gass et al., 1994; Filippi et al., 1995b; Miller et al., 1998). Although at first puzzling, there are a number of possible explanations for this observation. Firstly, as we have seen, conventional MRI has limited pathological specificity, and essentially detects changes in the relaxation properties of free water protons. An identical pattern of MRI signal abnormality will result from different pathological changes including oedema, demyelination, axonal loss or gliosis, not all of which result in sustained clinical deficit. Secondly, compensatory mechanisms involved in clinical recovery may not be detected by standard MRI techniques. Thirdly, disability in MS is a complex entity that may result from interactions between physical impairments in different brain systems (e.g. motor, sensory, visual). The most commonly used measurement instrument, the EDSS (Kurtzke, 1983), is limited by a bias toward locomotor function, non-linearity, and furthermore measures aspects of both impairment and disability. Finally, using newer MR techniques (including magnetization transfer imaging and NAA spectroscopy), subtle abnormalities have been detected in the white matter of MS patients distinct from conventional MRI-visible plaques, in the normal-appearing white matter (NAWM). Since MR diffusion imaging is sensitive to changes in the mobility of water molecules in the brain, it may be of value in investigating the pathological changes in MS lesions and NAWM.

Magnetic resonance diffusion imaging in MS

MR diffusion imaging can noninvasively measure the apparent diffusion coeffecient (ADC) of water molecules in the CNS (LeBihan and Breton, 1985) (see Chapter 2). The ADC is influenced by the presence of boundaries that restrict or hinder water diffusion, including axonal membranes, the myelin sheath and subcellular organelles. In MS, pathological damage to these structures, for example by axonal loss or demyelination, may be expected to increase the ADC of affected tissue.

Early studies reported higher water diffusion in MS plaques compared to NAWM (Larsson et al., 1992; Christiansen et al., 1993), and found evidence that early plaques had the highest diffusion values. It was also noted that NAWM in patients had higher diffusion than normal control white matter (Christiansen et al., 1993). These studies were limited by head motion (an inherent problem in diffusion imaging), an inability to measure diffusion in more than three directions, and restricted brain coverage. The diffusion studies described in this chapter represent methodological improvements on these initial studies.

The first study described in this chapter (section 4.2) investigated water diffusion throughout the brain NAWM in a population of MS patients and its relationship to water diffusion in focal lesions, using an EPI technique that minimizes the effect of motion. The second study (section 4.3) used the relatively recently developed technique of diffusion tensor imaging (DTI), which provides a fuller description of water diffusion. DTI permits the estimation of the structural property of anisotropy, which may reflect fibre tract integrity and orientation (see chapter 2). The third study (section 4.4) used DTI to study patients following

ischaemic stroke, in order to investigate the relationship between diffusion changes in a *single* focal cerebral lesion and the fibre tracts that traverse it.

4.2 An echoplanar MR diffusion study of water diffusion in the normal-appearing white matter MS and its relationship to water diffusion in focal lesions

Introduction

Because the NAWM often represents a larger tissue volume than MRI-visible focal lesions, even minor abnormalities of NAWM structure or function may have significant functional effects. This suggestion is supported by data from some groups demonstrating strong correlations between NAWM abnormalities and clinical deficits (e.g. Fu et al., 1998, van Buchem et al., 1998). It is therefore important to understand the mechanisms by which NAWM abnormalities originate; a fundamental question is whether they arise independently of focal lesions. If the pathogenetic mechanisms causing NAWM and focal lesions are closely linked, then the extent of structural damage in NAWM would be expected to correlate with that in focal lesions. To test this hypothesis a method that is able to detect and quantify subtle pathological changes is required. As we have seen, MR diffusion imaging is promising in this regard, being sensitive to the size, orientation and integrity of water spaces in tissue. The aims of the present study were: firstly, to investigate the relationship between water diffusion in the NAWM and within focal lesions in a representative cohort of patients with MS; secondly, to assess the spatial distribution of NAWM abnormalities; and thirdly, to

investigate the diffusion properties of lesions, which were subclassified according to the presence of T1 hypointensity [indicating severe axonal loss (van Walderveen et al., 1998)] or signal enhancement following contrast agent injection [indicating active inflammatory activity (Katz et al., 1993)].

Although MR diffusion imaging has relatively high spatial resolving power compared to other techniques (including NAA spectroscopy), its clinical application has until quite recently been limited by technical factors, including motion artefacts. An EPI technique largely eliminates motion artefact, allowing the rapid and reliable acquisition of diffusion data from the whole brain (typically in under three minutes). This allows a full assessment of the spatial distribution of NAWM abnormalities in the brain. The use of a fluid suppression technique reduces the contamination of regions of interest by rapidly diffusing cerebrospinal fluid (CSF), providing more accurate diffusion measurements (Kwong et al., 1991).

Patients and methods

Subjects. Forty patients with clinically definite MS (Poser et al., 1983; Lublin and Reingold, 1996) attending the National Hospital for Neurology and Neurosurgery were studied with approval from the combined National Hospital and Institute of Neurology ethics committee after giving informed written consent. No patients had received any immune-modifying treatment in the three months prior to the study. The clinical groups were defined as follows: benign (n=8) had a relapsing remitting course and minimal disability at 10 years disease duration; relapsing-remitting (n=9) had a history of relapses and remissions without progressive

deterioration; secondary progressive (n=13) had progressive deterioration for at least six months following an initial relapsing-remitting course; and primary progressive (n=10) had a progressive deterioration of at least 2 years from onset without relapses or remissions. A history and full neurological examination was performed, and the EDSS score (Kurtzke, 1983) was determined by a trained observer. Fourteen healthy age- and sex-matched controls were studied.

MRI:Conventional imaging. The field of view for all studies was 240mm x 240mm. After a sagittal localiser, fast spin echo images (with proton-density and T2-weighted contrast) were obtained at 28 contiguous 5mm axial slices (matrix size=256x256, TR=2000ms, T_{eff} =14/100). EPI diffusion studies were then performed without repositioning (see below), followed by multishot EPI scans (matrix size=256x256, TR=200ms, TE=30ms) at 16 x 5mm contiguous axial locations, matched in position and geometric distortion to the corresponding diffusion-weighted images. Finally, T1-weighted images (matrix size=256x256, TR=540ms, TE=20ms) were acquired five minutes after the administration of Gd-DTPA in all patients except the primary progressive group, and those with known allergies to contrast media. Previous studies have shown that the yield of enhancing lesions is low in the primary progressive group (Thompson et al., 1991).

MRI: Diffusion imaging. A single-shot spin echo EPI diffusion-weighted imaging sequence was used, with an inversion recovery pulse used to suppress the signal from cerebrospinal fluid (CSF) (Barker et al., 1997), improving lesion conspicuity in areas close to CSF spaces and reducing contamination of regions of interest by

partial volume of CSF (Kwong et al., 1991). Images were obtained from 16 contiguous 5mm slices. The parameters were as follows: matrix size=128x128, TR=5000ms, TI=1265ms, 10 gradient b factors up to 960 smm^{-2}, gradient strengths 0-22mT/m applied along the three principle gradient axes in turn. The ADCs corresponding to diffusion sensitisation along each axis (ADC_x, ADC_y and ADC_z) at each voxel were calculated using in-house software, which related the signal attenuation to the b factor (the degree of sensitization to diffusion, including inherent sensitization due to the imaging gradients) (Stejskal and Tanner, 1965) according to the following:

$$\frac{S}{S_0} = \exp(-bADC)$$

where S and S_0 represent the signal in the presence and absence of diffusion sensitive gradients respectively, ADC is the apparent diffusion coefficient and b is the gradient b factor which depends on the duration and magnitude of the applied diffusion gradients (LeBihan et al., 1985; LeBihan et al., 1996). From ADC_x, ADC_y and ADC_z , a directionally-averaged diffusion coefficient, ADC_{av}, was calculated as follows:

$$ADC_{av} = \frac{ADC_x + ADC_y + ADC_z}{3}$$

Providing the contribution of imaging gradient "cross terms" to the signal attenuation is negligible (as has been shown to be the case for the EPI sequence

used in this study), ADC_{av} provides a rotationally invariant measurement of diffusion. This removes the effect of the variation of diffusion with tissue direction (anisotropy), and is important when comparing similar brain regions across different subjects that may be oriented differently in the magnet.

Image analysis. Images were displayed and processed on a Sun workstation (Sun Microsystems, Mountain View, CA). Regions were identified on the high resolution EPI images (with reference to the conventional proton-density and T2-weighted scans) in frontal, parietal, temporal, occipital, cerebellar white matter and internal capsule bilaterally, and the splenium of the corpus callosum, in patients and normal subjects. The regions were defined according to strict anatomical criteria, and partial volume effects were minimized by inspecting the slices above and below the lesion. The genu of the corpus callosum was not examined due to its small size (and thus difficulty in avoiding partial volume). All NAWM regions were of uniform size (25 pixels or approximately $22mm^2$) and shape, and were obtained by a single observer (DJW) who was blinded to the clinical details. Regions of interest were transferred on to the calculated ADC_{av} maps and their mean ADC_{av} was determined. Lesions were identified on conventional proton-density and T2-weighted images and outlined using a semi-automated contouring program (*DispImage*, D Plummer, UCL Hospitals Trust) upon the high-resolution EPI images (non-diffusion weighted) before transferring them to the ADC_{av} maps. Each lesion was first classified as enhancing or non-enhancing and then the non-enhancing lesions were classified (using the post-contrast T1-weighted images) as T1 iso- or hypointense. T1 hypointensity was defined as reduced lesion signal intensity with respect to the surrounding NAWM.

The mean ADC_{av} was measured for each lesion. A mean ADC_{av} was calculated from the mean of all the lesions in each patient. A second mean ADC measure, weighted to take account of lesion size, was defined as:

$$ADC_{weighted} = \frac{\sum(ADC_{lesion} \times Area_{lesion})}{\sum Area_{lesion}}$$

where $ADC_{weighted}$ is the weighted measure, ADC_{lesion} and $Area_{lesion}$ represent the mean ADC and area of each individual lesion within the subject. The lesion load for each subject was calculated from the T2-wieghted EPI images using the semi-automated lesion areas and software developed at the Institute of Neurology.

Statistical analysis. An analysis of the ADC_{av} data was performed using mixed-model regression (Hand and Crowder, 1996), implemented by using SAS v6.12 PROC MIXED (SAS Institute Inc., Cary, North Carolina, USA). An unstructured covariance matrix was adopted. Probability values were obtained subsequent to a conversion of the restricted maximum likelihood (REML) Wald statistics to F ratios. The comparison of the control and MS patients is based on the difference between the REML control ADC_{av} estimate and the average of the four MS subtype ADC_{av} estimates. The correlation between mean NAWM ADC_{av} and both mean lesion ADC_{av} and $ADC_{weighted}$ in patients was assessed using a significance test of Spearman's correlation coefficient.

Results

Patients and controls did not differ significantly in either age (mean 38.4 years vs 43.7 years, p=0.13) or sex (male: female ratios 0.74: 1 and 0.75: 1 respectively). The clinical characteristics of the patients are shown in Table 4.1.

Table 4.1. *Characteristics of patients*

Multiple sclerosis subtype	Number of patients	Mean age (years) (SD)	Mean disease duration (years)	Median EDSS
Benign	8	44(5)	16.4	3.0
Relapsing- remitting	9	33(8)	5.8	4.0
Secondary progressive	13	40(8)	12.2	6.0
Primary progressive	10	57(12)	15.0	6.8

Diffusion-weighted images of good quality were obtained in all patients and controls, without visible evidence of motion artefact.

Findings in lesions

Lesions appeared as bright areas on ADC_{av} maps (Fig. 4.1) and had significantly higher ADC_{av} values (median ADC_{av}=0.96 $x10^{-3}mm^2s^{-1}$) than patient NAWM or control white matter ($p<0.001$). T1-hypointense lesions (median ADC_{av}=1.05 $x10^{-3}mm^2s^{-1}$) had significantly higher ADC_{av} values than non-T1 hypointense lesions (median ADC_{av}=0.95 $x10^{-3}mm^2s^{-1}$) ($p<0.001$). There was no statistically significant difference between ADC_{av} values in enhancing (median ADC_{av}=0.94 x $10^{-3}mm^2s^{-1}$) and non-enhancing (median ADC_{av}=0.96 $x10^{-3}mm^2s^{-1}$) lesions. There was no significant correlation between mean lesion ADC_{av} and EDSS.

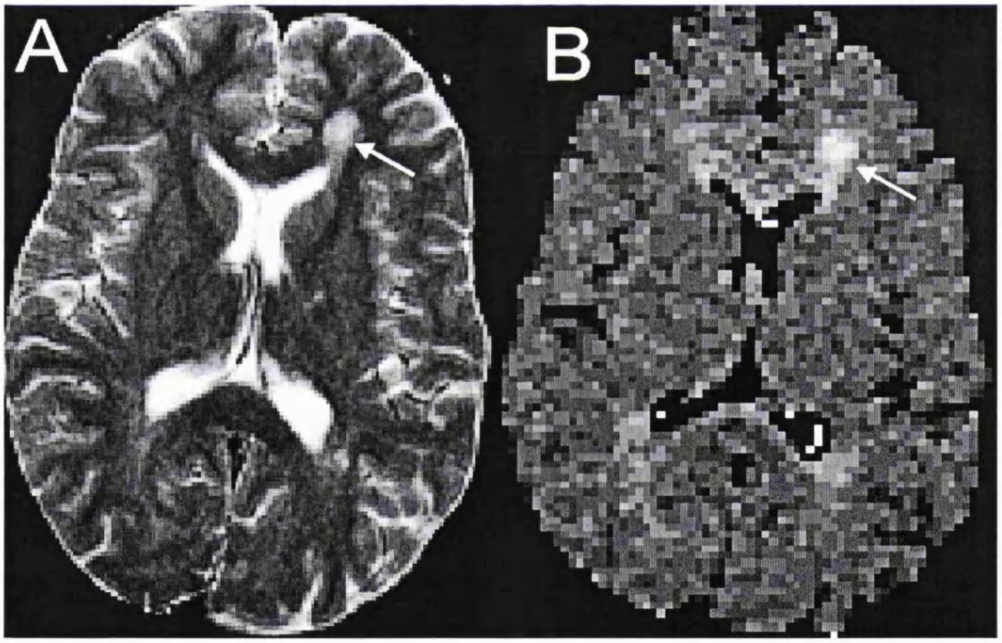

Figure 4.1 (A) T2-weighted image of a patient with clinically definite MS, showing a lesion in the left frontal region (arrowed). **(B)** Mean apparent diffusion coefficient (ADC_{av}) map. Bright voxels correspond to high ADC_{av} values.

Findings in control white matter and patient NAWM

The mixed model regression analysis of all available NAWM region data revealed a significant effect of subtype (i.e. benign, relapsing-remitting, primary progressive, secondary progressive or control) ($p=0.022$). Controls consistently showed a lower mean ADC_{av} than the patient subgroups, but there was no statistically significant difference between the different MS disease groups ($p=0.22$). These results suggest that the lower ADC_{av} in controls accounts for the effect of subtype. When all regions were considered together, the mean ADC_{av} was significantly higher in patients than controls ($p=0.008$).

There was a significant effect of anatomical region ($p=0.0001$) upon NAWM ADC_{av}; the corpus callosum consistently showed the highest mean ADC_{av} in all groups. The interaction between region and subtype approached statistical significance ($P=0.0565$), suggesting that different brain regions in patients show different degrees of ADC_{av} elevation compared to controls. We therefore averaged data by region in order to investigate this effect (Table 4.2). Patients had a higher mean ADC_{av} than controls for all regions examined; this was most significant ($P<0.05$) for the callosal, cerebellar, temporal and frontal regions. No significant correlation was found between mean NAWM ADC_{av} and disability (EDSS).

Correlations between NAWM and lesion ADC_{av}

Lesions had significantly higher ADC_{av} values than patient NAWM ($p<0.001$) or control white matter ($p<0.001$). The mean lesion ADC_{av} was strongly correlated with the mean NAWM ADC_{av} ($r=0.67$, $p<0.001$) (Fig 4.2); the weighted mean

lesion diffusion coefficient, $ADC_{weighted}$ showed a similar correlation with NAWM ADC_{av} ($r=0.60$, $p<0.001$). T2-weighted EPI lesion load did not correlate with mean NAWM ADC_{av} ($r=0.023$, $p=0.89$).

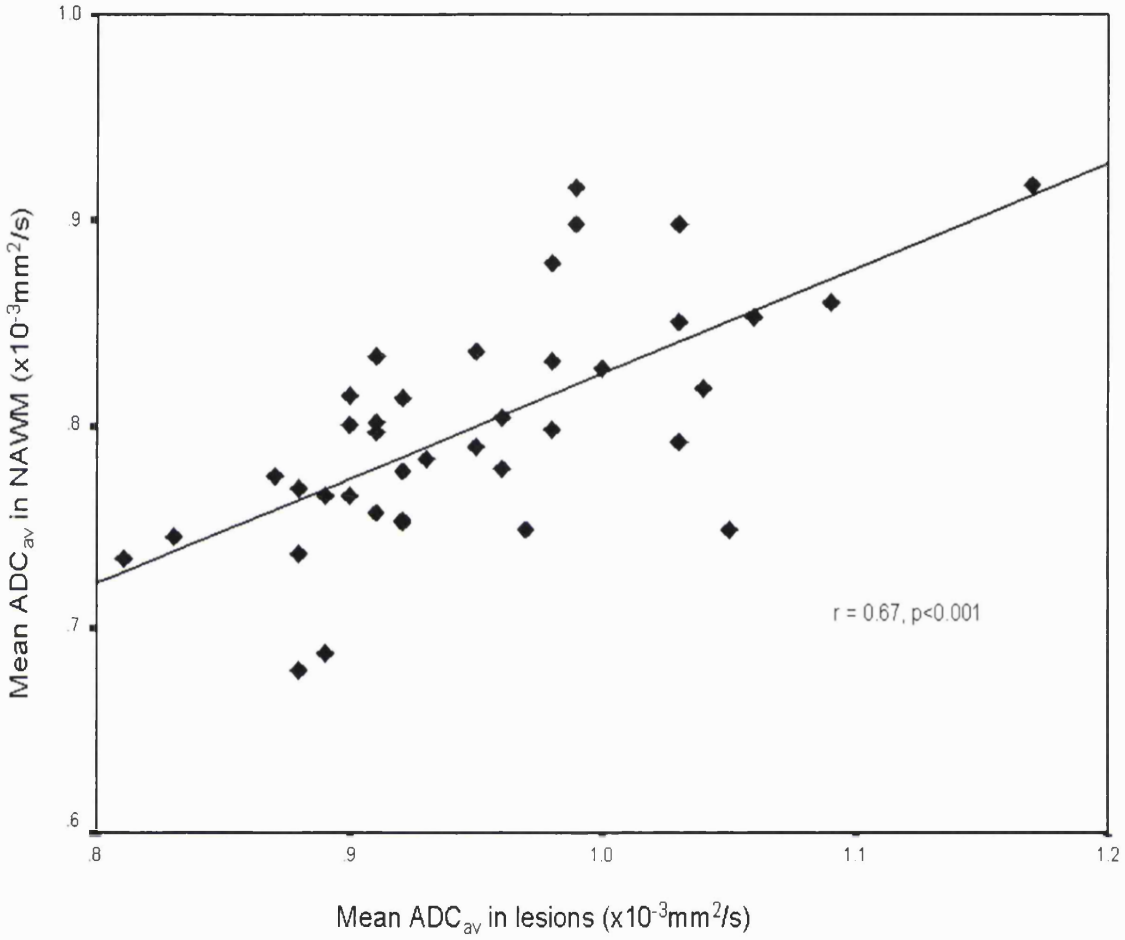

Fig. 4.2. Correlation between mean ADC_{av} in NAWM and mean ADC_{av} in lesions for each patient.

Table 4.2. *Regional ADC values (x10 $^{-3}$ mm ^{2}/s) in normal appearing white matter regions.*

	CONTROLS (182 regions)		PATIENTS (472 regions)			
Region	**Mean**	**Range**	**Mean**	**Range**	**Estimated difference in means**	**Significance of difference**
Frontal	0.75	0.67-0.98	0.78	0.69-0.91	0.03	0.07
Parietal	0.77	0.67-0.89	0.78	0.62-0.98	0.01	0.66
Capsule	0.73	0.64-0.87	0.76	0.60-0.93	0.03	0.20
Callosum	0.85	0.62-1.01	0.92	0.58-1.20	0.08	0.03*
Temporal	0.75	0.66-0.83	0.81	0.64-0.99	0.06	0.02*
Occipital	0.76	0.66-0.90	0.81	0.66-0.99	0.05	0.04*
Cerebellum	0.75	0.56-0.99	0.81	0.64-1.00	0.06	0.03*
All regions	0.76	0.69-0.87	0.80	0.68-0.92	0.04	0.008*

*$p<0.05$. All results obtained by mixed model regression. Not corrected for multiple comparisons

Discussion

This study provides quantitative data on the anatomical distribution of water diffusion abnormalities in the NAWM, and their relationship to those in lesions in MS patients. It has shown firstly that water diffusion abnormalities in NAWM are widespread throughout the brain; and secondly that there is a graded relationship between the mean ADC_{av} in NAWM and the mean ADC_{av} in lesions, a finding which suggests that the processes causing structural damage in NAWM and lesions are closely linked.

Findings in control white matter

The ADC_{av} measurements in control white matter are in good agreement with those from other MR diffusion imaging techniques (Pierpaoli et al., 1996; Falconer et al., 1997; Droogan et al., 1999; Ulug and van Zijl, 1999), but also provide regional measurements that have not previously been reported in detail. The highest ADC_{av} was consistently found in the corpus callosum, in agreement with previous work in smaller numbers of subjects using CSF-suppressed diffusion imaging (Falconer et al., 1997) and DTI (Ulug and van Zijl, 1999). The corpus callosum is highly anisotropic, containing tightly-packed, similarly oriented axons that exhibit higher diffusion along than across them (Pierpaoli et al., 1996). Since the ADC_{av} is a directionally averaged measure of diffusion, it should not necessarily be influenced by anisotropy; the reason for higher diffusion in the corpus callosum is thus not clear, and merits further study. These findings are unlikely to be due to CSF contamination since a CSF-suppressed method was

used, and suggest that in studies comparing ADC_{av} between patient and control groups it is important to anatomically match regions of interest, or to compensate for the anatomical variation of the ADC_{av} in other ways.

Findings in NAWM

The observation of a significantly increased ADC_{av} in the NAWM of patients with MS compared to normal controls is in agreement with other studies (Christiansen et al., 1993; Horsfield et al., 1996; Droogan et al., 1999). Due to the large number of different regions examined (requiring multiple statistical comparisons) and the limited population sample size, the regional findings in the present study should be considered exploratory, and require confirmation in a larger population. Nonetheless, there was a significant overall difference in NAWM ADC_{av} between patients and controls ($p<0.008$), and a significantly elevated patient ADC_{av} compared to controls in several brain regions examined. These data are consistent with widespread structural abnormality in the NAWM of MS patients, in keeping with findings using relaxation time measurements (Ormerod et al., 1986; Miller et al., 1989a) MT imaging (Dousset et al., 1992; Loevner et al., 1995) and proton NMR spectroscopy (Davie et al., 1994; Husted et al., 1994; Sarchielli et al., 1999). Of the seven brain regions studied, the ADC_{av} was significantly elevated in callosal, cerebellar, temporal and occipital white matter, with the largest difference in the corpus callosum. Diffuse and focal structural damage to the corpus callosum are both well documented in MS. A non-significant trend toward ADC_{av} elevation was noted in the internal capsule and the frontal and parietal NAWM. Less severe abnormality in the internal capsule NAWM than other regions has previously been

reported using MT imaging (Loevner et al., 1995; Leary et al., 1999), which could relate to the relative rarity of focal abnormalities in the region of the internal capsules (Brownell and Hughes, 1962; Narayanan et al., 1997).

Histopathological and biochemical studies have reported astrocytosis, demyelination, perivascular inflammation and oedema in the NAWM of patients with MS (Allen and McKeown, 1979; Newcombe et al., 1980), and an increase in tissue water (Tourtellotte and Parker, 1968). Recent work has also described extensive axonal loss in corpus callosum NAWM (Evangelou et al., 2000). These processes, with the exception of astrogliosis, would be expected to increase the amount of freely diffusing extracellular water in NAWM, thus elevating the ADC_{av}. Abnormalities of neurofilament phosphorylation have also been reported in NAWM (Trapp et al., 1998), which may increase the mobility of intracellular water.

The strong and significant graded relationship between mean lesion ADC_{av} and mean NAWM ADC_{av} suggests an association between the extent of structural damage in lesions and that in the NAWM. Although the basis of this relationship remains speculative, several mechanisms may contribute. The well-described transection of axonal cylinders in the lesions of MS (Ferguson et al., 1997; Trapp et al., 1998) may cause remote NAWM abnormalities by anterograde or retrograde degeneration. A reduced NAA concentration has been found to extend beyond regions containing visible lesions, consistent with axonal degeneration into surrounding NAWM (Narayanan et al., 1997). Our data are consistent with this hypothesis, since patients with the most severe axonal damage in lesions would be expected to have the most pathology in NAWM. However, the similar correlations between both the mean lesion ADC_{av} and the size-weighted mean lesion ADC_{av}

with NAWM ADC_{av}, and the lack of correlation between T2-weighted lesion load and NAWM ADC_{av}, suggest that NAWM abnormalities are not solely due to Wallerian degeneration of fibres traversing macroscopic lesions. Another possibility is that active lesions influence water diffusion in remote areas of NAWM by the spread of diffusible molecules (e.g. cytokines) associated with inflammation (Moreau et al., 1996).

There are increasing data to suggest that structural changes in NAWM precede (and may trigger) the development of focal lesions (Goodkin et al., 1998; Filippi et al., 1998; Pike et al., 1998). One mechanism linking lesion and NAWM pathology may thus be that a continuous low-grade process of inflammatory BBB leakage occurs in NAWM, which reaches a threshold, beyond which severe and irreversible BBB damage occurs and a focal lesion emerges.

Rather than being directly linked, the pathological processes in lesions and NAWM may both be driven by a common pathogenetic mechanism that varies in severity between different patients. The mechanisms accounting for pathological heterogeneity in MS are not well understood, but genetic factors might play a role; the distribution of MRI abnormalities differs between Japanese and Caucasian patients (Nakashima et al., 1999), and it is possible that genotype also affects pathological severity in lesions and NAWM (Miller, 1999). This suggestion is supported by recent studies suggesting that different subgroups of patients exhibit markedly different patterns in the extent and topology of oligodendrocyte damage within lesions (Luchinetti et al., 1999).

Finally, it cannot be excluded that in some patients NAWM and lesion abnormalities are due to independent processes, a suggestion supported by the considerable NAWM abnormalities in primary progressive MS, in which there is a

relative paucity of cerebral lesions (Thompson et al., 1991; Leary et al., 1999).

In summary, the present study has shown that there is an anatomically widespread elevation of the mean ADC_{av} in MS NAWM, which shows a robust correlation with the mean ADC_{av} in lesions. This suggests that at least some of the NAWM abnormalities in MS do not arise independently of focal lesions (or *vice versa*). MR diffusion imaging is a useful tool with which to investigate mechanisms of structural damage in lesions and NAWM, and the relationship between them. Longitudinal clinical studies and histopathological correlations will help to further clarify the pathogenesis of these abnormalities.

4.3 Diffusion tensor imaging of lesions and normal-appearing white matter in multiple sclerosis

Introduction

In the previous study, ADC measurements were made in lesions and NAWM of patients with MS by obtaining diffusion-weighted images sensitized to diffusion in three different directions. As discussed in chapter 2, this approach does not fully describe the motion of water molecules in the brain, particularly in regions where the tissue structure is directional, for example in white matter fibre tracts. Specifically, it is not possible to accurately estimate diffusion anisotropy, a property that may be of particular relevance in MS. Intact white matter fibre tracts generally exhibit high anisotropy, which should be affected by pathological damage in MS, for example by demyelination or axonal loss. Accurate quantification of diffusion anisotropy requires estimation of the diffusion tensor.

In addition to the accurate quantification of diffusion anisotropy (Pierpaoli and Basser, 1996) a further important advantage of estimating the diffusion tensor is that the quantities derived from it are rotationally invariant: that is, the same measurements for a particular brain structure will be obtained regardless of patient orientation (this may under some circumstances be true for diffusion measurements derived from three axis data, but cannot be assumed).

A DTI study was performed in MS patients with evidence of active disease on Gd-DTPA enhanced T1-weighted MRI scans. The aim was to systematically investigate the structural properties of NAWM and lesions (acute and chronic, T1 hypointense and T1 isointense) in patients, and the white matter of normal controls. The properties measured were mean diffusivity (MD), a measure of the magnitude of diffusion analogous to the ADC_{av} measured in the previous study; and fractional anisotropy (FA), a measure of diffusion anisotropy estimated from the diffusion tensor. This study investigated the relative sensitivity of MD and FA in the differentiation of lesion subtypes and of patient NAWM from control white matter, and the relationship between MD and FA, to ascertain whether they provide independent or complementary structural information.

It was hypothesized that pathological changes in the NAWM (whether predominantly axonal loss or gliosis), and in lesions (due to demyelination and/or other pathologies) should reduce anisotropy compared to control and patient white matter respectively, due to a reduction of the structural coherence of fibre tracts. Increases in diffusion in NAWM and plaques compared to control and patient white matter respectively were anticipated, in line with previous studies. It was anticipated that larger abnormalities would be found in acute inflammatory lesions compared to chronic lesions due to the presence of extracellular oedema, and in

T1 hypointense compared to T1-isointense lesions, due to a greater degree of axonal loss.

Patients and methods

Patients Six patients (mean age 34.2 +/-4.2 years; one male, five females) with clinically definite MS [ascertained using the Poser criteria (Poser et al.,1983)] attending the National Hospital for Neurology and Neurosurgery, London, were studied. A full neurological history and examination was performed, and disability was assessed using the EDSS (Kurtzke, 1983). Five had relapsing-remitting, one secondary progressive MS. Six normal healthy age and sex matched controls (mean age 34.3+/-8.9 years; one male, five females) were also studied.

MRI methods. High resolution mildly- and heavily-T2-weighted images were acquired at 26 contiguous 5mm axial slice positions covering the whole brain (TR=2000ms, TE=30/120, matrix size=256x256), followed by diffusion-weighted EPI images with no repositioning (TE=78ms, matrix size=96x96.) Diffusion gradients at 4 b values increasing from ~0 to 700 sec/mm2 were applied in each of 7 non-collinear directions) at 10 slice locations centred upon the lateral ventricles matched to the T2-weighted image slices. Five acquisitions of each set of diffusion data were performed and co-added following magnitude reconstruction to improve the signal to noise ratio. Cardiac gating was used; image acquisition was triggered from every second R wave monitored using a pulse oximeter. The diffusion tensor, MD and FA were calculated on a pixel by pixel basis (Basser et al., 1994; Basser and Pierpaoli, 1996). FA was chosen as it provided excellent

contrast between white matter tracts and cortical grey matter. After DTI, T1-weighted images were acquired (TR=540ms, TE=20ms, matrix size=256 x 256) 5 minutes after the administration of Gd-DTPA (0.1mmol/kg).

Region analysis. Lesions were outlined upon the T2-weighted images using a semi-automated technique; enhancement and T1 hypointensity were defined as previously. Rectangular NAWM regions of uniform size were defined in similar anatomical areas to the lesions (frontal WM, parietal WM, temporal WM, occipital WM) on the T2-weighted images. In order to allow the accurate transfer of regions between the T2-weighted images and the quantitative DTI maps, the latter were interpolated to the same matrix size as the T2-weighted images. For each region, MD and FA were measured. The geometric distortions of the EPI diffusion-weighted images were minimal at the slice positions studied; the accuracy of mapping was confirmed by correct registration of the outlined brain and ventricles between the two sets of images (T2- and DTI) for each patient.

Statistical analysis. The MD and FA values for each set of regions (control NAWM, patient NAWM, non-enhancing lesions, enhancing lesions, T1 hypointensities) were compared using the Mann-Whitney U test. The relationship between MD and FA was assessed by a significance test of Spearman's correlation coefficient.

Results

The median EDSS of the patients was 3.9 (range 1.0-7.0); the median disease

duration was 3.5 years (range 1.0-17.0 years). The following numbers of regions were studied: 261 areas of white matter in controls; 206 areas of NAWM in patients; 270 lesions, of which 25 were enhancing, 15 were T1-hypointense and 230 T1-isointense. Some lesions were clearly seen on both MD and FA maps, particularly those that enhanced. An example of a conspicuous, enhancing lesion is shown in Fig. 4.3.

The results are summarised in Table 4.3 and Figs. 4.4 and 4.5. MD was higher ($p<0.001$), and FA lower ($p<0.001$), in patient NAWM compared to control WM. Lesions had higher MD ($p<0.001$) and lower FA ($p<0.001$) than NAWM. MD was higher ($p=0.03$), and FA lower ($p<0.001$) in enhancing compared to non-enhancing lesions. MD was higher ($p=0.002$), and FA tended to be lower ($p=0.17$), in T1 hypointense non-enhancing lesions compared to T1 isointense non-enhancing lesions. There was a modest inverse correlation between MD and FA for all regions studied (Spearman's rho =-0.45, $p<0.001$) (Fig 4.6).

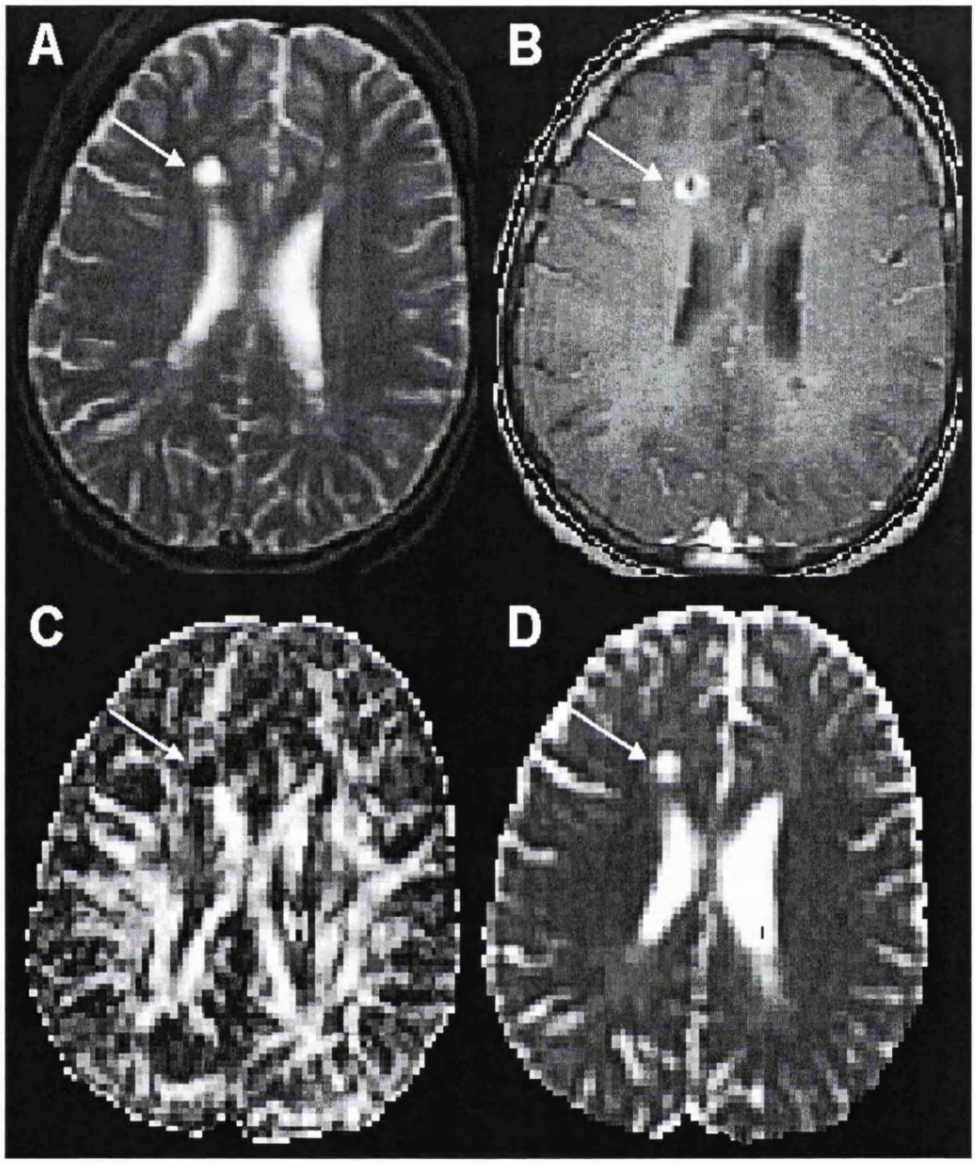

Fig. 4.3. Images acquired at an axial brain slice in a patient with MS. A lesion is present in the right frontal region (arrowed). **(A)** Conventional T2-weighted scan shows a typical area of high signal; **(B)** Post-contrast T1-weighted scan shows 'ring' enhancement; **(C)** Map derived from DTI of calculated FA at each voxel. Intact white matter tracts have high FA (bright voxels). Disruption of tissue integrity causes a loss of FA in the lesion (dark voxels, arrowed). **(D)** Map of MD. The lesion shows increased MD (bright voxels) compared to surrounding tissue; this may reflect acute oedema. The right side of the brain appears to the left side of each panel.

Table 4.3. *Fractional anisotropy and mean diffusivity for different lesion subtypes*

		FRACTIONAL ANISOTROPY (dimensionless units)				MEAN DIFFUSIVITY ($x10^{-3}mm^2/sec$)			
	Number of regions	**Minimum**	**Maximum**	**Mean (SD)**	**Median**	**Minimum**	**Maximum**	**Mean (SD)**	**Median**
NAWM (control)	261	0.29	0.87	0.60 (0.13)	0.60	0.59	1.10	0.84 (0.08)	0.84
NAWM (MS)	206	0.26	0.84	0.56 (0.12)	0.56	0.69	1.17	0.88 (0.08)	0.87
Lesions (all)	270	0.25	0.83	0.50 (0.12)	0.48	0.74	2.12	1.11 (0.21)	1.05
Lesions (NE, I)	230	0.25	0.83	0.51 (0.12)	0.49	0.74	2.12	1.09 (0.21)	1.03
Lesions (NE, H)	15	0.31	0.58	0.47 (0.08)	0.46	1.00	1.80	1.24 (0.21)	1.25
Lesions (NE, I+H)	245	0.25	0.83	0.51 (0.12)	0.49	0.74	2.12	1.10 (0.22)	1.04
Lesions (E)	25	0.25	0.60	0.38 (0.09)	0.36	0.90	1.57	1.16 (0.17)	1.14

NAWM = normal appearing white matter, E = enhancing, NE = non-enhancing, I = isointense, H = hypointense, SD = standard deviation

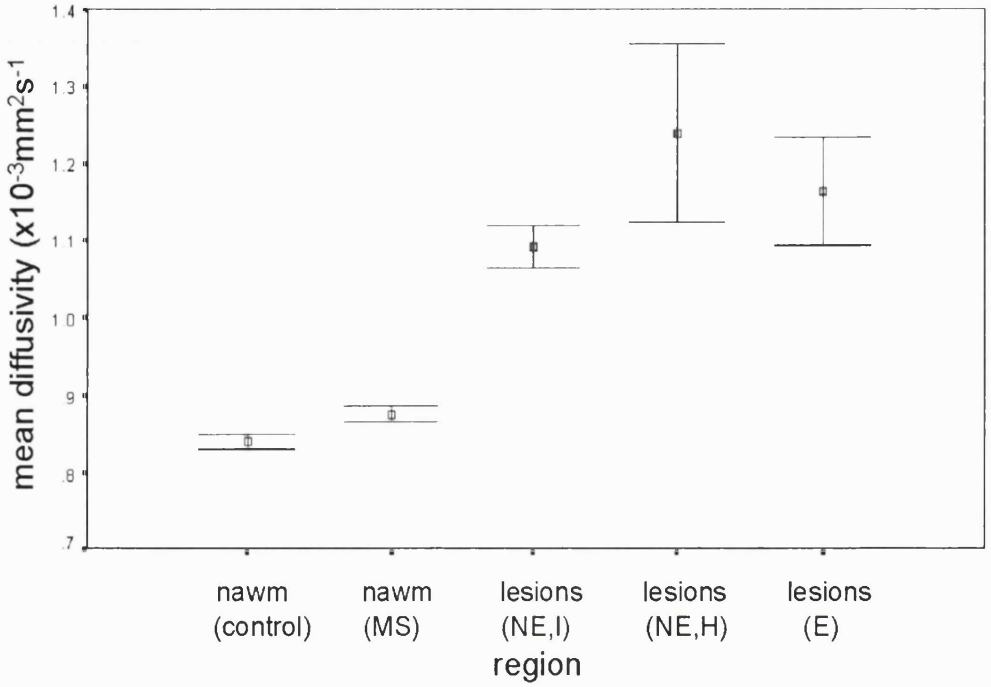

Fig. 4.4. MD for different types of region. Boxes represent the mean values, whiskers represent 95% confidence intervals. (E=enhancing; NE = non-enhancing; I=T1-isointense; H=T1-hypointense).

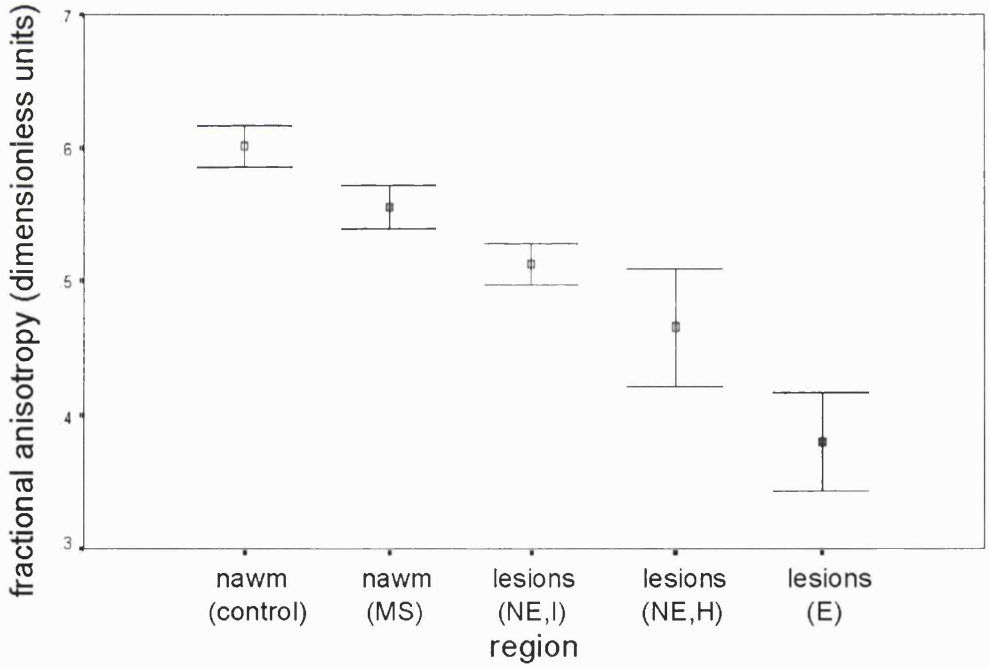

Fig. 4.5. FA for different types of region. Boxes represent the mean values, whiskers represent 95% confidence intervals.

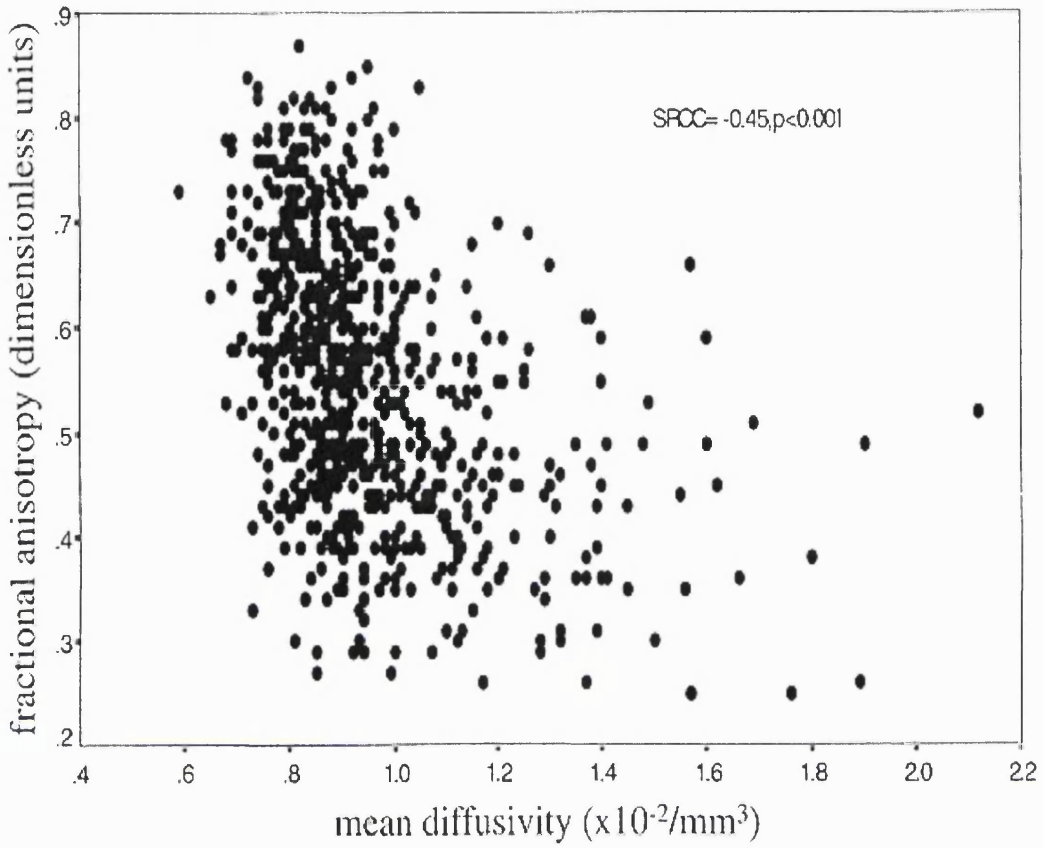

Fig. 4.6. Scatter plot of fractional anisotropy against mean diffusivity for all regions studied showing a modest inverse correlation ($r=-0.45$, $p<0.001$). This suggests that they may provide partially independent and complementary data for evaluating tissue structure.

Discussion

This study provides new quantitative structural information on the NAWM and lesions in MS. The full diffusion tensor was calculated to provide rotationally invariant diffusion information, including precise quantification of diffusion anisotropy. The diffusion characteristics in NAWM and lesions with different degrees of pathological severity and acute inflammatory activity were measured.

Findings in NAWM

In this study, patient NAWM showed significantly higher MD, and lower FA, than control white matter. These findings consolidate previous diffusion studies, but also expand upon them by demonstrating a reduction in diffusion anisotropy. Histopathological and MRI data from a variety of techniques already discussed (including MT imaging and NMR spectroscopy), converge to indicate a diffuse abnormality of structure in NAWM. In particular, studies of NAA concentrations using NMR spectroscopy suggest that axonal damage or dysfunction occurs in the NAWM of MS patients (Davie et al., 1995; Sarchielli et al., 1999). Axonal loss, with an expanded extracellular space, has been demonstrated in histopathological studies of NAWM (Allen and McKeown, 1979; Evangelou et al., 2000), as has an increase in water content (Tourtellotte and Parker, 1968). These abnormalities may contribute to the pattern of diffusion changes (increased MD, reduced FA) described in the present study.

Mean diffusivity findings in lesions

The finding of raised MD in lesions compared to NAWM is consistent with previous studies showing an increased lesion ADC (Larsson et al., 1992; Christiansen et al., 1993) and suggests a net loss of structural barriers to water molecular motion in plaques. Higher MD was observed in acute (enhancing) compared to chronic (non-enhancing) lesions. Post-mortem studies have confirmed that lesion enhancement reflects inflammation, blood brain barrier leakage and oedema (Katz et al., 1993; Bruck et al., 1997). There is also evidence

that axonal loss can occur in acute lesions (Trapp et al., 1998). The present findings in acute lesions could thus be explained by an expansion of the extracellular space due to a combination of vasogenic oedema and axonal loss. In the population of acute lesions studied the effects of these processes outweigh those which could potentially restrict water molecular motion, such as the accumulation of inflammatory cells including macrophages and the presence of myelin breakdown products (Graham et al., 1995; Gass et al., 1998). There is evidence from proton NMR spectroscopy that acute MS lesions contain lipid products of myelin breakdown (Davie et al., 1997); further work combining diffusion MRI with proton NMR spectroscopy may help to clarify the effect of these products on water diffusion.

The previous study using three axis diffusion in a representative population of 40 MS patients did not show a significant difference between the magnitude of water diffusion in acute (enhancing) compared to chronic (non-enhancing) lesions, by contrast with the present study. One explanation for this apparent discrepancy may be that in the present investigation all patients had evidence of active disease on Gd-DTPA enhanced scans, with mean disease duration 3.5 years, whereas in the previous study the mean disease duration was 12.5 years and many patients were clinically stable at the time of MRI scanning. It is thus possible firstly, that a higher proportion of the non-enhancing lesions in the previous study are older and show more severe structural damage in comparison to those in the present study; and secondly, that the diffusion properties of enhancing lesions differ between clinically active and clinically stable patients.

There was a large range of MD values in chronic (non-enhancing) plaques, suggesting considerable pathological heterogeneity. Possible contributory

processes include gliosis, which might reduce diffusion (Christiansen et al., 1993). On the other hand, persisting demyelination and axonal loss would be expected to increase diffusion by expanding the extracellular space (Barnes et al., 1991). The highest MD values were observed in T1-hypointense plaques, which probably represent destructive lesions containing extensive axonal loss (van Walderveen et al., 1998). The data reported here are consistent with those obtained from a navigated spin echo diffusion study which also reported that T1 hypointense lesions exhibit higher diffusion values than T1 isointense lesions (Droogan et al., 1999), and with the data reported in the previous section. In this regard, MD appears to give complementary information to T1-weighted images, with the advantage that it is inherently quantitative.

Anisotropy findings in lesions

Quantitative data on the anisotropy properties of lesions in MS have not previously been described. This study shows that lesions (considered together) have significantly lower FA than NAWM, and that acute (enhancing) lesions have significantly lower FA than chronic (non-enhancing) lesions. Moreover, FA proved more sensitive in discriminating between acute and chronic lesions than MD, as judged by the magnitude and significance of the observed differences. A study of the animal model EAE using DWI acquired with diffusion sensitisation in three directions demonstrated lower anisotropy in acute compared to chronic lesions (Verhoye et al., 1996) in keeping with data from the present study. The FA differences in enhancing and non-enhancing lesions could at least partly be accounted for by acute vasogenic oedema.

T1-hypointense lesions had lower FA than T1-isointense lesions, as anticipated from the greater degree of presumed axonal loss. The lowest FA, seen in acute enhancing lesions, suggests that extracellular oedema too has a marked effect on tissue FA. It will be of interest to measure FA as lesions evolve to determine how much of the structural loss is permanent; changes due to oedema should be reversible, whereas axonal loss may cause a persistent reduction in FA.

Future questions for DTI in MS

It is likely that a complex interaction between the pathological features of MS plaques - oedema, demyelination, axonal loss and gliosis - determines diffusion measurements. The data presented suggest that of these, oedema and axonal loss contribute most to water diffusion changes since enhancement and T1-hypointensity are associated with the most significant diffusion changes in FA and MD respectively. Ideally, experimental and post-mortem studies correlating the DTI changes and histopathology in MS are needed in order to establish the pathological basis of the diffusion MRI findings.

DTI is likely to further illuminate the pathophysiological changes occurring within MS lesions, particularly when employed in longitudinal studies of lesion evolution together with other MRI techniques including NAA spectroscopy and magnetisation transfer imaging. That the correlation observed between FA and MD for all regions studied was modest implies that they may provide partially independent and complementary data for evaluating brain pathology. Measurement of both diffusivity and anisotropy may improve the ability to detect specific pathological changes, and warrants further investigation.

The relatively small number of patients in this study is offset by the large number of lesions and NAWM regions examined, allowing a systematic characterisation of their structural properties. However, the present sample size does not permit an investigation of the relationship of DTI changes with the clinical course or level of disability. Future studies will examine the relationship of DTI changes to clinical deficit, and the natural history of diffusion changes within lesions.

4.4 Diffusion tensor imaging of corticospinal tract degeneration after stroke

Introduction

The work described in the previous section has shown that anisotropy is reduced, and diffusivity increased, in the lesions and NAWM of patients with MS. The pathological substrates of these abnormalities are not known. MS is a complex disease in which many pathological processes - including oedema, demyelination, axonal loss and gliosis - are involved. This makes it difficult to assess the contribution of each pathological element to observed changes in diffusion measurements. A previous investigation (section 4.2) indicates that the abnormalities in NAWM are closely linked to the degree of structural damage in lesions, raising the possibility that fibre transection within lesions causes subsequent degeneration into surrounding NAWM. If this is the case then a single lesion in a white matter fibre pathway should cause structural abnormalities in the pathway remote from itself in comparison to an unaffected pathway. In MS, the opportunity to examine the effect of a single lesion upon white matter tracts is rare

due to the multifocal nature of the disease. The present study has therefore investigated patients with the clinically much commoner situation of a single focal ischaemic lesion in order to assess the impact of this pathology on fibres traversing it. Although the pathological changes within an infarct are quite different to those within a demyelinating plaque, it does provide an opportunity to test the general hypothesis that focal damage along a fibre pathway causes distal degenerative changes.

Diffusion MRI has recently generated considerable interest due to its ability to reveal early pathophysiological changes in acute stroke (Prichard and Grossman, 1999), but less attention has been paid to structural changes in fibre tracts beyond the area of infarction. As we have seen, DTI allows quantification of the amount (diffusivity) and directional coherence (anisotropy) of water diffusion in healthy and pathological white matter tracts. Anisotropy measurement shows promise in detecting the degree of fibre damage in MS (section 4.3). Furthermore, the diffusion tensor provides the direction of diffusion along a fibre tract (described by a principle *eigenvector*), allowing *in vivo* maps of white matter fibre trajectories to be constructed (Pierpaoli et al., 1996).

Wallerian degeneration - the anterograde degeneration of axons and their myelin sheaths after proximal axonal or cell body injury – commonly follows focal damage to the CNS, including ischaemic stroke. These histological changes should cause measurable changes in parameters derived from the diffusion tensor due to their effects on water mobility. The aim of the present study was to quantitate measures of the magnitude (MD) and anisotropy (FA) of water diffusion within primary cerebral infarction and the associated descending corticospinal tract using DTI in five patients following acute ischaemic stroke.

Patients and methods

DTI (echo-planar imaging TE=78ms, 96x96 matrix, 4 diffusion b values increasing from 0 to ~700 s mm^{-2} applied in 7 non-collinear directions) and conventional T2-weighted MRI (TR=2000, TE=120, matrix 256x256) were used to study five patients (three male, two female; mean age 58 years) with resolving hemiplegia four to six months following middle cerebral artery territory infarction (four right-sided; one left-sided), and five normal controls (three male, two female; mean age 37 years). The diffusion tensor was estimated. MD and FA were measured in regions along the corticospinal tracts (internal capsule, cerebral peduncle and pons) and within the region of infarction, and in matched contralateral regions. Regions were defined upon the EPI images acquired in the absence of diffusion sensitisation with reference to the conventional MR images, and then transferred to maps of MD and FA. Statistical comparisons between the right and left sides were performed in patients and controls using the Mann-Whitney U test. Maps of the principle eigenvector were generated to depict the local fibre direction at each voxel using software developed at the Institute of Neurology (*DiffMapMP*, Dr Geoff Parker).

Results

T2-weighted-MRI showed high signal consistent with cerebral infarction in all patients, but only minor changes (hyperintensity) in the affected corticospinal tract of one patient. Using DTI the infarct was demonstrated in each case as an area of reduced FA and increased MD (Fig. 4.7). The ipsilateral corticospinal tract

showed reduced anisotropy on axial and coronal images (Fig. 4.8), but no visible change in diffusivity. Furthermore, eigenvector maps in patients revealed loss of coherence of the eigenvectors in the tract ipsilateral to the stroke, in contrast to the integrity of the decending corticospinal tract observed on the unaffected side (Fig. 4.8).

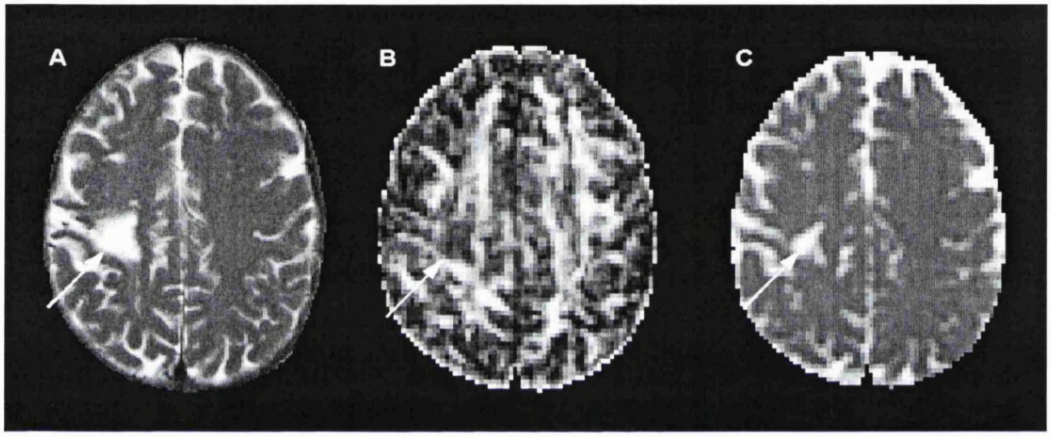

Fig. 4.7. (A) T2-weighted MRI, (B) and (C) DTI maps at an axial brain slice at the level of the corona radiata showing a right middle cerebral artery infarct (arrowed) in a 58-year old woman. (A) The infarct is shown as a region of high signal on a T2 weighted image. (B) FA map (in which areas of high anisotropy appear bright) shows reduced values in the infarct consistent with a loss of tissue integrity and orientation. (C) MD map (in which areas of high diffusion appear bright), showing increased water diffusion in the infarct.

Quantitative measurements of FA and MD confirmed statistically significant diffusion changes in the infarction and the ipsilateral descending corticospinal tract compared to matched contralateral regions (Table 4.4). Infarct regions showed reduced FA (mean 0.29 vs 0.48, $p<0.001$) and increased MD

(mean 1.75 vs 0.91, $p<0.001$). In the corticospinal tract distal to the infarct, DTI revealed significantly reduced FA (overall mean 0.61 vs 0.73, $p<0.001$), but without significant change in MD (overall mean 0.96 vs 0.95, $p=0.88$); this pattern was confirmed in each patient considered individually. In control subjects, no significant differences were detected between the right and left sides in FA (overall mean 0.83 vs 0.82, $p=0.51$) or MD (overall mean 0.92 vs 0.92, $p=0.63$) at any level examined.

Fig. 4.8

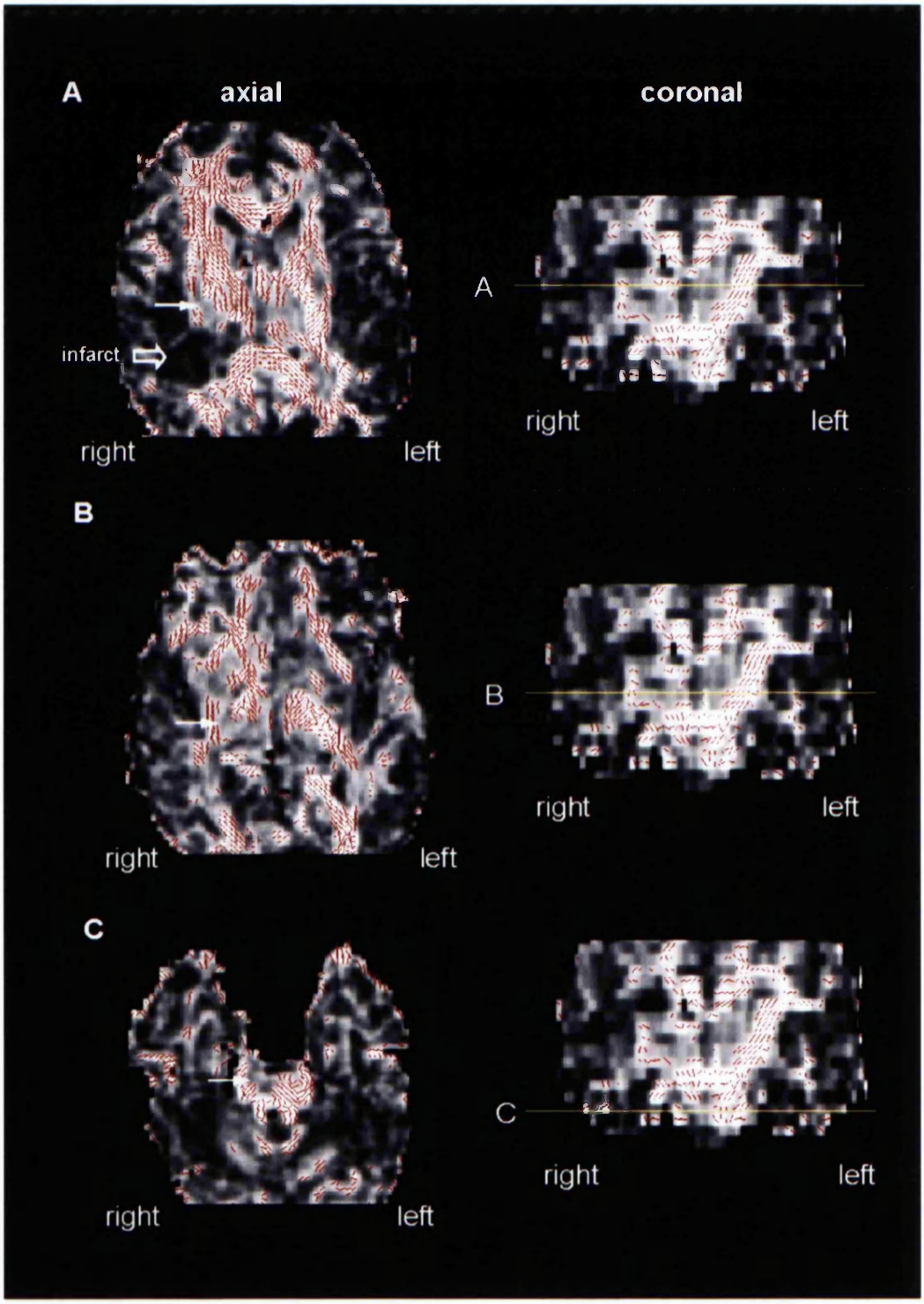

Fig. 4.8. DTI of a 45-year old man two months after right middle cerebral artery ischaemic stroke. **(A)**, **(B)**, and **(C)** show axial levels through the brain (left of panel). Coronal images (right of panel) show the intact left descending corticospinal tracts; horizontal yellow lines show the locations of the axial slices. The grey-scale images are FA maps with the principle eigenvectors - depicting local fibre direction - overlaid upon them (red lines). The open arrow in (A) indicates the infarct; small closed arrows in (A), (B) and (C) (left of panel) show the damaged corticospinal tract.

Table 4.4 *Mean values (SD) of FA (dimensionless units) and MD ($x10^{-3}mm^2s^{-1}$), in infarct regions in patients, and at different corticospinal trac levels in patients and controls. Asterisks indicate where right and left sides show a statistical difference ($p<0.01$, Mann-Whitney U test).*

	Patient group (n=5)				**Control group (n=5)**			
	Infarct side		**Unaffected side**		**Right**		**Left**	
	FA	MD	FA	MD	FA	MD	FA	MD
Infarct	0.29 (0.08)*	1.75 (0.34)*	0.48 (0.15)	0.91 (0.19)	-	-	-	-
Internal Capsule	0.65 (0.09)*	0.79 (0.18)	0.80 (0.08)	0.79 (0.11)	0.81 (0.06)	0.80 (0.07)	0.80 (0.06)	0.81 (0.04)
Cerebral Peduncles	0.66 (0.08)*	0.93 (0.16)	0.78 (0.05)	0.96 (0.25)	0.86 (0.05)	1.04 (0.12)	0.86 (0.05)	1.02 (0.15)
Pons	0.61 (0.12)*	1.10 (0.21)	0.68 (0.10)	1.09 (0.19)	0.82 (0.10)	1.07 (0.18)	0.78 (0.11)	1.08 (0.15)
All corticospinal tract regions	0.61 (0.13)*	0.96 (0.24)	0.73 (0.12)	0.95 (0.21)	0.83 (0.07)	0.92 (0.17)	0.82 (0.07)	0.92 (0.16)

Discussion

This study has demonstrated reduced FA with preservation of MD in the corticospinal tract distal to cerebral infarction. This pattern of diffusion changes is similar to that observed in experimental animal models of Wallerian degeneration in the peripheral nervous system (Beaulieu et al., 1996). Wallerian degeneration involves breakdown of the myelin sheath and disintegration of axonal microfilaments (Graham and Lantos, 1997). Loss of integrity of these directional structures is consistent with our observation of reduced anisotropy in the corticospinal tract ipsilateral to cerebral infarction. Although disruption of myelin and axons might be expected to increase the mobility (MD) of water molecules, an accumulation of cellular debris from the breakdown of axons may hinder water molecule motion (Beaulieu et al., 1996). Furthermore, Wallerian degeneration is characterised histologically by glial proliferation (Graham and Lantos, 1997), which would also be expected to restrict water molecule mobility. Both of these factors may contribute to the relative preservation of MD in the affected pathways. Replacement of the intact anisotropic microstructure by disorganised glial proliferation may also underlie the marked reduction in FA demonstrated in affected corticospinal tracts.

The primary infarct showed a different pattern of DTI abnormalities to those found in the associated corticospinal tract. Large MD increases were seen in all patients compared to matched contralateral brain regions (group mean 1.75 vs 0.91, $p<0.001$), consistent with previous reports of elevated water diffusion after the acute phase (>10 days) of cerebral infarction (Lutsep et al., 1997). Moreover, anisotropy was markedly reduced in the infarct in comparison to contralateral

regions (FA group mean 0.29 vs 0.48, $p<0.001$), a finding to the authors knowledge not previously reported in human subjects but in keeping with experimental data in animals following transient cerebral hypoxia-ischaemia showing reduced white matter anisotropy (Thornton et al., 1997). In a longstanding cerebral infarct it is thought that cell lysis and loss of normal tissue architecture expand the extracellular space, allowing water molecules to diffuse more freely (Knight et al., 1994). These changes would account for the increased diffusivity and reduced anisotropy demonstrated in regions of infarction.

The difference in diffusion properties between the primary lesion and the degenerated tract (reduced FA with increased MD in the infarct; reduced FA with preserved MD in the corticospinal tract) may allow DTI to distinguish between the primary lesion and associated Wallerian degeneration, which is not possible on conventional MRI. A second advantage of DTI is the ability to generate eigenvector maps, which provide a striking visual comparison between the trajectories of the affected and the intact corticospinal tracts (Figure 4.8). Finally, the finding of minor T2-weighted signal change in only one patient, in contrast to DTI abnormalities in all five cases indicates the higher sensitivity for DTI to detect Wallerian degeneration.

This preliminary study indicates that DTI can visualise and quantify changes in the integrity and orientation of white matter tracts transected by a focal ischaemic lesion that are consistent with Wallerian degeneration. These findings highlight the potential of DTI to detect and monitor the structural changes in cerebral infarction and associated degeneration of fibre pathways; longitudinal DTI studies may provide a better understanding of the pattern of clinical evolution following stroke.

The results of this study may also have implications for understanding mechanisms of NAWM abnormality in MS. The present data indicate that Wallerian degeneration may have a distinct pattern of diffusion characteristics, namely reduced anisotropy but with relative preservation of diffusivity, although studies on larger numbers of subjects are needed to confirm this. A DTI study in MS (section 4.3) demonstrated a reduction in anisotropy in NAWM, but with an additional concomitant increase in mean diffusivity. This suggests that the pathology in MS NAWM differs from the Wallerian degeneration of corticospinal axons after stroke. Differences in the relative extent of axonal loss and gliosis in the two situations may contribute. In MS other diffuse processes, including microscopic areas of inflammation or demyelination may also affect the magnitude of water diffusion in NAWM. Further studies correlating MRI diffusion measurements with quantitative histopathological data are needed to clarify the mechanisms of MR diffusion abnormalities.

Chapter 5

Studies of brain structure and function: complementary use of diffusion tensor and functional magnetic resonance imaging

5.1 Background

In chapter three, fMRI was used to investigate brain activation during monocular visual stimulation in normal controls and patients following recovery from optic neuritis. A more extensive pattern of activation induced by affected eye stimulation in patients was interpreted according to available information on connections between the activated regions, derived largely from neuroanatomical studies in other species. This approach to understanding functional imaging data is widely (and necessarily) employed due to the absence of definitive information on cerebral connections in humans *in vivo*.

DTI, as we have seen, provides information on the orientation and integrity of fibre pathways that is not accessible using conventional MRI methods. It may be a valuable tool for mapping the fibre tracts in the brain, thus enabling functional imaging data to be interpreted more effectively. This chapter presents two studies which aimed to demonstrate the feasibility and potential of combining the two imaging methods in the same subject(s), allowing information about brain structure and function to be obtained in a single NMR experiment. Some of the limitations of the approach are discussed.

The first study used fMRI and DTI to investigate mechanisms of motor recovery in a patient who made an excellent motor recovery following a traumatic brain injury to the internal capsule causing a dense hemiplegia. It was hypothesized that the information obtained on cortical activation using fMRI would be complementary to that obtained on the integrity of subcortical motor pathways using DTI. The second study investigated the pattern of activation in the visual cortex induced by a simple monocular visual stimulus, in conjunction with DTI to measure anisotropy and visualize the fibre orientation of the main visual projection pathways in humans.

5.2 Complementary use of diffusion tensor and functional magnetic resonance imaging in a traumatic injury of the internal capsule

Introduction

Recovery of function, although varied in extent and time course, frequently follows CNS damage of vascular, inflammatory or traumatic origin. Understanding recovery mechanisms is important, because they may help to explain the variation in clinical outcomes and allow for the rational planning of rehabilitation strategies. Explanations suggested to contribute to recovery include the resolution of acute reversible factors - including inflammation, haemorrhage and oedema - and the recruitment of undamaged brain areas by the release of inhibition or formation of new connections. Studies in stroke provide evidence for the recruitment of cortical areas in the undamaged hemisphere (Chollet et al., 1991; Weiller et al., 1992) and the expansion of representation into cortical areas

adjacent to the lesion site (Weiller et al., 1992; Nudo et al., 1996). In attempts to find prognostic markers, studies have examined structural parameters including volume of infarcted tissue (Binkowski et al., 1996) and lesion location (Binkowski et al., 1996; Fries et al., 1993) derived from CT or MRI scans. These imaging techniques provide no information about the integrity or directionality of fibre tracts within lesions, and furthermore lack pathological specificity. These limitations may in part explain the absence of a strong relationship between the volume or location of tissue damage and functional motor outcome.

DTI may complement the findings from functional imaging studies by giving insights into relationships between the degree of disruption of tract integrity (as indicated by changes in anisotropy) or orientation and the functional consequences. The use of fMRI in the investigation of motor system organization in human subjects is well established (e.g. Rao et al., 1993; Rao et al., 1995; Kim et al., 1993) and has been discussed (see chapter 2). Focal traumatic brain injuries have not been widely studied with either fMRI or DTI, but these techniques should provide complementary structural and functional information relevant to motor recovery mechanisms. The present study applied these techniques to a patient following recovery from a traumatic focal injury to the internal capsule. The specific question addressed was: in the patient studied, what were the relative contributions of reversible factors (i.e. those not causing a permanent loss of structural integrity in affected tracts) associated with the injury, and cortical reorganization, to recovery?

Case Report

A 21-year-old man suffered a penetrating brain injury to his right orbit due to an assault with a snooker cue. He lost consciousness and was initially unresponsive. When admitted to hospital he had recovered consciousness and had a dense left hemiplegia associated with sensory disturbance. A CT scan revealed a posterior defect of the right orbit with a large intracerebral bleed extending from the right frontal lobe, through the right basal ganglia and into right parietal cortex (Fig. 5.1). He made an excellent physical recovery over the next month. When examined 18 months later, at the time of the present study, motor examination revealed minimal dystonic posturing of the fingers of the outstretched left hand and of the left foot with a left sided reflex emphasis and extensor plantar response, but no detectable pyramidal weakness. There was some mild bradykinesia in the left hand but no tremor. His gait was slow with reasonable arm swing but mild dystonic posturing of the left foot (predominantly inversion). Some alteration of light touch sensation on the left side persisted. Cognitive testing showed mild deficits in verbal memory and impaired executive skills with abulia.

Methods

Informed written consent was obtained for all experiments. The patient was studied with fMRI and DTI. In addition, five healthy controls (mean age 28.4 years +/-5.3) were studied with DTI. All images were acquired in the axial plane with a 24 x 24cm field of view. Mildly and heavily T2-weighted images

(TE=42/84ms, TR = 2000ms, matrix 256x256) were used to assess the extent of the remaining lesion site in the patient.

Functional MRI. In the fMRI studies 20 second epochs of unilateral simple paced finger tapping (2.5Hz) alternated with rest. T2*-weighted gradient echo echoplanar imaging (EPI) data depicting blood oxygenation level dependent (BOLD) contrast were acquired (matrix size 96 x 96) at each of 10 5mm thick slice locations (interslice gap 0.5mm) through motor cortex. TR was 4000ms, giving five time points per epoch at each location; a total of 120 time points (24 epochs) were collected in 8 minutes. A high resolution inversion recovery gradient echo EPI dataset (TR=6000ms, TE=40ms, TI=200ms, 48 x 3mm contiguous axial slices) covering the whole brain was also acquired to superimpose the activation maps upon. Task monitoring for mirror movements and accurate performance was by direct observation (DJW). Three experiments were performed with each hand to ensure acceptable reproducibility of results. One study was rejected due to inaccurate paradigm performance. The standardized power of MR signal change at the frequency of the periodic alternation between tapping and rest conditions was estimated at each voxel by iterated least squares fit of a sinusoidal regression model (Bullmore et al., 1996b), as described fully in chapter 3. Activated voxels were colour coded (as described in the legend to Figure 5.2) and superimposed on the grey scale backround of the patient's anatomical EPI dataset coregistered in standard space to form a generic brain activation map (Brammer et al., 1997). The Talairach grid (Talairach and Tournoux, 1988) was superimposed upon the activation maps to assist anatomical localization.

DTI. DTI was performed as described previously (4 b values increasing from ~0-700 sec/mm2 applied in 7 non-collinear directions) at 10 slice locations corresponding to a subset of those of the conventional spin echo images through the basal ganglia. These were chosen to optimally demonstrate the corticospinal tracts. These data were acquired in two blocks of five slices due to a limitation on total image storage. For each dataset the total number of images acquired was 980. The diffusion tensor was estimated, from which FA values, eigenvalues and eigenvectors were calculated. Images were displayed on a Sun workstation (Sun microsystems, Mountain View, California, USA), and regions in anterior and posterior internal capsule were defined upon the FA maps with reference to the corresponding T2-weighted images. Regions were away from areas of significant geometric distortion on the echoplanar images. In order to display fibre directions colour maps were generated as described by Pierpaoli (1997). In these maps, the principle eigenvector components for each voxel (|ex|, |ey|, |ez|) are shown in red, green or blue respectively. For greater clarity, each value was modulated by FA, and the resulting map was overlaid upon the FA template.

Results

The original CT scan at the time of injury revealed an area of increased signal extending from the frontal lobe through the basal ganglia to parietal cortex. There was some distortion of the right lateral ventricle, oedema and mild mass effect (Fig. 5.1). On the MRI performed at the time of the study, 18 months after the injury, an area of heterogeneous increased signal was seen on both heavily and mildly T2-weighted mages extending from the frontal lobe into the right basal

ganglia (Fig. 5.1), involving the caudate and lentiform nuclei and the internal capsule but with some sparing of the right thalamus.

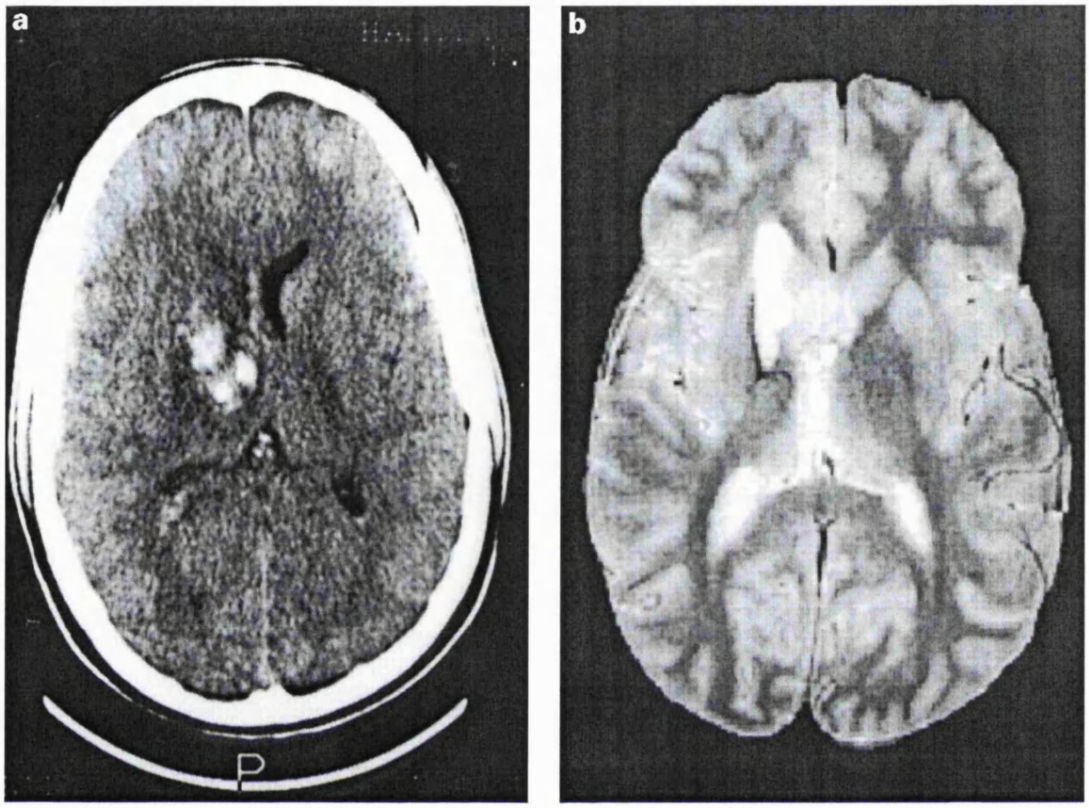

Fig. 5.1. CT and MRI in a traumatic brain injury to the internal capsule. **(A)** CT taken on the day of the injury. Note high signal (haemorrhage) in the region of the left anterior internal capsule with mass effect and oedema. **(B)** Mildly T2-weighted MRI taken 18 months after the injury. Note persistent high signal abnormality in region of left caudate and lentiform nuclei extending into the genu and posterior limb of the internal capsule.

fMRI activation maps (Fig 5.2) showed activation in contralateral primary motor cortex and supplementary motor cortex in response to finger tapping of each hand. Tapping the recovered hand elicited a small area of activation in the ipsilateral primary motor cortex. Accurate mapping of basal ganglia activations was not possible due to limited brain coverage. fMRI findings from simple paced

finger tapping in 10 normal subjects have been reported elsewhere (Werring et al., 1997).

FA maps gave a clear demonstration of white matter tract anatomy in both controls and the patient (Fig. 5.3). The maps, derived from images through the level of the internal capsule and basal ganglia, showed marked loss of tissue integrity (low FA values) in the region of the lesion site and anterior limb of the internal capsule compared to the unaffected side. In contrast, FA values in the posterior limb of the internal capsule were well preserved bilaterally. All control subjects had high FA values in both limbs of the internal capsule (table 5.1). Maps derived from the diffusion tensor which encoded the components of the eigenvalue of the principle eigenvector as red (|ex|), green (|ey|) and blue (|ez|) (with modulation by FA), showed the dominant diffusion direction in the anisotropic posterior limb in controls to be predominantly in the through-slice (z) direction (Fig 5.4A). In the patient, a small region of preserved anisotropy with diffusion predominantly in this (z) direction was seen in the middle third of the posterior limb of the internal capsule (Fig 5.4B) on the affected side. The direction of anisotropy in the anterior limb of the internal capsule in controls was predominantly in the horizontal anteroposterior (y) direction. In the patient this directionality was entirely lost on the affected side but not the uninjured side.

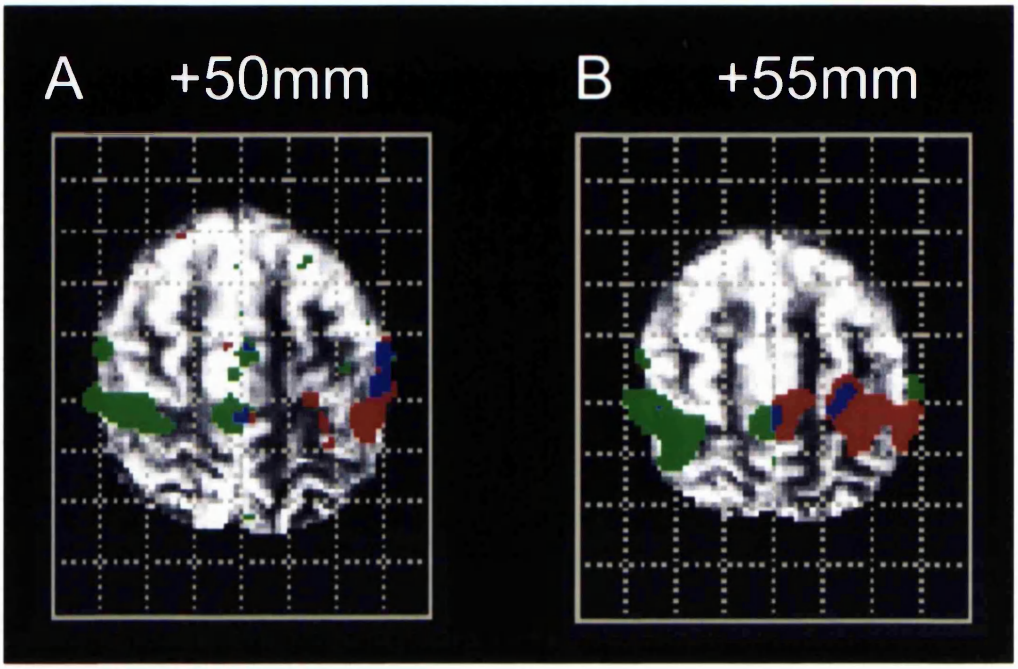

Fig. 5.2. Generic brain activation maps derived from two axial slices of fMRI data representing motor cortex (Talairach z co-ordinates +50mm and +55mm) in the patient described (see text). Voxels activated by right (unaffected) finger tapping are coloured red; voxels activated by left (recovered) finger tapping are coloured green; voxels activated by tapping both sides are coloured blue. The voxel-wise probability of false positive activation $p<0.0001$. The right side of the brain is to the left side of the panel.

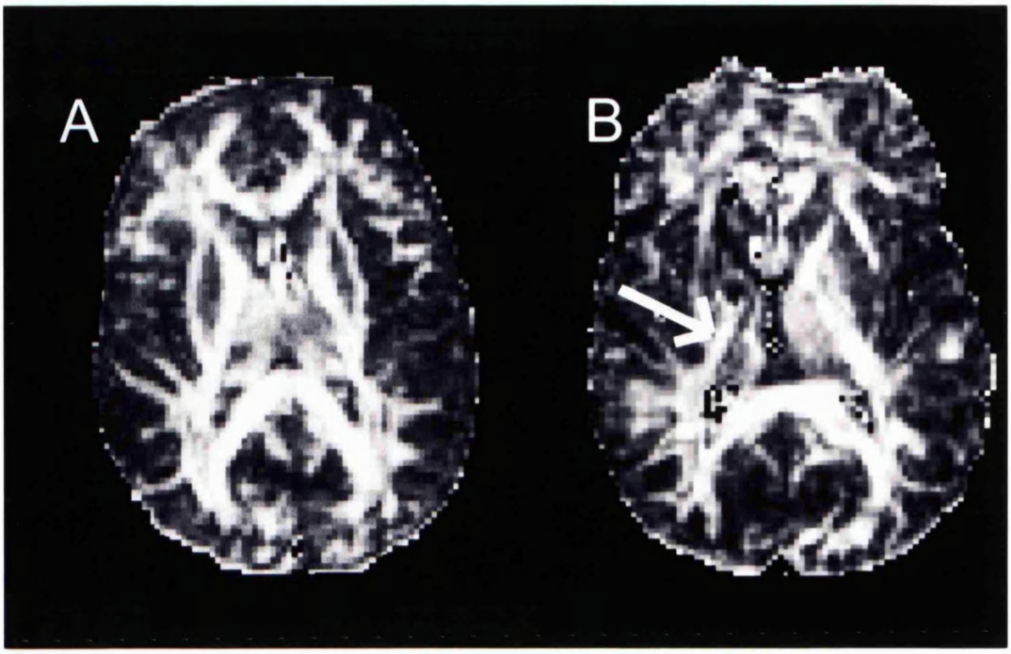

Fig. 5.3. FA maps from axial slices through the pyramidal tracts. **(A)** Normal control and **(B)** patient. A region of preserved FA in the posterior limb of the internal capsule (in the expected location of the pyramidal tract) in the patient is arrowed.

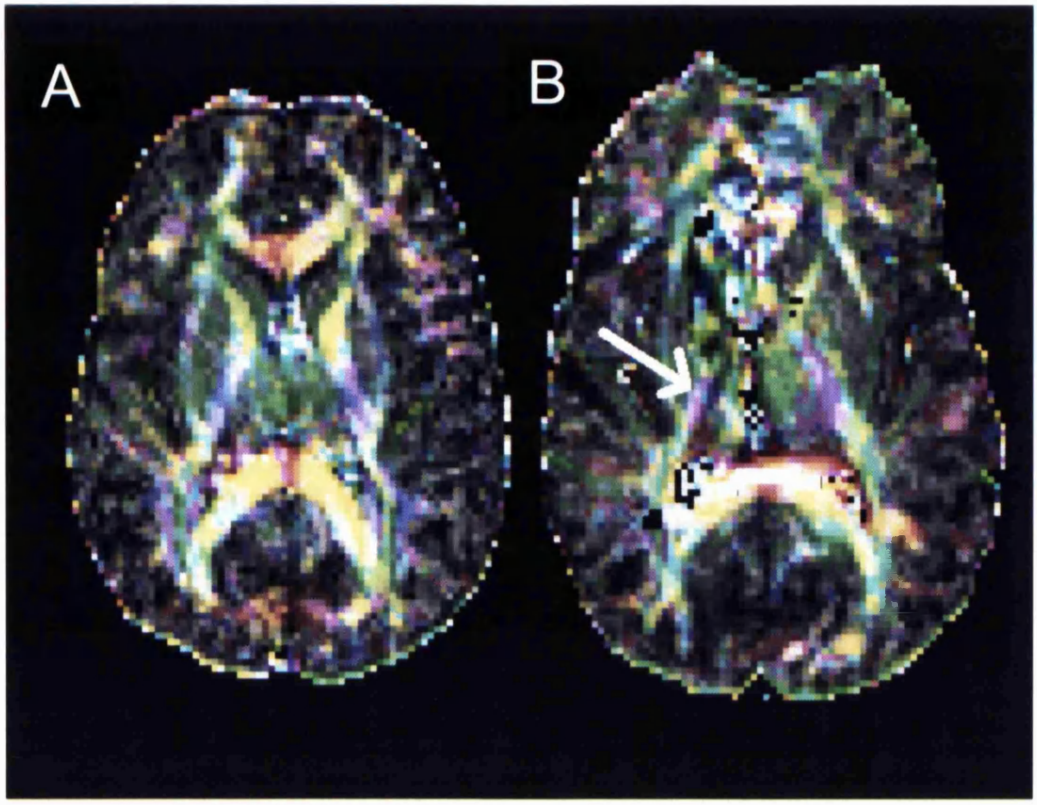

Fig. 5.4. Colour maps derived from DTI data depicting axial slices throught the level of the basal ganglia. The principle eigenvector components for each voxel ($|e_x|$, $|e_y|$, and $|e_z|$), modulated by FA, are displayed as red, green and blue, respectively, and overlaid upon a grey-scale FA map. **(A)** Normal control. Note that the predominant diffusion direction in the anterior limb of the internal capsule is in the y direction (green); in the posterior limb the z direction (blue); and in the genu and splenium of the corpus callosum in the x direction (red). **(B)** Patient (described in the text). In the middle third of the posterior limb of the internal capsule there is a region of preserved z direction diffusion (blue) representing the intact pyramidal tract (arrowed). The white voxels in the splenium of the corpus callosum represent a loss of diffusion information, which may be a result of rostrocaudal motion during the cardiac cycle. The right side of the brain is on the left side of each panel.

Table 5.1 *Fractional anisotropy (FA) values in the internal capsules of the patient studied and five normal controls.*

	Fractional Anisotropy (dimensionless units) +/-SD			
	Anterior limb		Posterior limb	
Subject	**Right**	**Left**	**Right**	**Left**
Patient	0.29 +/-0.14	0.78+/-0.13	0.72+/-0.08	0.80+/-0.05
Control 1	0.76+/-0.07	0.82+/-0.10	0.82+/-0.08	0.81+/-0.08
Control 2	0.72+/-0.09	0.72+/-0.09	0.86+/-0.09	0.86+/-0.06
Control 3	0.76+/-0.08	0.69+/-0.16	0.77+/-0.06	0.81+/-0.07
Control 4	0.73+/-0.06	0.68+/-0.08	0.80+/-0.08	0.80+/-0.08
Control 5	0.74+/-0.06	0.81+/-0.07	0.82+/-0.10	0.85+/-0.08

Discussion

The patient presented is an example of neurological recovery from a focal traumatic brain injury. The dramatic early recovery may have been due to two possible mechanisms, or a combination of both: firstly, the resolution of reversible factors (e.g. oedema, haemorrhage and mass effect) affecting motor pathway function with a subsequent return of function in the intact motor tracts; or secondly, some form of cortical reorganization to compensate for irreversible damage to subcortical motor pathways. Our experiment aimed to determine the contributions of these mechanisms by performing fMRI and DTI 18 months after the injury. The fMRI maps obtained from motor tasks with either the unaffected or recovered hand suggest that similar cortical areas (mainly contralateral primary

motor cortex) are involved in hand movement on each side. This in turn suggests that similar anatomical pathways (classical crossed corticospinal projections) are being utilized in each case, and that despite the severe nature of the right-sided injury these corticospinal fibres had been spared. A region of preserved structural integrity in the middle portion of the posterior limb of the internal capsule on the patient's right side is clearly demonstrated on the FA maps (Fig. 5.3), in contrast to the reduced anisotropy (implying reduced tissue structure) in the right sided anterior capsular limb. The highest degree of diffusion in this anisotropic posterior region was shown to be predominantly in the z direction by examining eigenvector, consistent with the expected orientation of corticospinal tract fibres. These diffusion findings support the preservation of the integrity and directionality of the pyramidal tract on the injured side; this information is not obtainable from any other in vivo imaging technique.

A classical view of the organization of fibres at the level of the internal capsule is of a single homunculus, in which there is a somatotopic representation of primary motor areas. In this description, the head is represented in the anterior limb, the mouth in the genu, the upper limb in the anterior part and lower limb the posterior part of the posterior capsular limb (Penfield and Boldrey, 1937). However, more recent studies using injections of the neuroanatomical tracer, horseradish peroxidase (HRP), into cortical motor areas of primates, have challenged this model (Fries et al., 1993). These investigators suggest that supplementary motor area (SMA) fibres descend to run horizontally in the anterior limb towards the genu. Dorsolateral premotor cortex projects via the genu, whilst primary motor cortex (both hand and foot areas) project via the middle third of the posterior limb. Our results are in good agreement with these anatomical data: the

horizontal orientation of anterior limb fibres in controls and on the uninjured side is clearly demonstrated (shown in green in Fig 4a and 4b). On the injured side, the area of preserved anisotropy in the z direction (blue) is in the middle third of the posterior limb, in keeping with pyramidal tract preservation and the excellent motor recovery observed.

Fries et al (1993) also studied 23 patients with capsular or striatocapsular strokes which they divided into those affecting four anatomical regions: (1) the basal ganglia only, (2) the anterior limb and basal ganglia, (3) the posterior limb only and (4) the posterior limb and thalamus. They found that all groups apart from the latter made an excellent motor recovery. Our case sustained structural damage to the basal ganglia, anterior limb and genu, but less severe damage to the thalamus, so although of traumatic rather than vascular origin might have been expected to make a good motor recovery on this basis. Based on their clinical findings, Fries et al (1993) challenged the traditional concept of a hierarchical motor system in which primary motor cortex projects via the corticospinal tract and is modulated by premotor and supplementary motor area (SMA)s (which contribute to planning and preparation for willed movement). The authors suggested that because SMA, premotor areas and primary motor areas descend in parallel via the anterior capsule, genu and posterior capsule respectively, they may substitute for each other functionally during recovery from a hemiparesis. According to this model, the subject described here would have damaged mainly the descending SMA projections, which might be expected to result in a compensatory increase in premotor and primary motor cortex activity. No evidence was found for this mechanism (in the form of increased activation in contralateral premotor or primary motor areas on tapping the recovered hand) in

the present study. The finding of areas of ipsilateral primary motor cortex activation in response to tapping the recovered hand is more suggestive of a recruitment of ipsilateral pathways, as suggested by previous PET studies in motor stroke (Chollet et al., 1991; Weiller et al., 1992). However, the variability in lateralization of cortical activation between the dominant and non-dominant hand may be considerable in fMRI experiments in normal subjects (Kim et al., 1993; Werring et al., 1998). From this single case study, the contribution of the fMRI findings to recovery remains undetermined.

That preservation of the pyramidal tract is a predictor of good clinical recovery has been suggested by other investigators. Binkowski et al (1996) studied motor recovery from hemiparetic ischaemic stroke in 23 patients using glucose PET and conventional MRI. They found that patients with a large volume of damage to the pyramidal tract on proton-density MRI on average had a worse outcome than those in whom this tract is spared, but no correlation was found between lesion size and change in a clinical motor score. They also found, in common with Fries et al (1993), that thalamic hypometabolism was a predictor of poor outcome. FA may prove to be a more sensitive measure of functionally important tract damage than volume of altered signal on conventional MR images, and may therefore relate more strongly to outcome following a focal lesion affecting the motor pathway. Further studies are required to address this possibility.

The low FA values seen in the anterior limb of the internal capsule on the affected side reflect irreversible structural damage to fibres in this region, probably including axonal loss and a distortion of ventricular anatomy creating a CSF-filled cavity. Since the tracts contained in this area are not as clinically important for

limb motor control in either traditional (Penfield and Boldrey, 1937) or more recent (Fries et al., 1993) anatomical models of capsule organization as the posteriorly located pyramidal tracts, this structural damage has not resulted in a severe permanent disturbance of motor function. A contribution to afferent fibre tracts in the anterior limb of the internal capsule is made by thalamo-cortical projections, which are involved in the perception of sensory information. The loss of integrity of fibres in this area is thus consistent with the residual sensory deficit shown in the patient studied.

The nuclei of the basal ganglia have complex roles in both motor control and behaviour. In a review of 240 cases of lesions to the basal ganglia from a variety of causes, Bhatia and Marsden (Bhatia and Marsden, 1994) found dystonia and abulia to be among the commonest symptoms, occurring in 36% and 13% of lesions respectively. Both of these symptoms were present in the case described here, in which unilateral lentiform and caudate nuclei damage occurred.

A limitation of the present data is the long interval between the injury and the study. This raises the possibility that during the acute recovery process some reorganisation of cortical function took place but that this had diminished by the time of our fMRI experiment. This question may only be addressed by a longitudinal study design. The potential power of a serial study is demonstrated by recent data, which indicate that dynamic changes in the corticospinal tract neuronal integrity or function, and in the pattern of motor cortex activation, accompany motor recovery in MS relapse affecting corticospinal tract function (Reddy et al., 2000). A return of the concentration of NAA in the pyramidal tract towards normal values was observed in parallel with clinical recovery and a

reduction in the abnormal cortical activation pattern observed soon after the onset of the deficit.

DTI studies at the time of injury would have been helpful in assessing the extent and duration of the structural changes occurring at the site of trauma, and the degree and time course of recovery of pyramidal tract integrity. Although DTI has provided unique and important information about the recovery of structural integrity in the damaged corticospinal tract of the patient studied, it has not been definitively proven that functional conduction in the pathway was acutely impaired at the time of injury, with subsequent resolution. Evidence for this could be obtained using a neurophysiological technique such as transcranial magnetic stimulation, although this technique should be used with caution in focal brain injury due to the possibility of epileptogenesis. In future studies, a multi-modal approach incorporating functional neuroimaging together with neurophysiology might be the most informative.

A technical limitation of the present data is the resolution of the diffusion weighted images, which may introduce artifacts into the anisotropy measurements obtained (Pierpaoli et al., 1996). The voxel dimensions used (2.5 x 2.5 x 5mm) are perhaps larger than optimal, and could result in artifacts due to partial volume (sampling of a mix of tissue types within a voxel). Furthermore, fibres with different trajectories may cross within a single voxel, causing possible misinterpretation of the diffusion tensor. However, increasing resolution results in a reduced signal to noise ratio, which may also lead to errors in FA estimation (since FA is known to be noise-dependent). It was found that the voxel size employed in our study provided the best currently available trade-off between resolution and signal to noise.

In summary, the findings of this study suggest that the clinical recovery observed in this case was not due to extensive cortical reorganisation, but mainly to the survival of existing motor (pyramidal) pathways. The preservation of both the integrity and direction of the pyramidal tract on the injured side have been demonstrated using DTI; these features are not visualized using standard imaging methods. Furthermore, this is the first study to use DTI to evaluate a traumatic brain injury. The initial hemiplegia was most likely to be due to a disruption of function in the pyramidal tract due to reversible factors, probably including impaired conduction due to oedema and/or mass effect in the region of the injury. Irreversible damage sustained to the anterior internal capsule and basal ganglia nuclei account for the persisting contralateral sensory deficit and hemidystonia. This case study demonstrates the potential value of combining maps of brain activation and white matter tract organization, derived from fMRI and DTI data respectively, to elucidate the mechanisms of recovery and persistent deficit resulting from a focal brain lesion in an individual patient.

5.3 A direct demonstration of both structure and function in the visual system: combining DTI with functional magnetic resonance imaging

Introduction

Present knowledge of the connections between brain areas in man remains imprecise, being derived largely from invasive techniques including post-mortem studies and neuroanatomical tracer experiments in other species. These connections are important in understanding the interactions (or functional

integration) between areas (Friston et al., 1997). As we have seen, DTI can probe structural properties of tissue not accessible to other methods, and may represent a unique tool for mapping fibre tracts noninvasively in the living human brain. The eigenvector associated with the largest principle diffusivity (eigenvalue) of the diffusion tensor is referred to as the "principle eigenvector", and coincides with the main direction of the local fibre tract (Pierpaoli et al, 1996). Thus, a map of the principle eigenvector conveys directional information about fibre orientation (see chapter 4).

There are technical limitations that must be considered when inferring connectivity from DTI. In particular, in areas where the arrangement of fibre tracts is not coherent, anisotropy measurements will be low, and the vector field of fibre direction relatively poorly defined. Despite these limitations, there has been some promising work attempting to use DTI to elucidate brain connectivity (Makris et al, 1997; Basser, 1998; Jones et al, 1999; Pierpaoli et al, 1998; Conturo et al., 1999). There is also evidence that DTI can provide information that is clinically relevant in neurological recovery (Makris et al, 1997; section 5.2).

To localize activated regions in fMRI experiments, they are mapped on to an anatomical template, often a conventional T1-weighted spin echo image. Such templates reveal macroscopic anatomy, including grey-white matter contrast, but do not give information about tract integrity or direction. A further limitation of conventional (i.e. non-EPI) anatomical templates is that they have different geometric distortions to the EPI functional images. Registration and spatial transformation algorithms are therefore used, which may cause inaccuracies in localising activations. Performing DTI in a practical time frame requires EPI; thus, DTI-derived maps will have more similar geometric distortions to the EPI

functional images than conventional MR images. The present study exploits the fact that EPI is used for both techniques to overlay fMRI activation maps on to a DTI structural template. Matched acquisition parameters (including receiver bandwidth and echo train length) were used to ensure similar geometric distortions in both sets of images, removing the need for formal registration algorithms, provided there is negligible subject motion between scans. This leads to two potential advantages over other mapping methods: the accuracy of functional localization to a subject's individual anatomy may be improved (compared to using conventional T1-weighted templates); and the relationship between functional activation and the structural properties (including anisotropy) and trajectories of brain pathways (revealed by the direction of the principle eigenvector) may be explored. Experiments were performed in healthy subjects using a visual stimulus, firstly to demonstrate the feasibility of combining DTI and fMRI maps to show fibre tract anatomy in relation to activations, and secondly to quantify anisotropy in white matter tracts and functionally activated regions.

Methods

Five normal subjects were studied (2 female, 3 male; mean age 27.6 years +/- 2.1). In the fMRI experiments 120 T2*-weighted gradient echo EPI images depicting blood oxygenation level dependent (BOLD) contrast at each of 10 5mm thick slices (interslice gap 0.5mm) through visual cortex were acquired as previously described (chapter three). 20-second epochs of unilateral or bilateral 8Hz flash photic stimulus alternated with rest (darkness). After motion correction (Brammer et al, 1997), data were analysed by cross-correlation to a boxcar response function

(Bandettini et al, 1993) using STIMULATE software (Strupp et al, 1996). Voxels exceeding a correlation coefficient of 0.25 were displayed; only clusters larger than a single voxel were accepted for further analysis.

DTI was performed immediately following fMRI, with no repositioning. Images were acquired in two sets of 5 non-contiguous 5mm slices (interslice gap 0.5mm) as described previously, to give ten slice locations identical to the fMRI data. To increase signal to noise without introducing motion artefacts, seven repetitions of the complete set were collected and then averaged after magnitude reconstruction. Receiver bandwidth, echo spacing and field of view were matched to the fMRI sequence. Mean diffusivity and FA were calculated at each voxel (Basser et al, 1996). The fMRI activation maps were overlayed upon FA maps on a Sun workstation (Sun Microsystems, Mountain View, CA) using software developed at the Institute of Neurology by Dr GJM Parker. Principle eigenvector maps were generated; for clarity of presentation the intensity of each vector element was weighted by the FA in each voxel.

Activated regions were defined upon fMRI maps using a semi-automated contouring technique (*DispImage*; D Plummer, UCL hospitals trust) and transposed on to FA maps. Regions of interest delineating the optic radiation bilaterally were obtained from the DTI images acquired in the absence of diffusion sensitization. FA was measured within activated regions and in the optic radiations.

Results

The geometric distortions in the unprocessed T2*-weighted functional and EPI diffusion images were similar by visual inspection; this was confirmed formally by transferring a brain outline from one image to the other (Fig. 5.5). All subjects showed activation in primary visual cortex, with variable additional activation of more lateral and anterior extrastriate areas. FA and eigenvector maps clearly demonstrated white matter tracts (Fig 5.6). Overlay of fMRI maps on to DTI anisotropy maps revealed activated voxels to be almost exclusively in regions of low FA (Fig. 5.6). FA values for the optic radiation were significantly higher (mean 0.69 +/- 0.03) than FA values within activated regions (mean 0.40 +/-0.14); $p < 0.001$, Mann-Whitney U test. (Table 5.2 and Fig.5.7).

Table 5.2. *FA in activated regions and optic radiation for five healthy subjects.*

Subject	Mean FA activated regions (SD)/ dimensionless units	Mean FA optic radiation (SD)/ dimensionless units
1	0.38 +/-0.12	0.65 +/-0.08
2	0.43 +/-0.04	0.70 +/-0.03
3	0.33 +/-0.08	0.70 +/-0.03
4	0.50 +/-0.15	0.71 +/-0.01
5	0.37 +/-0.07	0.70 +/-0.04

Principle eigenvector maps revealed the expected anteroposterior orientation of the optic radiation, as well as demonstrating fibre trajectories in the corpus callosum and internal capsule (Fig 5.8). The relationship between the eigenvectors describing the orientation of the optic radiation and the activation in visual cortex was also shown.

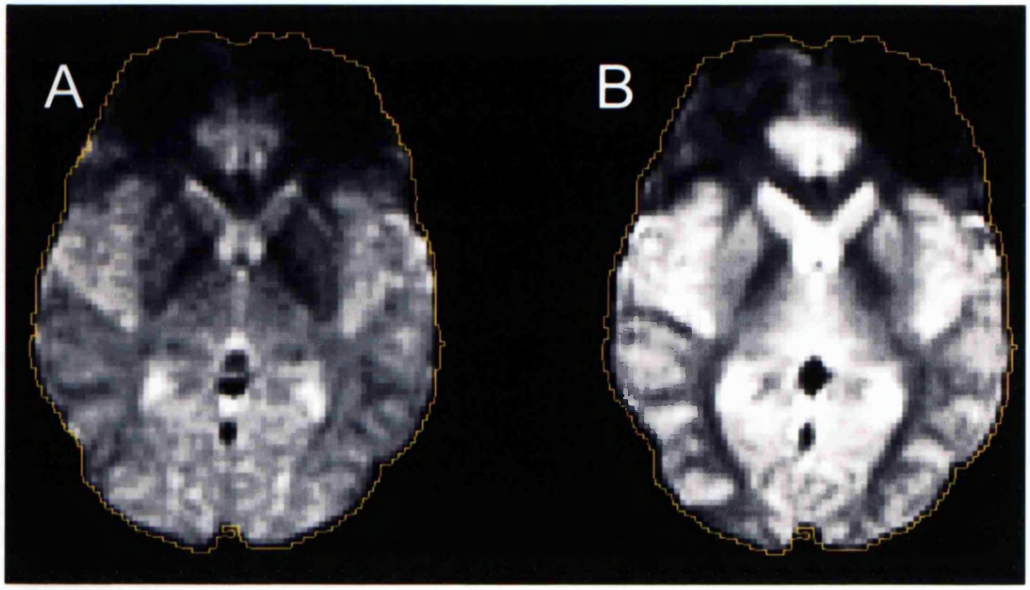

Fig. 5.5. (A) Unprocessed axial image acquired during DTI without diffusion sensitization (b=0) from a healthy 25 year old subject. **(B)** Unprocessed axial T2* weighted image from fMRI time series acquired during the same scanning session. The yellow boundary is an automated contour region around the whole brain, which was defined on image (A) and then transposed directly on to image (B).

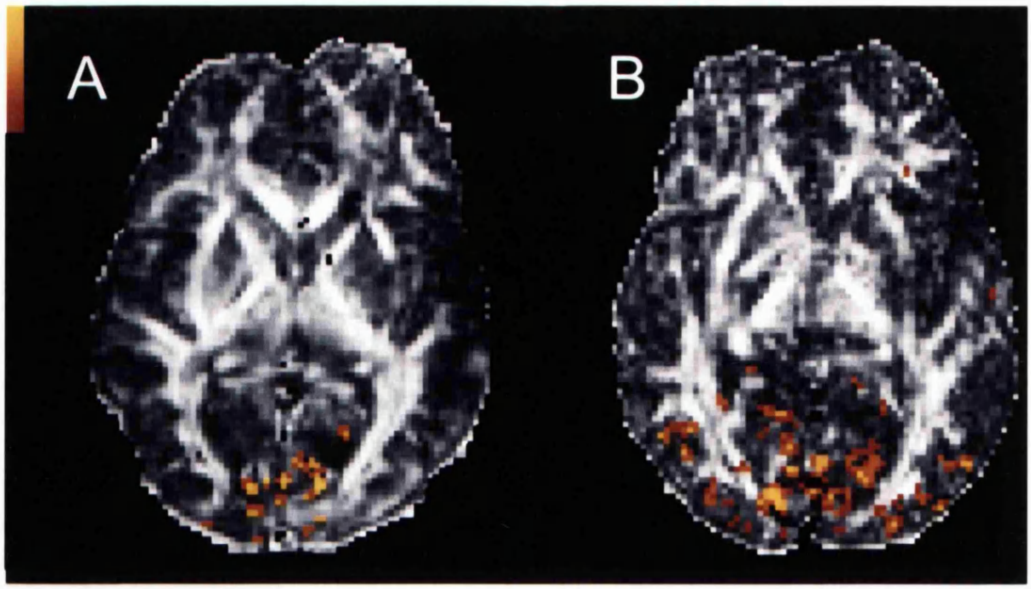

Fig. 5.6. fMRI activation maps (hotwire scale) obtained during 8Hz monocular stimulation of the right eye overlaid upon FA maps (grey scale) in **(A)** the same subject as Fig. 5.5 and **(B)** a healthy 30 year old subject. The colour scale represents the degree of correlation with a boxcar reference waveform, ranging from 0.25 (red) to > 0.5 (yellow).

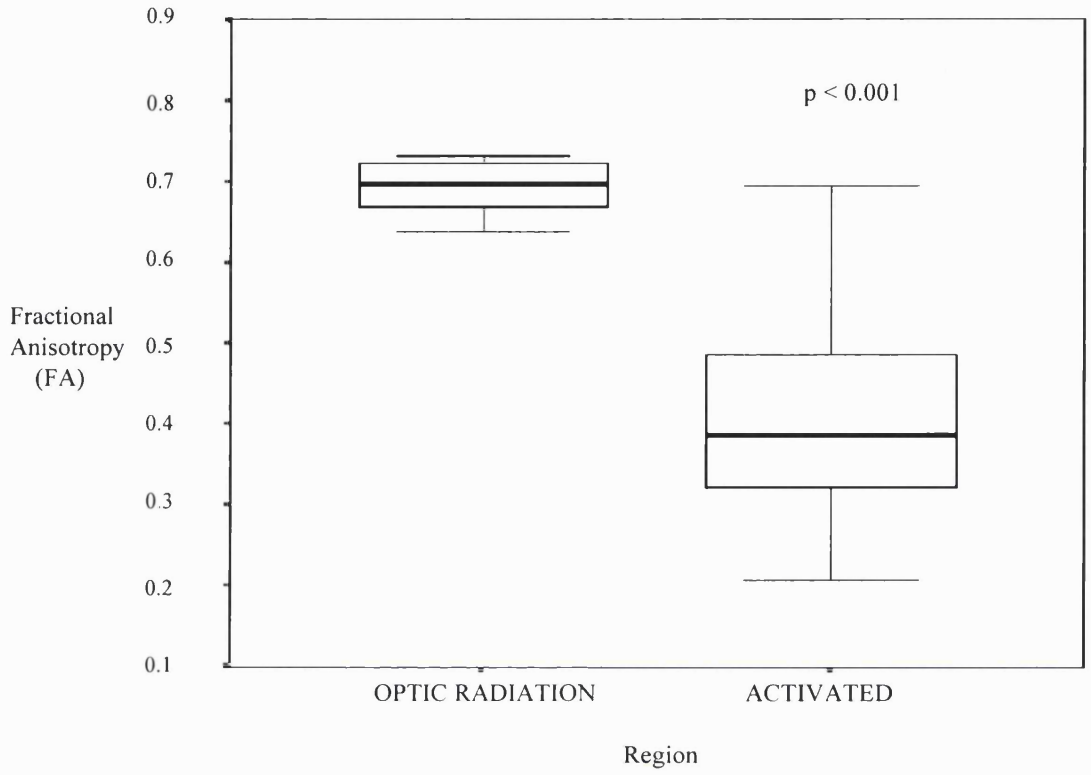

Fig 5.7. Fractional anisotropy (dimensionless units) in activated regions and in optic radiation white matter. Boxes show the interquartile ranges; bold bars represent the median; error bars show total data ranges.

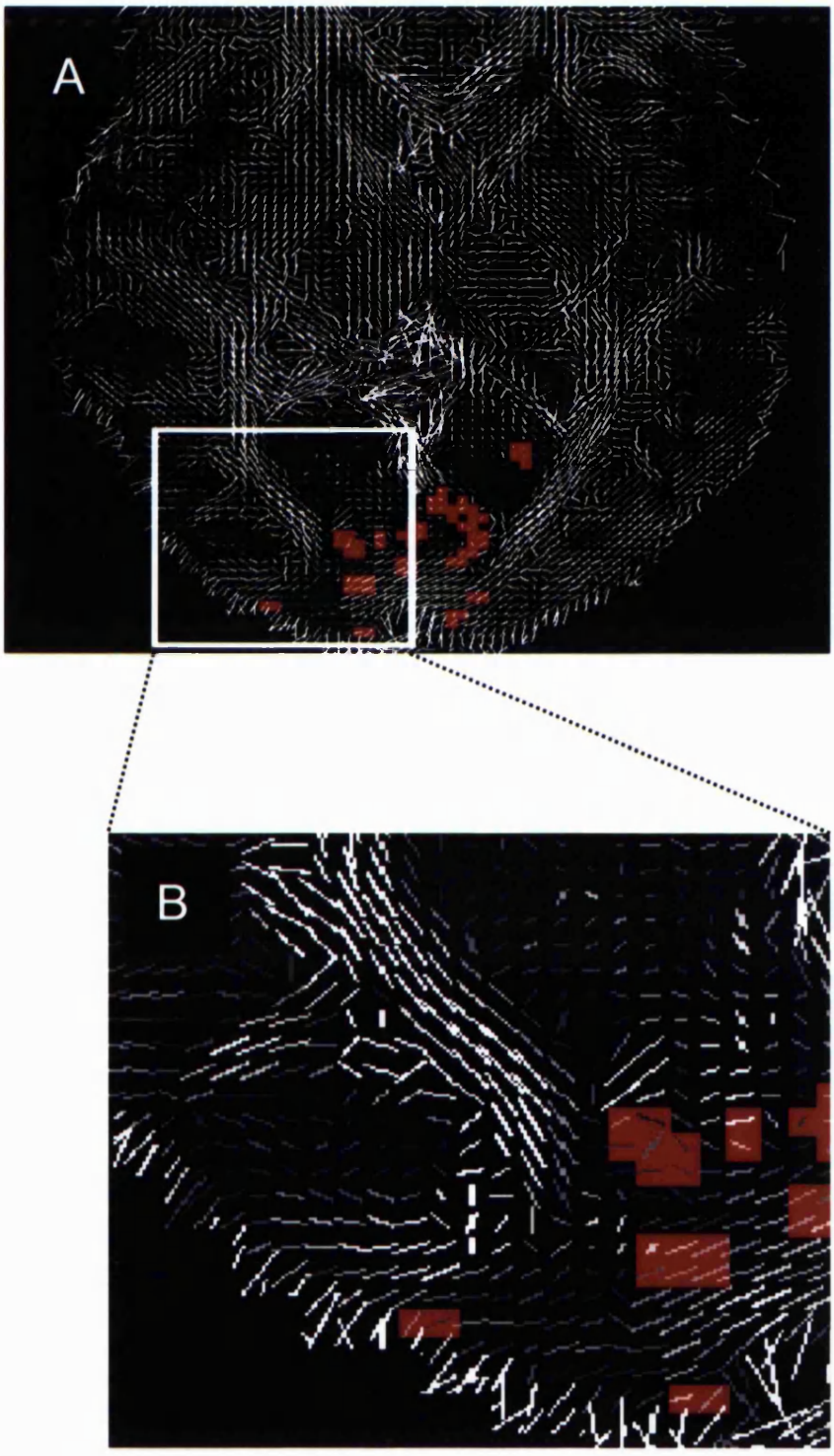

Fig. 5.8. DTI and fMRI data from an axial slice through the optic radiation in a healthy 25 year old subject. **(A)** Activated voxels (coloured red) overlaid upon a principle eigenvector map (grey scale needles). The grey-scale value is proportional to FA, whilst the length and direction of each needle represent the magnitude and direction of the principle eigenvector at each voxel, respectively. **(B)** Enlargement of inset region to show in closer detail the relationship between the principle eigenvectors and activated voxels.

Discussion

This study has shown that it is possible to overlay fMRI activation maps on to a DTI template without formal registration or transformation algorithms by employing closely matched EPI sequences for both datasets. This provides, in a single map, complementary information about fibre tract integrity and orientation in relation to regions of activation. Furthermore, FA provides a method of classifying the structural properties of brain tissue that may be of interest when combined with fMRI studies.

Since the predominant source of geometric distortion in EPI images is the presence of susceptibility gradients during the readout echo train, these distortions should depend largely on the readout bandwidth, echo spacing and echo train length. Although the sequences used for fMRI and DTI differed slightly (relatively short echo gradient echo EPI for the former, and long echo spin echo prepared EPI for the latter), these three main parameters were matched, so that the geometric effects on both image sets are similar or identical.

Significantly lower anisotropy was found in activated visual cortex than in the optic radiation, consistent with the anticipated localization of areas of activation to grey matter containing mainly neuronal cell bodies, with relatively isotropic diffusion. It is a generally agreed assumption that the main site of brain metabolism (and therefore BOLD signal change) is in populations of neuronal cell bodies within grey matter. Studies using fMRI at higher field (4T) in conjunction with optical imaging (Menon et al, 1995) indicate that grey matter capillaries provide the greatest contribution to the BOLD signal change at 4T, although the localization of the BOLD effect may vary with field strength. The relatively low

vascularity of white matter compared to grey matter (Rempp et al, 1994) may also contribute to these observations.

Although with careful sequence matching it is possible to overlay fMRI and DTI maps without formal registration, the underlying image data may require registration to generate activation and FA maps. fMRI images must generally be corrected for motion (Brammer et al, 1997); DTI images may also require registration (Haselgrove and Moore, 1996; Symms et al, 1997) or other correction strategies to correct for eddy current induced distortions. On the scanner used for the present work, however, such corrections are usually not required, and none were applied to the diffusion images in the current study. There was no significant rim artefact or other evidence of misregistration characteristic of eddy current-induced distortions in the FA maps. Even if registration is required to map activation maps upon FA templates, only simple linear techniques are needed to overcome the rigid body motion, image stretching and image shear to which the fMRI and DTI data are subject. The more complex, and potentially less accurate, non-linear warping necessary to match EPI data to conventional "spin warp" spin or gradient echo images, is not required.

A limitation of DTI is that in each voxel the diffusion tensor represents an average of the tissue sampled, and it is likely that with our voxel size some partial volume artifact is present. Furthermore, a voxel may contain small tracts with differing directions, resulting in a misleading average impression of tract direction. In such areas of incoherent fibre trajectories, anisotropy will be low, and the vector field poorly defined. This is probably the main limitation of DTI in assessing fibre direction, although future improvements in resolution may help to obtain increasingly accurate information about tract orientation and connectivity.

Improved resolution results in a reduced signal-to-noise ratio, however, which may affect FA estimation since there is a systematic overestimation of diffusion anisotropy as noise increases. At present DTI appears to be useful in accurately depicting the larger fibre pathways in the brain (including the corpus callosum, corticospinal tracts and optic radiation), and although the technical limitations of fibre incoherence must be considered, DTI shows considerable promise for the future study of brain connectivity. The problem of image noise may complicate the statistical analysis of diffusion data. Although in our experiment there is undoubtedly a large and significant difference in FA between activated voxels and white matter tracts, more work is required to develop better methods of analysing diffusion data statistically if more subtle effects are to be detected.

The principle of combining the two modalities may in the future be applied to group analyses, although this presents the methodological problem of transforming DTI maps into a standard space whilst maintaining meaningful quantitative information. Probabilistic information about connectivity might be obtained from the diffusion tensor and used in mathematical models of functional integration such as structural equation modelling (Friston et al, 1998d).

Water diffusion in human brain tissue is modified by brain pathology, for example ischaemia (Warach et al, 1992), demyelination (Larsson et al, 1992) and tumours (LeBihan et al, 1993). It is likely that the study of pathological changes within fibre tracts using DTI and fMRI will contribute further to our understanding of links between brain structure and function in health and in neurological disease. The combination of the techniques may provide, for example, an opportunity to assess the impact of subcortical pathology on tract anisotropy and cortical function.

Conclusion

DTI provides important structural information about brain anatomy not obtainable by other noninvasive imaging techniques; this information is complementary to fMRI studies. DTI allows the classification and investigation of brain tissue by its anisotropy characteristics, and has the potential to define the connectivity between brain regions. With the careful choice of imaging parameters, fMRI activation maps can be overlaid upon a fractional anisotropy template without registration or transformation. Visual cortex regions activated during photic stimulation show lower anisotropy than the optic radiation. Combining DTI and fMRI in this novel way, particularly to explore the functional consequences of pathological disruption of tracts, will illuminate links between brain structure and function in the future.

Chapter 6

Conclusions

This final chapter is presented in two parts: firstly, the main findings of the work contained in the thesis are briefly summarized, and their contribution to understanding mechanisms of neurological damage and recovery (with particular reference to demyelinating disease) are discussed; and secondly, some possible directions for future work using MR diffusion and fMRI techniques are suggested.

6.1 Summary of experimental work and its contribution to understanding mechanisms of nervous system damage and recovery

Mechanisms of recovery

The excellent clinical recovery characteristic of certain demyelinating diseases - in particular, in the early stages of MS - has been emphasized. Although in other neurological diseases from which recovery may occur - most notably stroke - there is evidence that cerebral adaptive mechanisms play a role (see chapter 3 for a brief overview), the possibility that similar changes contribute to recovery in demyelinating diseases has received relatively little attention. The fMRI experiments described in this thesis represent an attempt to investigate the role of cerebral reorganization in the recovery from demyelination.

The work described in chapter 3 tested the hypothesis that a different cerebral response to visual stimulation is found in patients who have recovered from optic neuritis, a model of demyelination in a clinically eloquent pathway, in comparison to healthy volunteers. A selected population of patients with clinical and paraclinical evidence of isolated optic nerve demyelination was studied. In these patients, the pattern of brain activation on stimulation of the recovered eye was abnormal, in both its anatomical distribution and its temporal relationship to the visual stimulus. Unlike the response elicited in controls, which was confined to the occipital visual cortex, patients showed widespread additional activation in other areas - including in the insula-claustrum, lateral temporal and posterior parietal cortices - with peak fMRI signal observed during the baseline experimental condition. A similar pattern of extra-occipital response was seen in two separate studies on the same patients using different experimental epoch lengths. The extra-occipital regions activated in patients have extensive connections to visual cortical areas, and some have been proposed as areas of multimodal sensory integration; possible mechanisms by which they may contribute to the recovery process are discussed in detail in chapter 3.

The patients studied were selected according to strict clinical and radiological criteria, designed to include only those with isolated optic nerve demyelination. They are not representative of patients with clinically definite MS. Furthermore, the interval between documented visual loss in the affected eye, and the fMRI study was in all cases over six months, and in most cases greater than ten years; in this time no patients had developed other areas of demyelination. Although the patients are thus a highly selected and rather atypical group, the strict selection criteria allow a clearer interpretation of the data by eliminating the

problems of multifocal lesions (with complex functional effects) likely to be present in patients with clinically definite MS. The studies reported thus provide evidence that the cerebral response to visual stimuli may be modified by an episode of optic nerve demyelination.

These results do not allow a definitive assessment of the contribution of the change in distribution of cerebral activity to functional recovery. The fact that the patients with the longest VEP latencies show the greatest extra-occipital response, and the graded relationship between extra-occipital activated volume and VEP latency suggest that the extra-occipital areas may have a role in compensating for VEP delay. However, more data is required to definitively establish this relationship; the group we have investigated are unusual in that five of seven had normal VEP latencies at the time of the study (Jones et al., 1993); the inclusion of additional patients with persisting VEP delay would therefore be very helpful in this regard. The available data indicate that the changes reported are enduring, given the long interval between presentation and study for most of the cases.

A characteristic feature of the extra-occipital responses in patients is that the peak fMRI response consistently occurs during the baseline condition of the experiment. The data presented - from both the short and long epoch studies - are *not* consistent with a fixed delay in the neural or haemodynamic response in these extra-occipital regions since in both cases the timing of the extra-occipital response was out of phase with respect to the periods of stimulation. The explanation that best fits the observed data is of an increased degree of neural activity in extra-occipital regions during the resting (dark) phase; this may reflect either excitatory or inhibitory synaptic events. Estimation of neurotransmitter

cycling rates suggests that synaptic activity in the baseline phase is not negligible and may not be constant during task performance (Shulman et al., 1998). One possible mechanism is that the extra-occipital areas are inhibited during the baseline condition and released (i.e. disinhibited) at the onset of visual stimulation. Although baseline responses in healthy subjects have been reported in the PET and fMRI literature in a variety of cognitive experiments (see for example Clark et al., 1996; Bullmore et al., 1996a; Shulman et al., 1997; Binder et al., 1999), they have only rarely been noted in simple visual stimulation experiments similar to the present work (Guy et al., 1999). There are a small number of reports of baseline responses in patients with CNS disease during simple visual stimulation: preliminary studies in children with periventricular leukomalacia have reported a "deactivation" of the anterior part of the visual cortex (Sie et al., 1998), but it is possible that the sedation used contributed to this response, in addition to the pathology. The data reported in this thesis suggest that baseline fMRI responses may be relevant to the physiological response after pathological damage to the adult CNS, and are deserving of further investigation.

The work described may have implications for our understanding of recovery in demyelinating diseases. Much previous experimental and clinical work has focused upon changes occurring at the site of demyelination in an affected pathway - including resolution of oedema and inflammation, and changes in the distribution and concentration of ionic channels - which are likely to play an important role in recovery of function (see chapter 1). The data presented in this thesis suggest that a functional reorganization in areas of the brain remote from a demyelinating lesion may also be associated with recovery of function. The contribution (if any) of the observed changes to functional recovery is not yet

clear. It is, for example, possible that the reorganized pattern represents an epiphenomenon perhaps due to visual misperception in patients [although visual acuity and gross colour perception typically recover fully after optic neuritis, higher level deficits in visual processing are well described (e.g. Mullen and Plant, 1986)]. It is important to distinguish between these possibilities, since if the adaptive response is shown to be beneficial it may be of value in developing or monitoring new rehabilitation strategies to improve functional outcome after demyelinating relapses.

The concept of cerebral adaptation contributing to functional recovery in demyelinated pathways may contribute to our understanding of the natural history of MS. The initial typical relapsing-remitting phase is characterized by intermittent, often modest neurological impairment, with good recovery from individual relapses. In the majority of patients, this disease pattern subsequently transforms into a phase of progressive disability. Why does this transition occur?

A traditional view of symptom production in the relapsing phase attributes clinical deficit to active inflammatory lesions in eloquent anatomical pathways. Inflammatory myelin loss, glial cell destruction and reactive gliosis with relative axon sparing contribute to conduction disturbances, which subsequently resolve with the reduction of inflammation, remyelination, and reorganization of sodium channels (see chapter 1 for a fuller discussion). A loss of efficiency of these repair processes has been suggested to account for the conversion to progressive MS. However, this explanation does not account for evidence that areas of active focal inflammation on enhanced MRI exceed clinical evidence of activity by a factor of 10 or more (Thompson et al., 1991); the latter observation is unlikely to be fully explained by lesions being located in non-eloquent areas.

This model of deficits in the relapsing phase has also been challenged by a renewed interest in the axonal loss that has long been known to occur in MS lesions. Recent work has elegantly demonstrated axon transection in inflammatory lesions even at very early stages of the disease (Fergusson et al., 1997; Trapp et al., 1998). It therefore seems likely that axon transection is a frequent feature of inflammatory demyelinating lesions at all stages of MS, mediated either by immune mechanisms or by the effects of persistent demyelination. Indirect evidence that axonal loss occurs in relapsing MS is also provided by measurement of NAA using proton NMR spectroscopy, and of cerebral atrophy (Narayanan et al., 1997; Losseff et al., 1996). If permanent axon damage begins at disease onset, local repair processes at the sites of demyelinating plaques do not provide a completely satisfactory explanation of recovery from relapse in the early disease stages. Cerebral adaptation to the ongoing axonal loss may be one contributory mechanism, analogous to the plastic cortical changes observed during functional recovery following motor stroke. Since adaptive cortical reorganization is not detected by standard MRI methods, it may also contribute to the clinical silence of many MRI lesions, and the lack of clear correlation between MRI abnormalities and clinical disability.

The present work is relevant in this context as it provides preliminary evidence for enduring changes in cerebral functional organization following recovery from a demyelinating lesion known to be associated with axonal loss (optic neuritis). A pathophysiological model that fits the available data can be summarized as follows: in relapsing-remitting disease, some clinical deficits are caused by reversible conduction disturbances resulting from inflammatory demyelination. Axon loss occurs in a significant proportion of inflammatory

lesions, but either causes temporary functional loss, or is clinically silent due to cerebral adaptation to persistently abnormal conduction in affected pathways. As the number of lost axons increases in important fibre tracts, the capacity of the brain to compensate is exceeded, resulting in irreversible and progressive disability. This model is attractive, but does not adequately explain certain aspects of MS; for example, approximately 10% of patients have a progressive disease pattern from onset. It is possible that in some patients, at some stages of the disease, clinical progression results from widely distributed structural damage in the NAWM, which are more apt to exceed compensatory mechanisms.

Mechanisms of CNS damage

Neurological deficit in MS can be attributed broadly to at least two main mechanisms: acute inflammatory demyelination in lesions, and persistent axon and/or myelin loss in lesions and NAWM. The lack of pathological specificity of conventional MRI has been discussed in chapters 1 and 4. MR diffusion imaging offers the prospect of improved detection or differentiation of the pathological processes in MS. In chapter 4, MR diffusion imaging was used to investigate a representative sample of patients with clinically definite MS. The key questions addressed were: can diffusion imaging detect heterogeneity of structure in MS lesions and subtle pathology in the NAWM? ; how anatomically widespread are the NAWM abnormalities? ; and finally, are the structural changes in NAWM related to those in lesions? The work presented provided answers to these questions, and consolidated previous diffusion studies. Firstly, the data confirm that water diffusion measurements are elevated in the lesions and NAWM of

patients with MS; this was shown both with an EPI 3-axis diffusion technique and with DTI. Secondly, considerable heterogeneity of diffusion characteristics was observed in MS lesions; T1 hypointense lesions exhibit higher water diffusion than non-T1 hypointense lesions, indicating that diffusion measurements may reflect the degree of persistent structural damage. Subsequent data from other laboratories have since confirmed this observation (Bammer et al., 1999; Iannucci et al., 1999). Thirdly, the data indicate that abnormalities of the NAWM in MS patients are anatomically widespread, and suggest that the corpus callosum may be particularly affected.

The data also emphasize the complex behaviour of water diffusion in the NAWM, since differences in the apparent degree of abnormality of ADC values are found in different brain regions. Finally, a relationship was found between diffusion measurements in the NAMW and in lesions, suggesting that the underlying mechanisms of tissue damage are likely to be linked. These mechanisms require further investigation, but one contributory process may be that axonal damage within lesions causes degeneration of traversing fibres into surrounding NAWM, as suggested by NAA spectroscopy studies (Narayanan et al., 1995). Other mechanisms, not directly related to focal lesions (e.g. diffuse inflammatory or degenerative processes in the NAWM) may also contribute, however. Whether focal lesions are a prerequisite for the development of NAWM abnormality (or *vice versa)* are important outstanding questions with potential therapeutic implications.

The DTI studies described in chapter 4 demonstrated abnormalities in diffusion anisotropy in both lesions and NAWM. An irreversible reduction in anisotropy may represent a permanent loss of structural integrity due to persistent

demyelination, axonal loss, gliosis, or a combination of factors. Furthermore, studies in patients with stroke (as a potential model of isolated focal CNS damage) indicate that a persistent loss of diffusion anisotropy, with a relative preservation in diffusivity, may be a pattern that is characteristic of fibre degeneration (Wallerian degeneration). This may have implications for the investigation of mechanisms of damage to the NAWM in MS.

Exploring links between structure and function

In chapter 5, experiments were performed to determine the feasibility of combining diffusion and fMRI in a single study in an individual, to investigate tract organization and functional activation patterns respectively. The work presented aimed to determine whether this combination provides information of potential interest, firstly in a study of recovery mechanisms in a patient following traumatic brain injury; and secondly in the visual system of healthy individuals. It was shown that information about fibre orientation and integrity, and functional activation in response to a task, may successfully be obtained in a single study. Information from both MR diffusion and fMRI studies can be directly displayed on a single map, providing that acquisition parameters are closely matched for both imaging techniques. This allows an exploration of the relationship of activated regions to the orientation and anisotropy of white matter tracts.

The study of a patient with a traumatic injury of the internal capsule demonstrated that such information may have clinical relevance and may shed light on mechanisms of recovery and persistent deficit. In particular, the relative contributions of reversible factors at the site of injury (e.g. oedema, inflammation),

sparing of axons, and reorganization of cortical function, may be specifically addressed using this combination of imaging modalities.

6.2 Discussion of the potential for future work

fMRI studies of recovery in demyelinating disease

Optic neuritis

The advantages of optic neuritis as a model of demyelination with which to increase our understanding of demyelinating disease mechanisms have been discussed (chapter 3). The work described therein has generated a number of questions that may be investigated in future studies. Studying larger numbers of patients who fulfil similar selection criteria, but who have a range of VEP latencies (delayed and non-delayed) would help to clarify the contribution of VEP delay to the abnormal pattern of cerebral activation. Evidence for a role in recovery may also be obtained by performing serial studies from the time of onset of symptoms. If the time course of recruitment of the extra-occipital areas parallels the recovery of vision or of the VEP, this would suggest a role in the recovery process. However, to definitively demonstrate a *change* in the cerebral response, related to the clinical episode, a prospective study of the activation pattern before, during, and after the onset of symptoms is needed. It is generally impractical to study patients before the onset of symptoms, but a longitudinal study of patients in the initial stages after presentation is likely to be of considerable interest, and is currently underway at the Institute of Neurology.

Another way to investigate the question of the relevance of these activation patterns to recovery is to study patients with a poor recovery (clinically and/or electrophysiologically) from optic neuritis, or with optic neuropathies due to different pathologies from which recovery is less complete. Examples of such processes include anterior ischaemic optic neuropathy, in which the optic nerve head is infarcted, causing a persistent loss of visual function. If a similar pattern of extra-occipital activation is also seen in these patients, this would suggest that it does not have a major role in the recovery process following optic neuritis, although a possible confounding factor is that the degree of persistent visual input disruption may differ between the two conditions. VEP studies and pattern electroretinography may be of value in this regard.

More detailed tests of visual function than the simple clinical measures used in the present work (acuity and colour appreciation) may be of interest, for example those investigating spatial frequency discrimination, colour contrast sensitivity or motion perception, which may be subtly impaired to variable extents following optic neuritis (e.g. Mullen and Plant, 1986). It is possible to design functional imaging experiments to detect the cerebral responses to various aspects of visual function, for example colour perception (e.g. Lueck et al., 1991), allowing an investigation of the relationship between the extent of recovery of different aspects of visual function, and compensatory functional activation patterns.

The possible contribution from ongoing cerebral activity (not directly rellated to the experimental stimulus) on the results presented (i.e. extra-occipital activation during the baseline condition) is difficult to control for using the

experimental design used in the present work. Factors including eye movements or changes in alertness could therefore influence cerebral activity during the resting phase. Future experiments could be improved by providing a better specified baseline period by, for example, monitoring eye movement, using a fixation cross, and asking the subject to make a response (e.g. pressing a button) to confirm vigilance and compliance. Event-related fMRI studies with continuous measurements of absolute fMRI signal values may demonstrate definitively whether extra-occipital areas after optic neuritis show a delayed excitatory or a "disinhibitory" response to a visual stimulus.

The studies described in this thesis were limited to data collected from only a proportion of the brain volume (approximately 50-60%) due to technical limitations in the amount of data that could be collected at the desired spatial resolution and SNR during the experiments. It would be desirable to image the entire brain in future studies, firstly, so that no changes in the distribution of cerebral response are missed; and secondly, to make the generation of group maps more straightforward by avoiding registration problems caused by partial brain overlap between subjects.

Motor recovery

The work in this thesis has largely focused upon isolated demyelination in the visual system, since optic neuritis has a number of methodological advantages that have previously been discussed. Motor disability is common in MS, but may reflect disease at a number of levels of the CNS, from the spinal cord to the motor cortex. It is thus not always straightforward to attribute particular deficits to

particular lesions, especially in patients of long disease duration. Despite these difficulties, there have been to date a small number of studies of motor deficits in patients with clinically definite MS. A preliminary study indicates that good recovery from a monoparesis may be associated with an increased extent of cerebral activation on moving the recovering limb (Yousry et al., 1998). A subsequent serial study of a single patient suggests that dynamic changes in motor activation pattern, and in the concentration of N-acetyl aspartate in the appropriate internal capsule, accompany clinical recovery from limb weakness caused by MS (Reddy et al., 2000). Another recent study (Lee et al., 2000) investigated 12 patients who had recovered from limb weakness in the context of MS, and found evidence for a posterior shift in the location of motor cortex activation on tapping the recovered hand, in comparison to healthy controls. Ipsilateral motor cortex activation was also noted, which correlated with the T2-weighted MRI lesion load. This relationship, between a measure of "disease burden" and of the degree of cortical reorganization, supports the hypothesis that the cortical changes are in fact adaptive and contribute to recovery. However, the limited pathological specificity and variable functional significance of signal change detected by conventional MRI have been emphasized previously. Further fMRI studies investigating motor recovery in MS are needed to confirm and extend these observations, and are likely to provide a greater understanding of the role of cortical adaptation in recovery, particularly when combined with techniques sensitive to the degree of structural damage (including axonal loss) in affected pathways (see below). The way in which demyelination (in which multifocal and diffuse tissue abnormalities play a role) may affect the morphology and magnitude of the cerebral BOLD response also requires further investigation.

The spinal cord is a common site for demyelinating lesions, and pathology at this site is likely to contribute substantially to motor disability in MS (Losseff et al., 1996). There is evidence that spinal damage due to trauma induces plastic changes in cerebral sensorimotor pathways (Danziger et al., 1996, Roelcke et al., 1997). The possibility of a similar reorganization occurring after spinal demyelination has not been widely studied, although one preliminary study suggested that an expanded area of supplementary motor cortex is activated on moving the previously more affected hand following asymmetric transverse myelitis affecting the cervical segments (Cramer et al., 1998). It will be of considerable interest to study cerebral motor activation in patients from the onset of acute spinal cord syndromes caused by demyelinating or other pathologies. The differences in cerebral activation between patients showing a rapid and complete recovery, and those with a poorer recovery could be investigated, although the problem of task performance and monitoring is a potential problem in persistently disabled patients (Frackowiack, 1998). Differences between different clinical subgroups of MS patients may also be of interest. fMRI during tactile or vibratory sensory stimulation to the periphery has received relatively little attention in comparison to motor experiments, but may represent a useful way of investigating the cortical response to disruption of somatosensory pathways (see, for an example of this approach Danziger et al., 1994). It will also be of interest to combine functional imaging studies with neurophysiological measures of central sensory and motor pathway conduction.

Neurological rehabilitation

Functional imaging has the potential to study some fundamental questions relating to the effects of neurological rehabilitation on recovery. As has been discussed, the first question to address before investigating the impact of rehabilitation is whether particular changes in cerebral activation contribute to functional recovery; it is, for example, possible that certain "maladaptive" reorganization patterns are associated with a poor outcome. However, if particular patterns of cerebral plasticity can be shown to be important in functional recovery, fMRI may be valuable in determining whether they can be altered by different patterns of motor or sensory experience at each stage of the recovery process. The effects of physical therapy on motor activation patterns at different stages of recovery could be investigated, and both aspects subsequently related to ultimate functional outcome. A similar approach could be used to study the effects of other therapeutic interventions (e.g. drug treatments aimed at reducing abnormal patterns of muscle tone) upon cerebral activation patterns and functional outcome. A specific and important question is: when do treatment interventions need to be targeted in order to maximize the speed and extent of functional recovery? Although clinical endpoints will remain the most important test of the effectiveness of treatments, the study of plastic changes using functional imaging may help to elucidate the underlying mechanisms of therapeutic effect upon the recovery process. This could in turn have important implications for the rational design of clinical neurorehabilitation strategies, the most appropriate selection of patients and the optimum timing of intervention.

Diffusion studies of tissue damage in MS

Diffusion imaging methods, particularly DTI, may provide a powerful new tool with which to investigate mechanisms of damage in lesions and NAWM in MS. The potential importance of NAWM abnormalities in the generation of disability in MS has previously been discussed. It has been suggested that diffusion imaging may be a way of quantifying the integrity of fibre pathways in the brain and provide a putative marker for fibre degeneration (wallerian degeneration). Studies using proton NMR spectroscopy suggest that wallerian degeneration may contribute to structural damage in NAWM (e.g. Narayanan et al., 1997), but the technical limitations of this imaging method, in particular its limited spatial resolution, have made this hypothesis difficult to investigate. DTI may allow the extent of wallerian degeneration in a white matter tract to be quantified and related to the extent of structural damage in lesions located in connected brain regions. The corpus callosum is an easily identifiable structure that is commonly involved in MS, and is large enough to be reliably investigated with MR diffusion imaging. One approach might be to measure anisotropy in segments of the corpus callosum and test for relationship with the anisotropy in lesions in connected areas of white matter. The known topographic organization of interhemispheric connecting fibres would predict that the two anisotropy measurements would correlate if fibre degeneration has occurred. A recent post-mortem study has shown a strong correlation between axon density in corpus callosum segments and T2-weighted lesion load in the corresponding hemispheric regions (Evangelou et al., 2000).

Another possible way of investigating mechanisms of lesion and NAWM tissue damage is to examine the evolution of lesion diffusion characteristics

serially, and to seek diffusion abnormalities in connected areas of NAWM following lesion appearance. A serial diffusion MRI study in MS patients with clinical and MRI evidence of disease activity over one year has been undertaken at the Institute of Neurology. Contralateral NAWM regions, matched as far as possible to lesion location, were examined in order to investigate whether measurable diffusion changes occur in anatomically connected regions before or after lesion appearance. Preliminary data indicate that such changes in connected brain regions may occur, supporting the concept that damage or dysfunction of fibres traversing lesions plays a role in NAWM abnormalities (Werring et al., 2000).

A definitive understanding of the pathological substrates of increased diffusivity and reduced diffusion anisotropy in lesions and NAWM will require a correlative MR and histopathological study. The wide range of diffusivity and anisotropy values seen in lesions (Chapter 4) is perhaps unsurprising given the great heterogeneity of pathological changes in MS plaques. A large recent histological study has emphasized that a number of different pathogenic mechanisms, with different degrees of damage to myelin and oligodendrocytes, may operate in MS lesions (Luchinetti et al., 1999).

The methodological limitations of the diffusion tensor techniques that are commonly used at present must be remembered when interpreting diffusion data. In particular, the limited spatial resolution may give a misleading impression of fibre integrity: for example, if there are two sets of fibres with different orientations crossing within a voxel, a low diffusion anisotropy may result. Subsequent selective damage to one set of fibres may then theoretically cause an *elevation* of anisotropy (Pierpaoli et al., 1998). Technical developments, for

example high angular resolution DTI, may in the future allow a clearer depiction of small fibre trajectories within the brain. It may also be possible to measure water diffusion properties reliably in the optic nerves and spinal cord. These structures have clearly defined clinical functions and provide valuable models for investigating mechanisms of impairment and recovery in demyelination. Although the small size and anatomical characteristics of these regions (in particular the proximity of bony structures and their susceptibility to motion) create considerable technical challenges, technical advances in spatial resolution, geometric distortions and motion correction strategies may make MR diffusion imaging useful in clinical studies in the foreseeable future.

Exploring links between structure and function

The potential for DTI to demonstrate the trajectories of fibre pathways has generated interest in its complementary application with functional imaging techniques. In Chapter 5, a preliminary attempt to combine data from DTI and fMRI in normal subjects during simple visual stimulation was presented. The integrity and orientation of visual pathways was directly related to activation in connected areas of visual cortex. It will be of great interest in the future to apply similar methods to the study of demyelinating (or other) lesions in eloquent pathways. The effects upon tract integrity may then be linked to the pattern of cerebral activation during a task expected to involve the affected pathway. In this way the relationship between the nature, extent, and location of tissue damage, and the degree of cortical adaptive response may be investigated and correlated with clinical or paraclinical (for example neurophysiological) measures of recovery. It

may be possible to explore the key question of why patients with apparently identical neurological damage may show a range of clinical outcomes.

A particular question of interest is the extent to which local mechanisms at the site of CNS injuries, and reorganization of the cortex, contribute to recovery in humans. DTI, by providing novel microstructural information may be of particular value in studying reversible and irreversible changes in tract integrity at the injury site, whilst fMRI is helpful in mapping cortical activation patterns in response to tasks involving the affected pathway. A first attempt to combine the two techniques in the same patient, in a clinical setting, was also presented in Chapter 5. This study indicated that axonal sparing was a major determinant of clinical recovery following a traumatic injury of the internal capsule. This type of approach is likely to contribute to further understanding of recovery mechanisms, particularly in the motor system (Rowe and Frackowiack, 1999). Furthermore, insight may be gained into mechanisms of deficit due to the function disconnection of cerebral areas following tract injury. Longitudinal studies may be valuable in assessing the evolution of structural changes at the injury site together with the cortical activation pattern, and their relationship to the subsequent pattern of clinical evolution.

The approach used in chapter 5 – i.e. directly overlaying activations upon DTI derived maps – is feasible in subjects in which motion can be minimized between experiments. This may be more difficult to ensure in motor studies, or in patients with disabilities; image registration techniques to combine data from the different modalities in a composite volume may therefore be helpful. A preliminary study in the motor system has used this approach to combine DTI and fMRI data in a normal subject (Pfeiffer et al., 2000).

As will be apparent from the previous discussion, the importance of understanding the relationship between structure and function and *vice versa* cannot be over-emphasized in clinical neuroscience. A full understanding of the organization of the nervous system will require mapping of not only the brain areas specialized for certain functions, but also the anatomical fibre systems connecting them. Previous methods of elucidating fibre connections have relied on histological impregnation techniques such as the Golgi method, and the study of tract degeneration in response to experimental or other injury (Brodal, 1969). These methods are limited in their applicability to clinical studies. Upon this background, DTI is potentially a very useful technique for the non-invasive mapping of fibre pathways. The degree of connectedness between intracerebral voxels can be estimated by examining parameters derived from the diffusion tensor, often including the principle eigenvector. Using algorithms that vary in complexity, the most likely trajectory for fibre tracts originating from any given seed point can be estimated. This field is the subject of considerable interest at present and is likely to develop rapidly (see for example Jones et al., 1999; Conturo et al., 1999). Few studies have applied this methodology to the study of pathological changes affecting tracts, but it is possible that in due course the effects of lesions upon fibre integrity and direction will be visualized directly, and related to clinical findings. A recent study has, for example, demonstrated a deviation of white matter fibres adjacent to a brain tumour, with little associated motor deficit (Wieshmann et al., 2000). The study of patients with motor stroke presented in Chapter 4 provides an illustration of the impact of a single focal brain lesion upon the integrity and orientation of a connected fibre tract. The concept of diaschisis, widely invoked to explain the functional effects of brain lesions, may

be investigated using the direct visualization of fibre tracts using DTI, together with fMRI activation studies.

6.3 Concluding remarks

The central themes addressed by this thesis are the mechanisms underlying recovery and persistent damage to the CNS in demyelinating disease. In relation to the first of these, evidence has been obtained for a reorganization of the cerebral response to visual stimulation in patients following recovery from isolated optic neuritis, compared to normal individuals. Although the work should be considered as preliminary, it clearly demonstrates the value of using fMRI in the investigation of demyelinating disease mechanisms. The concept of cortical adaptation in response to persistent fibre damage in eloquent tracts can be incorporated into current models of MS pathophysiology in which axonal loss occurs in MS lesions at the earliest disease stages. Further studies - in patients with varying degrees of clinical and electrophysiological recovery from optic neuritis, and in patients studied serially during the recovery process - are likely to provide further insights into the potential contribution of cortical reorganization to recovery.

Diffusion imaging has been shown to be sensitive to structural heterogeneity in lesions, and to subtle abnormalities in NAWM in MS; it therefore shows promise in the investigation of mechanisms of tissue damage in lesions and NAWM. Diffusion measurements did not correlate with clinical measures of disability, though further studies of larger clinical cohorts are needed. In particular, it will be of interest to determine whether diffusion anisotropy in eloquent tracts correlates with appropriate functional deficits.

The relationship between the degree of diffusion abnormality in lesions and that in NAWM suggests that their underlying pathogenetic mechanisms may be linked. The complex influences on diffusion measurements have been explored, underlining the need for carefully conceived and executed experimental studies. The studies presented here show the promise of anisotropy measurements in the investigation of subtle NAWM pathology, and the work in stroke suggests that anisotropy may be sensitive to fibre degeneration. The technical limitations of DTI (in particular its limited spatial resolution) currently limit its application to the larger fibre tracts, but methodological improvements are likely to emerge in the near future. Finally, the complementary use of MR diffusion imaging studies of aspects of tissue structure, together with fMRI studies of brain function, will provide insight into the complex relationships between the extent and nature of tissue damage, the cortical response to the damage, and the clinical outcome from demyelinating and other neurological diseases.

References

Adams RD and Kubik CS. The morbid anatomy of the demyelinating diseases. Am J Med 1952; 12: 510-46.

Allen I and McKeown S. A histological, histochemical and biochemical study of the macroscopically normal white matter in multiple sclerosis. J Neurol Sci 1979; 41: 81-91.

Arnold DL, Matthews PM, Francis GS, O'Connor J, Antel JP. Proton magnetic resonance spectroscopic imaging for metabolic characterization of demyelinating plaques. Ann Neurol 1992; 31: 235-41.

Atlas SW, Howard RS, Maldjian J et al. Functional magnetic resonance imaging of regional brain activity in patients with intracerebral gliomas: findings and implications for clinical management. Neurosurgery 1996; 38: 329-338.

Bakshi R, Miletich RS, Emmet ML, Kinkel WR. High resolution fluorodeoxyglucose positron emission tomography shows both global and regional cerebral hypometabolism in multiple sclerosis. J Neuroimaging 1998; 8: 228-34.

Bammer R, Augustin M, Seifert T, Strasser-Fuchs S, Hartung HP, Fazekas F. High resolution magnetic resonance diffusion tensor imaging in patients with multiple sclerosis [abstract]. Multiple Sclerosis 1999; 5 (Suppl 1): 211.

Bandettini P, Jesmanowicz A, Wong EC, Hyde JS. Processing strategies for time-course data sets in functional MRI of the human brain. Magn Reson Med 1993; 30: 161-73.

Bandettini P, Wong EC, Binder J, et al. Functional MR imaging using the BOLD approach. Dynamic characteristics and data analysis. In: Le Bihan D, ed. Diffusion and perfusion magnetic resonance imaging. New York: Raven Press, 1995a: pp335-51.

Bandettini PA, Davis TL, Kwong KK et al. FMRI and PET demonstrate sustained blood oxygenation and flow enhancement during extended visual stimulation durations [abstract]. Proc Int Soc Magn Reson Med 1995b; 1: 453.

Bandettini P and Wong EC. Echo-Planar Magnetic Resonance Imaging of Human Brain Activation. In: Schmitt, M.K. Stehling, R.Turner, eds. Echo-planar imaging: theory, technique and application. Berlin: Springer, 1998: pp493-531.

Barker GJ, Clark CA, Franconi F, Symms M. A CSF-suppressed, EPI based pulse sequence for diffusion tensor and apparent diffusion constant measurement in multiple sclerosis [abstract]. Proc Int Soc Magn Reson Med 1997; 1: 223.

Barkhof F, Filippi M, Miller DH, et al. Comparison of MRI criteria at first presentation to predict conversion to clinically definite multiple sclerosis, Brain 1997; 120: 2059-69.

Barnes D, Munro PM, Youl BD, Prineas JW, McDonald WI. The longstanding MS lesion. A quantitative MRI and electron microscopic study. Brain 1991; 114: 1271-80.

Basser PJ, Le Bihan D, Mattiello J. Estimation of the effective self-diffusion tensor from the NMR spin echo. J Magn Reson Series B 1994; 103: 247-54.

Basser PJ and Pierpaoli C, Microstructural and physiological features of tissues elucidated by quantitative diffusion tensor MRI. J Magn Reson Series B 1996; 111: 209-19.

Basser,P.J. Fiber-tractography via diffusion tensor MRI (DT-MRI) [abstract] 1998. Proc Int Soc Magn Reson Med 1998; 2: 1226.

Beaulieu C and Allen PS. Determinants of anisotropic water diffusion in nerves. Magn Reson Med 1994; 31: 394-400.

Belliveau JW, Kennedy DN, McKinstry RC. Functional mapping of the human visual cortex by magnetic resonance imaging. Science 1991; 254: 716-19.

Benecke R, Meyer BU, Freund HJ. Reorganisation of descending motor pathways in patients after hemispherectomy and severe hemispheric lesions demonstrated by magnetic brain stimulation. Exp Brain Res 1991; 83: 419-26.

Berthier M, Starskein S, Leigurda R. Behavioural effects of damage to the right insula and surrounding regions. Cortex 1987; 23: 673-8.

Bhatia KP and Marsden CD. The behavioural and motor consequences of focal lesions of the basal ganglia in man. Brain 1994; 117: 859-76.

Binder JR, Frost JA, Hammeke TA, Bellgowan PS, Rao SM, Cox RW Conceptual processing during the conscious resting state. A fMRI study. J Cogn Neurosci 1999; 11: 80-95.

Binkowski F, Seitz RJ, Arnold S, Classen J, Benecke R, Freund H-J. Thalamic metabolism and corticospinal tract integrity determine motor recovery in stroke. Ann Neurol 1996; 39: 460-70.

Black JA, Felts P, Smith KJ, Kocsis JD, Waxman SG. Distribution of sodium channels in chronically demyelinated spinal cord axons: immuno-ultrastructural localization and electrophysiological observations. Brain Res 1991; 544: 59-70.

Blinkenberg M, Rune K, Jonsson A, et al. Cerebral metabolism in a case of MS with acute mental disorder. Acta Neurol Scand 1996; 94: 310-13.

Brady TJ. Future prospects for MR imaging [abstract]. Proc Soc Magn Reson Med 1991; 1: 2.

Brammer M.J, Bullmore ET, Simmons A, Williams SCR, Grasby PM, Howard RJ, Woodruff PWR, Rabe-Hesketh S. Generic brain activation mapping in fMRI: a nonparametric approach. Magn Reson Imaging 1997; 15: 763-70.

Brewer JB, Zhao Z, Desmond JE, Glover GH, Gabrieli JD. Making memories: brain activity that predicts how well visual experience will be remembered. Science 1998; 281: 1185-7.

Brex PA, O'Riordan JI, Miszkiel KA, et al. Multisequence MRI in clinically isolated syndromes and the early development of MS. Neurology 1999; 53: 1184-90

Brodal A. Neurological Anatomy. London: Oxford University Press, 1969. pp5-30.

Brooks DJ, Leenders KL, Head G, Marshall J, Legg NJ, Jones T. Studies on regional cerebral oxygen utilisation and cognitive function in MS. J Neurol Neurosurg Psychiatry 1984; 47: 1182-91.

Brownell B and Hughes JT. The distribution of plaques in the cerebrum in multiple sclerosis. J Neurol Neurosurg Psychiatry 1962; 25: 315-20.

Bruck W, Schmeid M, Suchanek G, et al. Oligodendrocytes in the early course of multiple sclerosis. Ann Neurol 1994; 35: 65-73.

Bruck W, Bitsch A, Kolenda H, Bruck Y, Stiefel M, Lassmann H. Inflammatory central nervous system demyelination: correlation of MRI findings with lesion pathology. Ann Neurol 1997; 42: 783-93.

Brusa A, Mortimer C, Jones SJ. Clinical evaluation of VEPs to interleaved checkerboard reversal stimulation of central, hemi- and peripheral fields. Electroenceph Clin Neurophysiol 1995; 96: 485-94.

Buchkremer-Ratzmann I, and Witte OW. Extended brain disinhibition following small prothrombotic lesions in rat frontal cortex. NeuroReport 1997; 8: 519-22.

Buckner RL, Bandettini PA, O'Craven KM, et al. Detection of cortical activation during averaged single trials of a cognitive task using functional magnetic resonance imaging. Proc Nat Acad Sci USA 1996; 93: 14878-83.

Bullmore ET, Rabe-Hesketh S, Morris RG, et al. Functional magnetic resonance image analysis of a large-scale neurocognitive network. Neuroimage 1996a; 4: 16-33.

Bullmore ET, Brammer MJ, Williams SCR, et al. Statistical methods of estimation and inference for functional MR image analysis. Magn Reson Med 1996b; 35: 261-77.

Bullmore ET, Brammer MJ, Rabe-Hesketh S, et al. Methods for diagnosis and treatment of stimulus-correlated motion in generic brain activation studies using fMRI. Human Brain Mapping 1999; 7: 38-48.

Calvert GA, Brammer MJ, Iversen SD. Crossmodal identification. Trends in Cognitive Sciences 1998; 2: 247-253.

Cannella B, Raine CS. The adhesion molecule and cytokine profile of multiple sclerosis lesions. Ann Neurol 1995; 37: 424-35.

Carswell R. Pathological Anatomy: Illustrations of the Elementary Forms of Disease. London: Orme, Brown, Green and Longman 1838.

Chacko LW. The laminar pattern of the lateral geniculate body in the primate. J Neurol Neurosurg Psychiatry 1948; 11: 211-24.

Charcot JM Histologie de la sclerose en plaque. Gazette Hôpital (Paris) 1868; 41: 554-66.

Chataway J, Feakes R, Corradu F, et al. The genetics of multiple sclerosis: principles, background and updated results of the United Kingdom systematic genome screen. Brain 1998; 121: 1869-87.

Chenevert TL, Brunberg JA, Pipe JG. Anisotropic diffusion in human white matter: demonstration with MR techniques in vivo. Radiology 1990; 177: 401-5.

Chien D, Buxton RB, Kwong KK, Brady TJ, Rosen BR. MR diffusion imaging of the human brain. J Comp Assist Tomogr 1990; 14: 514-20.

Chiu SY, Ritchie JM. Evidence for the presence of potassium channels in the paranodal region of acutely demyelinated mammalian single nerve fibres. J Physiol (Lond) 1981; 313: 415-37.

Chollet F, Di Piero V, Wise RSJ, Brooks DJ, Dolan RJ, Frackowiak RSJ. The functional anatomy of motor recovery after stroke in humans: a study with positron emission tomography. Ann Neurol 1991; 29: 63-71.

Christiansen P, Gideon P, Thomsen M, et al. Increased water self-diffusion in chronic plaques and in apparently normal white matter in patients with multiple sclerosis. Acta Neurol Scand 1993; 87: 195-9.

Ciaramitaro VM, Todd WE, Rosenquist AC. Disinhibition of the superior colliculus restores orienting to visual stimuli in the hemianopic field of the cat. J Comp Neurol 1997;387:568-587.

Clark VP, Keil K, Ma J, et al. Functional magnetic resonance imaging of human visual cortex during face matching: a comparison with positron emission tomography. Neuroimage 1996; 4: 1-15.

Cohen,M.S. and Bookheimer,S.Y. Localisation of brain function using magnetic resonance imaging. Trends in Neuroscience 1994; 17: 268-77.

Compston DA, Batchelor JR, Earl CJ, McDonald WI. Factors influencing the risk of MS developing in patients with optic neuritis. Brain 1978; 101: 495-511.

Compston DA, Vakerelis BN, Paul E, McDonald WI, Batchelor JR, Mims CA. Viral infection in patients with multiple sclerosis and HLA-DR matched controls. Brain 1986; 109: 325-44.

Connolly M, Van Essen D. The representation of the visual field in parvocellular and magnocellular layers of the lateral geniculate nucleus in the Macaque monkey. J Comp Neurol 1984; 226: 544-64.

Conturo TE, Lori NF, Cull TS, et al. Tracking neuronal fibre pathways in the living human brain. Proc Nat Acad Sci USA 1999; 96: 10422-7.

Cox RW. Analysis and visualisation of 3D fMRI data [abstract]. Proc Soc Magn Reson Med 1995; 2: 834.

Cramer SC, Fray L, Tievsky A, et al. Patterns of cortical activation after recovery from myelitis [abstract]. Neuroimage 1998; 7: S485.

Cramer SC, Nelles G, Benson RR, et al. A functional MRI study of subjects recovered from hemiparetic stroke. Stroke 1997; 28: 2518-27.

Danziger N, Remy P, Pidoux B, et al. A clinical and neurophysiological study of a patient with an extensive transection of the spinal cord sparing only a part of one anterolateral quadrant. Brain 1996; 119: 1835-48.

Davie CA, Hawkins CP, Barker GJ, et al. Serial proton magnetic resonance spectroscopy in acute multiple sclerosis. Brain 1994; 117: 49-58.

Davie CA, Barker GJ, Webb S, et al. Persistent functional deficit in multiple sclerosis and autosomal dominant cerebellar ataxia is associated with axonal loss. Brain 1995; 118: 1583-92.

Davie CA, Barker GJ, Thompson AJ, Tofts PS, McDonald WI, Miller DH. 1H magnetic resonance spectroscopy of chronic cerebral white matter lesions and normal appearing white matter in multiple sclerosis. J Neurol Neurosurg Psychiatry 1997; 63: 736-42.

Davis FA, Jacobson S. Altered thermal sensitivity in injured and demyelinated nerve: a possible model of temperature effects in multiple sclerosis. J Neurol Neurosurg Psychiatry 1971; 34: 551-61.

Dean G. Annual incidence, prevalence and mortality of MS in white South African-born and in white immigrants to South Africa. Br Med J 1967; 2: 842-5.

deLacoste MC, Kirkpatrick JB, Ross ED. Topography of the human corpus callosum. J Neuropath Exp Neurol 1985; 44: 578-91.

DeStefano N, Narayanan S, Mathews PM, Francis GS, Antel JP, Arnold DL. *In vivo* evidence for axonal dysfunction remote from focal lesions of the type seen in multiple sclerosis. Brain 1999; 122: 1933-9.

Diao Y-C, Wang Y-K, Pu M-L. Binocular responses of cortical cells and the callosal projection in the albino rat. Exp Brain Res 1983; 49: 410-18.

Doran M, Hajnal JV, Van Bruggen N. Normal and abnormal white matter tracts shown by MR imaging using directional diffusion weighted sequences. J Comput Assist Tomogr 1990; 14: 865-73.

Dousset V, Grossman RI, Ramer KN, et al. Experimental allergic encephalomyelitis and multiple sclerosis: lesion characterisation with magnetisation transfer imaging. Radiology 1992; 182: 483-91.

Droogan AG, Clark CA, Franconi F, et al. Comparison of echoplanar and navigated spin echo diffusion-weighted imaging techniques used to detect multiple sclerosis lesions [abstract]. Proc Int Soc Magn Reson Med 1997; 3: 1714.

Droogan AG, Clark CA, Werring DJ, Barker GJ, McDonald WI, Miller DH. Comparison of multiple sclerosis clinical subgroups using navigated spin echo diffusion-weighted imaging. Magn Reson Imaging 1999; 17: 653-61.

Eames RA, Jacobson SG, McDonald WI. Pathological changes in the optic chiasm of the cat following local injection of diphtheria toxin. J Neurol Sci 1977; 32: 381-93.

Edan G, Miller DH, Clanet M, et al. Therapeutic effect of mitoxanthrone combined with methylprednisolone in multiple sclerosis: a randomised multi-centre study of active disease using MRI and clinical criteria. J Neurol Neurosurg Psychiatry 1997; 62: 112-18.

Eden GF, VanMeter JW, Rumsey JM, Maisog JM, Woods RP, Zeffiro TA. Abnormal processing of visual motion in dyslexia revealed by functional brain imaging. Nature 1996; 382: 66-9.

Elian M and Dean G. Multiple sclerosis among the United Kingdom-born children of immigrants from the West Indies. J Neurol Neurosurg Psychiatry 1987; 50: 327-32.

Engel SA, Glover GH, Wandell BA. Retinotopic organization in human visual cortex and the spatial precision of functional MRI. Cereb Cortex 1997; 7: 181-92

England JD, Gamboni F, Levinson SR, Finger TE. Changed distribution of sodium channels along demyelinated axons. Proc Nat Acad Sci USA 1990; 87: 6777-80.

Evangelou N, Esiri MM, Smith S, Palace J, Matthews PM. Quantitative pathological evidence for axonal loss in normal appearing white matter in multiple sclerosis. Ann Neurol 2000; 47: 391-5.

Falconer JC and Narayana PA. Cerebrospinal fluid-suppressed high-resolution diffusion imaging of human brain. Magn Reson Med 1997; 37: 119-23.

Fazekas F, Offenbacher H, Fuchs S, et al. Criteria for an increased specificity of MRI interpretation in elderly subjects with suspected multiple sclerosis. Neurology 1988; 38: 1822-5.

Feinberg DA and Mark AS. Human brain motion and cerebrospinal fluid circulation demonstrated with MR velocity imaging. Radiology 1987; 163: 793-9.

Felts PA, Baker TA, Smith KJ. Conduction in segmentally demyelinated mammalian central axons. J Neurosci 1997; 17: 7267-77.

Ferguson B, Matyszak MK, Esiri MM, Perry VH. Axonal damage in acute multiple sclerosis lesions. Brain 1997; 120: 393-9.

Ferrier D. Cerebral localisation in its practical relations. Brain 1889; 12: 36-58.

Fieschi C, Gasperini C, Ristori G. Differential diagnosis in multiple sclerosis. In: Multiple sclerosis: clinical challenges and controversies, eds Thompson AJ, Polman C, Hohlfield R. Dunitz: London, 1997.

Filippi M, Campi A, Dousset V, et al. A magnetization transfer study of normal-appearing white matter in multiple sclerosis. Neurology 1995a; 45: 478-82.

Filippi M, Paty DW, Kappos L, et al. Correlations between changes in disability and T2-weighted brain MRI activity in multiple sclerosis. A follow-up study. Neurology 1995b; 45: 255-60.

Filippi M, Rocca MA, Martino G, Horsfield MA, Comi G. Magnetization transfer changes in the normal appearing white matter precede the appearance of enhancing lesions in patients with multiple sclerosis. Ann Neurol 1998; 43: 809-14.

Foreman SD, Cohen JD, Fitzgerald M, Eddy WF, Mintun MA, Noll DC. Improved assessment of significant activation in functional magnetic resonance imaging (fMRI): use of a cluster-size threshold. Magn Reson Med 1995; 33: 636-47.

Fox PT and Raichle ME. Stimulus rate determines regional brain blood flow in striate cortex. Ann Neurol 1985; 17: 303-5.

Frackowiak RSJ. The cerebral basis of functional recovery. In: Human Brain Function. Eds Dolan RJ, Frackowiak RSJ, Mazziotta J, Friston K. San Diego: Academic Press, 1998: pp275-299.

Frahm J, Merboldt KD, Hanicke W, Kleinschmidt A, Boecker H. Brain or vein–oxygenation or flow? On signal physiology in functional MRI of human brain activation. NMR Biomed 1994; 7: 45-53.

Frahm J, Gunnar K, Merboldt K-D, Kleinshmidt A. Dynamic uncoupling and recoupling of perfusion and oxidative metabolism during focal brain activation in man. Magn Reson Med 1996; 35: 143-8.

Fries W, Danek A, Scheidtmann K, Hamburger C. Motor recovery following capsular stroke: role of descending pathways from multiple motor areas. Brain 1993; 116: 369-82.

Friston KJ, Frith,CD, Frackowiak RSJ. Time-dependent changes in effective connectivity measured with PET. Human Brain Mapping 1993; 1: 69-80.

Friston KJ, Holmes AP, Worsley KJ, Poline JP, Frith CD, Frackowiak RSJ. Statistical Parametric Maps in Functional Imaging: A General Linear Approach. Human Brain Mapping 1995; **2**: 189-210

Friston KJ, Williams S, Howard R, Frackowiak RSJ, Turner R. Movement-related effects in fMRI time series. Magn Reson Med 1996; 35: 346-55.

Friston KJ, Price CJ, Buechel C, Frackowiak RJ. A taxonomy of study design. In: Human Brain Function. Eds Dolan RJ, Frackowiak RSJ, Mazziotta J, Friston K. San Diego: Academic Press, 1998a.

Friston KJ, Fletcher P, Josephs O, Holmes A, Rugg MD, Turner R. Event-related fMRI: characterising differential responses. Neuroimage 1998b; 7: 30-40.

Friston KJ, Josephs O, Rees G, Turner R. Nonlinear event-related responses in fMRI. Magn Reson Med 1998c; 39: 41-52.

Friston, K.J., and Frackowiak, RSJ. Images of the future: a Philosophical Coda. In: Frackowiak RS, Friston KJ, Frith CD, Dolan RJ, Mazziotta JC, eds. Human Brain Function. San Diego: Academic Press, 1998d.

Frost JA, Binder JR, Springer JA, et al. Language processing is strongly left lateralized in both sexes: Evidence from functional MRI. Brain 1999; 122: 199-208.

Frostig RD, Lieke EE, Ts'o DY, Grinvald A. Cortical functional architecture and local coupling between neuronal activity and the microcirculation revealed by in vivo high resolution optical imaging of intrinsic signals. Proc Nat Acad Sci USA 1990; 87: 6082-6.

Fu L, Matthews PM, De Stefano N, et al. Imaging axonal damage of normal-appearing white matter in multiple sclerosis. Brain 1998; 121: 103-13.

Fulton JF. Observations on the vascularity of the human occipital lobe during visual activity. Brain 1928; 51: 310-20.

Gallo P, Piccinno M, Pagni S, Tavalato B. Interleukin-2 levels in serum and cerebrospinal fluid of multiple sclerosis patients. Ann Neurol 1988; 24: 795-7.

Gareau PJ, Gati JS, Menon RS, et al. Reduced visual evoked responses in MS patients with optic neuritis: comparison of functional magnetic resonance imaging and visual evoked potentials. Multiple Sclerosis 1999; 5: 161-4.

Gass A, Barker GJ, Kidd D, et al. Correlation of magnetization transfer ratio with clinical disability in multiple sclerosis. Ann Neurol 1994; 36: 62-7.

Gass A, Barker GJ, MacManus D, et al. High resolution magnetic resonance of the anterior visual pathways in patients with optic neuropathies using fast spin echo and phased array local coils. J Neurol Neurosurg Psychiatry 1995; 58: 562-5.

Gass A, Gaa J, Schreiber W, et al. Assessment of the apparent diffusion coefficient in contrast-enhancing and chronic lesions [abstract]. Proc Int Soc Magn Reson Med 1998; 2: 1328.

Geschwind N. Disconnexion syndromes in animals and man. Brain 1965; 88: 237-94.

Ghatak NR, Hirano A, Litjmaer H, Zimmerman HM. Asymptomatic demyelinated plaque in the spinal cord. Arch Neurol 1974; 30: 484-6.

Giovannoni G. Cerebrospinal fluid and serum nitric oxide metabolites in patients with multiple sclerosis. Multiple Sclerosis 1998; 4 : 27-30.

Gitelman DR, Nobre AC, Parrish TB. A large-scale distributed network for covert spatial attention. Brain 1999;122: 1093-1106.

Goodkin DE, Rooney WD, Sloan R, et al. A serial study of new MS lesions and the white matter from which they arise. Neurology 1998; 51: 1689-97.

Graham DI and Lantos PL, eds. Greenfield's neuropathology; 6th edn. London: Arnold, 1997, pp104-7.

Graham GD, Zhong J, Guarnaccia JB. Echo-planar imaging of water diffusion and diffusion anisotropy within multiple sclerosis plaques [abstract]. Proc Int Soc Magn Reson Med 1995; 1: 278.

Guy CN, Ffytche DH, Brovelli A, Chumillas J. fMRI and EEG responses to periodic visual stimulation. Neuroimage 1999; 10: 125-48.

Hadjikhani N and Roland P. Cross-modal transfer of information between the tactile and the visual representations in the human brain: a positron emission tomographic study. J Neurosci 1998; 18: 1072-84.

Halliday AM, McDonald WI, Mushin J. Delayed visual evoked response in optic neuritis. Lancet 1972; 1: 982-5.

Hammond SR, McLeod JG, Macaskill P, English D. The epidemiology of multiple sclerosis in three Australian cities: Perth, Newcastle and Hobart. Brain 1988; 111: 1-25.

Hand D and Crowder M. Practical longitudinal data analysis. London: Chapman and Hall, 1996.

Harris JO, Frank JA, Patronas N, McFarlin DE, McFarland HF. Serial gadolinium-enhanced MRI scans in patients with early, relapsing-remitting multiple sclerosis: implications for clinical trials and natural history. Ann Neurol 1991; 29: 548-55.

Haselgrove JC and Moore JR. Correction for distortion of echo-planar images used to calculate the apparent diffusion coefficient. Magn Reson Med 1996; 36: 960-64.

Hathout GM, Kirlew KA, So GJK, et al. MR imaging signal response to sustained stimulation in human visual cortex. J Magn Reson Imaging 1994; 4: 537-43.

Hawkins CP, Munroe PMG, MacKenzie F, et al. Duration and selectivity of blood-brain barrier breakdown in chronic relapsing experimental allergic encephalomyelitis studied using gadolinium-DTPA and protein markers. Brain 1990; 113: 365-78.

Hedera P, Lai S, Haacke EM, et al. Abnormal connectivity of the visual pathways in human albinos demonstrated by susceptibility-sensitised MRI. Neurology 1994; 44: 1921-6.

Hertz-Pannier L, Gaillard WD, Mott SH, et al. Noninvasive assessment of language dominance in children and adolescents with functional MRI: a preliminary study. Neurology 1997; 48: 1003-1012.

Hiehle JF, Grossman RI, Ramer KN, Gonzalez-Scarano F, Cohen JA. Magnetization transfer effects in MR-detected multiple sclerosis lesions: comparison with gadolinium-enhanced spin-echo images and nonenhanced T1-weighted images. Am J Neuroradiol 1995; 16: 69-77.

Hikosaka O, Wurtz RH. Visual and oculomotor functions of monkey substantia migra pars reticulata. I. Relation of visual and auditory responses to saccades. J Neurophysiol 1983; 49: 1230-53.

Horsfield MA, Lai M, Webb SL, et al. Apparent diffusion coefficients in benign and secondary progressive multiple sclerosis by nuclear magnetic resonance. Magn Reson Med 1996; 36: 393-400.

Howard R, Williams S, Bullmore E, et al. Cortical response to exogenous visual stimulation during visual hallucinations. Lancet 1995; 345: 8941.

Howseman A, Porter D, Hutton C, Josephs O, Turner R. Blood oxygenation level dependent signal time courses during prolonged visual stimulation. Magn Reson Imaging 1998; 16: 1-11.

Husted CA, Goodin DS, Hugg JW, et al. Biochemical alterations in multiple sclerosis lesions and normal-appearing white matter detected by in vivo ^{31}P and ^{1}H spectroscopic imaging. Ann Neurol 1994; 36: 157-65.

Iannucci G, Cercignani M, Rocca A, Pratesi A, Comi G, Filippi M. Diffusion imaging characteristics of MS lesions [abstract]. Multiple Sclerosis 1999; 5 (suppl): 212.

IFNB Multiple Sclerosis Study Group. Interferon beta-1b is effective in relapsing-remitting multiple sclerosis. 1.Clinical results of a multicenter, randomized, double-blind, placebo-controlled trial. Neurology 1993; 43: 655-61.

Ingvar DH. Patterns of brain activity revealed by measurements of regional cerebral blood flow. In: The Coupling of Function, Metabolism and Blood Flow in the Brain. Munksgaard: Copenhagen, 1975.

Isaac C, Li DK, Genton M, et al. Multiple sclerosis: a serial study using MRI in relapsing patients. Neurology 1988; 38: 1511-15.

Jack CR, Thompson RM, Butts RK et al. Sensory motor cortex: correlation of presurgical mapping with functional MR imaging and invasive cortical mapping. Radiology 194; 190: 85-92.

Jacobson SJ, Eames RA, McDonald WI. Optic nerve fibre lesions in adult cats: pattern of recovery of spatial vision. Exp Brain Res 1979; 36: 491-508.

Jezzard P and Balaban RS. Correction for geometric distortion in echo planar images from B(0) field variations. Magn Reson Med 1995; 34: 65-73.

Jones DK, Simmons A, Williams SC, Horsfield MA. Non-invasive assessment of axonal fiber connectivity in the human brain via diffusion tensor MRI. Magn Reson Med 1999; 42: 37-41.

Jones SJ. Visual evoked potentials after optic neuritis. Effect of time interval, age and disease dissemination. J Neurol 1993; 240: 489-94.

Jones DK, Simmons A, Williams SCR, Horsfield MA. Non-invasive assessment of structural connectivity in white matter by diffusion tensor MRI [abstract]. Proc Int Soc Magn Reson Med 1998; 1: 531.

Katz B and Schmitt OH. Electrical interaction between two adjacent nerve fibres. J Physiol (London) 1940; 97: 471-88.

Katz D, Taubenberger JK, Cannella B, McFarlin DE, Raine CS, MacFarland H. Correlation between MRI findings and lesion development in chronic active multiple sclerosis. Ann Neurol 1993; 34: 661-69.

Kermode AG, Thompson AJ, Tofts P, et al. Breakdown of the blood-brain barrier precedes symptoms and other MRI signs of new lesions in multiple sclerosis. Pathogenetic and clinical implications. Brain 1990; 113: 1477-89.

Kidd D, Thorpe JW, Kendall BE, et al. MRI dynamics of brain and spinal cord in progressive multiple sclerosis. J Neurol Neurosurg Psychiatry 1996; 60: 15-19.

Kidd D, Barkhof F, McConnell R, Algra PR, Allen IV, Revesz T. Cortical lesions in multiple sclerosis. Brain 1999; 122: 17-26.

Kim S-G, Ashe J, Hendrich K, et al. Functional magnetic resonance imaging of motor cortex: hemispheric asymmetry and handedness. Science 1993; 261: 615-17.

Knight RA, Dereski MO, Helpern JA, et al. Magnetic resonance imaging of evolving focal ischaemia. Stroke 1994; 25: 1252-62.

Koller H, Bucholz J, Siebler M. Cerebrospinal fluid from multiple sclerosis patients inactivates neuronal Na^+ current. Brain 1996; 119: 457-63.

Krabbe K, Gideon P, Wagn P, Hansen U, Thomsen C, Madsen F. MR diffusion imaging of human intracranial tumours. Neuroradiology 1997; 39: 483-9.

Kriss A, Francis DA, Cuendet F, et al. Recovery after optic neuritis in childhood. J Neurol Neurosurg Psychiatry 1988; 51: 1253-8.

Kuhn MJ, Johnson KA, Davis KR. Wallerian Degeneration: Evaluation with MR Imaging. Radiology 1988; 168: 199-202.

Kupfer C, Chumbley L, De C. Downer J. Quantitative histology of optic nerve, optic tract and lateral geniculate nucleus of man. J Anat 1967; 101: 393-401.

Kurtzke JF. Rating neurologic impairment in multiple sclerosis: an expanded disability status scale (EDSS). Neurology 1983; 33: 1444-52.

Kwong KK, McKinstry RC, Chien D, Crawley AP, Pearhman JD, Rosen BR. CSF-suppressed quantitative single-shot diffusion imaging. Magn Reson Med 1991; 21: 157-63.

Kwong KK, Belliveau JW, Chesler DA, et al. Dynamic magnetic resonance imaging of human brain activity during primary sensory stimulation. Proc Nat Acad Sci USA 1992; 89: 5675-9.

Lai S, Hopkins AL, Haacke EM, et al. Identification of vascular structures as a major source of signal contrast in high resolution 2D and 3D functional activation imaging of the motor cortex at 1.5T: preliminary results. Magn Reson Med 1993; 3: 387-92.

Langkilde AR, Rostrup E, Frederiksen JL, Larsson HBW. Functional MR imaging of the visual cortex in patients with previous optic neuritis [abstract]. Proc Int Soc Magn Reson Med 1999; 2: 818.

Larsson HBW, Federiksen J, Kjaer L, Henriksen O, Olesen J. In vivo determination of T_1 and T_2 in the brains of patients with severe but stable multiple sclerosis. Magnetic Resonance in Medicine 1988; 7: 43-55.

Larsson HB, Thomsen C, Frederiksen J, Stubgaard M, Henriksen O. In vivo magnetic resonance diffusion measurement in the brain of patients with multiple sclerosis. Magn Reson Imaging. 1992; 10: 7-12.

Lassman H. Comparative neuropathology of chronic experimental allergic encephalomyelitis and multiple sclerosis. Schriftenreihe Neurologie 1983; 25: 1-135.

Lassman H. Neuropathology of multiple sclerosis. In: Compston DAS, ed. McAlpine's Multiple Sclerosis. 3rd edition. Edinburgh: Churchill Livingstone, 1998.

Lassmann H, Suchanek G, Ozawa K Histopathology and blood-cerebrospinal fluid barrier in multiple sclerosis. Ann Neurol 1994; 36: S42-S46.

Le Bihan D and Breton E. Imagerie de diffusion in vivo par resonance magnetique nucleaire. C R Acad Sc Paris 1985; 301: 1109-12.

Le Bihan D, Breton E, Lallemand D, Grenier P, Cabanis E, Laval-Jeantet M. MR imaging of intravoxel incoherent motions: applications to diffusion and perfusion in neurologic disorders. Radiology 1986; 161: 401-7.

LeBihan D, Breton E, Lallemand D, Aubin M-L, Vignaud J, Lavalleantet M. Separation of diffusion and perfusion in intravoxel incoherent motion MR imaging. Radiology 1988; 168: 497-505.

LeBihan D, Douek P, Argyropoulou M, Turner R, Patronas N. Diffusion and perfusion magnetic resonance imaging in brain tumours. Top Magn Reson Imaging 1993; 5: 25-31.

LeBihan D. Can fMRI detect decreased neuronal activity? [abstract]. Proc Int Soc Magn Reson Med 1995; 1: 452.

LeBihan D, Breton E, Lallemend D, Grenier P, Cabanis E, Laval-Jeantet M. MR imaging of intravoxel incoherent motions. Radiology 1996; 161: 401-7

LeGros Clark WE. The laminar organization and cell content of the lateral geniculate body in the monkey. J Anat 1941; 75: 419-33.

Le TH and Hu X. Retrospective estimation and correction of physiological artifacts in fMRI by direct extraction of physiological activity from MR data. Magn Reson Med 1996; 35: 290-8.

Leary SM, Silver NC, Stevenson VL, Barker GJ, Miller DH, Thompson AJ. Magnetization transfer of normal appearing white matter in primary progressive multiple sclerosis. Multiple Sclerosis 1999; 5: 313-16.

Lee MA, Smith S, Palace J, et al. Spatial mapping of T2 gadolinium-enhancing T1 lesion volumes in multiple sclerosis; evidence for distinct mechanisms of lesion genesis? Brain 1999; 122: 1261-70.

Lee M, Reddy H, Johansem-Berg H, Pendlebury S, Jenkinson M, Smith S, Palace J, Matthews PM. The motor cortex shows adaptive functional changes to brain injury from multiple sclerosis. Ann Neurol 2000; 47: 606-13.

Lehericy S, van de Moortele PF, Lobel E et al. Somatotopic organisation of striatal activation during finger and toe movement: a 3T magnetic resonance imaging study Ann Neurol 1998; 44: 398-404.

LeVay S, Wiesel TN, Hubel DH. The development of ocular dominance columns in normal and visually deprived monkeys. J Comp Neurol 1980; 191: 1-51.

LeVay S, Connolly M, Houde J, Van Essen DC. The complete pattern of ocular dominance stripes in the striate cortex and visual field of the macaque monkey. J Neurosci 1985; 5: 486-501.

Lewis RA, Sumner AJ, Brown MJ, Asbury AK. Multifocal demyelinating neuropathy with persistent conduction block. Neurology 1982; 32: 958-64.

Li Y, Jiang N, Powers C, Chopp M. Neuronal damage and plasticity identified by microtubule-associated protein 2, growth-associated protein 43, and cyclin D1 immunoreactivity after focal cerebral ischaemia in rats. Stroke 1998; 29: 1972-80.

Loevner LA, Grossman RI, Cohen JA, Lexa FJ, Kessler D, Kolson DL. Microscopic disease in normal-appearing white matter on conventional MR images in patients with multiple sclerosis: assessment with magnetization-transfer measurements. Radiology 1995; 196: 511-15.

Losseff NA, Webb SL, O'Riordan JI, et al. Spinal cord atrophy and disability in multiple sclerosis. A new reproducible and sensitive MRI method with potential to monitor disease progression. Brain 1996a; 119: 701-8.

Losseff NA, Wang L, Lai HM, et al. Progressive cerebral atrophy in multiple sclerosis: a serial MRI study. Brain 1996b; 119: 2009-20.

Losseff NA, Miller DH. Measures of brain and spinal cord atrophy in multiple sclerosis. J Neurol Neurosurg Psychiatry 1998; 64: S102-5.

Lublin FD, Reingold SC. Defining the clinical course of multiple sclerosis: results of an international survey. Neurology 1996; 46: 907-11.

Luchinetti C, Bruck W, Parisi J, Scheithauer B, Rodriguez M, Lassmann H. A quantitative analysis of oligodendrocytes in multiple sclerosis lesions. A study of 113 cases. Brain 1999; 122: 2279-95.

Lueck CJ, Zeki S, Friston KJ, et al. The colour centre in the cerebral cortex of man. Nature 1989; 340: 386-9.

Lumsden CE. The neuropathology of multiple sclerosis. In: Handbook of clinical neurology, Eds Vinken PK, Bruyn GW, pp271-309. Amsterdam: North Holland Publishing Company, 1970.

Lutsep HL, Albers GW, DeCrespigny A, Kamat GN, Marks MP, Moseley ME. Clinical utility of diffusion-weighted magnetic resonance imaging in the assessment of ischaemic stroke. Ann Neurol 1997; 41: 574-80.

MacFadyen DJ, Drance SM, Douglas GR, et al. The retinal nerve fibre layer, neuroretinal rim area, and visual evoked potentials in MS. Neurology 1988; 38: 353-8.

Maeda M, Kawamura Y, Tamagawa Y, et al. Intravoxel incoherent motion (IVIM) MRI in intracranial, extraaxial tumors and cysts. J Comput Assist Tomogr 1992; 16: 514-8.

Makris N, Worth AJ, Sorensen B, et al. Morphometry of in vivo human white matter association pathways with diffusion-weighted magnetic resonance imaging. Ann Neurol 1997; 42: 951-62.

Matthews B. Symptoms and signs of multiple sclerosis. In: Compston DAS, ed. McAlpine's Multiple Sclerosis. London: Churchill Livingstone, 1998.

Matthews PM, Francis G, Antel J, Arnold DL. Proton magnetic resonance spectroscopy for metabolic characterization of plaques in multiple sclerosis [published erratum appears in Neurology 1991; 41: 1828]. Neurology 1991; 41: 1251-6.

McDonald CT, Burkhalter A. Organization of long-range inhibitory connections within rat visual cortex. J Neurosci 1993; 13: 768-781.

McDonald WI. Conduction velocity of cutaneous afferent fibres during experimental demyelination. Proceedings of the University of Otago Medical School 1961; 39: 29-30.

McDonald WI. The effects of experimental demyelination on conduction in peripheral nerve: a histopathological and electrophysiological study. II. Electrophysiological observations. Brain 1963; 86: 501-24.

McDonald WI, Sears TA. The effects of experimental demyelination on conduction in the central nervous system. Brain 1970; 93: 583-98.

McDonald WI. Conduction in the optic nerve. Trans Ophth Soc UK 1976; 96: 352-4.

McDonald WI. Miller DH, Barnes D. The pathological evolution of multiple sclerosis. Neuropath Appl Neurobiol 1992; 18: 319-34.

McDonald WI, Miller DH, Thompson AJ. Are magnetic resonance imaging findings predictive of clinical outcome in therapeutic trials in multiple sclerosis? The dilemma of interferon-β. Ann Neurol 1994; 36: 14-18.

McDonald WI. The pathophysiology of MS. In: Compston DAS, ed. McAlpine's Multiple Sclerosis, London: Churchill Livingstone, 1998.

McFarland HF, Frank JA, Albert PS, et al. Using gadolinium-enhanced magnetic resonance imaging lesions to monitor disease activity in multiple sclerosis. Ann Neurol 1992; 32: 758-66.

McKhann GM, Cornblath DR, Griffin JW, et al. Acute motor axonal neuropathy: A frequent cause of acute flaccid paralysis in China. Ann Neurol 1993; 33: 333-42.

McLeod JG. Electrophysiological studies in the Guillain-Barre syndrome. Ann Neurol 1981; 9: S20-27.

Menon,R., Ogawa,S., Hu,S., Strupp,J.P., Anderson,P., Ugurbil,K. BOLD based functional MRI at 4 Tesla includes a capillary bed contribution: echo-planar imaging correlates with previous optical imaging using intrinsic signals. Magn Reson Med 1995; 33: 453-9.

Menon RS, Ogawa S, Strupp JP, Ugurbil K. Ocular dominance in human V1 demonstrated by functional magnetic resonance imaging. J Neurophysiol 1997; 77: 2780-7.

Merboldt KD, Hanicke W, Frahm J. Self-diffusion NMR imaging using stimulated echoes. J MRI 1985; 64: 479-86.

Mesulam MM and Mufson EJ. In: Jones, EG and Peters A, eds. The insula of Reil in man and monkey: architectonics, connectivity and function. New York: Plenum Press, 1986.

Mesulam M. From sensation to cognition. Brain 1998; 121: 1013-52.

Miller DH, Albert PS, Barkhof F, et al. Guidelines for using magnetic resonance imaging techniques in monitoring the treatment of multiple sclerosis. Ann Neurol 1996; 39: 6-16.

Miller DH, Johnson G, Tofts PS, MacManus D, McDonald WI. Precise relaxation time measurements of normal-appearing white matter in inflammatory central nervous system disease. Magn Reson Med 1989a; 11: 331-6.

Miller DH, Ormerod IE, Rudge P, Kendall BE, Moseley IF, McDonald WI. The early risk of MS following isolated acute syndromes of the brainstem and spinal cord. Ann Neurol 1989b; 26: 635-9.

Miller DH, Rudge P, Johnson G, et al. Serial gadolinium enhanced magnetic resonance imaging in multiple sclerosis. Brain 1988; 111: 927-39.

Miller DH, Austin SJ, Connelly A, Youl BD, Gadian DG, McDonald WI. Proton magnetic resonance spectroscopy of an acute and chronic lesion in multiple sclerosis. Lancet 1991; 337: 8-9.

Miller DH, Grossman RI, Reingold SC, McFarland HF. The role of magnetic resonance imaging techniques in understanding and managing multiple sclerosis. Brain 1998; 121: 3-24.

Miller DH. Clinical and magnetic resonance imaging heterogeneity in multiple sclerosis. J Neurol Neurosurg Psychiatry 1999; 67: 139.

Moll C, Mourre C, Lazdunski M, Ulrich J. Increase of sodium channels in demyelinated lesions of multiple sclerosis. Brain Res 1991; 556: 311-16.

Moreau T, Thorpe J, Miller D, et al. Reduction in new lesion formation in multiple sclerosis following lymphocyte depletion with CAMPATH-1H. Lancet 1994; 344: 298-301.

Moreau T, Hale G, Waldmann H, Isaacs J, Wing M, Compston DAS. Cytokine release increases conduction block in partially demyelinated pathways due to multiple sclerosis. Brain 1996; 119: 225-37.

Morris GL, Mueller WM, Yetkin FZ et al. Functional magnetic resonance imaging in partial epilepsy. Epilepsia 1994; 35: 1194-8.

Moseley ME, Cohen Y, Mintorovitch J, et al. Early detection of regional cerebral ischaemia in cats: comparison of diffusion- and T2-weighted MRI and spectroscopy. Magn Reson Med 1990; 2: 330-46.

Mufson EJ and Mesulam MM. Thalamic connections of the insula in the rhesus monkey and comments on the paralimbic connectivity of the medial pulvinar nucleus. J Comp Neurol 1984; 277: 109-120.

Mullen KT and Plant GT. Colour and luminance vision in human optic neuritis. Brain 1986; 109: 1-13.

Mumford CJ, Wood NW, Kellar Wood H, Thorpe JW, Miller DH, Compston DA. The British Isles survey of multiple sclerosis in twins. Neurology 1994; 44: 11-15.

Nakashima I, Fujihara K, Okita N, et al. Clinical and MRI study of brainstem and cerebellar involvement in Japanese patients with multiple sclerosis. J Neurol Neurosurg Psychiatry 1999; 67: 153-7.

Namerow NS, Thompson LR. Plaques, symptoms, and the remitting course of multiple sclerosis. Neurology 1969; 19: 765-74.

Narayanan S, Fu L, Pioro E, DeStefano N, Collins DL, et al. Imaging of axonal damage in multiple sclerosis: spatial distribution of magnetic resonance imaging lesions. Ann Neurol 1997; 41: 385-91.

Newcombe J, Cuzner ML, Roytta M, Frey H. White matter proteins in multiple sclerosis. J Neurochem 1980; 34: 700-708.

Nieuollon A, Cheramy A, Glowinski J. Release of dopamine evoked by electrical stimulation of the motor and visual areas of the cerebral cortex in both caudate nuclei and in the substantia nigra in the cat. Brain Res 1978; 145: 69-83.

Nitschke MF, Kleinschmidt A, Wessel K, Frahm J. Somatotopic motor representation in the human anterior cerebellum. A high-resolution functional MRI study. Brain 1996; 119: 1023-9.

Noguchi K, Watanabe N, Nagayoshi T, Kanazawa T, Toyoshima S, Shimizu M, Seto H. Role of diffusion-weighted echo-planar MRI in distinguishing between brain abscess and tumour: a preliminary report. Neuroradiology 1999; 41: 171-4.

Nudo RJ, Wise BM, SiFuentes F, Milliken GW. Neural substrates for the effects of rehabilitative training on motor recovery after ischemic infarct. Science 1996; 272: 1791-4.

Nusbaum AO, Tang CY, Wei T, Buchsbaum MS, Atlas SW. Whole-brain diffusion MR histograms differ between MS subtypes. Neurology 2000; 54: 1421-7.

Offenbacher H, Fazekas F, Schmidt R, Freidl W, Flooh E, Payer F, Lechner H. Assessment of MRI criteria for a diagnosis of MS. Neurology 1993; 43: 905-9.

Ogawa S, Lee TM, Nayak AS, Glynn P. Oxygenation-sensitive contrast in magnetic resonance images of rodent brain at high magnetic fields. Magn Reson Med 1990; 14: 68-78.

Ogawa S, Tank DW, Menon R, et al. Intrinsic signal changes accompanying sensory stimulation: Functional brain mapping with magnetic resonance imaging. Proc Nat Acad Sci USA 1992; 89: 5951-5.

Okazi MM, McNamara JO, Nadler JV Kainate and quisqualate receptor autoradiography in rat brain after angular bundle kindling. Neuroscience 1990; 37: 135-142.

Olsen CR and Graybiel AM. Sensory maps in the claustrum of the cat. Nature 1980; 288: 479-81.

Ordidge RJ, Helpern JA, Qing ZQ, Knight RA, Nagesh V. Correction of motional artifacts in diffusion-weighted MR images using navigator echoes. Magn Reson Imaging 1994; 12: 455-60.

O'Riordan JI, Thompson AJ, Kingsley DPE, et al. The prognostic value of brain MRI in clinically isolated syndromes of the CNS. A 10-year follow-up. Brain 1998; 121: 495-503.

Ormerod IE, Johnson G, MacManus D, du Boulay EP, McDonald WI. Relaxation times of apparently normal cerebral white matter in multiple sclerosis. Acta Radiol Suppl. 1986; 369: 382-4.

Ormerod IEC, Miller DH, McDonald WI, et al. The role of magnetic resonance imaging in the assessment of multiple sclerosis and isolated neurological lesions: a quantitative study. Brain 1987; 110: 1579-1616.

Palmer E, Ashby P, Hajek VE. Ipsilateral fast corticospinal pathways do not account for recovery in stroke. Ann Neurol 1992; 32: 519-25.

Parisi V and Bucci GM. Visual evoked potentials after photostress in patients with primary open angle glaucoma and ocular hypertension. Invest Ophthalmol Vis Sci 1992; 33: 436-42.

Parisi V, Pierelli F, Restuccia R, et al. Impaired VEP after photostress response in MS patients previously affected by optic neuritis. Electroenceph Clin Neurophysiol 1998; 108: 73-9.

Pathologic damage in MS assessed by diffusion-weighted and magnetization transfer MRI. Cercignani M, Iannucci G, Rocca M, Comi G, Horsfield MA, Filippi M. Neurology 2000; 54: 1139-44.

Paty DW, Li DK. UBC MS/MRI Study Group and the IFNN Multiple Sclerosis Study Group. Interferon beta-1b is effective in relapsing-remitting multiple sclerosis. II. MRI analysis results of a multicenter, randomized, double-blind, placebo-controlled trial. Neurology 1993; 43: 662-7.

Pauling L and Coryell CD. The properties and structure of hemoglobin, oxyhemoglobin and carbonmonoxyhemoglobin. Proc Nat Acad Sci USA 1936; 22: 210-16.

Penfield JW, Boldrey E. Somatic motor and sensory representation in the cerebral cortex of man as studied by electrical stimulation. Brain 1937; 60: 389-443.

Perry VH, Cowey A. The ganglion cell and cone distributions in the monkey's retina: implications for central magnification factors. Vision Research 1985; 25: 1795-1810.

Persson HE, Sachs C. Visual evoked potentials elicited by pattern reversal during provoked visual impairment in multiple sclerosis. Brain 1981; 104: 369-82.

Pfeiffer PN, Sicotte NL, Mattiello, et al. Functional and structural mapping of human motor systems [abstract]. Neuroimage 2000; 11: 873.

Phadke JF. Survival patterns and causes of death in patients with multiple sclerosis: results from an epidemiological survey in north-east Scotland. J Neurol, Neurosurg Psychiatry 1987; 50: 523-31.

Phillips CG, Zeki S, Barlow HB. Localization of function in the cerebral cortex. Past, present and future. Brain 1984; 107: 327-61.

Pierpaoli C and Basser PJ. Toward a quantitative assessment of diffusion anisotropy. Magn Reson Med 1996; 36: 893-906.

Pierpaoli C, Jezzard P, Basser P, Barnett A, Di Chiro G. Diffusion tensor MR imaging of the human brain. Radiology 1996; 201: 637-648.

Pierpaoli C. Oh no! One more method for colour mapping of fibre tract direction using diffusion MR imaging data [abstract]. Proc Int Soc Magn Reson Med 1997; 2: 1741.

Pierpaoli C, Barnett A, Virta A, Penix L, Chen R. Diffusion MRI of Wallerian degeneration. A new tool to investigate neural connectivity in vivo? [abstract]. Proc Int Soc Magn Reson Med 1998; 2: 1247.

Pike GB, DeStefano N, Narayanan S, Francis G, Antel J, Arnold DL. A longitudinal study of magnetization transfer in multiple sclerosis [abstract]. Proc Int Soc Magn Reson Med 1998; 1: 122.

Porac C and Coren S. The dominant eye. Psychol Bull 1976; 83: 880-97.

Poser CM, Paty DW, Scheinber L, et al. New diagnostic criteria for multiple sclerosis: guidelines for research protocols. Ann Neurol 1983; 13:227-31.

Pozzilli C, Fieschi C, Perani D, et al. Relationship between corpus callosum atrophy and cerebral metabolic asymmetries in MS. J Neurol Sci 1992; 112: 51-7.

Prichard JW and Cummings J. The insistent call from functional MRI. Neurology 1997; 48: 797-800.

Prichard JW and Grossman RI. New reasons for early use of MRI in stroke. Neurology 1999; 52: 1733-6.

Prineas J and Connel F. Remyelination in multiple sclerosis. Ann Neurol 1979; 5: 22-31.

Rao SM, Binder JR, Bandettini PA, et al. Functional magnetic resonance imaging of complex human movements. Neurology 1993; 43: 2311-18.

Rao SM, Binder JR, Hammeke TA, et al. Somatotopic mapping of the human primary motor cortex with functional magnetic resonance imaging. Neurology 1995; 45: 919-24.

Rasminsky M, Kearney RE, Aguayo AJ, Bray GM. Conduction of nervous impulses in spinal roots and peripheral nerves of dystrophic mice. Brain Res 1978; 143: 71-85.

Reddy H, Narayanan S, Matthews PM, et al. Relating axonal injury to functional recovery in MS. Neurology 2000; 54: 236-9.

Redford DJ, Kapoor R, Smith KJ. Nitric oxide donors reversibly block axonal conduction; demyelinated axons are especially susceptible. Brain 1997; 120: 2149-57.

Rempp KA, Brix G, Wenz F., Becker CR, Guchel F, Lorenz WJ. Quantification of rCBF and volume with dynamic susceptibility contrast-enhanced MRI. Radiology 1994; 193: 637-41.

Renshaw PF, Yurgelun-Todd DA, Cohen BM. Greater haemodynamic response to photic stimulation in schizophrenic patients: An echoplanar MRI study. Am J Psychiatry 1994; 151: 1493-5.

Rivera-Quinones C, MacGavern D, Schmelzer JD, Hunter SF, Low PA, Rodriguez M. Absence of neurological deficits following extensive demyelination in a class I-deficient murine model of multiple sclerosis. Nature Med 1998; 4: 187-93.

Roelcke U, Curt A, Otte A, et al. Influence of spinal cord injury on cerebral sensorimotor systems: a PET study. J Neurol Neurosurg Psychiatry 1997; 62: 61-5.

Rombouts SA, Barkhof F, Sprenger M, Valk J, Scheltens P. The functional basis of oclular dominance: functional MRI (fMRI) findings. Neurosci Lett 1996; 221: 1-4.

Rombouts SARB, Lazeron RHC, Scheltens P, Uitdehaag BMJ, Sprenger M, Valk J, Barkhof F. Visual activation patterns in patients with optic neuritis: An fMRI pilot study. Neurology 1998; 50: 1896-9.

Ron MA, Callanan MM, Warrington EK. Cognitive abnormalities in multiple sclerosis: a psychometric and MRI study. Psychological Medicine 1991; 21: 59-68.

Rosa MG, Gattass R, Fiorani Junior M. Complete pattern of ocular dominance stripes in V1 of a New World monkey, Cebus apella. Exp Brain Res 1988; 72: 645-8.

Rowe JB, Frackowiak RS The impact of brain imaging technology on our understanding of motor function and dysfunction. Curr Opin Neurobiol 1999; 9: 728-34.

Roy C and Sherrington C. On the regulation of the blood supply of the brain. J Physiol 1890; 11: 85-108.

Rudick RA, Fisher E, Lee JC, Simon J, Jacobs L. Use of the brain parenchymal fraction to measure whole brain atrophy in relapsing-remitting MS. Multiple Sclerosis Collaborative Research Group. Neurology 1999; 53:1698-704.

Runmarker B and Andersen O. Prognostic factors in a multiple sclerosis incidence cohort with twenty five years follow up. Brain 1993;116:117-134.

Sadovnik AD and Baird PA. The familial nature of multiple sclerosis: age-corrected empiric recurrence risks for children and siblings of parents. Neurology 1988; 38: 990-1.

Sahraie A, Weiskrantz L, Barbur JL, Simmons A, Williams SC, Brammer MJ. Pattern of neuronal activity associated with conscious and unconscious processing of visual signals. Proc Nat Acad Sci USA 1997; 17: 9406-11.

Sailer M, O'Riordan JI, Thompson AJ, et al. Quantitative MRI in patients with clinically isolated syndromes suggestive of demyelination. Neurology 1999; 52: 599-606.

Sandell JH, Schiller PH. Effect of cooling area 18 on striate cortex cells in the squirrel monkey. J Neurophysiol 1982; 48: 38-48.

Sarchielli P, Presciutti O, Pellicoli GP, et al. Absolute quantification of brain metabolites by proton magnetic resonance spectroscopy in normal-appearing white matter of multiple sclerosis patients. Brain 1999; 122: 513-21.

Schneider W, Noll DC, Cohen JD. Functional topographic mapping of the cortical ribbon in human vision with conventional MRI scanners. Nature 1993; 365: 150-3.

Schroder J, Wenz F, Schad LR, Baudenstel K, Knopp MV. Sensorimotor cortex and supplementary motor area changes in schizophrenia. A study with functional magnetic resonance imaging. Br J Psychiatry 1995; 167, 197-201.

Sclabassi RJ, Namerow NS, Enns NF. Somatosensory response to stimulus trains in patients with multiple sclerosis. Electroenceph Clin Neurophysiol 1974; 37: 23-33.

Seil FJ. Tissue culture studies of demyelinating disease: a critical review. Ann Neurol 1977; 2: 345-55.

Sereno MI, Dale AM, Reppas JB et al. Borders of multiple visual areas in humans revealed by functional magnetic resonance imaging. Science 1995; 268: 889-93.

Sherk H. In: Jones EG. and Peters A, eds. The Claustrum and the Cerebral Cortex. New York: Plenum Press, 1986.

Shibasaki H, McDonald WI, Kuroiwa Y. Racial modification of clinical picture of multiple sclerosis; comparison between British and Japanese patients. J Neurol Sci 1981; 49: 253-71.

Shulman RG, Fiez JA, Corbetta M, et al. Common blood flow changes across visual tasks: II. Decreases in cerebral cortex. J Cogn Neurosci 1997; 9: 648-63.

Shulman RG and Rothman DL Interpreting functional imaging studies in terms of neurotransmitter cycling. Proc Nat Acad Sci USA 1998; 95:11993-8.

Sie LTL, Rombouts SARB, Scheltens P, Valk J, van der Knaap MS. Functional MRI of the visual cortex in sedated children with periventricular echodensities [abstract]. Neuroimage 1998; 7: S494.

Smith KJ and McDonald WI. Spontaneous and evoked electrical discharges from a central demyelinating lesion. J Neurol Sci 1982; 55: 39-47.

Smith KJ, Blakemore WF, McDonald WI. Central remyelination restores secure conduction. Nature 1979; 280: 395-6.

Steel DHW and Waldock A. Measurement of the retinal nerve fibre layer with scanning laser polarimetry in patients with previous demyelinating optic neuritis. J Neurol Neurosurg Psychiatry 1998; 64: 505-9.

Stejsjkal EO and Tanner JE. Spin diffusion measurements: spin echoes in the presence of a time-dependent field gradient. J Chem Phys 1965; 42: 288-92.

Stevenson VL, Leary SM, Losseff NA, et al. Spinal cord atrophy and disability in MS: A longitudinal study. Neurology 1998; 51: 234-8.

Stewart WA, Hall LD, Berry K, Paty DW. Correlation between NMR scan and brain slice data in multiple sclerosis [letter]. Lancet 1984; 2: 412.

Stone J. The naso-temporal division of the cat's retina. J Comp Neurol 1966; 126: 585-600.

Stone J, Leicester J, Sherman SM. The naso-temporal division of the monkey's retina. J Comp Neurol 1973; 150: 333-48.

Stone LA, Frank JA, Albert PS et al. The effect of interferon-β on blood brain barrier disruptions demonstrated by contrast-enhanced magnetic resonance imaging in relapsing-remitting multiple sclerosis. Ann Neurol 1995; 37: 611-19.

Strupp JP. Stimulate: a GUI based fMRI analysis software package [abstract]. Neuroimage 1996; 3: S607.

Swadlow HA. Properties of antidromically activated callosal neurons responsive to callosal input in rabbit binocular cortex. Exp Neurol 1974; 43: 424-44.

Swingler RJ, Compston DAS. The clinical features of multiple sclerosis in South East Wales. Q J Med 1992; 83: 325-37.

Symms MR, Barker GJ, Franconi F, Clark CA. Correction of eddy-current distortions in diffusion-weighted echo-planar images with a two-dimensional registration technique [abstract]. Proc Int Soc Magn Reson Med 1997; 2: 1723.

Talairach J and Tournoux P. Co-planar stereotaxic atlas of the human brain. New York: Thieme Medical, 1988.

Taylor DG and Bushell MC. The spatial mapping of translational diffusion coefficients by the NMR imaging technique. Phys Med Biol 1985; 30: 345-9.

Thomas CG and Menon RS. Amplitude response and stimulus presentation frequency response of human primary visual cortex using BOLD EPI at 4T. Magn Reson Med 1998; 40: 203-9.

Thompson AJ, Kermode AG, MacManus DG, et al. Patterns of disease activity in multiple sclerosis: clinical and magnetic resonance imaging study. Br Med J 1990; 300: 631-4.

Thompson AJ, Kermode AG, Wicks D, et al 1992. Major differences in the dynamics of primary and secondary multiple sclerosis. Ann Neurol 1991; 29: 53-62.

Thompson AJ, Polman CH, Miller DH, et al. Primary progressive multiple sclerosis. Brain 1997; 120: 1085-96.

Thompson AJ, Montalban X, Barkhof F, Brochet B, Filippi M, Miller DH, Polman CH, Stevenson VL, McDonald WI. New diagnostic criteria for primary progressive multiple sclerosis. Ann Neurol 2000; 47: 831-5.

Thornton JS, Ordidge RJ, Penrice J, et al. Anisotropic water diffusion in white and gray matter of the neonatal piglet brain before and after transient hypoxia-ischaemia. Magn Reson Imaging 1997; 15: 433-40.

Thorpe JW, Kidd D, Moseley IF, et al. Spinal MRI in patients with suspected multiple sclerosis and negative brain MRI. Brain 1996; 119: 709-14.

Thulborn KR, Waterton JC, Matthews PM, Radda GK. Oxygenation dependence of the transverse relaxation time of water protons in whole blood at high field. Biochem Biophys Acta 1982; 714: 265-70.

Tourtellotte WW and Parker JA. Some spaces and barriers in postmortem multiple sclerosis. In Brain Barrier Systems, eds Lajtha A and Ford DH: Progress in Brain research 29: 493-525. Amsterdam: Elsevier, 1968.

Tracey I, Hamberg LM, Guimaraes AR, Hunter G, Chang I, Navia BA, Gonzalez RG. Increased cerebral blood volume in HIV-positive patients detected by functional MRI. Neurology 1998; 50: 1821-6.

Trapp BD, Peterson J, Ransohof RM, Rudick R, Mork S, Bo L. Axonal transection in the lesions of multiple sclerosis. N Engl J Medicine 1998; 388: 278-85.

Trapp BD, Ransohoff RM, Fisher E, et al. Neurodegeneration in multiple sclerosis: relationship to neurological disability. The Neuroscientist 1999; 5: 48-57.

Truyen L, van Waesberghe JHTM, van Walderveen MAA, et al. Accumulation of hypointense lesions ("black holes") on T1 SE MRI in multiple sclerosis correlates with disease progression. Neurology 1996; 47: 1469-76.

Tsukada N, Miyagi K, Matsuda M, Yanagisawa N, Yone K. Tumour necrosis factor and interleukin-1 in the CSF and sera of patients with multiple sclerosis. J Neurol Sci 1991; 104: 230-34.

Tsumoto T and Suda K. Effects of stimulation of the dorsocaudal claustrum on activities of striate cortex neurones in the cat. Brain Res 1982; 240: 345-59.

Tsuruda JS, Chew WM, Moseley ME, Norman D. Diffusion-weighted MR imaging of the brain: value of differentiating extraaxial cysts and epidermoid tumors. Am J Roentgenol 1990; 155: 1059-65.

Turner R and Le Bihan D. Single-shot diffusion imaging at 2.0 Tesla, J Magn Reson Imaging 1990; 86: 445-52.

Turner R, LeBihan D, Moonen TW, Despres D, Frank J. Echo-planar time course MRI of cat brain oxygenation changes. Magn Reson Med 1991; 27: 159-66.

Tychsen L, Burkhalter A. Nasotemporal asymmetries in V1: Ocular dominance columns of infant, adult and strabismic macaque monkeys. J Comp Neurol 1997; 388:32-46.

Uhlenbrock D, Sehlen S. The value of T1-weighted images in the differentiation between MS white matter lesions and subcortical arteriosclerotic encephalopathy (SAE). Neuroradiology 1989; 31: 203-12.

Ulrich J and Groebke-Lorenz W. The optic nerve in multiple sclerosis. A morphological study with retrospective clinico-pathological correlations. J Neuropath Exp Neurol 1976; 3: 149-59.

Ulug AM and van Zijl PCM. Orientation-independent diffusion imaging without tensor diagonalisation: anisotropy definitions based on physical attributes of the diffusion ellipsoid. JMRI 1999; 9: 804-13.

van Buchem M, Udupa J, McGowan J et al. Global volumetric estimation of disease burden in multiple sclerosis based on magnetization transfer imaging. AJNR 1997; 18: 1287-90.

van Buchem MA, Grossman RI, Armstrong C, Polansky M, Miki Y, Heyning FH, et al. Correlation of volumetric magnetization transfer imaging with clinical data in MS. Neurology 1998; 50: 1609-17.

van Walderveen MA, Barkhof F, Hommes OR, et al. Correlating MRI and clinical disease activity in multiple sclerosis: relevance of hypointense lesions on T1-weighted spin-echo MRI in multiple sclerosis. Neurology 1995; 45: 1684-90.

van Walderveen MA, Kamphorst W, Scheltens Ph et al. Histopathologic correlate of hypointense lesions on T_1-weighted spin-echo MRI in multiple sclerosis. Neurology 1998; 50: 1282-8.

van Waesberghe JH, Castelijns JA, Scheltens P, Truyen L, Lycklana A Nijeholt GJ, Hoogenraad FG, Polman CH, Valk J, Barkhof F. Comparison of four potential MR parameters for severe tissue destruction in multiple sclerosis lesions. Magn Reson Imaging 1997; 15: 155-62.

Varela FJ, Singer W. Neuronal dynamics in the visual corticothalamic pathway revealed through binocular rivalry. Exp Brain Res 1987; 66: 10-20.

Verhoye MR, 's-Gravenmade EJ, Raman ER, Van Reempts J, Van der Linden A. In vivo noninvasive determination of abnormal water diffusion in the rat brain studied in an animal model for multiple sclerosis by diffusion-weighted NMR imaging. Magn Reson Imaging 1996; 14: 521-532.

Wagner AD, Schacter DL, Rotte M, et al. Building memories: remembering and forgetting of verbal experiences as predicted by brain activity. Science 1998; 281: 1188-91.

Warach S, Chien D, Li W, Ronthal M, Edelman RR. Fast magnetic resonance diffusion-weighted imaging of acute human stroke. Neurology 1992; 42: 1717-23.

Weiller C, Chollet F, Friston KJ, Wise RJS, Frackowiak RSJ. Functional reorganization of the brain in recovery from capsulostriatal infarction in man. Ann Neurol 1992; 33: 463-472.

Weiller C, Ramsay SC, Wise RJS, Frackowiak RSJ. Individual patterns of functional reorganization in the human cerebral cortex after capsular infarction. Ann Neurol 1993; 33: 181-189.

Weinshenker BG, Bass B, Rice GPA, et al. The natural history of multiple sclerosis: a geographically based study. 1.Clinical course and disability. Brain 1989; 112: 133-46.

Weller M, Stevens A, Sommer N, Melma A, Dichgans J, Wietholter A. Comparative analysis of cytokine patterns in immunological, infections and oncological neurological disorders. J Neurol Sci 1991; 104: 215-21.

Werring DJ, Barker GJ, MacManus DG, Thompson AJ, Miller DH. Lateralisation of motor cortex activation in right-handed subjects demonstrated by functional magnetic resonance imaging [abstract]. J Neurol Neurosurg Psych 1997; 64: 702.

Werring DJ, Brassat D, Droogan AG, et al. The pathogenesis of lesions and normal-appearing white matter changes in multiple sclerosis. A serial diffusion MRI study. Brain 2000; 123: 1667-76.

Wieshmann UC, Franconi F, Symms MR, Clark CA, Barker GJ, Shorvon SD. The variability and accuracy of the apparent diffusion coefficient in diffusion weighted EPI [abstract]. Proc Int Soc Magn Reson Med 1997; 3: 1748.

Wieshmann UC, Symms MR, Parker GJM, Clark CA, Lemieux L, Barker GJ, Shorvon SD. Diffusion tensor imaging demonstrates deviation of fibres in normal appearing white matter adjacent to a brain tumour. J Neurol Neurosurg Psychiatry 2000; 68: 501-503.

Willoughby EW, Grochowski E, Li DKB, Oger J, Kastrukoff LF, Paty DW. Serial magnetic resonance scanning in multiple sclerosis: a second prospective study in relapsing patients. Ann Neurol 1989; 25: 43-9.

Woods RP, Cherry SR, Mazziotta JC. Rapid automated algorithm for aligning and reslicing PET images. J Comput Assist Tomogr 1992; 16: 620-33.

Youl BD, Turano G, Miller DH et al. The pathophysiology of acute optic neuritis: an association of gadolinium leakage with clinical and electrophysiological deficits. Brain 1991; 114: 2437-50.

Young IR, Hall AS, Pallis CA, Legg NJ, Bydder GM, Steiner RE. Nuclear magnetic resonance imaging of the brain in multiple sclerosis. Lancet 1981; 2: 1063-6.

Yousry TA, Berry I, Filippi M. Functional magnetic resonance imaging in MS. J Neurol Neurosurg Psychiatry 1998;64(suppl): S85-S87.

Zeki S and Bartels A. The asynchrony of consciousness. Proc R Soc Lond B Biol Sci 1998; 265: 1583-5.